Journal of Communications

ISSN 1796-2021

Volume 6, Number 7, October 2011

Contents

Special Issue: Advances in Wireless Communications and Networks

Guest Editors: Khan Mohammad Iftekharuddin, Mohammed Nazrul Islam, Mohammad Ataul Karim, and Mohammad Abdus Salam

Special Issue on Advances in Wireless Communications and Networks

Guest Editorial

K. M. Iftekharuddin
Old Dominion University
Department of Electrical & Computer Engineering
231 Kaufman Hall Norfolk, Virginia 23529, USA

M. N. Islam
State University of New York, Farmingdale
Department of Security Systems
2350 Broadhollow Road
Farmingdale, New York 11735, USA

M. A. Karim
Old Dominion University
Office of Research
4111 Monarch Way, Suite 203
Norfolk, Virginia 23508, USA

M. A. Salam
Southern University
Department of Computer Science
Baton Rouge, Louisiana 70813, USA

Wireless communication has been growing significantly in recent years with the development of communications systems, network architecture and sensors. Wireless systems will play important role in future internet and information systems. . Intense research in wireless systems includes developments in many application areas such as medical, agriculture, and military. This special issue on advances in wireless systems presents research trends and recent developments in the areas of multi-antenna sensing system, radio power optimization, reliable routing protocols, digital filter design, and mobile ad hoc networks.

The special issue invited papers from around the world which prompted a significant number of submissions. In addition, a selected number of authors were invited from the IEEE International Conference on Computer and Information Technology held on December 23-25, 2010 in Dhaka, Bangladesh. We received a total of thirteen submissions which went through rigorous review process by the experts in the field. Seven papers are finally selected for publication to appear in the special issue of the journal. The authors represent academic and/or research institutions from Bangladesh, China, India, Thailand, and United Kingdom.

The first paper deals with the primary user detection in cognitive radio systems. Alghamdi and Ahmed developed an optimum linear combiner multi-antenna based spectrum sensing technique using the multitaper spectrum estimation method. They showed through analyses and simulation that the proposed optimal technique requires a signal-to-noise ratio (SNR) of the order of -12 dB to achieve a probability of detection of 99.99% at a false alarm rate of 1% with additive white Gaussian noise.

Han, Wang, Liu and Zhu investigate the power allocation in coordinated multi-point transmission system with remote radio units power constraints. They developed a modified water-filling power allocation technique in order to obtain the optimum downlink sum capacity with a minimum complexity. Simulation results made it obvious that the proposed method can achieve the near-optimal sum data rate utilizing relatively more transmit power.

An efficient cluster head selection method is proposed in the third paper, which is based on sensor nodes' energy per unit cost. Debroy, Sadi, and Imran showed through experimentation that adoption of certain selection criterion in the proposed method can increase the system lifetime and maximize data communication significantly as compared to similar approaches in the literature.

The fourth paper presents a methodology to improve the performance of orthogonal frequency division multiple access system by employing adaptive resource allocation based on channel state information (CSI). Sivridis, Wang, and Choi minimize the effect of errors from imperfect CSI in fast fading environment and hence optimize the overhead load

doi:10.4304/jcm.6.7.509-511

and uplink resources used for feedback purpose. Effectiveness of the proposed scheme is demonstrated through simulation in providing a higher overall fairness and system throughput.

Channa and Ahmed propose an efficient routing scheme for post-disaster ad hoc communication networks based on the shortest possible routes with all reliable nodes. The technique detects packet forwarding misbehavior caused by network fault or congestion in an active route and reroutes packets through other reliable route. Theoretical analyses and simulation results verify the significant performance improvement in terms of packet delivery ratio and delay in the presence of network fault with a reasonable increase in routing overhead.

The impact of weighting factor and crossover probability on the design of low pass finite-duration impulse response digital filter as well as on the convergence behavior of the differential evolution (DE) technique is investigated by Chattopadhyay, Sanyal and Chandra in the fifth paper. The DE-optimized filter is then incorporated in a quadrature phase shift keying (QPSK) modulated system for pulse shaping purpose. Performance of the QPSK system is quantified in terms of bit error rate in order to obtain the optimized control parameters for the filter design.

The final paper proposes an adaptive receiver power routing protocol for mobile ad hoc wireless network. Bello, Bakalis, Rapajic, Anang and Eneh investigate the impact of environment and signal path loss on the quality of service and throughput performance. Analytical and simulation results show that the proposed protocol increases the throughput by 62% as compared to conventional dynamic source routing protocol. The average received power for individual nodes is claimed to 1×10^{10} watt compared to 5×10^{2} watt in conventional model.

The guest editors would like to express their sincere gratitude to the reviewers, who have finished their reviews in the shortest possible time and dedicated their precious time to ensure the quality of this special issue. Finally, the guest editors would extend their sincere appreciation to the Associate Editor-in-Chief, Dr. Haohong Wang for providing them with this opportunity and facilitating preparation of an excellent journal special issue.

Khan Mohammad Iftekharuddin is a Professor in the department of Electrical and Computer Engineering at the Old Dominion University (ODU). He directs the Vision lab at ODU. Prior to joining ODU, he was in the Electrical and Computer Engineering department at University of Memphis (UoM). He was also an associated faculty in the Institute for Intelligent Systems at U of M. Further, he held a joint appointment with the joint graduate program in biomedical engineering at the U of M and University of Tennessee at Memphis. Prior to U of M, he was on the faculty of the departments of Computer Science and Electrical & Computer Engineering at North Dakota State University. His research interests include biomedical image analysis, sensor signal acquisition and modeling, digital, optical and multimedia signal and image processing, optical computing and interconnection, applications of artificial-neural inference techniques, automatic target recognition (ATR) and biologically inspired ATR. Dr. Iftekharuddin is the author of five book chapters and more than hundred refereed journal papers and conference proceedings. He is an associate editor for *Optical Engineering, International Journal of Imaging, Open Cybernetics and Systemic Journal* and *International Journal of Tomography and Statistics*, He has served as guest editor for seven journal special issues. He is an elected fellow of SPIE, a senior member of IEEE, a member of IEEE CS and OSA. He obtained his B.Sc. degree from Bangladesh Institute of Technology in 1989. He received an M.S. and a Ph.D. both in electrical engineering from the University of Dayton in 1991 and 1995, respectively.

Mohammed Nazrul Islam is an Assistant Professor in the Department of Security Systems at the State University of New York at Farmingdale. He received his BS and MS in Electrical and Electronic Engineering from Bangladesh University of Engineering and Technology in 1991 and 1994, respectively, and his PhD from Muroran Institute of Technology, Japan in 1999. Prior to joining Farmingdale, he worked as a Research Scientist and Adjunct Assistant Professor at Old Dominion University. He also served respectively as an Associate Professor at Bangladesh University of Engineering and Technology, as a Postdoctoral Research Fellow at the University of South Alabama and as a Visiting Assistant Professor at the University of West Florida. He authored and co-authored more than 110 publications in refereed journals and conference proceedings. His research interests include optical communication, wireless communication, digital image processing and solid state devices. He is a Senior Member of IEEE and a Member of SPIE.

Mohammad Ataul Karim is Vice President for Research of Old Dominion University in Norfolk, Virginia. Previously, he served as dean of engineering at the City University of New York. His research areas include information processing, pattern recognition, computing, displays, and electro-optical devices and systems. Dr. Karim is author of 18 books, 7 book chapters, and over 360 articles. He is North American Editor of *Optics & Laser Technology* and an Associate Editor of the *IEEE Transactions on Education.* He has served as guest editor for over 25 journal special issues. Professor Karim is an elected fellow of the Institution of Electrical and Electronics Engineers (IEEE), Optical Society of America (OSA), Society of Photo-Instrumentation Engineers (SPIE), the Institute of Physics (InstP), the Institution of Engineering & Technology (IET), and Bangladesh Academy of Sciences. He received his BS in physics in 1976 from the University of Dacca, Bangladesh, and MS degrees in both physics and electrical engineering, and a Ph.D. in electrical engineering from the University of Alabama respectively in 1978, 1979, and 1981.

Mohammad Abdus Salam is an Associate Professor in the Department of Computer Science at Southern University, Baton Rouge, Louisiana. He received his BS degree in Electrical and Electronics Engineering from Bangladesh Institute of Technology, Rajshahi in 1991 and MS and Ph.D. degrees from Fukui University, Japan, respectively in 1998 and 2001. Prior to 2005, he worked as an adjunct faculty member of Mathematics and Computer Science at the City University of New York at York College, and as a postdoctoral fellow in the Department of Electrical and Computer Engineering at the University of South Alabama, Mobile, Alabama. He is a member of IEEE, IEICE (Japan), and AIAA. His research interests include wireless communication, error-control coding, and sensor networks.

Optimal and Suboptimal Multi Antenna Spectrum Sensing Techniques with Master Node Cooperation for Cognitive Radio Systems

Owayed A. Alghamdi and Mohammed Z. Ahmed
Mobile Communications Research Group
University of Plymouth
Plymouth PL4 8AA, UK
{owayed.alghamdi, m.ahmed}@plymouth.ac.uk

***Abstract*—In this paper, we consider the primary user detection problem in cognitive radio systems by using multi antenna at the cognitive radio receiver. An optimal linear combiner multi antenna based spectrum sensing technique is proposed using the multitaper spectrum estimation method. A suboptimal square law combiner multi antenna based technique, using the multitaper method, is also proposed. The decision statistics' probability density functions of the proposed techniques are derived theoretically. Probabilities of detection and false alarm formulae are presented using the Neyman Pearson criterion. Both proposed techniques are derived when energy detector is used. Based on our results, we found that the general likelihood ratio detector1 (GLRD1) and the blind GLRD that are proposed in the literature, require signal to noise ratios SNRs=7.5 and 9.6 dB, respectively to achieve a probability of detection of 99.99% at false alarm 1% with additive white Gaussian noise (AWGN) using 4 antennas and 16 samples for sensing. In our proposed optimal and suboptimal techniques, the required SNRs are found as −12 and −7.5 dB, respectively to achieve the same probabilities in the same conditions. Of course, this result gives an indication that even GLRD multi antenna based spectrum sensing techniques are blind in their philosophy, but that comes at the expense of their performance. Simulation results that confirm the theoretical work are also presented. An AWGN and Rayleigh flat fading environments are examined in the results. Finally, a new concept of cooperative spectrum sensing, the master node, is introduced.**

***Index Terms*—cognitive radio, spectrum sensing, multitaper spectrum estimation method, multi antenna spectrum sensing, cooperative spectrum sensing**

I. Introduction

Cognitive radio(CR) [1] is a new technology in the wireless communications world that has changed the policy of the spectrum assignment from static to a more flexible paradigm. In a CR network, a spectrum subband that is already licensed to a primary user (PR), can be used opportunistically at a specific time and location by an unlicensed user (i.e., secondary user), which is the CR. This new concept of spectrum access can satisfy the ever increasing demand for spectrum resources, and reduce the underutilized spectrum. Additionally, it can provide communications anywhere at any time [2]. An IEEE 802.22 wireless regional area network (WRAN) is the first CR standard, which operates on the spectrum that is allocated to TV services [3, 4].

In order to use the vacant subband, CR must sense its surrounding radio frequency (RF) environment before using it. Using an accurate spectrum sensing techniques allows CR to opportunistically exploit that unused spectrum, and protect the PR user from interference. Thus, spectrum sensing is a key functional factor in CR systems.

Matched filtering is classified as a high performance spectrum sensing technique. However, it requires a full knowledge of every PR's transmitted signal [5, 6]. A cyclostationary detector has a good performance, but requires knowledge of the PR's cyclic frequencies and requires long time to complete sensing [5-8]. On the other hand, an energy detector (ED), which is called a periodogram or radiometer, is simple, but has a poor performance at a low signal to noise ratio (SNR). The reason behind this, is that ED uses single rectangular tapering, which causes spectral leakage and large variance [9].

The multitaper spectrum estimation method (MTM) [10] produces single spectrum estimate with minimum spectral leakage and variance using an orthonormal family of tapers, the Discrete Prolate Slepian Sequences (DPSS) [11]. Haykin, on the other hand, suggests that MTM is an efficient spectrum sensing technique in CR systems [2]. MTM is an approximation of the optimal spectrum estimate, the maximum-likelihood method but at reduced computation [12, 13]. Haykin in [14], presented MTM's spectrum sensing tutorial and experiment results. The MTM parameters, half time bandwidth product NW, and the number of tapers K used in MTM, are recommended as ranges in his work. In our previous work, the MTM's parameters have been optimized as in [15]. The optimal NW is found as 4 and K=5 tapers is the optimal number of tapers. Optimal MTM parameters give the highest performance, and minimize the complexity when using MTM. The probabilities of detection and false alarm formulae of multitaper based spectrum sensing in additive white

Manuscript received January 25, 2011; revised May 1, 2011; accepted June 5, 2011.

Gaussian noise (AWGN) have been derived using the Neyman-Pearson criterion as in our work in [16].

Multi antenna in wireless communications allow for an increased data rate, and improve the spatial diversity [17]. Thus, a CR user can use it for both communications and spectrum sensing. Multi antenna spectrum sensing techniques and issues in CR systems have been investigated in [18-25].

Two main ED-based multi antenna spectrum sensing techniques, the linear coherent combining, and the selection processing are considered in [18]. In [19], each antenna is connected to an ED, where the PR's signal is present when more than one antenna decides so. In [20, 21], using the ED-based square law combining (SLC) technique in orthogonal frequency division multiplexing (OFDM)–multi input multi output (MIMO) based CR, resulted in significant improvements to the performance compared with using a single antenna. Generally, these works depend on ED, which has a poor performance in low SNR, and that is not practical in CR applications.

In [22], general likelihood ratio detectors (GLRDs) using multi antenna are derived with different assumptions. GLRD1 is derived assuming that only the channel gain is unknown, and is estimated using maximum likelihood (ML) estimation. Blind GLRD is derived when, signal variance, noise variance, and channel gain are all unknown to the CR, and it requires estimating these parameters as well. GLRD is derived in [23], assuming that the PR user had three different signal sources. Deriving asymptotic performance of GLRDs at different assumptions can be found in [24]. We can say that even GLRDs, in some cases, do not need prior information about the PR's signal, the channel, and the noise, they depend on estimating, which degrades the performance significantly and requires high SNR to work. In [25], we proposed local-MTM-singular value decomposition (Local-MTM-SVD) multi antenna based spectrum sensing technique as an efficient technique. Our results show a significant improvement in the performance compared to using single antenna.

In this paper, we consider CR spectrum sensing using multi antenna to detect an inverse fast Fourier transform/fast Fourier transform (IFFT/FFT) PR's transmitted signal (e.g., OFDM). Our CR user is assumed to be an IFFT/FFT based signal processing (e.g., OFDM). This will allow for the practical use of MTM in spectrum sensing. We propose the use of linear combiner-MTM based (MTM-LC) spectrum sensing, which is optimal when the channel coefficients can be known by CR, and that is possible when the PR's signaling is known. Blind channel equalization methods can, also, be used in such cases. The linear combining here increases the SNR, and using MTM minimizes the spectral leakage, and improves the variance of the estimate. A suboptimal multi antenna spectrum sensing technique has been proposed, square low combining-MTM based (MTM-SLC). In MTM-SLC, the MTM is performed through each antenna separately, and then the final spectrum estimate can be averaged over all the antennas' estimates. MTM-SLC, improves the performance at low SNR, and does not require coherent detection. Our proposed techniques have been derived theoretically and compared to simulation. The same techniques have been derived as well for ED and comparison between different techniques is presented in the results. Decision statistics' probability density functions (PDFs) of the proposed techniques have been defined for different hypothesis at different cases for both MTM, and ED. Additionally, we introduce a new cooperation concept, the master node (MN) cooperation. In MN, a single CR node can be supported by advanced hardware components, and advanced signal processing. This improves the detection's probability, minimizes the overall CR network complexity, minimizes the over head that is required when all CR's nodes share sensing, and accelerates the decision process.

The rest of the paper is organized as follows: Section II defines the model for the system under consideration, and reviews MTM and ED spectrum sensing techniques. Section III presents the theoretical aspect of the proposed multi antenna MTM-based detectors, and the same detectors when using ED in an AWGN environment. Section IV presents the works in a multipath fading environment. Section V defines the MN-Cooperation concept and compares it to the existing classical cooperation algorithms. Section VI presents the results and Section VII concludes the paper.

II. System Model

In our system model, we consider the OFDM signaling scheme for the PR user. The PR transmitter with N subcarriers (N-IFFT/FFT) transmits OFDM-quadrature phase shift keying (OFDM-QPSK) signal with energy E_s over each subcarrier, and symbol duration T_s. The CR transceiver is supported by the (N-IFFT/FFT) processor as well, so as to perform both tasks of communications and sensing. The number of antennas, M is added to the CR for both spectrum sensing and communications. Fig. 1 shows a representative diagram of multi antenna based spectrum sensing in CR systems.

In the global cooperation scenario, the number of CRs G cooperate their spectrum sensing decisions using binary digits to a main CR base station (CR-BS), which performs the "OR" rule cooperation and declares the final decision to the CR's nodes.

The received PR signal, at the CR receiver, is sampled to generate a finite discrete time samples series $\{x_{t,m}; t = 0,1,\dots,N-1, m = 1,\dots,M\}$, where m denotes the antenna number, and t is the time index. The discrete time samples are dot multiplied with different tapers $v_{(t,k)}(N,W)$ (tapers are DPSS). The associated eigenvalue of the k^{th}taper is $\lambda_k(N,W)$. The product is applied to a Fourier transform to compute the energy concentrated in the bandwidth $(-W,W)$ centered at frequency f. The half time bandwidth product is NW. The total number of generated tapers is $2NW$.

In order to evaluate the performance of the proposed techniques, we review two different types of probabilities at each frequency bin f_i, the probability of detection $P_d(f_i)$ and the probability of false alarm $P_f(f_i)$.

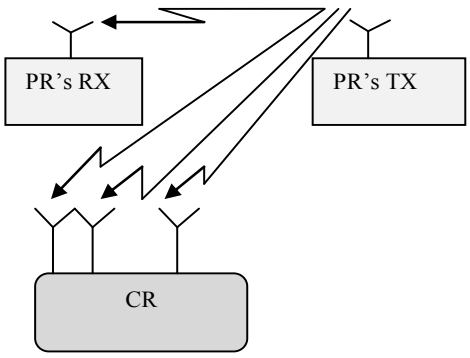

Figure 1. Multi antenna based spectrum sensing in CR systems.

$P_d(f_i)$, is the probability that the CR node (sensor) correctly decides the presence of the PR's signal, and $P_f(f_i)$ is the probability that the CR node (sensor) decides the PR's signal is present when it is absent.

The binary hypothesis test for CR spectrum sensing at the l^{th} time, and using the m^{th} antenna branch is given by:

$$\mathcal{H}_0: \quad x_{t,m}(l) = w_{t,m}(l)$$
$$\mathcal{H}_1: \quad x_{t,m}(l) = s_t(l) + w_{t,m}(l) \qquad (1)$$

where l=0,1,…,L-1 is OFDM block's index, and $x_{t,m}(l)$, $w_{t,m}(l)$, and $s_t(l)$ denote the CR received, noise at the branch m, and PR's transmitted samples. The transmitted PR signal is distorted by the zero mean AWGN, $w_{t,m}(l) \sim \mathcal{CN}(0, \sigma_w^2)$ at the output from the different antenna branches, which are independent and with identical variance σ_w^2. Note that at each frequency bin of CR FFT, $\mathcal{H}_0$ indicates no PR signal present, while $\mathcal{H}_1$ means there is a PR signal present.

The time instant l comes from the samples over different OFDM blocks, and the time instant t comes from the samples from the same OFDM block (i.e., IFFT/FFT samples). Thus, the spectrum sensing time in seconds is $(L)(N)(T_s)$, where T_s represents symbol duration, L represents the number of OFDM blocks that were used in sensing, and N is the number of samples per OFDM block (i.e., FFT size).

For K orthonormal tapers used in the MTM, there will be K different eigenspectrums produced from each antenna defined as:

$$Y_{k,m}(f_i) = \sum_{t=0}^{N-1} v_{(t,k)}(N,W)(x_{t,m}(l))e^{-j2\pi f_i t} \qquad (2)$$

where, $f_i = 0, \frac{1}{N}, \frac{2}{N}, \dots, \frac{N-1}{N}$ are the normalized frequency bins. The power spectrum estimate given by Thomson theoretical work is defined as [10]:

$$S_{MTM}^m(f_i) = \frac{\sum_{k=0}^{K-1} \lambda_k(N,W) \left|Y_{k,m}(f_i)\right|^2}{\sum_{k=0}^{K-1} \lambda_k(N,W)} \qquad (3)$$

On the other hand, the energy detector, when the samples are taken at uniform time spacing, gives the power spectrum density estimation as [9]:

$$S_{ED}^m(f_i) = \left|\sum_{t=0}^{N-1} x_{t,m}(l)e^{-j2\pi f_i t}\right|^2 \qquad (4)$$

The decision statistic over L using MTM is defined for the m^{th}antenna as follows:

$$DEC_{MTM}^m(f_i) = \sum_{l=0}^{L-1} \frac{\sum_{k=0}^{K-1} \lambda_k(N,W) \left|\sum_{t=0}^{N-1} v_{(t,k)}(N,W) x_{t,m}(l) e^{-j2\pi f_i t}\right|^2}{\sum_{k=0}^{K-1} \lambda_k(N,W)} \qquad (5)$$

Using the energy detector, the decision statistic over L is defined for the m^{th} antenna as follows:

$$DEC_{ED}^m(f_i) = \sum_{l=0}^{L-1} \left|\sum_{t=0}^{N-1} x_{t,m}(l)e^{-j2\pi f_i t}\right|^2 \qquad (6)$$

For single antenna MTM-based spectrum sensing, and according to the central limit theorem, if the number of samples L, is large, the decision statistic, $DEC_{MTM}^m(f_i)$ is asymptotically normally distributed with mean (E) [16]:

$$E[DEC_{MTM}^m(f_i)] = \begin{cases} LK\sigma_w^2 & \mathcal{H}_0 \\ LK(E_s + \sigma_w^2) & \mathcal{H}_1 \end{cases} \qquad (7)$$

and variance (VAR)

$$VAR\left(DEC_{MTM}^m(f_i)\right) = \begin{cases} 2LC^2\lambda_\Sigma\sigma_w^4 & \mathcal{H}_0 \\ 2LC^2\lambda_\Sigma\sigma_w^2(\sigma_w^2 + 2E_s) & \mathcal{H}_1 \end{cases} \qquad (8)$$

where λ_Σ, is defined as follows:

$$\begin{aligned} \lambda_\Sigma \; = & \sum_{k=0}^{K-1} \lambda_k^2(N,W) + 2\lambda_0(N,W)\lambda_1(N,W) \\ & + 2\lambda_0(N,W)\lambda_2(N,W) + \cdots \\ & + 2\lambda_0(N,W)\lambda_{K-1}(N,W) \\ & + 2\lambda_1(N,W)\lambda_2(N,W) + 2\lambda_1(N,W)\lambda_3(N,W) \\ & + \cdots + 2\lambda_1(N,W)\lambda_{K-1}(N,W) + \cdots \\ & + 2\lambda_{K-2}(N,W)\lambda_{K-1}(N,W) \end{aligned}$$

and $C = E[\frac{1}{\sum_{k=0}^{K-1} \lambda_k(N,W)}] = \frac{1}{\sum_{k=0}^{K-1} \lambda_k(N,W)}$

On the other hand for the energy detector, and at the same assumption, the decision statistic, $DEC_{ED}^m(f_i)$ has the mean [26]:

$$E[\, DEC_{ED}^m(f_i)] = \begin{cases} L\sigma_w^2 & \mathcal{H}_0 \\ L(E_s + \sigma_w^2) & \mathcal{H}_1 \end{cases} \qquad (9)$$

and variance

$$VAR\left(DEC_{ED}^m(f_i)\right) = \begin{cases} 2L\sigma_w^4 & \mathcal{H}_0 \\ 2L\sigma_w^2(\sigma_w^2 + 2E_s) & \mathcal{H}_1 \end{cases} \qquad (10)$$

For a normally distributed decision statistic, $DEC(f_i)$, the probabilities of detection, $P_d(f_i)$, and false alarm, $P_f(f_i)$ are defined as follow:

$$\begin{aligned} P_d(f_i) &= P(DEC(f_i) > \gamma / \mathcal{H}_1) \\ &= Q\left(\frac{\gamma - E[DEC(f_i)/\mathcal{H}_1]}{\sqrt{VAR(DEC(f_i)/\mathcal{H}_1)}}\right) \qquad (11) \\ P_f(f_i) &= P(DEC(f_i) > \gamma / \mathcal{H}_0) \end{aligned}$$

$$= Q\left(\frac{\gamma - E[DEC(f_i)/\mathcal{H}_0]}{\sqrt{VAR(DEC(f_i)/\mathcal{H}_0)}}\right) \quad (12)$$

The probability of miss detection $P_{mi}(f_i)$ can be defined as:

$$P_{mi}(f_i) = P(DEC(f_i) < \gamma / \mathcal{H}_1)$$
$$= 1 - Q\left(\frac{\gamma - E[DEC(f_i)/\mathcal{H}_1]}{\sqrt{VAR(DEC(f_i)/\mathcal{H}_1)}}\right) \quad (13)$$

The term $Q(\xi)$ is the complementary cumulative distribution function, $Q(\xi) = \frac{1}{\sqrt{2\pi}}\int_{\xi}^{\infty} e^{-\frac{t^2}{2}}\,dt$, and γ represents the chosen threshold. Note that γ can be controlled based on $L\sigma_w^2$. The signal to noise ratio is defined as SNR $= \frac{E_s}{\sigma_w^2}$ for each antenna branch when they are identical.

The different probabilities in (11), (12), and (13) can be calculated based on the means (*Es*), and the variances (*VARs*) for the different techniques at the different hypotheses as in (7) to (10). Thus, the different probabilities of MTM using single antenna can be redefined as follow [16]:

$$P_d^{MTM}(f_i) = Q\left(\frac{\gamma - LK(E_s+\sigma_w^2)}{\sqrt{2LC^2\lambda_\Sigma\sigma_w^2(\sigma_w^2+2E_s)}}\right) \quad (14)$$

$$P_f^{MTM}(f_i) = Q\left(\frac{\gamma - LK\sigma_w^2}{\sqrt{2LC^2\lambda_\Sigma\sigma_w^4}}\right) \quad (15)$$

$$P_{mi}^{MTM}(f_i) = 1 - Q\left(\frac{\gamma - LK(E_s+\sigma_w^2)}{\sqrt{2LC^2\lambda_\Sigma\sigma_w^2(\sigma_w^2+2E_s)}}\right) \quad (16)$$

The number of samples required by MTM using single antenna (L^{MTM}) can be written as [16]:

$$L^{MTM} = \left(\frac{a^{MTM} - b^{MTM}}{KE_s}\right)^2 \quad (17)$$

where

$$a^{MTM} = \sqrt{2C^2\lambda_\Sigma\sigma_w^4}\,Q^{-1}\left(P_f^{MTM}(f_i)\right)$$

and

$$b^{MTM} = \sqrt{2C^2\lambda_\Sigma\sigma_w^2(\sigma_w^2+2E_s)}\,Q^{-1}\left(P_d^{MTM}(f_i)\right)$$

Substituting (9) and (10) in (11), (12), and (13), gives the different probabilities for the ED case.

III. Proposed Multi Antenna Based Spectrum Sensing Techniques

In this section of the paper, we present the theoretical and analytical works of the proposed two spectrum sensing techniques. The first proposed technique is the square law combining-MTM based (MTM-SLC) technique, which can be developed by using number of the antennas, *M* at the CR receiver for spectrum sensing based on MTM. The decision statistic is performed via each antenna branch separately using MTM over *L* samples, and then the overall decision statistic is calculated by summing the outputs decision statistics from the different antenna branches as square law combining. MTM-SLC is compared theoretically and analytically to the energy detector-square law combining (ED-SLC) as can be seen below.

The decision statistics in (5) and (6) can be redefined for square law combining using *M* antennas for both techniques MTM, and ED respectively as follow:

$$DEC_{MTM-SLC}(f_i) = \sum_{m=1}^{M}\sum_{l=0}^{L-1}\frac{\sum_{k=0}^{K-1}\lambda_k(N,W)\left|\sum_{t=0}^{N-1}v_{(t,k)}(N,W)x_{t,m}(l)e^{-j2\pi f_i t}\right|^2}{\sum_{k=0}^{K-1}\lambda_k(N,W)} \quad (18)$$

and

$$DEC_{ED-SLC}(f_i) = \sum_{m=1}^{M}\sum_{l=0}^{L-1}\left|\sum_{t=0}^{N-1}x_{t,m}(l)e^{-j2\pi f_i t}\right|^2 \quad (19)$$

From (18) and (19) the decision statistic using square law combining is a sum of identical and independent normally distributed *M* antennas decision statistics. Thus, the mean of the $DEC_{MTM-SLC}(f_i)$ using *M* antennas can be defined as follows:

$$E[DEC_{MTM-SLC}(f_i)] = \begin{cases} MLK\sigma_w^2 & \mathcal{H}_0 \\ MLK(E_s+\sigma_w^2) & \mathcal{H}_1 \end{cases} \quad (20)$$

and the variance can be defined as follows:

$$VAR\left(DEC_{MTM-SLC}(f_i)\right) = \begin{cases} 2MLC^2\lambda_\Sigma\sigma_w^4 & \mathcal{H}_0 \\ 2MLC^2\lambda_\Sigma\sigma_w^2(\sigma_w^2+2E_s) & \mathcal{H}_1 \end{cases} \quad (21)$$

In the ED case, the mean of the decision statistic, $DEC_{ED-SLC}(f_i)$ using square law combining through *M* antennas can be defined as follows:

$$E[DEC_{ED-SLC}(f_i)] = \begin{cases} ML\sigma_w^2 & \mathcal{H}_0 \\ ML(E_s+\sigma_w^2) & \mathcal{H}_1 \end{cases} \quad (22)$$

and the variance is defined as follows:

$$VAR(DEC_{ED-SLC}(f_i)) = \begin{cases} 2ML\sigma_w^4 & \mathcal{H}_0 \\ 2ML\sigma_w^2(\sigma_w^2+2E_s) & \mathcal{H}_1 \end{cases} \quad (23)$$

The different probabilities can be redefined for the square law combining technique using *M* antennas for both MTM, and ED cases by substituting the means and variances defined in (20), (21), (22), and (23) in (11), (12), and (13). The threshold, γ in this case, is controlled by the term $LM\sigma_w^2$.

The second proposed technique is the MTM based-Linear combiner (MTM-LC) of the received samples from different *M* antennas at the CR receiver. The received data samples at the CR receiver are summed from the different *M* antenna branches in the time domain to be as follows:

$$x_t(l) = \sum_{m=1}^{M} x_{t,m}(l) \quad (24)$$

Then the eigenspectrums of the resulted new received samples, $x_t(l)$, can be written as follows:

$$Y_k(f_i) = \sum_{t=0}^{N-1} v_t^{(k)}(N,W)x_t(l)e^{-j2\pi f_i t} \quad (25)$$

The MTM-LC decision statistic over *L* samples can be defined as follows:

$$DEC_{MTM-LC}(f_i) = \sum_{l=0}^{L-1} \frac{\sum_{k=0}^{K-1} \lambda_k(N,W) \left| \sum_{t=0}^{N-1} v_{(t,k)}(N,W) x_t(l) e^{-j2\pi f_i t} \right|^2}{\sum_{k=0}^{K-1} \lambda_k(N,W)} \quad (26)$$

In order to derive the different probabilities expressions of $DEC_{MTM-LC}(f_i)$, we need to derive the mean (E), and the variance (VAR) for the different hypotheses. We follow our theoretical derivation of the MTM-single based as in [16]. The linear combiner binary hypothesis can be defined as follows:

$$\mathcal{H}_0: \ x_t(l) = w_{t,1}(l) + w_{t,2}(l) + \cdots \ w_{t,M}(l)$$
$$\mathcal{H}_1: \ x_t(l) = s_t(l) + w_{t,1}(l) + \cdots s_t(l) + \ w_{t,M}(l) \quad (27)$$

The main different in $\mathcal{H}_0$ between MTM, and MTM-LC is the effect of the combined noise signals from different antenna. Thus, the mean for K correlated Gaussian samples of the decision statistic in (26), $E[DEC_{MTM-LC}(f_i)/\ \mathcal{H}_0]$ can be defined as follows:

$$E[DEC_{MTM-LC}(f_i)/\ \mathcal{H}_0] = C. \sum_{l=0}^{L-1} \Big(\sum_{k=0}^{K-1} (\lambda_k(N,W) . K \sum_{t=0}^{N-1} \sum_{t'=0}^{N-1} E[v_{(t,k)}(N,W) . v_{(t',k)}(N,W). x_t(l) x_{t'}(l)] \Big) \Big) \quad (28)$$

It can be shown that (28) can be simplified as:

$$E[DEC_{MTM-LC}(f_i)/\ \mathcal{H}_0] = \sum_{l=0}^{L-1} \sum_{t=0}^{N-1} (v_{(t,k)}(N,W). v_{(t',k)}(N,W)). K . E[x_t(l) x_{t'}(l)] \quad (29)$$

From the definition of the DPSS, we have [11]:

$$\sum_{t=0}^{N-1} v_{(t,k)}(N,W). v_{(t,k')}(N,W) = \begin{cases} 1, & k = k' \\ 0, & k \neq k' \end{cases} \quad (30)$$

In the remaining parts of the paper, the terms $w_{t,m}(l)$, and $s_t(l)$ will be written as $w_m(l)$, and $s(l)$ respectively for simplification.

The orthonormality of the sequences can be used to simplify (29), over L (L here is for MTM-LC technique, which is different from that for MTM-SLC) sensed samples, when $t = t'$as follows:

$$E[DEC_{MTM-LC}(f_i)/\ \mathcal{H}_0] = \sum_{l=0}^{L-1} K. E[x_t^2(l)]$$

$$= LK. E[\big(w_1(l) + w_2(l) + \cdots + w_M(l)\big)\big(w_1(l) + w_2(l) + \cdots + w_M(l)\big)] = LK. E[w_1^2(l) + w_1(l)w_2(l) + w_1(l)w_3(l) + \cdots + w_1(l)w_M(l) + w_2^2(l) + w_2(l)w_1(l) + w_2(l)w_3(l) + \cdots + w_2(l)w_M(l) + \cdots + w_M^2(l) + w_M(l)w_1(l) + w_M(l)w_2(l) + \cdots + w_M(l)w_{M-1}(l)] \quad (31)$$

since $E[w_i(l)w_j(l)] = 0$, for $i \neq j$, and $i, j = 1,2, \ldots M$, then (31) can be rewritten as follows:

$$E[DEC_{MTM-LC}(f_i)/\ \mathcal{H}_0] = LK. (E[w_1^2(l)] + E[w_2^2(l)] + \cdots + E[w_M^2(l)])$$

$$= LK. ((E[w_1(l)])^2 + VAR(w_1(l)) + (E[w_2(l)])^2 + VAR(w_2(l)) + \cdots + (E[w_M(l)])^2 + VAR(w_M(l))) \quad (32)$$

Finally, $E[w_m(l)] = 0$, and $VAR\big(w_m(l)\big) = \sigma_w^2$, then (32) can be written as follows:

$$E[DEC_{MTM-LC}(f_i)/\ \mathcal{H}_0] = MLK\sigma_w^2 \quad (33)$$

The variance of K correlated Gaussian samples in (26), $VAR(DEC_{MTM-LC}(f_i)/\ \mathcal{H}_0)$ over L sensed samples when $t = t'$, can be defined as follows:

$$VAR(DEC_{MTM-LC}(f_i)/\ \mathcal{H}_0) = \beta L. \left(\sum_{t=0}^{N-1} v_{(t,k)}^2(N,W) \right)^2 . VAR\big(x_t^2(l)\big) \quad (34)$$

$$= \beta L\ . VAR(w_1^2(l) + w_1(l)w_2(l) + w_1(l)w_3(l) + \cdots + w_1(l)w_M(l) + w_2^2(l) + w_2(l)w_1(l) + w_2(l)w_3(l) + \cdots + w_2(l)w_M(l) + \cdots + w_M^2(l) + w_M(l)w_1(l) + w_M(l)w_2(l) + \cdots w_M(l)w_{M-1}(l)\ ) \quad (35)$$

where β is defined as follows:

$$\beta = C^2\ \lambda_\Sigma \quad (36)$$

Then, (35) can be simplified as follows:

$$VAR(DEC_{MTM-LC}(f_i)/\ \mathcal{H}_0) = \beta L\ (VAR\big(w_1^2(l)\big) + VAR\big(w_2^2(l)\big) + \cdots + \ VAR\big(w_M^2(l)\big) + VAR\big(2w_1(l)w_2(l)\big) + VAR\big(2w_1(l)w_3(l)\big) + \cdots + VAR(2w_1(l)w_M(l)) + VAR\big(2w_2(l)w_3(l)\big) + VAR\big(2w_2(l)w_4(l)\big) + \cdots + VAR\ \Big(2w_2(l)w_M(l)\Big) + \cdots + VAR\big(2w_M(l)w_{M-1}(l)\big)\Big)$$

$$= \beta L\Bigg(VAR\big(w_1^2(l)\big) + VAR\big(w_2^2(l)\big) + \cdots + VAR\big(w_M^2(l)\big) + \binom{M}{2} VAR\ \Big(2w_i(l)w_j(l)\Big)\Bigg) \quad (37)$$

where $VAR\big(w_m^2(l)\big) = 2\sigma_w^4$, and $VAR\ \Big(2w_i(l)w_j(l)\Big) = 4\sigma_w^4, \forall\ i \neq j, and\ i, j = 1,2, \ldots M$. Finally, (37) can be written as follows:

$$VAR(DEC_{MTM-LC}(f_i)/\ \mathcal{H}_0) = \beta L\ (M(2\sigma_w^4) + 2\binom{M}{2}\ (2\sigma_w^4))$$

$$= \beta L\ \left(M(2\sigma_w^4) + 2\left(\frac{M!}{(M-2)!\,2!}\right)(2\sigma_w^4)\right)$$

$$= \beta L\ M^2(2\sigma_w^4) \quad (38)$$

When the PR's signal is present, the

$E[DEC_{MTM-LC}(f_i)/\mathcal{H}_1]$ over L sensed samples when $t = t'$, can be defined as follows:

$$\begin{aligned}E[DEC_{MTM-LC}(f_i)/\mathcal{H}_1] &= LK.E[\big(s(l)+w_1(l)+s(l)+w_2(l)\\ &+\cdots+s(l)+w_M(l)\big)\big(s(l)+w_1(l)\\ &+s(l)+w_2(l)+\cdots+s(l)+w_M(l)\big)]\end{aligned}$$

$$\begin{aligned}&= LK.E[M^2s^2(l)+w_1^2(l)+w_2^2(l)+\cdots+w_M^2(l)\\ &+s(l)w_1(l)+s(l)w_2(l)+\cdots\\ &+s(l)w_M(l)+\cdots\\ &+w_M(l)s(l)]\end{aligned}$$

$$\begin{aligned}&= LK.(E[M^2s^2(l)]+2M.E[s(l)].E[w_m(l)]+\\ &E[w_1^2(l)]+E[w_2^2(l)]+\cdots+\\ &E[w_M^2(l)])\end{aligned} \quad (39)$$

where $E[M^2s^2(l)] = M^2E_s$, $E[w_m(l)] = 0$, and $E[w_m^2(l)] = ((E[w_m(l)])^2 + VAR(w_m(l))) = 0 + \sigma_w^2$, then (38) can be simplified as follows:

$$\begin{aligned}E[DEC_{MTM-LC}(f_i)/\mathcal{H}_1] &= LK(M^2E_s + M\sigma_w^2)\\ &= MLK(ME_s + \sigma_w^2)\end{aligned} \quad (40)$$

The variance, $VAR(DEC_{MTM-LC}(f_i)/\mathcal{H}_1)$ can be defined as follows:

$$\begin{aligned}&VAR(DEC_{MTM-LC}(f_i)/\mathcal{H}_1)\\ &= \beta L.VAR\big(M^2s^2(l)+w_1^2(l)+w_2^2(l)\\ &+\cdots+w_M^2(l)+s(l)w_1(l)+s(l)w_2(l)\\ &+\cdots+s(l)w_M(l)+\cdots\\ &+w_M(l)s(l)\big)\end{aligned}$$

$$\begin{aligned}&= \beta L\Big(VAR\big(2Ms(l)w_1(l)\big)+VAR\big(2Ms(l)w_2(l)\big)+\cdots\\ &+VAR\big(2Ms(l)w_M(l)\big)+VAR\big(w_1^2(l)\big)\\ &+VAR\big(w_2^2(l)\big)+\cdots+VAR\big(w_M^2(l)\big)\\ &+\binom{M}{2}.VAR\left(2w_i(l)w_j(l)\right)\Big),\ \forall\ i\\ &\neq j, and\ i,j = 1,2,\dots M\\ &= \beta L(M(4M^2)E_s\sigma_w^2 + M(2\sigma_w^4)\\ &+2\left(\frac{M!}{(M-2)!\,2!}\right)(2\sigma_w^4))\\ &= \beta L\big(M(4M^2)E_s\sigma_w^2 + M^2(2\sigma_w^4)\big)\\ &= 2\beta LM^2\sigma_w^2\,(\sigma_w^2 + 2ME_s)\end{aligned} \quad (41)$$

Finally, the different MTM-LC hypotheses' mean, and variance can be summarized as follow:

$$E\big(DEC_{MTM-LC}(f_i)\big) = \begin{cases}MLK\sigma_w^2 & \mathcal{H}_0\\ MLK(ME_s+\sigma_w^2) & \mathcal{H}_1\end{cases} \quad (42)$$

$$VAR\big(DEC_{MTM-LC}(f_i)\big) = \begin{cases}2\beta L\,M^2\sigma_w^4 & \mathcal{H}_0\\ 2\beta LM^2\sigma_w^2\,(\sigma_w^2+2ME_s)\,\mathcal{H}_1\end{cases} \quad (43)$$

The same derivation steps can be followed for $DEC_{ED-LC}(f_i)$, then the different hypotheses' mean, and variance can be written as follow:

$$E[DEC_{ED-LC}(f_i)] = \begin{cases}ML\sigma_w^2 & \mathcal{H}_0\\ ML(ME_s+\sigma_w^2) & \mathcal{H}_1\end{cases} \quad (44)$$

$$VAR\big(DEC_{ED-LC}(f_i)\big) = \begin{cases}2M^2L\sigma_w^4 & \mathcal{H}_0\\ 2M^2L\sigma_w^2(\sigma_w^2+2ME_s)\,\mathcal{H}_1\end{cases} \quad (45)$$

The different probabilities, P_d^{MTM-LC}, P_f^{MTM-LC}, and P_{mi}^{MTM-LC} shown in (11), (12), and (13) can be calculated based on the means (*E*s), and the variances (*VAR*s) for the MTM-LC at the different hypotheses as in (42) and (43). The same procedures can be done for the ED-LC technique. The threshold, γ, in this case, is controlled by the term $LM\sigma_w^2$.

The MTM's mean is *K* times ED's mean for both hypotheses, and the difference in the variance is defined as the variance factor (*VF*), which can be written as follows:

$$VF = C^2\,\lambda_\Sigma = \beta \quad (46)$$

The number of samples, $L^{MTM-SLC}$(i.e., OFDM blocks) needed to achieve predefined probabilities of detection, $P_d^{MTM-SLC}$, and false alarm, $P_f^{MTM-SLC}$ in the MTM-SLC technique can be written using the resulted MTM-SLC probabilities of detection and false alarm formulae as follows:

$$L^{MTM-SLC} = \left(\frac{a^{MTM-SLC} - b^{MTM-SLC}}{MKE_s}\right)^2 \quad (47)$$

where

$$a^{MTM-SLC} = \sqrt{2VFM\sigma_w^4}\,Q^{-1}\left(P_f^{MTM-SLC}(f_i)\right)$$

and

$$b^{MTM-SLC} = \sqrt{2VFM\sigma_w^2(\sigma_w^2+2E_s)}\,Q^{-1}\left(P_d^{MTM-SLC}(f_i)\right)$$

The derivation of $L^{MTM-SLC}$ is detailed in the Appendix.

The MTM-LC's samples, L^{MTM-LC}, can be defined as follows:

$$L^{MTM-LC} = \left(\frac{a^{MTM-LC} - b^{MTM-LC}}{M^2KE_s}\right)^2 \quad (48)$$

where

$$a^{MTM-LC} = \sqrt{2VFM^2\sigma_w^4}\,Q^{-1}\left(P_f^{MTM-LC}(f_i)\right)$$

and

$$b^{MTM-LC} = \sqrt{2VFM^2\sigma_w^2(\sigma_w^2+2ME_s)}\,Q^{-1}\left(P_d^{MTM-LC}(f_i)\right)$$

This can be written in (dB) as follows:

$$L_{dB} = 10log_{10}(L)$$

Substituting *VF*=1, and *K*=1 in (47), and (48) produces the number of samples, *L* for ED-SLC, and ED-LC respectively.

IV. Multi Path Fading Enviornment

The channel model that is assumed in this paper is similar to that in [27], where an AWGN is added to the PR's signal at the CR's receiver. In the multipath fading environment, (1) can be rewritten as follows:

$$\mathcal{H}_0: \ x_{t,m}(l) = w_{t,m}(l)$$

$$\mathcal{H}_1: \ x_{t,m}(l) = \sum_{p=0}^{P-1} h_{p,m} s_{t-p}(l) + w_{t,m}(l) \quad (49)$$

where the discrete channel impulse response between the PR's transmitter and CR's m^{th} branch is represented by $h_{p,m}, p = 0,1,\dots,P-1$, and P is the total number of resolvable paths. The discrete frequency response of the channel through the m^{th} branch is obtained by taking the N point FFT, with $N \geq P$ as follows [28]:

$$H_m(f_i) = \sum_{p=0}^{P-1} h_{p,m} e^{-j2\pi f_i p} \quad (50)$$

In such an environment, using MTM-SLC and ED-SLC does not need co-phasing to cancel the effect of the channel of each antenna branch. Since the decision statistic will be performed via each CR's antenna branch independently, the MTM-SLC's decision statistic can be approximated to Gaussian, and then (20) and (21) can be rewritten as:

$$E\left(DEC_{MTM-SLC}(f_i)\right) = \begin{cases} MLK\sigma_w^2 & \mathcal{H}_0 \\ LK\left(E_s\left(\sum_{m=0}^{M-1}|H_m(f_i)|^2\right) + M\sigma_w^2\right) & \mathcal{H}_1 \end{cases} \quad (51)$$

$$VAR\left(DEC_{MTM-SLC}(f_i)\right) = \begin{cases} 2MLC^2\lambda_\Sigma\sigma_w^4 & \mathcal{H}_0 \\ 2LC^2\lambda_\Sigma\sigma_w^2\left(M\sigma_w^2 + 2E_s\left(\sum_{m=0}^{M-1}|H_m(f_i)|^2\right)\right) & \mathcal{H}_1 \end{cases} \quad (52)$$

In practice, $|H_m(f_i)|^2$ can be estimated a priori during the time that PR's transmitter occupies a specific band with specific power [28]. In this paper, we assume that the channel gain between the PR's transmitter and the CR's receiver is constant during the spectrum sensing duration, and this is useful for application like in IEEE802.22. When applying MTM-LC and ED-LC, the CR wants to coherently add up the signals from different branches by co-phasing, which requires knowing the channel coefficients a priori via training sequences or pilot signals. Blind channel equalization techniques [29] are very useful in such cases.

V. Master- Node Cooperation

In order to resolve the multipath fading effect, shadowing, and noise uncertainty on the CR's spectrum sensing, different cooperative spectrum sensing techniques have been proposed in literature. Fig. 2 shows the cooperative spectrum sensing scenario in a centralized CR networks. Basically, these techniques are classified into soft and hard cooperation techniques. In the soft

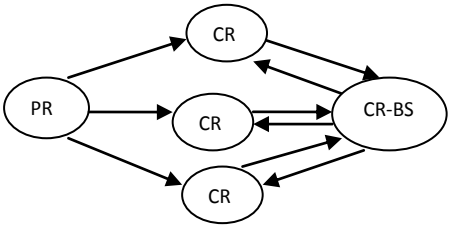

Figure 2. Classical cooperative spectrum sensing scenario in a centralized CR network.

technique, a number of CR users sense the PR's signal and then resend the real measurements to the main CR-BS that applies a specific fusion rule, and then declares the final decision. In hard cooperation, each CR's user decides about the PR's signal locally and independently from the other CRs, then a binary digit represents the state of the PR's signal in a specific band is sent to the CR-BS that applies a binary fusion rule to declare the final decision to the CR network.

An optimal linear soft cooperation algorithm has been proposed in [26], where the performance is optimized by linearly combining the individual CRs' local test statistics at the CR-BS. In [30], the authors propose an optimal soft cooperation algorithm based on the deflection coefficient maximization criterion. The cooperative spectrum sensing performance using likelihood ratio test (LRT)-soft combination has been evaluated in [31]. It is found that the LRT-soft cooperation outperforms AND-hard cooperation in term of performance.

An OR-hard cooperation algorithm has been proposed in [32], where the CR-BS declares that the PR's signal is present in the band under sensing when at least one CR user decides the signal is present.

The joint probability of detection, Q_d, and the joint probability of false alarm, Q_f, of the OR rule combining at the CR-BS using *G* CR nodes (sensors) with identical probabilities of detection and false alarm are given by:

$$Q_d = 1 - \prod_{g=1}^{G}(1 - P_{d,g}) \quad (53)$$

$$Q_f = 1 - \prod_{g=1}^{G}(1 - P_{f,g}) \quad (54)$$

where $P_{d,g}$, $P_{f,g}$ represent the probabilities of detection and false alarm achieved by the g^{th} CR node (sensor).

The multitaper singular value decomposition spectrum sensing technique (MTM-SVD) [2, 14], can be classified as soft cooperation with multi measurements from different tapers [7]. Our work in [25], ends the need for huge overhead feedback to the CR-BS in MTM-SVD by proposing the efficient multi antenna based spectrum sensing technique, the Local-MTM-SVD.

The work in [33] shows that, including the decision from CR user with a low SNR in the cooperation at the CR-BS degrades the probability of detection. Thus, the authors propose a fusion rule at the CR-BS that uses only the reliable decisions, which come from the CR users with a high SNR. The main drawbacks here are the requirements for SNR estimation, and in addition to sending decisions from different CR users to the CR-BS,

each CR has to send its own estimated SNR to the CR-BS. Different hard cooperation optimization algorithms have been proposed in [34-38]. The common objectives of these works are minimizing the number of binary bits sent to the CR-BS that would require wideband control channel, or by choosing the CRs with the reliable decisions to cooperate at the main station, while at the same time, keeping the probability of opportunity high.

Generally, implementing spectrum sensing at each CR in the cooperative CR network, decoding or amplifying the sensed signals and then sending the results to a main CR-BS, have the following main challenges:

1) The need for sensing units at each CR that will increase the hardware cost, the system complexity, the sensing delay and power consumption.
2) The need for sending the sensed information or decisions to a main CR-BS, which requires more signal processing at both sides, the CR's terminals and CR-BS.
3) The need for control channels and huge overhead feedback to send the sensed information from all CRs to the CR-BS. Additionally, algorithms for information sharing and coordination are required in such cases [39].
4) Additional information such as the SNRs at different CRs has to be sent to the main CR-BS in optimized cooperative sensing.
5) The availability of some CRs in the network with reliable decisions is not guaranteed at all time. Thus, cooperating the sensed information produces more errors.

In order to face such challenges, the CR system needs to minimize the spectrum sensing processing in the CR network and insure that the performance is kept high. Supporting the CR network with an ideal CR node can satisfy the two above conditions. Adding highly advanced hardware and software components to a single CR node in the CR network, and excluding the others CRs is a good solution. In this solution, the spectrum sensing using advanced high performance techniques such as those proposed in this paper is performed at this ideal CR, and the final decision can be sent to the main CR-BS. The hardware components here should allow the ideal CR node to sense different frequency bands at the same time. Prior information about the different PR's signals must be known at this ideal node in order to resolves multipath fading. Training sequences and pilot signals are examples of this information.

Fig. 3 shows the MN-cooperative spectrum sensing scenario in a centralized CR networks. The work in [40], proposes implementing spectrum sensing using devices that are separate from the CR network and can be provided by the CR's service provider. In addition to the PR's and CR's system, a separate sensing system appears in their work. Of course, that would increase the overall system complexity, require more technical and management coordination protocols and sensing devices cannot be used in the CR's cycle.

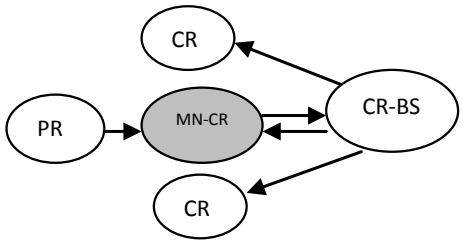

Figure 3. MN cooperative spectrum sensing scenario in a centralized CR network.

VI. Simulation Results

In our system, each node of the CR network uses 64-FFT with a sampling frequency 20 MHz. The PR user's transmitter uses 64-IFFT with symbol duration T_s =0.05μs, and transmits QPSK signal with normalized energy equal to 1 over each subcarrier. The CR nodes use the MTM and ED with *M*=1 antenna. The multi antenna techniques considered in this paper, MTM-SLC, MTM-LC, ED-SLC, ED-LC, and Local-MTM-SVD are examined with a different number of antennas *M*=2, and 4. In MTM techniques, the used half time bandwidth product is *NW*=4, and the number of tapers is *K*=5 [15]. In all cases of simulations, the results are averaged over 10^6 realizations. The channels considered in the simulation are AWGN with zero mean and variance σ_w^2, and Rayleigh flat fading. The performance is evaluated over a chosen frequency bin, when it is assumed that, the whole band under sensing is occupied by the PR's signal.

Fig. 4, and Fig. 5 show the probability of detection, P_d versus probability of false alarm, P_f using the different spectrum sensing techniques with a different number of antennas at AWGN with SNR=−10dB and 20 OFDM blocks (i.e., $L = 20$) used in sensing. Note that the number of samples used is $(L = 20) \times (N = 64) = 1280$, which approximately corresponds to the sensing time 64μs. Both figures show significant improvement in the performance using the proposed MTM with multi antenna techniques. Additionally, we can see how the Local-MTM-SVD technique has the same performance that is achieved by MTM-SLC in the same conditions. This suggests that MTM-SLC is more practical as it does not need the SVD process and gives the same performance with lower complexity. Using *M*=2 antennas, when $P_f = 10\%$, MTM-SLC, MTM-LC, ED-SLC, and ED-LC techniques have P_d =80, 95, 21, and 29% respectively. The MTM-LC outperforms MTM-SLC in terms of P_d by 5% for *M*=4 case, and by 14% for *M*=2 case, when $P_f = 10\%$ in the same conditions. ED techniques have a poorer performance compared to the others under the same conditions.

Fig. 6 shows the probability of detection, P_d versus probability of false alarm, P_f , using the different considered spectrum sensing techniques with number of antennas *M*=2 at Rayleigh flat fading with average SNR=−5dB and $L = 20$. It is clear that the MTM-LC and ED-LC' performances are affected by fading more than

that in MTM-SLC and ED-SLC. This is due to the destructive adding of the received signals from different antennas without co-phasing the channels coefficients. There is a significant outperforming of MTM against ED even in a fading environment, and the Local-MTM-SVD still has the same performance when using MTM-SLC in the same conditions. The probability of detection P_d's percentages when the false alarm is fixed to $P_f = 10\%$ using MTM-LC, MTM-SLC, ED-LC, ED-SLC, and Local-MTM-SVD are 77, 93, 62, 81, and 93 % respectively.

Fig. 7 shows the probabilities of detection, P_d that meet probability of false alarm, $P_f = 10\%$, versus the SNR at AWGN using MTM with single antenna, MTM-SLC, and MTM-LC with *M*=4 antennas, and $L = 50$ for spectrum sensing. We can see a noticeable improvement in the performance using both proposed techniques compared to MTM with single antenna. At SNR=−15dB, MTM-SLC outperforms MTM with single antenna in terms of probability of detection, P_d by 30%. On the other hand, MTM-LC outperforms MTM with single antenna by 66%. It can be seen from the figure that, our simulations match the theory.

Fig. 8 shows the comparison between the number of OFDM blocks, L required to achieve $P_d = 99\%$, and $P_f = 1\%$ at AWGN environment with different SNR using the different considered techniques with *M*=1, and 4 antennas. It is clear that the number of OFDM blocks used in the sensing process in the MTM system is lower than that for ED in all cases. Additionally, LC techniques require a lower number of OFDM blocks compared to SLC for both MTM, and ED cases in the same conditions. For example, from the figure at SNR=−15dB, the number of OFDM blocks *L* in dB that are required by ED only, ED-SLC, ED-LC, MTM only, MTM-SLC, and MTM-LC are 50, 42, 35, 32, 27, and 20 , or in *milli seconds* as 5, 0.792, 0.158, 0.08, 0.025, and 0.005 respectively. It is clear that the MTM-multi antenna based spectrum sensing techniques proposed in this paper, are faster than the others. For example, MTM-LC is faster than MTM only by 93.75% (i.e., faster by 0.075 *m seconds*), and ED-LC by 96.85%.

In OR-rule based cooperation, the resulted spectrum sensing decisions from the individual CR nodes are relayed to the main CR-BS, which applies the OR rule cooperation algorithm to declare the final decision to the CR network. Five CR nodes (i.e.,*G*=5) share the cooperation, with each supported by *M*=3 antennas. Fig. 9 shows the OR rule joint probability of detection, Q_d versus the joint probability of false alarm, Q_f for MTM-SLC, MTM-LC, ED-SLC, and ED-LC with *M*=3 antennas, and *G*=5 CR users at AWGN with SNR= − 12dB and *L*=20 OFDM blocks. At joint probability of false alarm, $Q_f = 10\%$, the joint probability of detection is $Q_d = 100\%$ using the MTM-LC, 92% using MTM-SLC, 45% using ED-LC, and 25% using ED-SLC.

The resulted probabilities of detection for MTM-SLC, MTM-LC, GLRD1 [22], and blind GLRD detector [22] using *M*=4 antennas at AWGN with SNR=−10dB when the false alarm is 1% and *L*=16, can be summarized as follow:

- Using MTM-SLC and MTM-LC gives a probability of detection 70, and 98% respectively.
- In the same conditions, the GLRD1 and the blind GLRD detectors have a probability of detection of 0%.

Therefore, our main conclusion here is that, the latter techniques can produce large harmful interference to PR users, or a very low probability of opportunity.

Additionally, the required SNRs in (dB) for MTM-SLC, MTM-LC, ED-SLC, ED-LC, GLRD1[22], and blind GLRD detector [22] to achieve a probability of detection of 99.99%, using *M*=4 antennas at AWGN when the false alarm is 1% and *L*=16 sensed samples, can be summarized as follow:

- The GLRD1 gives a probability of detection of 99.99% when the SNR=7.5 dB, and the blind GLRD, gives the same probability when the SNR =9.6 dB.
- The MTM-SLC and MTM-LC give the same probability of detection, when the SNR for them is −7.5, and −12dB respectively.

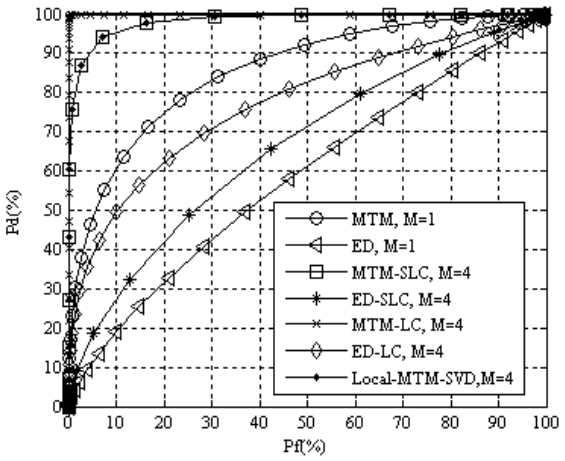

Figure 4. Probability of detection versus probability of false alarm using MTM and ED with *M*=1, and MTM-SLC, MTM-LC, ED-SLC, and ED-LC with *M*=4 antennas at AWGN with SNR=−10dB and $L = 20$.

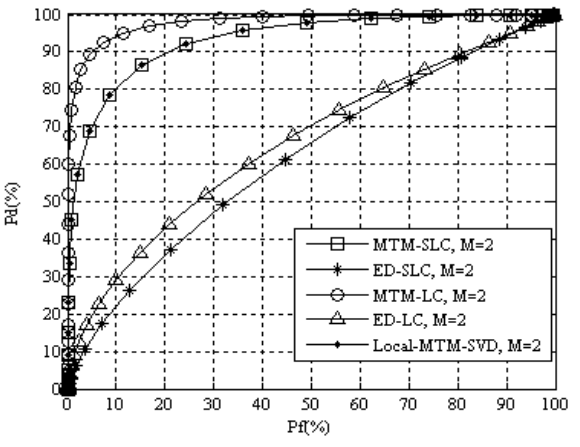

Figure 5. Probability of detection versus probability of false alarm using MTM-SLC, MTM-LC, ED-SLC, and ED-LC with number of antennas *M*=2, at AWGN with SNR=−10dB and $L = 20$.

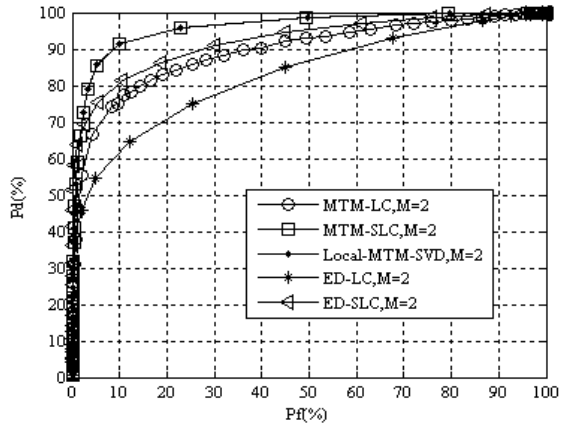

Figure 6. Probability of detection versus probability of false alarm using MTM-SLC, MTM-LC, ED-SLC, and ED-LC with M=2 antennas at Rayleigh flat fading with average SNR=−5dB and$L = 20$.

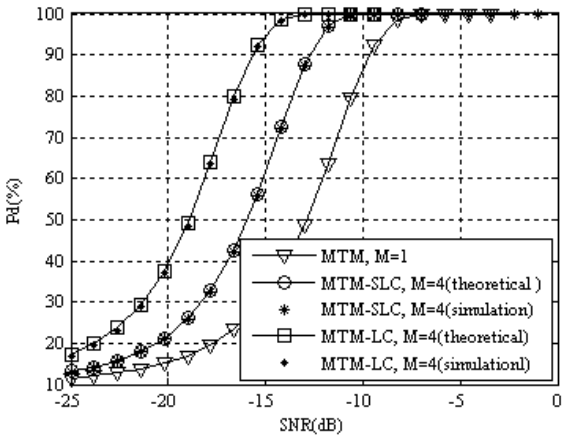

Figure 7. Probability of detection that meets $P_f = 10\%$ versus the SNR at AWGN using MTM, MTM-SLC, and MTM-LC spectrum sensing techniques with number of antennas M=4 and $L = 50$.

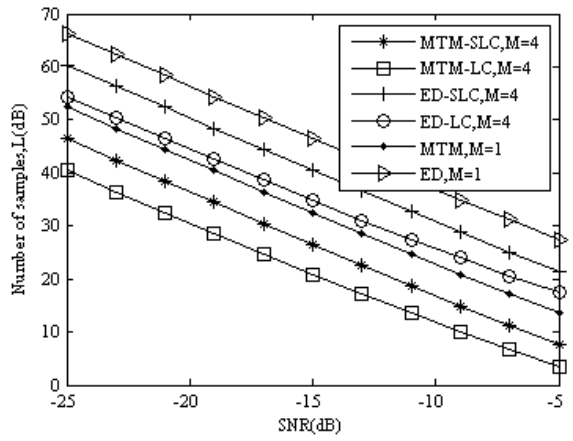

Figure 8. Numbers of samples (L) required to achieve $P_d = 99\%$, and $P_f = 1\%$ at AWGN with different SNR using MTM, MTM-SLC, MTM-LC, ED, ED-SLC, and ED-LC spectrum sensing techniques with number of antennas M=1, and 4.

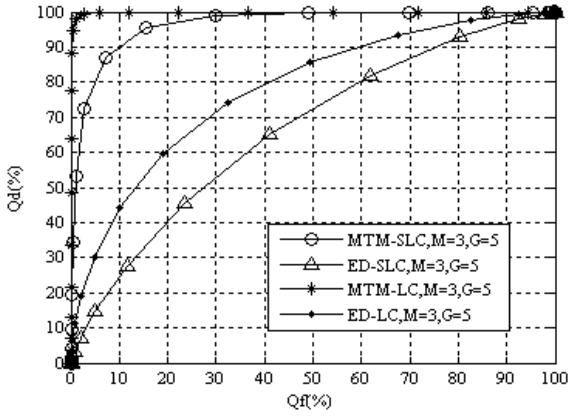

Figure 9. OR rule Joint Probability of detection versus joint probability of false alarm using MTM-SLC, MTM-LC, ED-SLC, and ED-LC spectrum sensing techniques with number of antennas M=3using 5 CR users (G=5) at AWGN with SNR=−12dB and L=20.

- The ED-SLC and ED-LC achieve the same probability of detection in the same conditions, when their SNRs are 5, and 0 dB respectively.

Thus, these techniques do not give a high performance unless the SNR is high, which is not practical in CR. It is clear that the MTM-LC has a 10dB SNR's gain compared to ED-LC, and 15dB compared to ED-SLC.

VII. Conclusion

In this paper, we propose different MTM-multi antenna based techniques as efficient CR spectrum sensing techniques. Theoretical work has been derived for the proposed techniques in AWGN, and multipath fading wireless environments. The ED-multi antenna based spectrum sensing techniques has been derived as well and compared to that of MTM, and the Local-MTM-SVD.

Using multi antenna in MTM-LC, and MTM-SLC gives more improvement in performance compared to that for ED-LC, ED-SLC. The Local-MTM-SVD spectrum sensing technique has the same performance when of MTM-SLC under the same conditions. Therefore, we can say that the MTM-SLC is more practical than Local-MTM-SVD as it does not need SVD processors, and that minimizes the complexity and the cost of the system. Moreover**,** based on our results, we found that the GLRD1 and the blind GLRD that are proposed in the literature, require SNRs=7.5 and 9.6 dB, respectively to achieve a probability of detection of 99.99% at false alarm 1% with AWGN using 4 antennas and 16 samples for sensing. In our proposed optimal and suboptimal techniques, the required SNRs are found as -12 and -7.5 dB, respectively to achieve the same probabilities in the same conditions.

In the multipath fading environment, adding the PR's signals received from different CR antennas might degrades the resulted combined signal destructively in MTM-LC, and ED-LC. Thus, such combining needs co-phasing to tolerate the multi path effects. However, we

believe that this is a main challenge in CR spectrum sensing and is still open issue. Blind equalization methods can be considered in such cases.

The proposed techniques represent local cooperation using multi antenna. These techniques can be added to one CR node to work as MN in the CR network. This is a practical solution to minimize the complexity of the CR network. The different hard and soft cooperation algorithms in the literature can be used here to improve the overall performance. The OR rule cooperation is used to cooperate the generated binary decisions from the individuals CR nodes at a main CR-BS. Then the final decision is declared to the CR nodes.

APPENDIX

The probabilities of detection and false alarm, $P_d^{MTM-SLC}(f_i)$, and $P_f^{MTM-SLC}(f_i)$ using MTM-SLC technique are defined as:

$$P_d^{MTM-SLC}(f_i) = Q\left(\frac{\gamma - L^{MTM-SLC}KM(E_s+\sigma_w^2)}{\sqrt{2LMC^2\lambda_\Sigma\sigma_w^2(\sigma_w^2+2E_s)}}\right) \quad (55)$$

$$P_f^{MTM-SLC}(f_i) = Q\left(\frac{\gamma - L^{MTM-SLC}KM\sigma_w^2}{\sqrt{2LMC^2\lambda_\Sigma\sigma_w^4}}\right) \quad (56)$$

In order to calculate the number of samples, $L^{MTM-SLC}$, which are required to achieve specific probabilities of detection and false alarm, the threshold, γ that used in both (55), and (56) are the same. Thus, after mathematical manipulation, the threshold form (55) can be defined as follows:

$$\gamma = Q^{-1}\left(P_d^{MTM-SLC}(f_i)\right)\sqrt{2LMC^2\lambda_\Sigma\sigma_w^2(\sigma_w^2+2E_s)} + LKM(E_s+\sigma_w^2) \quad (57)$$

using (56), the threshold can be defined as:

$$\gamma = Q^{-1}\left(P_f^{MTM-SLC}(f_i)\right)\sqrt{2LMC^2\lambda_\Sigma\sigma_w^4} + LKM\sigma_w^2 \quad (58)$$

Since the thresholds in (57) and (58) are equals, then $L^{MTM-SLC}$ can finally be defined as in (47). The same steps can be followed to derive the number of required samples, when MTM-LC, ED-SLC, and ED-LC are used for sensing.

REFERENCES

[1] J. Mitola and G. Q. Maguire, "Cognitive radio: making software radios more personal," *IEEE personal communications,* vol. 6, pp. 13-18, 1999.

[2] S. Haykin, "Cognitive radio: brain-empowered wireless communications," *IEEE journal on selected areas in communications,* vol. 23, pp. 201-220, 2005.

[3] C. Cordeiro, K. Challapali, D. Birru and N. Sai Shankar, "IEEE 802.22: the first worldwide wireless standard based on cognitive radios," in *New Frontiers in Dynamic Spectrum Access Networks, 2005. DySPAN 2005. 2005 First IEEE International Symposium on*, 2005, pp. 328-337.

[4] C. Stevenson, G. Chouinard, L. Zhongding, H. Wendong, S. Shellhammer and W. Caldwell, "IEEE 802.22: The first cognitive radio wireless regional area network standard," *Communications Magazine, IEEE,* vol. 47, pp. 130-138, 2009.

[5] I. F. Akyildiz, W. Y. Lee, M. C. Vuran and S. Mohanty, "NeXt generation/dynamic spectrum access/cognitive radio wireless networks: a survey," *Computer Networks,* vol. 50, pp. 2127-2159, 2006.

[6] T. Yucek and H. Arslan, "A survey of spectrum sensing algorithms for cognitive radio applications," *Communications Surveys & Tutorials, IEEE,* vol. 11, pp. 116-130, 2009.

[7] M. Jun, G. Y. Li and J. Biing Hwang, "Signal Processing in Cognitive Radio," *Proceedings of the IEEE,* vol. 97, pp. 805-823, 2009.

[8] Y. Zeng, Y. C. Liang, A. T. Hoang and R. Zhang, "A review on spectrum sensing for cognitive radio: challenges and solutions," *EURASIP Journal on Advances in Signal Processing,* vol. 2010, p. 2.

[9] D. B. Percival and A. T. Walden, *Spectral analysis for physical applications: multitaper and conventional univariate techniques*: Cambridge Univ Pr, 1993.

[10] D. J. Thomson, "Spectrum estimation and harmonic analysis," *Proceedings of the IEEE,* vol. 70, pp. 1055-1096, 1982.

[11] D. Slepian, "Prolate spheroidal wave functions, Fourier analysis, and uncertainty. V- The discrete case," *Bell System Technical Journal,* vol. 57, pp. 1371–1430, 1978.

[12] P. Stoica and T. Sundin, "On nonparametric spectral estimation," *Circuits, Systems, and Signal Processing,* vol. 18, pp. 169-181, 1999.

[13] D. J. Thomson, "Jackknifing multitaper spectrum estimates," *IEEE Signal Processing Magazine,* vol. 24, pp. 20-30, 2007.

[14] S. Haykin, D. J. Thomson and J. H. Reed, "Spectrum Sensing for Cognitive Radio," *Proceedings of the IEEE,* vol. 97, pp. 849-877, 2009.

[15] O. A. Alghamdi, M. A. Abu-Rgheff and M. Z. Ahmed, "MTM Parameters Optimization for 64-FFT Cognitive Radio Spectrum Sensing using Monte Carlo Simulation," in *EMERGING 2010 : The Second International Conference on Emerging Network Intelligence*, Florence-Italy, 2010, pp. 107-113.

[16] O. A. Alghamdi, M. Z. Ahmed and M. A. Abu-Rgheff, "Probabilities of Detection and False Alarm in Multitaper Based Spectrum Sensing for Cognitive Radio Systems in AWGN," presented at the The IEEE International Conference on Communication Systems (IEEE ICCS 2010), Singapore, 2010.

[17] A. Goldsmith, *Wireless communications*: Cambridge Univ Pr, 2005.

[18] A. Pandharipande and J. P. M. G. Linnartz, "Performance Analysis of Primary User Detection in a Multiple Antenna Cognitive Radio," in *Communications, 2007. ICC '07. IEEE International Conference on*, 2007, pp. 6482-6486.

[19] L. Jong-Hwan, B. Jun-Ho and H. Seung-Hoon, "Collaborative Spectrum Sensing using Energy Detector in Multiple Antenna System," in *Advanced Communication Technology, 2008. ICACT 2008. 10th International Conference on*, 2008, pp. 427-430.

[20] V. Kuppusamy and R. Mahapatra, "Primary user detection in OFDM based MIMO Cognitive Radio," in *Cognitive Radio Oriented Wireless Networks and Communications, 2008. CrownCom 2008. 3rd International Conference on*, 2008, pp. 1-5.

[21] M. Wei, W. Mu Qing, L. Dong and W. Meng Ling, "User sensing based on MIMO cognitive radio sensor networks," in *Computer Science and Information Technology, 2009. ICCSIT 2009. 2nd IEEE International Conference on*, 2009, pp. 205-208.

[22] A. Taherpour, M. Nasiri-Kenari and S. Gazor, "Multiple antenna spectrum sensing in cognitive radios," *Wireless Communications, IEEE Transactions on,* vol. 9, pp. 814-823, 2010.

[23] Z. Rui, L. Teng, L. Ying-Chang and Z. Yonghong, "Multi-antenna based spectrum sensing for cognitive radios: A GLRT approach," *Communications, IEEE Transactions on,* vol. 58, pp. 84-88, 2010.

[24] W. Pu, F. Jun, H. Ning and L. Hongbin, "Multiantenna-Assisted Spectrum Sensing for Cognitive Radio," *Vehicular Technology, IEEE Transactions on,* vol. 59, pp. 1791-1800, 2010.

[25] O. A. Alghamdi and M. A. Abu-Rgheff, "Local MTM-SVD based spectrum sensing in SIMO OFDM cognitive radio under bandwidth constraint," in *Cognitive Radio Oriented Wireless Networks & Communications (CROWNCOM), 2010 Proceedings of the Fifth International Conference on*, 2010, pp. 1-6.

[26] Q. Zhi, C. Shuguang and A. H. Sayed, "Optimal Linear Cooperation for Spectrum Sensing in Cognitive Radio Networks,"

Selected Topics in Signal Processing, IEEE Journal of, vol. 2, pp. 28-40, 2008.
[27] F. Sheikh, S. Masud and B. Bing, "Harmonic power detection in wideband cognitive radios," *Signal Processing, IET,* vol. 3, pp. 40-50, 2009.
[28] Q. Zhi, C. Shuguang, A. H. Sayed and H. V. Poor, "Optimal Multiband Joint Detection for Spectrum Sensing in Cognitive Radio Networks," *Signal Processing, IEEE Transactions on,* vol. 57, pp. 1128-1140, 2009.
[29] T. Lang and S. Perreau, "Multichannel blind identification: from subspace to maximum likelihood methods," *Proceedings of the IEEE,* vol. 86, pp. 1951-1968, 1998.
[30] B. Shen, S. Ullah and K. Kwak, "Deflection coefficient maximization criterion based optimal cooperative spectrum sensing," *AEU - International Journal of Electronics and Communications,* vol. 64, pp. 819-827, 2009.
[31] E. Visotsky, S. Kuffner and R. Peterson, "On collaborative detection of TV transmissions in support of dynamic spectrum sharing," in *New Frontiers in Dynamic Spectrum Access Networks, 2005. DySPAN 2005. 2005 First IEEE International Symposium on*, 2005, pp. 338-345.
[32] A. Ghasemi and E. S. Sousa, "Collaborative spectrum sensing for opportunistic access in fading environments," in *New Frontiers in Dynamic Spectrum Access Networks, 2005. DySPAN 2005. 2005 First IEEE International Symposium on*, 2005, pp. 131-136.
[33] Y. Zheng, X. Xie and L. Yang, "Cooperative Spectrum Sensing Based on SNR Comparison in Fusion Center for Cognitive Radio," 2009, pp. 212-216.
[34] Z. Wei, R. K. Mallik and K. Ben Letaief, "Cooperative Spectrum Sensing Optimization in Cognitive Radio Networks," in *Communications, 2008. ICC '08. IEEE International Conference on*, 2008, pp. 3411-3415.
[35] L. Wang, "Novel scheme for cooperation spectrum sensing in cognitive radio networks," in *Computer and Automation Engineering (ICCAE), 2010 The 2nd International Conference on*, 2010, pp. 371-375.
[36] A. Jamshidi, "Performance analysis of low average reporting bits cognitive radio schemes in bandwidth constraint control channels," *Communications, IET,* vol. 3, pp. 1544-1556, 2009.
[37] S. Chunhua, Z. Wei and K. B. Letaief, "Cooperative Spectrum Sensing for Cognitive Radios under Bandwidth Constraints," in *Wireless Communications and Networking Conference, 2007.WCNC 2007. IEEE*, 2007, pp. 1-5.
[38] S. Chunhua, Z. Wei and K. Ben, "Cluster-Based Cooperative Spectrum Sensing in Cognitive Radio Systems," in *Communications, 2007. ICC '07. IEEE International Conference on*, 2007, pp. 2511-2515.
[39] S. Hussain and X. Fernando, "Spectrum sensing in cognitive radio networks: Up-to-date techniques and future challenges," in *Science and Technology for Humanity (TIC-STH), 2009 IEEE Toronto International Conference*, 2009, pp. 736-741.
[40] H. Zhu, F. Rongfei and J. Hai, "Replacement of spectrum sensing in cognitive radio," *Wireless Communications, IEEE Transactions on,* vol. 8, pp. 2819-2826, 2009.

Owayed A. Alghamdi received the B.Sc. and M.Sc. degrees in Electrical Engineering with communications major from King Saud University, Riyadh, Saudi Arabia, in 2000 and 2007. Since 2001, he has worked with the Ministry of Interior (MOI) of Saudi Arabia as a telecommunication engineer, where he has gained theoretical and practical experience in different kinds of telecommunications.

Currently, he is a Ph.D. candidate in the Department of Electrical and Computer Engineering at University of Plymouth, Plymouth, UK. His research interests include statistical signal processing, detection and estimation theories, wireless communications and networking, cognitive radio, and cooperative communications.

Mohammed Zaki Ahmed graduated with a Master of Engineering (Information Engineering) and a Bachelor of Engineering (Communication Engineering) from the University of Plymouth, getting both degrees in 1999. He completed his PhD at the University of Plymouth(2003) and has been employed as a lecturer there since 2001.

He is currently an Associate Professor in the School of Computing and Mathematics. His current research includes error correction and signal processing as applied to communication, storage and wireless networks.

Block Diagonal Precoding Based Power Allocation for Coordinated Multi-Point Transmission

Jing Han
Broadband Wireless Communications and Multimedia Laboratory, Key Laboratory of Embedded System and Service Computing supported by Ministry of Education, Tongji University, Shanghai, China

Ping Wang[1,2], Fuqiang Liu[1], Yin Zhu[1]
[1]Broadband Wireless Communications and Multimedia Laboratory, Key Laboratory of Embedded System and Service Computing supported by Ministry of Education, Tongji University, Shanghai, China
[2] Shanghai Key Laboratory of Digital Media Processing and Transmission, Shanghai, China
Email: pwang@tongji.edu.cn

***Abstract*—This paper studies power allocation in coordinated multi-point (CoMP) transmission of 3GPP LTE-Advanced system with remote radio units(RRUs) power constraints. We apply block diagonal (BD) precoding to downlink transmission, and assume perfect knowledge of downlink channels and transmit messages at each transmit point. We propose a modified water-filling power (MWF) allocation algorithm in order to maximize the downlink sum capacity, at the same time the low complexity is achieved. The interior-point method is also used to solve the optimization problem. Simulations show that interior-point method converges after only a few iterative steps and the system capacity is near-optimal. As for complexity and power efficiency, MWF achieves a good compromise.**

***Index Terms*—CoMP, MU-MIMO, power allocation, optimization problem**

I. INTRODUCTION

In conventional cellular networks, intra-cell interference can be eliminated by Orthogonal Frequency Division Multiple Access (OFDMA). However, co-channel interference of adjacent cells is still a main factor to impact the system performance, especially for cell-edge user throughput. In order to meet the requirements of higher cell-edge throughput and spectrum efficiency of next generation broadband wireless communication system, 3GPP LTE-Advanced proposed a multi-cell MIMO technology named coordinated multiple point (CoMP) transmission and reception on August, 2008.

According to 3GPP [1], CoMP is mainly characterized into two categories: Joint Processing (JP) and Coordinated Scheduling/Beamforming (CS/CB). In JP, data intended for a particular UE is jointly processed and transmitted instantaneously from all the coordinated points, while in CS/CB data is only transmitted from the serving cell. Although CoMP naturally increases system complexity, it yields great capacity improvement and coverage benefits [2-3]. With these CoMP schemes, especially for CoMP JP, efficient power allocation schemes need to be designed to support joint radio resource management among coordinated cells. This is because the CoMP-JP transmission scheme is more likely to be an expansion of the traditional single cell MIMO transmission scheme, in which the system performance is largely influenced by power allocation. However, although there are plenty of literatures that consider power allocation scheme for cooperative multi-cell networks, to the author's best knowledge, relative study on CoMP system is few.

Reference [4-6] studied the power allocation scheme in CoMP system. Reference [4] considered the power allocation problem with carrier aggregation (CA). Reference [5] proposed an iterative algorithm of joint antenna selection and power allocation with the purpose of maximizing the sum rate of coordinated users. Reference [6] proposed a BS scheduling scheme based on threshold judgment and an iterative power allocation approach using NE theory. However, some system models of the literatures mentioned above are not practical. Reference [7] formulated the cooperative multi-cell power allocation as a network utility maximization problem and proposed an iterative algorithm that converges to the global optimum. Reference [8-9] studied the power allocation scheme based on zero-forcing precoding. All these algorithms are based on per-antenna power constraint. But, in our paper, we study the power allocation problem with per-RRU power constraint which fits the situation of CoMP.

In LTE system, eNodeB is composed of a base band unit (BBU) and several remote units (RRUs), each of which covers a cell. In 3GPP RAN1 #59bis meeting on January, 2010, an agreement was reached that CoMP techniques would only be applied in intra-eNodeB

Manuscript received January 30, 2011; revised April 25, 2011; accepted June 14, 2011.
Corresponding author: Ping Wang, e-mail: pwang@tongji.edu.cn

doi:10.4304/jcm.6.7.524-528

scenario for Rel-10 [10]. A block diagram of the system is shown in Fig.1.

In the paper, we will focus on power allocation in MU-CoMP-JP system with per-RRU power constraint. We adopt BD precoding transmission scheme, because we think it is a scheme with the greatest potential due to the fact that it has been used in most CoMP-related proposals

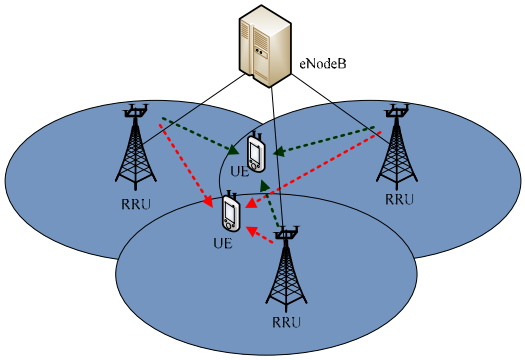

Fig.1 Network Topology of CoMP JP

submitted to 3GPP RAN1. In the paper, we first propose a MWF algorithm. The core is to find the range of height of the water surface by using a simple and efficient iterative algorithm in order to satisfy the RRU power constraint. We then study the power allocation problem from the mathematical aspect of view, and use the barrier method to find a near-optimal solution.

The rest of the paper is organized as follows. In section II, the system model of coordinated multi-point transmission with BD precoding and problem formulation will be described in detail. In section III, we propose the modified water-filling power allocation algorithm, and then present optimization solution algorithm by using interior-point methods. Simulation results are shown in Section IV. The conclusion follows in section V.

II. System Model and Problem Formulation

A. Network Architecture

We consider an intra-eNodeB CoMP system consisting of M RRUs with N users (UE) served. Each RRU and UE are equipped with n_T and n_R antennas, respectively. Since the system is using BD precoding, the number of antennas should meet the conditions $M \times n_T \geq N \times n_R$. We use $\mathbf{H}_k \in \mathbb{C}^{n_R \times (M \cdot n_T)}$ to represent the downlink channel from all the M cooperative RRUs to the k th user. Let $\mathbf{H} = \left[\mathbf{H}_1^T, \mathbf{H}_2^T, \cdots, \mathbf{H}_N^T\right]^T$ denote the channel of all users. The elements of $\mathbf{H}$ are assumed to be independent zero mean complex Gaussian random variables with unit variance. Thus, matrix $\mathbf{H}$ is full rank, which means each user has n_R independent spatial substreams of data. The received signal of the k th user can be denoted as

$$\mathbf{y}_k = \mathbf{H}_k \mathbf{U}_k \mathbf{s}_k + \sum_{i=1, i \neq k}^{N} \mathbf{H}_k \mathbf{U}_i \mathbf{s}_i + \mathbf{n}_k \ . \quad (1)$$

where $\mathbf{s}_k \in \mathbb{C}^{(M \cdot n_T) \times 1}$ indicates the transmitted symbols for the k th user. $\mathbf{n}_k \in \mathbb{C}^{N_R \times 1}$ is additive white complex Gaussian noise vector, normalized so that its covariance matrix is the identity matrix. $\tilde{\mathbf{H}}_k = \left[\mathbf{H}_1^T, \cdots, \mathbf{H}_{k-1}^T, \mathbf{H}_{k+1}^T, \cdots \mathbf{H}_N^T\right]^T$ represents all the users' channel expect the k th user. $\mathbf{U}_k$ is BD precoding matrix, which should satisfy $\tilde{\mathbf{H}}_k \mathbf{U}_k = \mathbf{0}$. Since $\tilde{\mathbf{H}}_k$ is assumed to be a full rank matrix, we have $rank(\tilde{\mathbf{H}}_k) = \min(n_R(N\text{-}1), n_T M) = n_R(N\text{-}1)$. We perform singular value decomposition (SVD) on $\tilde{\mathbf{H}}_k$.

$$\tilde{\mathbf{H}}_k = \tilde{\mathbf{U}}_k \tilde{\Sigma}_k \left[\tilde{\mathbf{V}}_k^{(1)}, \tilde{\mathbf{V}}_k^{(0)}\right]^* \quad (2)$$

where $\tilde{\mathbf{V}}_k^{(0)}$ holds the last $(n_T M - n_R(N\text{-}1))$ right singular vectors, which forms an orthogonal basis for the null space of $\tilde{\mathbf{H}}_k$. Thus, we have $\tilde{\mathbf{H}}_k \tilde{\mathbf{V}}_k^{(0)} = \mathbf{0}$, which means inter-user interference has been eliminated. We then perform SVD on $\mathbf{H}_k \tilde{\mathbf{V}}_k^{(0)}$ in order to decompose the channel into independent parallel sub-channels.

$$\mathbf{H}_k \tilde{\mathbf{V}}_k^{(0)} = \mathbf{U}_k \Sigma_k \left[\mathbf{V}_k^{(1)}, \mathbf{V}_k^{(0)}\right]^* \quad (3)$$

where Σ_k is a $n_R \times n_R$ diagonal matrix, whose element $\lambda_{kj}^{1/2} (j = 1, \cdots n_R)$ is the singular values of parallel sub-channels. $\mathbf{V}_k^{(1)}$ holds the n_R singular vectors with non-zero singular values. Thus, $\mathbf{U}_k = \mathbf{W}_k \mathbf{\Lambda}^{1/2}$ $= \tilde{\mathbf{V}}_k^{(0)} \mathbf{V}_k^{(1)} \mathbf{\Lambda}^{1/2}$, where $\mathbf{\Lambda} = diag(P_{k1}, P_{k2}, \cdots P_{kj}, \cdots, P_{kn_R})$ indicates the power allocated on the k th user's j th substream. The equivalent channel of user k now can be written as $\mathbf{H}_k \tilde{\mathbf{V}}_k^{(0)} \mathbf{V}_k^{(1)}$ consisting of n_R independent sub-channels, each of which has a gain of $\lambda_{kj}^{1/2} (j = 1, \ldots, n_R)$.

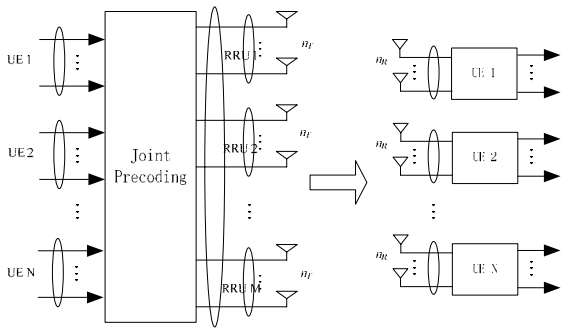

Fig.2 System Structure of Downlink CoMP-JP

B. Problem Formulation

BD precoding enables the system to transmit multiple data streams to each user while removing the inter-user interference. The whole system channel can now be seen as $N \times n_R$ independent parallel sub-channels. The rate of the j th sub-channel of the k th user is given by

$$R_{kj} = \log_2(1+\lambda_{kj}P_{kj}). \quad (4)$$

Define w_{kj}^{il} as an element of $\mathbf{W}_k$ representing a mapping relation between P_{kj} and the transmit power of the i th RRU's l th antenna. The total transmitting power of the i th RRU can be written as

$$P_{RRU_i} = \sum_{k=1}^{N}\sum_{j=1}^{n_R}\sum_{l=1}^{n_T}\left|w_{kj}^{il}\right|^2 P_{kj} \quad (\forall i = 1,\cdots M). \quad (5)$$

Let $P_{MAX\_PER\_RRU}$ be the power constraint of each RRU. Therefore, our optimization problem to maximize the sum rate with per-RRU power constraint can be formulated as

$$\text{(OP1)} \ \max_{P_{kj}} \sum_{k=1}^{N}\sum_{j=1}^{n_R}\log_2(1+\lambda_{kj}P_{kj}).$$

s.t.

$$\text{c1}: P_{kj} \ge 0 \quad (\forall k = 1,\cdots,N \quad \forall j = 1,\cdots,n_R)$$

$$\text{c2}: P_{RRU_i} \le P_{MAX\_PER\_RRU} \quad (\forall i = 1,\cdots M)$$

It is easy to notice that the objective function and constraints are all convex over the solution set. Thus, it is a convex optimization problem [11].

III. Power Allocation Algorithms

A. Modified Water-filling Power Allocation Algorithm (MWF)

Since the entire system has been decomposed into $N \times n_R$ independent sub-channels, one way of solving the optimal power allocation problem is using the conventional water-filling strategy. If P is the total volume of water filled into a vessel, the depth of water at each sub-channel is the power allocated to it, and $1/\lambda_{kj}$ traces out the bottom of the vessel [12].

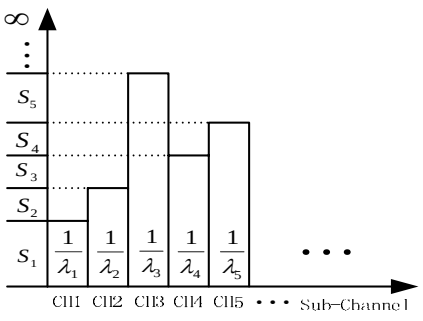

Fig.3 Intervals Divided by the Bottom of the Vessel

Here, we can not use the water-filling strategy directly because of the per-RRU power constraint. Let's define $\mu \in [0,+\infty)$ as the height of the water surface. The bottom of the vessel naturally divides $[0,+\infty)$ into $N \times n_R$ left-closed right-open intervals denoted by $S_1, S_2, \cdots, S_{N\times n_R}$ as shown in Fig.3. In MWF, we firstly determine which interval μ is in by using a simple iterative algorithm. Then we obtain μ by analyzing a set of linear functions. Our iterative algorithm works as follows.

Initialize $\alpha = N \times n_R + 1$.

Repeat

$\alpha = \alpha - 1, P = \min(S_\alpha)$.

Use water-filling algorithm to allocate power among sub-channels, and update P_{kj}.

Calculate P_{RRU_i} according to (5).

Until $P_{RRU_i} \le P_{MAX\_PER\_RRU} \quad (\forall i = 1,\cdots M)$.

Thus, we know $\mu \in S_\alpha$. And we can determine the value of P_{kj} according to (6).

$$P_{kj} = \begin{cases} \mu - 1/\lambda_{kj} & when\ \mu \ge 1/\lambda_{kj} \\ 0 & when\ \mu < 1/\lambda_{kj} \end{cases} \quad (6)$$

From (5) and (6), P_{RRU_i} can be written as a function of μ. That is to say, we now have M linear functions of one variable, each of which can be expressed as $P_{BS_i} = a_i\mu + b_i$ (a_i and b_i are coefficients). For each $P_{RRU_i} = P_{MAX\_PER\_RRU}$ $(\forall i = 1,\cdots M)$, we can get a corresponding μ_i. The water surface μ equals $\min(\mu_i)$. Finally, we calculate P_{kj} according to (6).

B. Interior-point Methods

Considering (OP1) is a convex optimization problem, we solve the problem by a particular interior-point algorithm, the barrier method. The main idea of the method is to approximately formulate the inequality constrained problem as an unconstrained problem by an indicator function. We construct the indicator function as

$$B(P_{kj}) = \sum_{k=1}^{N}\sum_{j=1}^{n_R}\ln(P_{kj}) + \sum_{i=1}^{M}\ln(P_{MAX\_PER\_RRU} - \sum_{k=1}^{N}\sum_{j=1}^{n_R}\sum_{l=1}^{n_T}\left|w_{kj}^{il}\right|^2 P_{kj}) \quad (7)$$

Hence, the barrier function is defined as:

$$G(P_{kj}, r) = -\sum_{k=1}^{N}\sum_{j=1}^{n_R}\log_2(1+\frac{\lambda_{kj}P_{kj}}{\sigma^2}) - rB(P_{kj}). \quad (8)$$

Since $r \in \mathbb{R}^+$ is very small, $G(P_{kj}, r)$ is an approximation of the original objective function. As r decreases, the approximation becomes more accurate. Also, when P_{kj} tends to the boundary of the feasible set S, $G(P_{kj}, r)$ increases to ∞. Thus, $B(P_{kj})$ builds a barrier at the boundary of S. (OP1) can now be simplified to the following equivalent problem (OP2) which can be easily solved.

$$\text{(OP2)} \quad \min G(P_{kj}, r)$$
$$\text{s.t.} \quad P_{kj} \in \operatorname{int} S$$

Let P_{kj}^* indicate the optimal solution. The barrier method can be described as follows.

Initialize $\widetilde{P_{kj}}$, r, coefficient $\beta \in (0,1)$, tolerance $\varepsilon > 0$.
Repeat
  Calculate P_{kj}^* by minimizing (9), starting at $\widetilde{P_{kj}}$.
  if $\left| rB(P_{kj}^*) \right| < \varepsilon$
    Break; We find the optimal solution.
  else
    Update $\widetilde{P_{kj}} = P_{kj}^*$ and $r = \beta r$;
  end

IV. Simulation Results

In this section, we perform computer simulations to evaluate the performance of the proposed intra-eNodeB power allocation algorithms and to compare it with other traditional method. We consider one single eNodeB with 3 RRUs. There are 2 users served at the same time. Each RRU has 4 antennas, and each user is equipped with 2 antennas. The channel $\mathbf{H}$ is assumed to be quasi-static flat Rayleigh fading and Rice fading with Rice factor equal to 10. Also, ideal channel estimation is used.

In the simulation, we compare MWF and interior-point methods with equal power allocation strategy. The initial values of parameters of interior-point algorithm are set as $\gamma = 1$, $\beta = 1/3$ and $\varepsilon = 10^{-3}$. We implement the algorithms under different power constraints of RRU.

It is shown in Fig.4 and Fig. 5 that CoMP has a gain over the traditional single cell MU-MIMO transmission scheme. This is because in CoMP-JP strategy there are more transmit antennas and the inter-cell interference is eliminated. The sum rate of 2 users of barrier method outperforms those of the other two algorithms under various RRU power constraints, since the barrier method approaches to the optimal solution on every iterative step. Besides, MWF has more obvious rate gain than equal power allocation when the power constraint of RRU is small, which is consistent with the property of traditional water-filling algorithm.

As for power efficiency, Fig.6 plots the data rate per watt. We can see that MWF has the highest power efficiency while the performance of the barrier method is relatively poor. That means in order to obtain the same data rate, the barrier method may require more transmit power.

Besides, the iterative number of MWF is related to the number of sub-channels, which is very small in practical system. However, the iterative number of barrier method is always kept in about 12 times in our simulation. Thus, we can see that MWF has much lower complexity and higher efficiency.

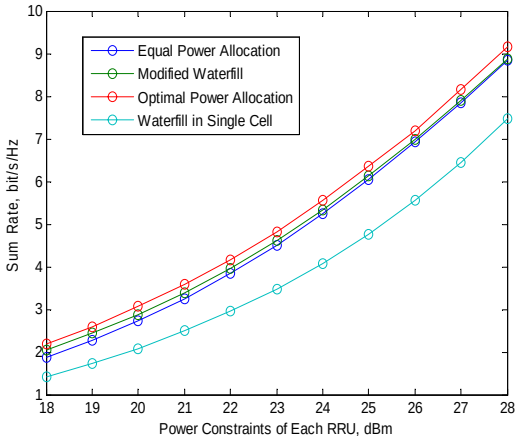

Fig.4 Sum Rate of the 2 users under Different Power Constraints, Rayleigh Fading

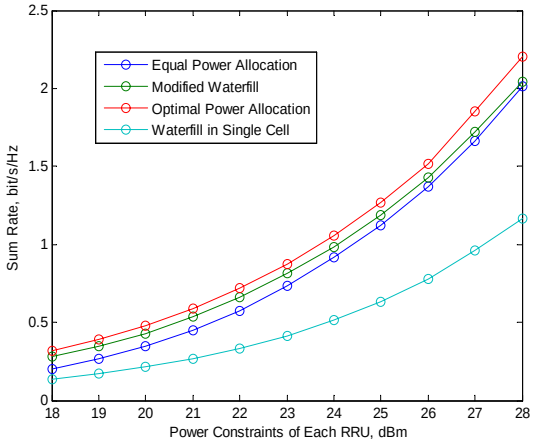

Fig. 5 Sum Rate of the 2 users under Different Power Constraints, Rice Fading

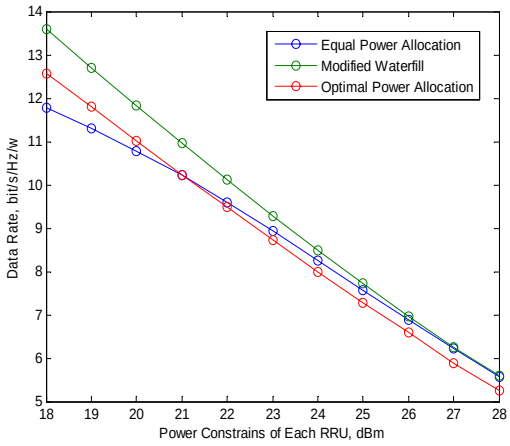

Fig.6 Bit Rate per Watt

V. CONCLUION

In this paper, we formulate the optimal power allocation problem with per-RRU power constraint in multi-user CoMP-JP network to achieve the maximal sum rate of the system. We first propose a MWF algorithm. The algorithm roughly determines the range of μ, before obtaining the sub-optimal solution through solving a set of equations. Since the power allocation problem is convex optimization, we then use barrier method to obtain the optimal solution. We construct the barrier function to transform the original equality constrained problem to an unconstrained problem which can be easily solved. Simulation results show that the barrier method can get the near-optimal sum data rate, while using relatively more transmit power. Considering the algorithm complexity and power efficiency, MWF is a good compromise alternative.

ACKNOWLEDGEMENT

This work was supported by the National Science and Technology Major Project of China under Grant 2011ZX03003-001, Sino-Finland International Cooperation Project under Grant 2010DFB10410, National Natural Science Foundation of China under Grant 61103179 and the Opening Project of Shanghai Key Laboratory of Digital Media Processing and Transmission under grant 2010KF04.

REFERENCES

[1] R1-092199, "Final Report of 3GPP TSG RAN WG1 #56bis v2.0.0", March, 2009.
[2] R1-100936, "CoMP JT in FDD downlink", Alcatel-Lucent Shanghai Bell, Alcatel-Lucent, RAN1#60, February, 2010.
[3] R1-101069, "Evaluation of DL CoMP for High Load and Low Load Scenarios", Huawei, RAN1#60, February, 2010.
[4] Wang Xiaoyong, Xiao Dengkun, Jing Xiaojun, "A Norvel Power Allocation Algorithm under CoMP with CA", 2nd IEEE International Conference on Broadband Network & Multimedia Technology (IC-BNMT), 2009, pp.66-70.
[5] Ji Qing, Xiaohui Li, Nai'an Liu, Yongqiang Hei and Guanghui Yu, "A Joint Antenna Selection and Power Allocation Algorithm for CoMP Systems", IEEE 24th International Conference on Advanced Information Networking and Applications Workshops, 2010, pp. 169-172.
[6] Yadong Liu, Gang Wu, Shu Fang, Xianxue Fan, "BS Scheduling and Iterative Power Allocation for the Multi-Cell Downlink MIMO Systems", 7th International Conference on Information, Communications and Signal Processing (ICICS), 2009.
[7] Yosia Hadisusanto, Lars Thiele, Volker Jungnickel, "Distributed Base Station Cooperation via Block-Diagonalization and Dual-Decomposition", IEEE Global Telecommunications Conference (GLOBECOM), 2008, pp.1-5.
[8] Yachen Wang, Jingsai Jiang, Yanhong Fan, Ye Li, "Coordinated Transmission with Block Diagonalization in MIMO Broadcast", 6th International Conference on Wireless Communications Networking and Mobile Computing (WiCOM), 2010.
[9] Niu Yanping, Tang Hong, Tang Lun, "Zero-forcing based coordinated multi-point transmission system and power allocation", Application Research of Computers, 27(5), 2010, pp.1918-1920.
[10] "Draft Report of 3GPP TSG RAN WG1 #59bis v0.1.0", January, 2010.
[11] Stephen Boyd and Lieven Vandenberghe, Convex Optimization, Cambridge University Press, 2004.
[12] David Tse and Pramod Viswanath, Fundamentals of Wireless Communication, Cambridge University Press, 2005.
[13] Quentin H. Spencer, A. Lee Swindlehurst, Martin Haardt, "Zero-Forcing Mehtods for Downlink Spatial Multiplexing in Multi-User MIMO Channels", IEEE Transactions on Signal Processing, 52(2), 2004, pp. 461-471.

Jing Han was born in Shanghai, China 1987. She received the BS Degree in communication engineering (2009) from Tongji University. Currently, she is a graduate student at Broadband Wireless Communications and Multimedia Laboratory in Tongji University. She has published 3 papers. Her research interest is resource allocation in wireless communication systems.

Ping Wang was born in China, 1978-2-28. He graduated from the department of computer science and engineering at Shanghai Jiaotong University, China and received Ph. D. degree in 2007. His major field of study is wireless communication. He joined the college of electronic and information engineering at Tongji University in 2007 and now is a lecturer. His current and previous interests include routing algorithms and resource management in wireless networks, vehicular ad hoc network and video transcoding.

Fuqiang Liu was born in China, 1963-3-7. He graduated from the department of automation at China University of Mining and received Ph. D. degree in 1996. His major field of study is signal processing. Now he is a professor in the department of information and communication engineering at Tongji University. His main research interests are in routing algorithms in wireless broadband access and image manipulation.

Yin Zhu was born in China, 1974. She received MS degree in Communication and Information system from Soochow University in 2003 and is a lecturer of University of Science and Technology of Suzhou. Now she is a Ph.D. candidate of Tongji University with research area in next generation broadcast wireless communication.

An Efficient Approach to Select Cluster Head in Wireless Sensor Networks

Bijan Kumar Debroy, Muhammad Sheikh Sadi, Md. Al Imran
Department of Computer Science & Engineering, Khulna University of Engineering & Technology, Khulna, Bangladesh
bjnroy@gmail.com, sheikhsadi@gmail.com, alimran13@gmail.com

***Abstract*—Enhancing lifetime of sensor nodes should be considered as the key design objective in Wireless Sensor Networks (WSN). A sensor node can only be equipped with a limited energy supply and it loses its energy during data communication. In some application scenarios, replenishment of energy resources might be impossible since the sensor nodes are distributed in remote environment. Hence, the nodes lose their energy quickly and become dead. The frequent topology changes due to the die of sensors make the network quite unstable. A good cluster head selection protocol is, therefore, required to enhance system lifetime and data communication. This paper proposes a new methodology for cluster head selection based on sensor nodes' energy per unit cost. Experimental study shows that the proposed method, by adopting few selection criteria on choosing cluster head, increases the system lifetime and maximize data communication in comparison to existing dominant approaches.**

***Index Terms*—Cluster Head Selection, Enhancing Lifetime, Sensor Nodes, Energy Dissipation**

I. Introduction

As part of the continued advances in Micro-Electro-Mechanical Systems (MEMS), Wireless Sensor Networks (WSN) has and will play a vital role in our daily lives. WSNs have a wide area of use, from medical to military, and from home to industry [1]. WSNs consist of low-power multi-functioning sensor nodes, operating in an unattended environment, with limited computational and sensing capabilities. A sensor node is a node in a wireless sensor network that is capable of performing some processing, gathering sensory information and communicating with other connected nodes in the network. The base stations are one or more distinguished components of the WSN with much more computational, energy and communication resources. They act as a gateway between sensor nodes and the end user [2]. Base Station is a central server by which users take information about environment. Cluster head maintain communication among sensors in a cluster and base station. Selecting cluster heads, before the routing takes place, is an important issue since location and energy level of cluster heads tends to make an effect on WSN. The basic objective of cluster head selection is to make the network useful and efficient [3]. Proper cluster head selection assures the proper clustering and proper clustering enables bandwidth reuses and increase system capacity by using the network topology among senders and receivers.

When studying the overall network design problem in WSN, there are many important aspects that need to be taken into consideration, such as the lifetime of node, smaller size of the sensor node, its hardware complexity and ultra-low energy consumption. Among them, enhancing lifetime should be considered as the key design objective, since a sensor node can only be equipped with a limited energy supply [4]. Sensors node last till their energy is fade away [5]. In some application scenarios, replenishment of energy resources might be impossible, and therefore sensor node lifetime shows a very strong dependency on battery lifetime [6]. The frequent topology changes due to the die of sensors make the network quite unstable. A good cluster head selection protocol is, therefore, required which is able to enhance the system lifetime and maximize data communication.

There are few existing protocols in WSNs in order to select cluster heads. A number of existing works select cluster heads randomly. As a result, same node can selected for current round, which was selected for previous round. The cluster may or may not be divided equally. There are some other works in the area of cluster head selection which fails to consider load balancing among cluster heads. Hence, it causes more loads for data recreation and processing for the cluster heads. For this unequal balancing, few heads die quickly for more energy consumption. The existing works, based on direct communication among the sensor nodes, need more energy to transmit data to base station and hence, the nodes die quickly. Hence, the research on efficient cluster head selection becomes necessary to enhance system life-time and maximize data communication in WSNs.

In this paper, Energy-Cost Ratio Based Cluster Head determining Protocol (ECRBCP) is proposed to select the cluster heads. Energy-Cost of networks is determined by the ratio of total amount of energy for all cluster heads to total network costs. For cluster head selection, nodes are chosen from the candidate nodes which have higher Energy-Cost ratio. Experimental analysis shows that

Manuscript received January 31, 2011; revised April 30, 2011; accepted June 5, 2011

doi:10.4304/jcm.6.7.529-539

ECRBCP outperform existing dominant approaches with respect to enhancing system lifetime and amount of data communication.

The remaining part of the journal paper is organized as follows: related work in Section II. In Section III, the network architecture and radio models are discussed. Section IV describes proposed methodology for determining cluster head. In Section V, experimental analysis of the proposed method is illustrated. Finally, Section VI concludes the paper.

II. Related Work

In Minimum-Transmission-Energy routing (MTE) [7], nodes route data destined ultimately for the base station through intermediate nodes. The intermediate nodes are chosen such that the transmit amplifier energy is minimized. Nodes adjust their transmit power to the minimum required level to reach their next-hop neighbor. This reduces interference with other transmissions and reduces the nodes energy dissipation. Communication with the next-hop neighbor occurs using a CSMA MAC protocol, and when collisions occur, the data are dropped. When a node receives data from one of its upstream neighbors, it forwards the data to its next-hop neighbor. This continues until the data reach the base station. Depending on the radio characteristics the total energy expended in the system might actually be greater using MTE routing than using direct communication protocol. In MTE routing, the nodes closest to the base station will be used to route a large number of data messages to the base station. Thus these nodes will die out quickly. In addition, since in the area nearer to the base station, nodes become dead, this area of the environment is no longer monitored. As a result, in these communications, there occurs more energy loss among router.

In static-clustering protocol [7], clusters are formed at first and remain unchanged for the entire system. The static clustering protocol is identical to LEACH [8] except the clusters are chosen a-priori and fixed. The clusters are formed using the simulated annealing algorithm as in LEACH-C [9]. Static clustering includes scheduled data communication from the cluster members to the cluster-head and data aggregation at the cluster-head. As the cluster head and the cluster remain same for each round, the selected static cluster head die quickly and thus the network lifetime cannot be maximized.

To meet the requirements of wireless micro-sensor network, LEACH, application-specific protocol architecture is developed. LEACH is a clustering-based protocol that includes the following properties: (a) randomized, adaptive, self-configuring cluster formation, (b) localized control for data transfers, (c) low-energy media access, and (d) data processing. In LEACH, the nodes organize themselves into local clusters, with one node acting as the cluster-head. All non-cluster-head nodes must transmit their data to the cluster-head, while the cluster-head node must receive data from all the cluster members, perform signal processing functions on the data (e.g., data aggregation), and transmit data to the remote base station. Therefore, cluster-head is more energy-intensive than other nodes. In the scenario, where all nodes are energy-limited, if the cluster-heads were chosen a priori and fixed throughout the system lifetime as in a static clustering algorithm, the cluster-head sensor nodes would quickly use their limited energy. Once the cluster-head runs out of energy, it is no longer operational. The LEACH incorporates randomized rotation of the high-energy cluster-head position such that it rotates among the sensors in order to avoid draining the battery of any one sensor in the network. In this way, the energy load associated with being a cluster-head is evenly distributed among the nodes. LEACH forms clusters by using a distributed algorithm, where nodes make autonomous decisions without any centralized intervention. In LEACH, distributed cluster formation can be done without knowing the exact location of any of the nodes in the network and any sensor node can act as cluster head. So, proper cluster head selection is not possible over time.

In order to produce better clusters by dispersing the cluster head nodes throughout the network a central control algorithm called LEACH-C [10] is developed. Unlike the LEACH, LEACH-C utilizes the central base station for the formation of cluster heads. During set-up phase of LEACH-C, each node sends information about its current location and energy level to the Base Station (BS). In addition to determining good clusters, the BS needs to ensure that the energy load is evenly distributed among all the nodes. To do this, the BS computes the average node energy, and whichever nodes have energy below this average cannot be cluster-heads for the current round. In LEACH-C, the nodes transmit their data to the cluster head node during each frame of data transfer and the cluster head aggregates the data and sends the resultant data to the BS. When the cluster head node's energy is depleted, the nodes in the cluster lose communication ability with the BS and are essentially dead. Furthermore a number of sensor nodes to be needed for the network ranges from hundreds to hundred-thousands, this technique will not appropriate [11].

In LEACH-F [12], the clusters are fixed and only the cluster heads are rotated. Here, a node should have to use a large amount of power to communicate with its cluster head when another cluster's head is nearer. For initial cluster formation, the LEACH-F also uses the same annealing algorithm as in LEACH-C. LEACH-F is more energy efficient than LEACH-C. But the LEACH-F cannot be implemented in practical real time systems, because the interference of signals is more. LEACH-F does not allow new nodes to be added to the system, and does not adjust its behavior based on nodes dyeing. That's why lifetime enhancement is tough.

Hang Su and Xi Zhang [1] have extended the existing analytical model to derive the optimized parameter and show its correctness by simulations. The analyses by the authors reveal the insight that the original analytical model underestimates the optimal number of clusters and thus needs to be modified. This research discusses the protocols for scenarios limited to sensors having correlated data. Nonetheless there are applications of

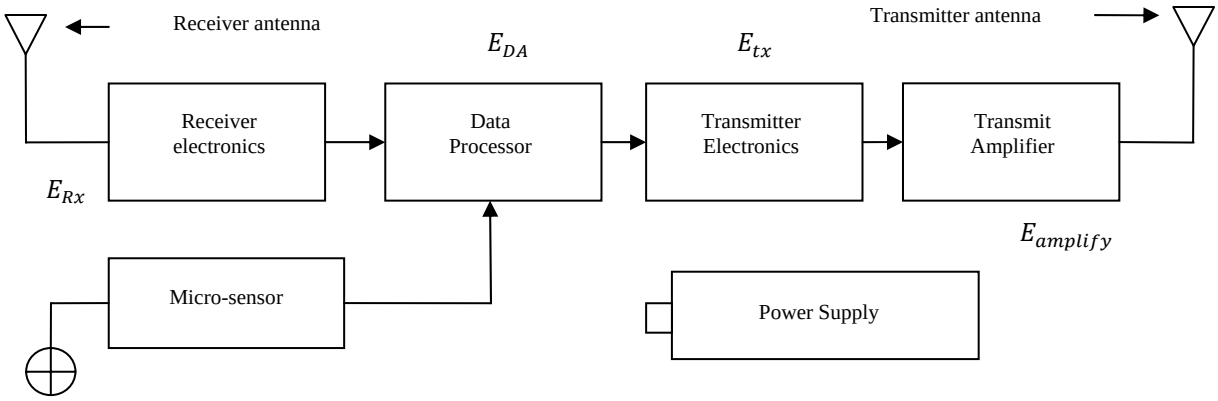

Figure 1: Radio energy dissipation model.

micro sensor networks devoid of the above limitation. For instance, sensor networks for medical monitoring applications may constitute dissimilar sensors located on and/or in the body which monitor vital signs. The prime focus of these networks is to maximizing quality of different parameters, which mainly forbids loss of information. In order to support the unique considerations of these networks, protocol architectures need to be developed.

III. Network Architecture And Radio Model

In ECRBCP, a sensor network model is considered with the following properties: (a) The base station is fixed and located far away from the sensor nodes, (b) Sensor nodes are energy constrained with uniform initial energy allocation, (c) Sensor nodes are equipped with power control capabilities to vary their communication power, (d) Each node in sensor network senses data and send to the local cluster heads to BS always, (e) Sensor nodes are immobile. As shown in the Figure 1**,** the sensor nodes are equipped with Transmitter antenna, Receiver antenna, Power Supply, Amplifier, Data Processor etc**.** Environmental information is sensed through micro-sensor, every kind of data operation is done through data processor and data communication through antenna [8]. The energy consumed throughout the entire sensor network can be described as the energy consumption for data communication to the cluster head that is energy communication factor E_{tx}. Energy dissipation for data communication to the cluster head is

$$E_{tx} = E_{amplify} + E_{processing} \quad (1)$$

Where, $E_{processing}$ is the energy consumed for data processing and $E_{amplify}$ is the energy consumed for signal amplification. If communication distance between the communicating nodes is d, and two different channel models is used in this communication then free space model has power loss of d^2 .

IV. Proposed Methodology For Determining Cluster Head

In ECRBCP, the clusters are formed using the central control algorithm by dispersing the cluster head nodes throughout the network. The advantage of using the centralized clustering algorithm is that the BS forms the cluster which is the most energy intensive task, so that the energy dissipation of the sensor nodes decreases and network lifetime increases. Here all sensor nodes send their current location and energy level to the base station and the base station forms the clusters for the network by taking enhanced and effective processing of the current information of whole network. The operation of ECRBCP is divided into rounds. Each round begins with set-up phase when the clusters are formed, followed by a steady-state phase when the data are transferred from the nodes to the central base station through their respective cluster-heads. The selection of sensor nodes are done in round of few seconds and in each round five cluster heads are selected in case of not more than hundreds sensor nodes in the network.

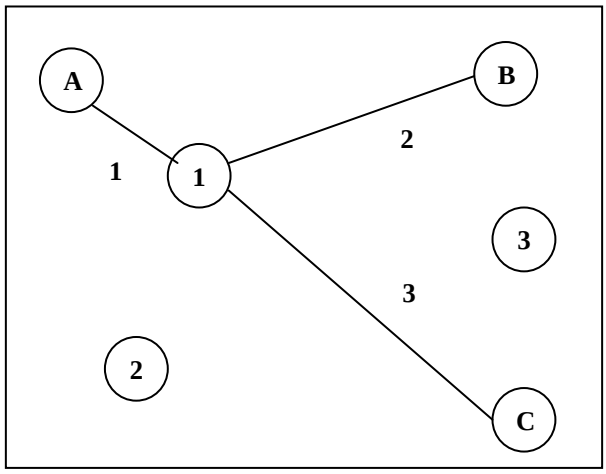

Figure 2: A sample Network Topology where circle denote node and edge denote distance in meter.

Energy-Cost of networks is determined by the ratio of total amount of energy for all cluster heads to total network costs. The cluster head candidates are selected from living nodes whose energy is higher than the average energy. For cluster head selection, nodes are chosen from the candidate nodes depending on higher Energy-Cost ratio. A network will have higher Energy-Cost ratio if the network reserve more power among cluster heads for reliable data transfer. For calculating a

neighbor node for any living node X, it follows the following equation:

$$Neighbor\ (X) = \min\ (dist\ (1), dist\ (2), dist\ (3), \ldots \ldots\ldots, dist\ (P)) \quad (2)$$

$$Here, 1, 2 \ldots P\ = \ Set\ of\ candidate\ nodes\ dist\ (i) = Absolute\_Distance\_Between(X, i)$$

Figure 2 is a sample topology where A, B, and C are candidates for cluster heads and 1, 2, 3 are non-cluster head nodes; distance between node 1 and A = 1m; distance between node 1 and B = 2m; and distance between node 1 and C = 3m. Then we have to determine that, under which cluster head, candidate node 1 will belong to. To determine the neighbor node for node A, B and C, the square distance is calculated between the candidate nodes and the non candidate nodes. If (x1, y1) be the coordinate of node 1 and (xa, ya) be the coordinate for node A, then the mathematical equation for distance calculation as

$$distance(A, 1) = (xa - x1)^2 + (ya - y1)^2 \quad (3)$$

In LEACH-C, to select the cluster head, Simulated Annealing algorithm [13] is used. The cost function *f(S)* in LEACH-C is defined as

$$f(S) = \sum_{i=1}^{N} \min\left(dist^2(i, s)\right) \text{ ,where } (s \in S) \quad (4)$$

Here, N is the number of sensor node and *dist (i, s)* is the distance between node *i* and node *s*. From last few equations, it can be derived that the Communication Cost (CC) is proportional to the Communication Distance (CD):

$$CC \propto CD \quad (5)$$

If the communication distance between cluster-head and the non cluster-head increases then the overall cost will increase and if the communication distance decreases then the overall cost will decrease. The energy consumed in data signal amplification can be expressed as

$$Energy\ Dissipation\ \propto CC \quad (6)$$

The communication cost is proportional to the energy dissipated. Hence, if the communication cost increases between the communicating nodes then more energy will be dissipated; and thus total energy consumption will also increase. Total Cost is determined by the summation of the minimum of the square distances between nearest neighbor among non cluster node and cluster head node. The relation of Energy-Cost and total cost can be shown as

$$Energy\text{-}Cost \propto \frac{1}{Total\ Cost} \quad (7)$$

Here, Energy-Cost and cost factor are related with vice-versa. So, as whole we can express energy-cost ratio and final expression of ECRBCP respectively

$$Energy\text{-}Cost \propto \frac{\sum \text{Energy of CLuster Head}}{Total\ Cost} \quad (8)$$

$$f(S) = \frac{\sum_{i=0}^{n-1} \text{Energy of CLuster Head}}{Total\ Cost} \quad (9)$$

Here, n=number of cluster head

Total cost for each candidate node all *s* in the set of candidate node *S*. In our analysis we found that, to minimize the communication cost those nodes are selected as cluster head that create a proper distribution of cluster heads in the network, that's why network coverage and load balancing is also addressed by this method. In ECRBCP the cluster head node's with higher sensor Energy-Cost ratio is more likely to become a set of cluster-head otherwise depends on probability as follows

$$P_d = \begin{cases} e^{-\frac{f(S)-f(S')}{\alpha_d}} & f(S') \leq f(S) \\ 1 & f(S') > f(S) \end{cases} \quad (10)$$

Where, α_d= $1000e^{d/20}$ and P_d is compared with an arbitrary value in the range of 0 to 1 if it bigger than that arbitrary value, then nodes in S' is become set of new cluster heads. If P_d is smaller than the arbitrary value then a new S' is created until an optimum set of cluster heads is found.

This protocol requires that each node know its location in order to generate a topology map. Sensors send information about their current location to base station selects a optimum set of cluster head comparing a Energy-Cost function where the Energy-Cost for each set of cluster head is determined by the ratio of the sum of energy of cluster heads and minimum square distances of each cluster head with their member nodes. The total cluster formation process is divided into a number of parts. Such as Initial Candidate selection, energy calculation, distance calculation, Energy-Cost function determination and then finally cluster formation. The proposed cluster head selection methodology for ECRBCP is as follows:

INITIALIZATION

Let,
N →total number of alive nodes
P →number of Cluster Head per round = 5% of total alive nodes
C[] →Set of Cluster Head Candidate
E → The current energy of a particular node
distance[] →contains distance between nodes
CH[] → contains node selected as cluster head
currentE_[] → Contain Current energy of nodes

The following function named as FIND_MIN_DIST uses to determine network cost is calculated for ECRBCP:

FIND_MIN_DIST (
$double * X1, double * Y1, int\ size1, double * X2, double * Y2, int\ size2, int * ch\_index, int * C)$

```
1. int newIndex, double dsquare, double minDist
2. size1 ←N, size2 ← P
3.for i→0 to size1-1
   begin
     minDist = 1000000;
    for i→0 to size2-1
        begin
                if (C[k]) then
                    dsquare = (X2[i] − X1[i]) *
(X2[i] − X1[i]) + (Y2[i] − Y1[i]) * (Y2[i] − Y1[i]);
                        if (dsquare < min_dist) then
                                min_dist = dsquare;
                                new_index = j;
                        end if
                end if
```

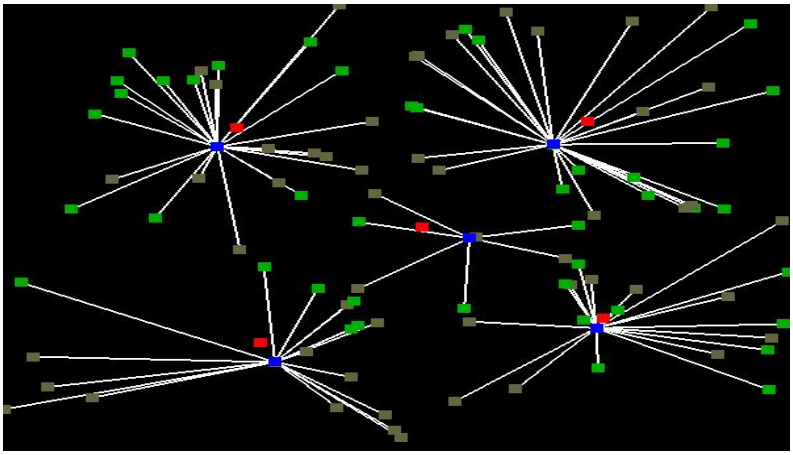

Figure 3: Clustering View of ECRBCP.

```
        end
    cost += min_dist;
    ch_index[i] = new_index;
    end
return cost;
```

The above function returns the cost of each set of cluster head, where the cost of each set of cluster head is defined by the sum of the minimum of the square distances of the cluster heads with its member nodes. This function also determines the neighbors of a cluster head. A node becomes a neighbor or member of a cluster head node only when it has the minimum cost with that cluster head node than others. Here X1, Y1 denotes the x and y coordinates respectively of any non cluster head or cluster node. And X2, Y2 denotes the x, y coordinate of cluster head nodes. By using following procedure cluster heads are selected:

1. Initialization
2. Calculate average energy of sensor nodes, $E_{ave} = \sum_{i=0}^{n-1} E_i$
3. Determine the nodes that are eligible for being Cluster Head

```
for I → 0to N-1
begin
    allnodes[i]=true;
    if(E_i < E_avg)
        C[i]=false;//not eligible for being cluster head
     else
        C[i]=true;//eligible for being cluster head
    end if
end
```

4. Find initial set C of P nodes for the Simmulated Anneling(SA) algorithm from eligible nodes
5. Find the energy-cost ratio of the initial set, C of CH node

```
/*chIndex[i] denotes the ith cluster head node of a set and nodeUnder array contains the no of member under a single Cluster head node, cluster Index array contains the node number of Cluster head for each node.*/
for I → 0 to P
begin
        Energy_Cos +=currentE_[chIndes[i]];
 end
/*determine the sum of the minimum of the square distances for each set of cluster head.*/
minCost = FIND_MIN_DIST(XN, YN, N, XC, YC, P, clusterIndex, allnodes);
Energy_Cost /=minCost; // summation of cluster heads energy divided by communication cost
```

6. Determine Cluster_Head_Energy value by adding current energy of cluster head in set C
7. Total_Network_Cost is determined by the summation of the minimum of the square distances between nearest neighbor among non cluster node {N-C} and cluster head node in set C. //Here N set of all nodes
8. Determine Energy-Cost ratio by dividing Cluster_Head_Energy/ Total_Network_Cost
9. Find new set C' of CH nodes
10. Determine Cluster_Head_Energy value by adding current energy of cluster head in set C'
11. Total_Network_Cost is determined by the summation of the minimum of the square distances between nearest neighbor among non cluster node {N-C'} and cluster head node in set C'. //Here N set of all nodes
12. Determine Energy-Cost ratio by dividing Cluster_Head_Energy/ Total_Network_Cost
13. Compare the ratio of C with C'
14. If energy-cost ratio of (C') > energy-cost ratio of(C), C' becomes new optimum. Otherwise depends on probability
15. Repeat 9 to 14 for a predefined times of iteration
16. Finally form the cluster with the optimum set of cluster head

The above procedure uses nodes energy at current round of iteration then compare with average energy of network and select cluster head randomly. Then SA is applied to maximizing the value of energy-cost function to determining good cluster head for reliable data communication within each round.

In Figure 3, blue nodes are selected for cluster head for a particular round. Red nodes denote virtual co-ordinates. Green nodes denote those nodes which have more than

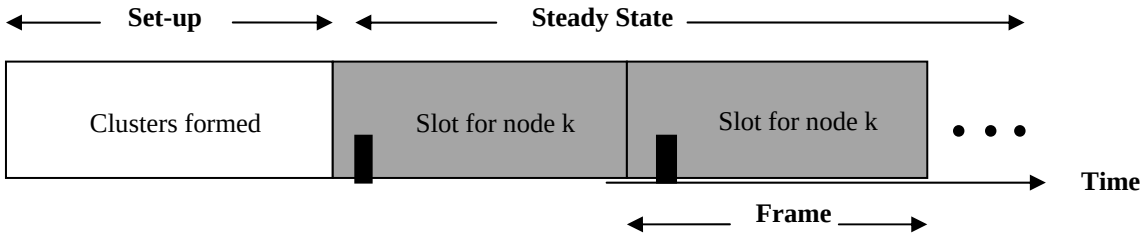

Figure 4: Time-line showing ECRBCP operation.

average energy and other nodes denote that they have not enough energy for cluster head. The steady-state operation is broken into frames where nodes send their data to the cluster-head (at most once per frame) during their allocated communication slot. Each slot in which a node transmits data is constant, so the time for a frame of data transfer depends on the number of nodes in the cluster.

In every time scheduling, above procedure are done in setup phase then steady-state begins. The steady-state operation is broken into frames where nodes send their data to the cluster-head at most once per frame during their allocated communication slot. Each slot in which a node transmits data is constant, so the time for a frame of data transfer depends on the number of nodes in the cluster. In addition, the set-up protocol does not guarantee that nodes are evenly distributed among the cluster-head nodes. Therefore the number of nodes per cluster is highly variable in ECRBCP and the amount of data each node can send to the cluster-head varies depending on the number of nodes in the cluster. To reduce energy dissipation, each non-cluster-head node uses power control to set the amount of communication power based on the received strength of the cluster-head advertisement. Furthermore, the radio of each non-cluster-head node is turned off until its allocated communication time. Since all the nodes have data to send to the cluster-head and the total bandwidth is fixed using a TDMA schedule is efficient use of bandwidth in addition to being energy efficient. The cluster-head must keep its receiver on to receive all the data from the nodes in the cluster. Once the cluster-head receives all the data, it can operate on the data (e.g., performing data aggregation) and then the resultant data are sent from the cluster-head to the base station. Since the base station may be far away and the data messages are large this is a high-energy communication. Figure 4 shows a flow graph of the steady-state operation. It also shows the time-line for a single round of ECRBCP, from the time clusters are formed during the set-up phase, through the steady-state operation when data are transferred from the nodes to the cluster-heads and forwarded to the base station. When a cluster-head has data to send, at the end of its frame it must sense the channel to see if anyone else is transmitting using the base station spreading code. If so, the cluster-head waits to transmit the data. Otherwise, the cluster-head sends the data using the base station spreading code.

Data aggregation is performed on all the unprocessed data at the base station or it can be performed locally at the cluster head. If the energy for communication is greater than the energy for computation, performing data aggregation locally at the cluster-head can reduce the overall system energy consumption, since much less data needs to be transmitted to the base station. The cluster-head must be awake to receive all the data from the nodes in the cluster. Once the cluster-head receives all the data, it performs data aggregation to enhance the common signal and reduce the uncorrelated noise among the signals. Assuming perfect correlation, all individual signals can be combined into a single representative signal. The resultant data are sent from the cluster-head to the base station. Otherwise, more energy could be required for data communication, since the base station may be far away from sensor nodes and communication messages are large.

This protocol is designed to enhance the system lifetime and data communication in WSN. In addition, ECRBCP is designed to enable maximum energy savings by enabling nodes to enter the sleep state where portions of the node are powered-down to save energy as often as possible.

V. Experimental Analysis

In this section we mention the packages are required for simulation in order to compare with other existing dominant protocols and draw some outlines from the experiments.

NS-2 simulator [14] package (ns-allinone-2.27) is used with a MIT wireless sensor package [15] for the simulation of ECRBCP. We use hundred sensor nodes those are randomly located in the 100m × 100m to 1000m × 1000m network topology. The base station is located at (x=50, y=175). The number of cluster heads for each round is 5% of the total alive nodes as the optimal number of cluster heads for an energy efficient clustering mentioned in LEACH.

The performance of ECRBCP is evaluated in comparison to other existing dominant protocols such as LEACH-C, LEACH and Static Clustering in terms of system lifetime, energy-dissipation, and amount of data transfer. Throughout the simulation we measure the metrics: (a) Number of Alive node: Performance of a network depends on the lifetime of each node, if the lifetime of the nodes increase then the network performs well and sensors transmit more data to the base station. (b) Energy Dissipation: The lifetime of a node and the amount of data being transmitted by the nodes depend on communication cost among them. If the required energy to transmit data among nodes is reduced then energy dissipation will be reduced. (c) Data received: It is

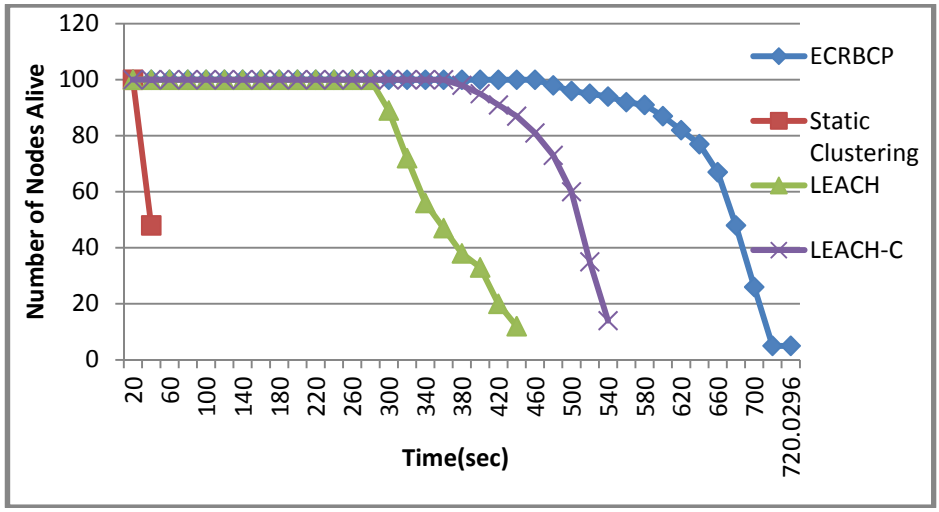

Figure 5: Number of Nodes Alive with respect to Network life time.

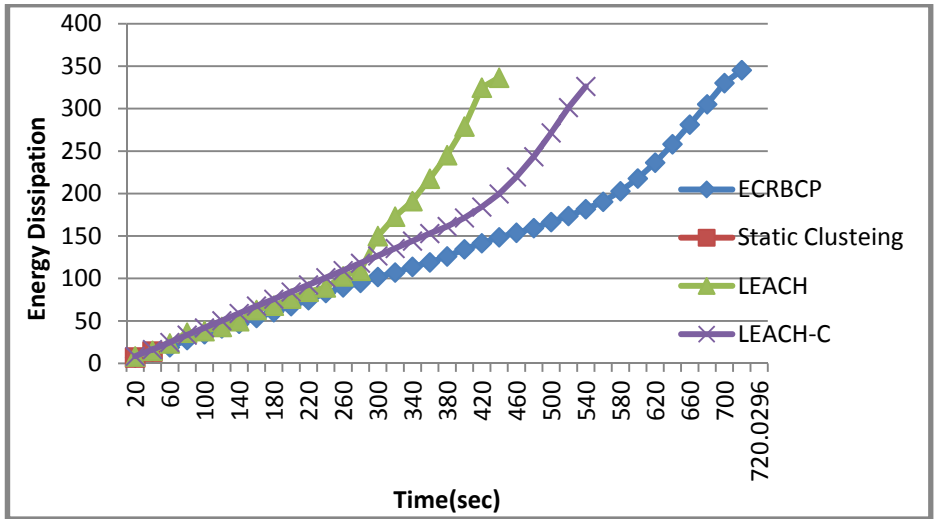

Figure 6: Amount of Energy Dissipation with respect to Time.

needed to know that how much data is received at the base station from the sensor networks. If the amount of data received is enough as it is expected then the network will perform well. (d) Initial energy: uniform energy supply is given among sensor nodes at the time of simulation start. (e) Network area: It denotes the area of the network as square meter. Few parameters such as cluster head, initial energy, network area, round time, location of base station were used in the simulation work. These parameters are listed in Table I.

Figure 5 shows the simulation curve of different protocol like ECRBCP, LEACH-C, LEACH and Static-Clustering. Where, x-axis denotes time and y-axis denotes number of node alive. This graph shows the number of nodes alive with respect to network life time in a 100*100 m^2 network area. The network lifetime depends on the time when the sensor nodes remain alive in a network. The simulation is started using 100 nodes. When the duration of nodes die is long, the network lifetime is also long. First node die is an important factor for evaluating overall network performance. First node alive time for ECRBCP is much better then LEACH-C and others. It also shows that the lifetime of the nodes of ECRBCP is longer than LEACH-C, LEACH, and also Static-clustering [3], [5], [7]. So the network lifetime of ECRBCP is longer than other protocols.

TABLE I.
SIMULATION PARAMETERS

Parameter	Value
Simulation Area(x, y)	100×100 to1000×1000m^2
Node's Initial Energy	2-5 joule
Simulation Time	3600 seconds
Base Station Location	(50,175)
Number of Nodes	100
Desired no. of Cluster	5
Round Time	20 seconds

Figure 6 shows the simulation curve of the amount of energy dissipation with respect to time in a 100*100 m^2network area. Here x-axis denotes time period and y-axis denotes energy dissipation of the network.

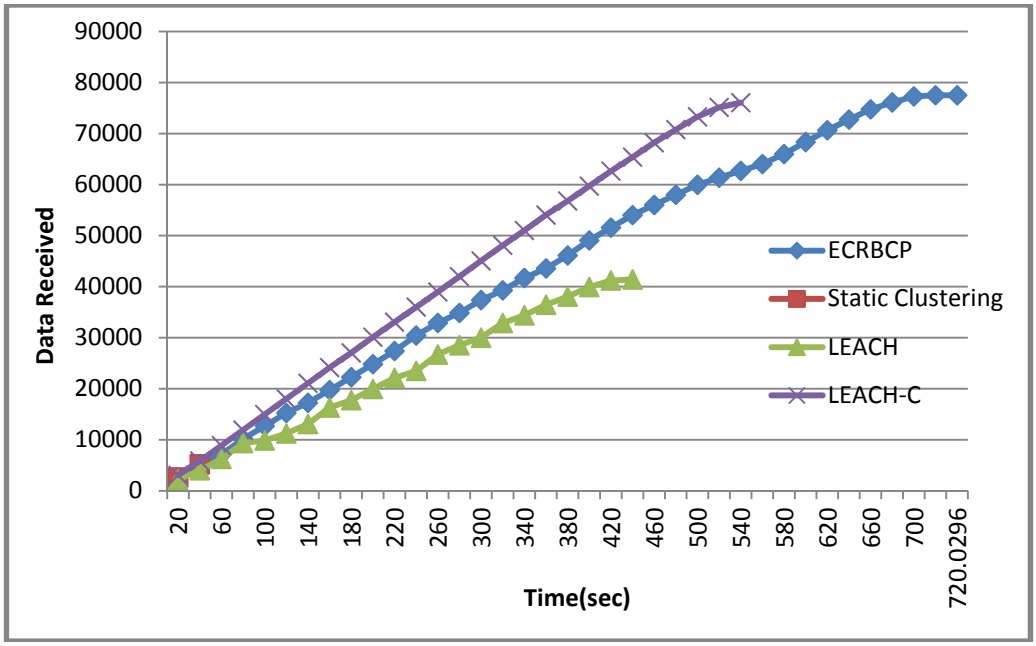

Figure 7: Amount of Data Received with respect to Network life time.

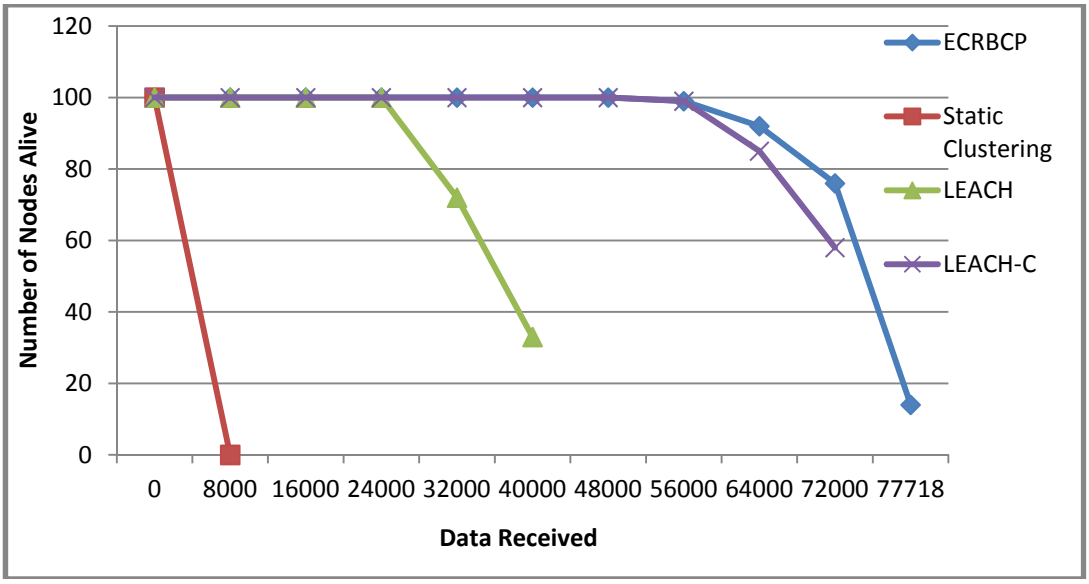

Figure 8: Number of Nodes Alive with respect to Amount of Data Received.

It can be observed that till 540 seconds, energy dissipation rate of ECRBCP is less than LEACH-C, LEACH, and Static-clustering, and that of LEACH-C is less than LEACH.

Figure 7 shows the simulation curve of the amount of data received with respect to network life time in a 100*100 m^2 network area. Where x-axis denotes time period and y-axis denotes data reception by the base station. The curve shows that till 540 seconds, the amount of data received by base station using ECRBCP is higher than LEACH but less than LEACH-C whereas LEACH-C is higher than LEACH and Static-Clustering. After 540 seconds, the amount of data received by base station using ECRBCP tends to increase than LEACH-C. Using simulation parameters as shown in Table I, 2% more data can be received using ECRBCP than LEACH-C and the difference will be more, if more initial energy for sensors is used.

Figure 8 shows the simulation curve of number of nodes alive with respect to amount of data message received in a 100*100 m^2 network area. Where x-axis denotes date reception and y-axis denotes number of node alive. After passing around 8000 unit of data to the base station, all the nodes of Static-Cluster are died and after passing around 40000 units of data packets to the base station, all the nodes of LEACH are died. But all nodes of both LEACH-C and ECRBCP are alive till around 60000 units of data packets are received by the base station. Then the die rate of nodes is increased for both of LEACH-C and ECRBCP. Using simulation parameters, it is showed that there is a proportional relationship among the parameter used for this figure. Though ECRBCP

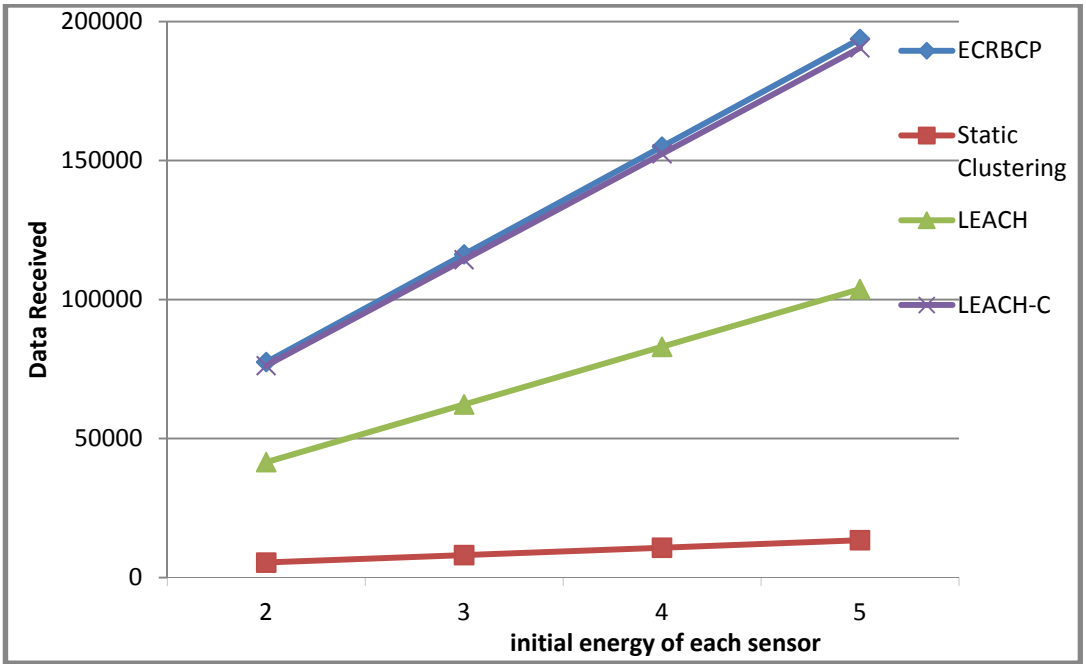

Figure 9: Data Received with respect to initial energy of each sensor.

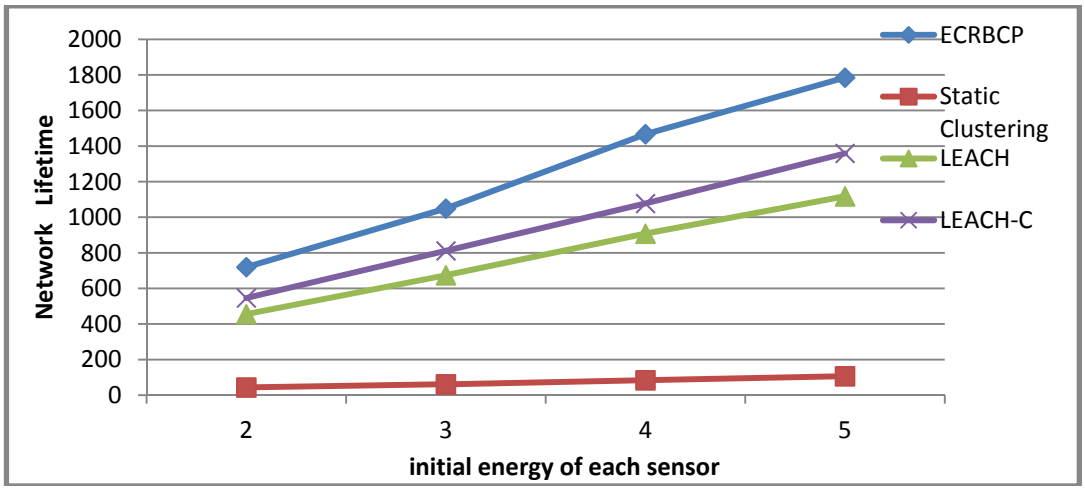

Figure 10: Initial energy of each sensor vs. Network Lifetime.

shows better result than other, some fluctuation can be occurred due to networks' undesired characteristics.

Figure 9 shows the simulation curve of total amount of data received by the base station with respect to uniform initial energy of each sensor. Where x-axis denotes initial energy of each sensor and y-axis denotes data received. Each curve denotes a method and in this graph each of the curve moves upward depending on the increase of initial energy of each sensor. Let a curve LEACH and see increase of one joule of uniform initial energy of each sensor of the network gives a large amount of total energy in the network for a simulation. As a result we get more amounts of data received by the base station. This graph denotes that there is a proportion relationship among uniform initial energy of each sensor nodes and total number of data received by the base station. If we use more initial energy for each sensor then get more data. And if we carefully observe that, 5 joule of initial energy of each sensor is used then we can make differentiation among the ending point of LEACH-C and ECRBCP. For large amount of initial energy of each sensor we must get better result for ECRBCP than LEACH-C.

Figure 10 shows the simulation curve of network lifetime with respect to initial energy of each sensor. Where x-axis denotes initial energy of each sensor and y-axis denotes network lifetime. An increase of one joule of initial energy of each sensor of the network gives a large amount total energy in the network for a simulation. As a result, lifetime for all method can be obtained. This graph denotes that there is a proportional relationship among initial energy of each sensor and network lifetime. It can be observed that, if 2 joule of initial energy of each sensor is used then clear differentiation among the network lifetime of each method can be drawn. So, for large amount of uniform initial energy of each sensor

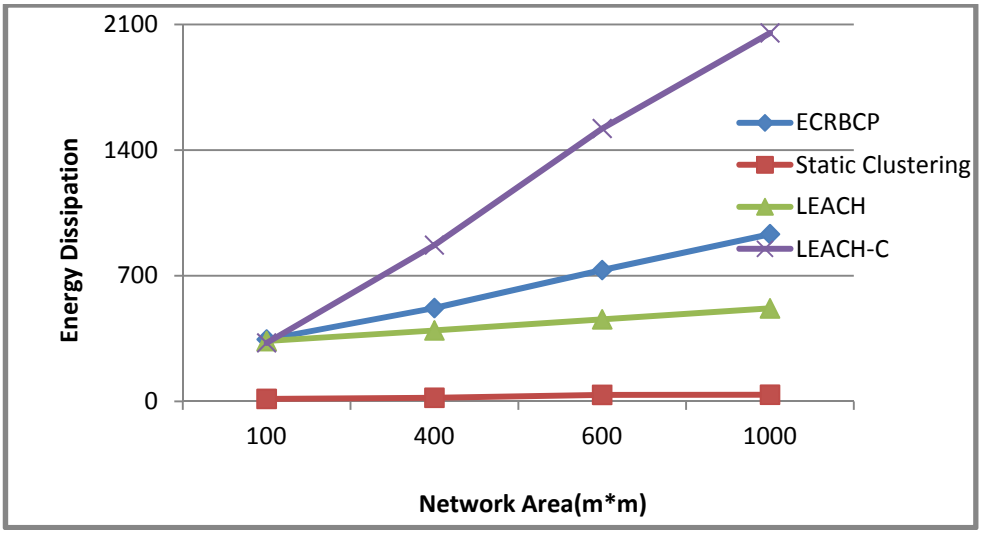

Figure 11: Amount of Energy Dissipation with respect to Network area.

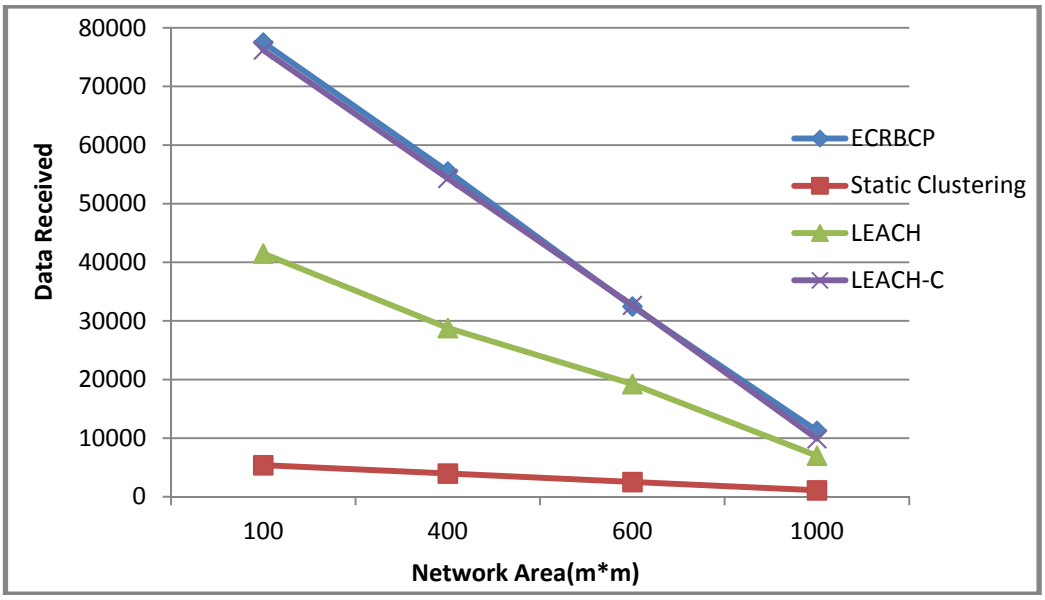

Figure 12: Amount of Data Received with respect to Network area.

make more percentage of differentiation between ECRBCP and other methods.

Figure 11 shows the simulation curve of energy dissipation with respect to network area. Where x-axis denotes network area and y-axis denotes energy dissipation. In this case, 2 joule is used as initial energy of each sensor node. When the network area increases then dissipation rate for each method is increased. In Static-Clustering and LEACH, energy dissipation are less than ECRBCP and LEACH-C. Since network lifetime of Static-Clustering and LEACH-C is too short. Among ECRBCP and LEACH-C, energy dissipation for ECRBCP is less than LEACH-C for any network area. This analysis is also a very important factor for large scale application of sensor networks.

Figure 12 shows the simulation curve of data received by base station with respect to network area. Where x-axis denotes network area and y-axis denotes data received by base station. We use 2 joule as initial energy of each sensor node. When the network area increases then dissipation rate for each methods is increased. So amount of data received by the base station decreases. In case of Static-Clustering and LEACH we got less data reception by the base station than ECRBCP and LEACH-C. Among ECRBCP and LEACH-C there are some fluctuation was occurred for lower initial energy of each sensor node. And we accomplished our goal to pick network scenario for long time as well as data for a large area of networks.

The comparisons show that ECRBCP has large advantages than other routing protocols. ECRBCP is effective because it increases the network lifetime, reduces the energy dissipation for data communication. One of the important factors for network lifetime increase is that the time required for first node die in simulation. Time taken for first node die of ECRBCP is better than other methods. As ECRBCP serve longer time than other methods, the network can serve for a long period,

producing high-level information about an environment that is monitored by the sensor nodes.

VI. CONCLUSIONS

This paper proposes a new approach to select cluster head based on higher energy-cost ratio where energy-cost ratio is determined by the ratio of total amount of energy for all cluster heads and total network costs. ECRBCP contributes to the study of wireless sensor networks by addressing the problem of increasing system lifetime and maximizing data communication via proper cluster head selection. ECRBCP utilizes the high-energy base station to perform most energy related tasks. ECRBCP shows its better performance, in considering four simulated metrics: a) number of nodes alive, (b) energy dissipation, (c) data received, d) initial energy, and e) network area, than existing dominant approaches.

In this paper we found that, to minimize the communication cost among sensors to cluster heads to base station, those nodes are selected as cluster heads that creates a proper distribution of cluster heads among the network, that's why network coverage and load balancing issue are also addressed by this method.

In this paper few specified methodologies are shown to enhance system lifetime and maximize data communication in wireless sensor networks. There are few other open scopes, to extend this research. For the selection of cluster head, few issues should be dealt with, e.g., total amount of data in previous round of data communication, remaining energy for the current round, and distance between cluster head and each sensor node. Furthermore, a high performance approximation algorithm, instead of Simulated Annealing Algorithm, can be developed to get a better solution.

REFERENCES

[1] A. Allirani, M. Suganthi, "An Energy Sorting Protocol (ESP) With Low Energy and Low Latency in Wireless Sensor Networks", *International Journal of Computer Science and Network Security*, vol. 8 no.11, pp. 208-214, November 2008.

[2] Kay Römer, Friedemann Mattern, "The Design Space of Wireless Sensor Networks", *IEEE Wireless Communications*, vol. 11 issue 6, pp. 54 – 61, December 2004.

[3] R. Sivaraman, V. R. Sarma Dhulipala, V. Aarthy, K. Kavitha "Energy comparison and Analysis for Cluster Based Environment in Wireless Sensor Networks", *International Journal of Recent Trends in Engineering*, vol. 2, no. 4, pp. 89-91, November 2009.

[4] I. F. Akyildiz, W. Su, Y. Sankarasubramaniam, E. Cayirci, "Wireless sensor networks: a survey". *Computer Networks*, vol. 38 issue 4, pp. 393-422, March 2002.

[5] Ali Hossein Alipour, Davood Key Khosravi, Abbas Mirzaei Somarin, "New method to decrease probability of failure nodes in WSNs", *International Journal of Computer and Network Security*, vol. 2, no. 2, pp. 38-40, February 2010.

[6] Eui-Hyun JUNG, Sung-Ho LEE, Jae-Won CHOI and Yong-Jin PARK, "A Cluster Head Selection Algorithm Adopting Sensing-Awareness and Sensor Density for Wireless Sensor Networks", *IEICE Transaction* on *Communications*, vol. E90-B, no. 9, pp. 2472-2480, September 2007.

[7] Wendi Beth Heinzelman, "Application-Specific Protocol Architectures for Wireless Networks," Ph.D. Dissertation, Massachusetts Institute of Technology, June 2000.

[8] Choon-Sung Nam, Hee-Jin Jeong, Dong-Ryeol Shin, "The Adaptive Cluster Head Selection in Wireless Sensor Networks" *IEEE International Workshop on Semantic Computing and Applications*, pp. 147 – 149, July 2008.

[9] Wendi Rabiner Heinzelman, Anantha Chandrakasan, Hari Balakrishnan, "Energy-Efficient Communication Protocol for Wireless Microsensor Networks", Proc. of 33rd *Hawaii International Conference on System Sciences*, vol. 8, pp. 208, January, 2000.

[10] Wendi B. Heinzelman, Anantha P. Chandrakasan, Hari Balakrishnan, "An Application-Specific Protocol Architecture for Wireless Microsensor Networks" *IEEE Transaction on Wireless Communications*, vol. 1, no. 4, pp. 660-670, October 2002.

[11] Guangyan Huang, Xiaowei Li, "Energy-Efficiency Analysis of Cluster-Based Routing Protocols in Wireless Sensor Networks", *IEEE Aerospace Conference*, pp. 8, July 2006.

[12] Kemal Akkaya, Mohamed Yonis, "A Survey on routing protocols for wireless sensor networks" *Journal of Ad Hoc Networks*, vol. 3, pp. 325—349, 2005.

[13] Siva D. Muruganathan, Daniel C. F. Ma, Rolly I. Bhasin, Abraham O. Fapojuwo, "A Centralized Energy-Efficient Routing Protocol for Wireless Sensor Network", *IEEE Radio Communications*, March 2005.

[14] The network simulator-2 [Online]. Available: http://www.isi.edu/nsnam/ns/

[15] MIT package [Online]. Available: http://www.ece.rochester.edu/~wheinzel/research.html

Bijan Kumar Debroy was born on 3rd February 1987 in a city of Bangladesh named Faridupur. He obtained his B.Sc. in Computer Science & Engineering in 2010 from Khulna University of Engineering & Technology, Khulna, Bangladesh. He has more than two international publications. Among them, two were published in 12th International Conference on Computer & Information Technology, Dec. 2009, Dhaka, Bangladesh and 13th International Conference on Computer & Information Technology, Dec. 2010, Dhaka, Bangladesh.

Dr. Muhammad Sheikh Sadi was born on 1st January 1978 in Dhaka city of Bangladesh. He obtained his B.Sc. in Electrical and Electronic & Engineering in 2000 from Khulna University of Engineering & Technology, Khulna, Bangladesh. In 2004, he obtained his M.Sc. in Computer Science & Engineering from Bangladesh University of Engineering & Technology, Dhaka, Bangladesh. In 2009, he obtained his Ph.D. PhD in Electrical and Computer Engineering from Curtin University, Australia. He has more than 15 peer reviewed publications.

Md. Al Imran was born on 13th December 1987 in a city of Bangladesh named Khulna. He obtained his B.Sc. in Computer Science & Engineering in 2010 from Khulna University of Engineering & Technology, Khulna, Bangladesh. He has more than two international publications. Among them, two were published in 12th International Conference on Computer & Information Technology, Dec. 2009 and 13th International Conference on Computer & Information Technology, Dec. 2010, Dhaka, Bangladesh.

Radio Resource Management for Fast Fading Environments

Leonidas Sivridis, Xinheng Wang, and Jinho Choi
School of Engineering
Swansea University, SA2 8PP, UK
email: {392924, x.wang, j.choi}@swansea.ac.uk

***Abstract*—Adaptive resource allocation based on perfect Channel State Information (CSI) can significantly improve the performance of Orthogonal Frequency Division Multiple Access (OFDMA) systems. However, in real systems, accurate CSI is impossible because of noisy channel estimates, channel feedback delays, and processing delays. Therefore, only imperfect CSI can be used for resource allocation purposes. In this paper, we minimize the impact of errors caused by imperfect CSI and evaluate the significance of periodic CSI feedback in a fast fading environment. In a fast fading environment, periodic CSI feedback requires a high overhead load; and the uplink resources reserved for feedback purposes are limited. Thus, we present a strategy that optimizes the usage of those uplink resources. Simulation results show that this strategy leads to a higher overall fairness and system throughput.**

***Index Terms*—orthogonal frequency division multiple access (OFDMA), partial CSI, Radio Resource Management, Call Admission Control, fast fading.**

I. Introduction

Orthogonal Frequency Division Multiple Access (OFDMA) is used on the downlink of the 3GPP Long Term Evolution (LTE) system as it is inherently able to combat frequency selective fading and offers degrees of freedom in radio resource management (RRM) by taking advantage of diversity effects [1]. Efficient RRM over an OFDMA system depends on accurate Channel State Information (CSI) at the transmitter side [2]. Its knowledge allows for the system bandwidth to be fully exploited through adaptation of the transmission parameters used on each OFDMA carrier. Although the system throughput can be improved with accurate CSI [2], this assumption is unrealistic. Noisy channel estimation, along with a delay between the moment of channel estimation and the actual transmission, results in imperfect or outdated CSI being used for RRM purposes. RRM in OFDMA systems involves the application of adaptive modulation/coding (AMC). AMC provides the flexibility to match the Modulation-Coding Scheme (MCS) to each user's channel conditions. It was concluded in [3] that AMC is not significantly affected by noisy channel estimation if a reasonably good estimator is used. However, when the mobility of the users is high, the CSI becomes more outdated, which will lead to errors in the resource assignments; and thus, to a decrease in overall system performance. As user mobility is a principal driving force for mobile-OFDMA based wireless systems such as LTE, it becomes more important to consider the time-varying nature of channels for resource allocation problems in order to further enhance the system throughput. In LTE, resources are allocated to users every 1msec [1] which allows for a quick response to the varying channel conditions of the link. However, under significant user mobility the small coherence time means that the CSI measurement reports need to be frequent; otherwise, the CSI used by the base-station (BS) to perform AMC will not be correlated with the current channel states. In this paper, we define correlated CSI (CCSI) as the CSI that is correlated to some degree with the current value of the channel. Frequent CSI measurement reports lead to increased system overhead requirements, especially when a large number of active users are present in the cell [4]. Instead of feeding back the instantaneous channel coefficients to the BS, it is feasible that users simply send the mean of the subchannel SNR distribution [5]. We define this knowledge as statistical CSI (SCSI). Using SCSI to perform resource allocation requires significantly less resources to be occupied for feedback purposes.

In practical systems, only imperfect/outdated CSI and SCSI can be used to perform resource allocation. Therefore, practical resource allocation schemes that account for CSI inaccuracy are required. The impact of imperfect and outdated CSI on the performance of adaptive OFDM has already been studied in the literature [3],[6]. Using SCSI to perform resource allocation for OFDMA systems has been analyzed in [5]. In this work we distinguish between these two different forms of partial CSI (SCSI and CCSI) and address CCSI and SCSI based resource allocation strategies for LTE systems.

Most works [7] – [9] on resource allocation for OFDMA systems under the partial CSI assumption do not differentiate between the SCSI and CCSI concepts. In [5], a comparison that focused on the continuous rate case (i.e Shannon capacity based formulation) was performed between the two cases. In the first part of this paper we compare the two cases for the more practically relevant case where only a discrete number of modulation and coding levels are available. In order to do so, we quantify the performance degradation created by CSI errors. These results are then applied to allocate resources to users with the objective of maximizing the overall system throughput while ensuring that the target bit error rates are kept below a given threshold and each users queue length is kept within stable bounds. We also investigate the impact of this maximization on the system throughput for both the SCSI and CCSI based resource allocation schemes.

The majority of research on OFDMA resource management does not consider the presence of a Call Admission Control (CAC) unit [7] – [9], [5]. The CAC unit limits the number of admitted flows in order to maintain the user QoS. Also, it distributes the network throughput between the supported services[10]. Motivated by our comparison between the CCSI and SCSI based resource allocation schemes in the second part of this paper we propose a strategy that leads to a good tradeoff between overhead consumption and fairness as well as throughput when

Manuscript Received December 01 2010; Revised May 01 2011; Accepted August 22 2011

doi:10.4304/jcm.6.7.540-548

the presence of the CAC unit is considered.

In summary our contributions are as follows:

Quantify the performance degradation due to CSI errors for both the SCSI and CCSI cases when only a discrete number of modulation and coding levels are available and a constraint on the target bit error rate is imposed.

Apply these results to a throughput maximizing scheduling algorithm and compare the performamce difference between the CCSI and SCSI based resource allocation schemes.

Propose a strategy that leads to a good tradeoff between overhead consumption and fairness as well as throughput when the presence of the CAC unit is considered.

The rest of this paper is organized as follows: the system model and the methodology used to calculate the probability of successfully selecting an MCS level is given in Section 2. The scheduling algorithm used in our simulations and the method proposed to make optimal use of the available resources for feedback is presented in Section 3. Simulation results are presented in Section 4. Finally, the paper is concluded in Section 5.

II. System Model

We consider a downlink OFDM system with K users and N subchannels. The time axis is divided into Transmission Time Intervals (TTIs). During each TTI, packets of fixed length arrive for each user at a given rate.We consider a downlink OFDM system with K users and N sub-channels. The time axis is divided into Transmission Time Intervals (TTIs) of length 1msec as specified in the LTE standard [1]. Each user accesses the same service whereas a CAC unit is assumed to limit the number of incoming flows so that the network can offer each flow its required QoS. If a request is accepted, the arriving packets are buffered in separate queues for each user. At the beginning of each TTI the BS schedules bandwidth transmission and allocates resources to each user according to their queue state and estimated/average SNR.

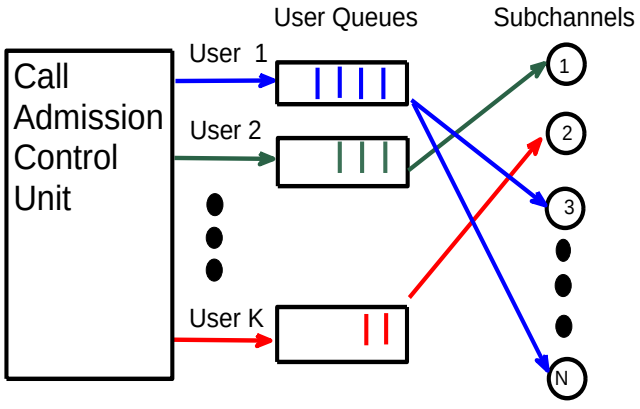

Figure 1. System Structure

A set of MCS levels are employed for AMC. Each MCS level is indexed by $m \in \{1, ..., M\}$, and its selection is determined by the value of the imperfect SNR which is denoted by $\hat{\gamma}$. The range of SNR values used for transmission is divided into M intervals by M SNR thresholds which are chosen in such a way that the information rate is supportable subject to a target BER constraint. These thresholds are denoted by Γ_m. Therefore, MCS m will be applied when $\Gamma_m \leq \gamma < \Gamma_{m+1}$. Also, it is assumed that $R_1 < R_2 < ..... < R_M$, where R_m is the spectral efficiency of MCS m. Each user k's channel gain on sub-channel n is denoted by h_{kn}. The channel gains are assumed to follow a complex Gaussian distribution with zero mean and unit variance, $h_{kn} \sim NC(0, 1)$.

Consider mobile user k whose outdated channel gain for sub-channel n is denoted by $\hat{h}_{kn}$ and the current channel gain which is denoted by h_{kn} . According to [3], when both $\hat{h}_{kn}$ and h_{kn} are complex Gaussian variables with a zero mean and unit variance, the conditional probability distribution function (pdf) $P(h_{kn}|\hat{h_{kn}})$ follows a complex Gaussian distribution with a mean equal to $\mu_k = \rho_k \hat{h_{kn}}$ and a variance of $\sigma_k = 1 - \rho_k^2$. In these expressions, ρ_k denotes the correlation coefficient between h_{kn} and $\hat{h}_{kn}$ and its value is $\rho_k = J_0(2\pi f_{d,k}\tau)$. Here, J_0 is the zeroth order Bessel function of the first kind, $f_{d,k}$ is the maximum Doppler frequency for user k, and τ is the channel feedback delay. In practical systems, if we can estimate the maximum Doppler frequency, this correlation coefficient can be obtained[11]. As $P(h_{kn}|\hat{h_{kn}})$ is Gaussian distributed, $P(|h_{kn}|\big|\hat{h_{kn}})$ follows a Ricean distribution. When the CSI is outdated, there will always be a nonzero probability of selecting an MCS level which is not optimized for the region where the current SNR lies (i.e selecting an MCS level which cannot meet the target BER). We define P_{knm} as the probability of successfully selecting an MCS level m on sub-channel n for user k. It is given as

$$P_{knm} = P(\gamma_{kn} > \Gamma_m) = Q_1\left(\frac{\rho_k\sqrt{\frac{\hat{\gamma}_{kn}}{\bar{\gamma}_{kn}}}}{\sigma_k}, \frac{\sqrt{\frac{\Gamma_m}{\bar{\gamma}_{kn}}}}{\sigma_k}\right), \quad (1)$$

where

$$Q_1(\alpha, \beta) = \int_\beta^\infty x I_o(\alpha x)\exp^{(-\frac{\alpha^2+\beta^2}{2})}, \quad (2)$$

is the Marcum Q function [12] and $\bar{\gamma}_{kn} = \frac{P_r}{N_o B}$ is user $k's$ mean SNR on sub-carrier n. The outdated and current SNR are $\hat{\gamma}_{kn} = \frac{P_r|h_{kn}|^2}{N_o}$ and $\gamma_{kn} = \frac{P_r|h_{kn}|^2}{N_o}$, respectively, where P_r is the received power and N_o is the noise spectral density. When SCSI is used to select MCS levels, P_{knm} for a Rayleigh fading channel becomes [13]

$$P_{knm} = P(\gamma_{kn} > \Gamma_m) = \exp\big(-\frac{\Gamma_m}{\bar{\gamma}_{kn}}\big). \quad (3)$$

As the use of outdated CSI or SCSI leads to errors when AMC is performed, it is useful to minimize them. In order to achieve optimal utilization of the available spectral resources whilst meeting the target BER requirements, the optimum MCS level m^* for each user k on subchannel n is chosen according to the following rule

$$m^* = \arg\max_m P_{knm} R_m \quad (4)$$

where P_{knm} is given by either (1) or (3) depending on whether outdated CSI or SCSI is used.

In this setting, we denote the maximum bandwidth normalized information rate that can be reliably transmitted by user k on subchannel n by G_{kn} which is given as

$$G_{kn} = P_{knm} R_m \quad (5)$$

The quantity G_{kn} is referred to as throughput throughout this paper.

III. SCHEDULING

A. Scheduling Algorithm

Scheduling generally aims to maximize the system throughput; however, user fairness needs to also be accounted for. Algorithms that simply maximize the system throughput lead to starvation of users at the cell edge and to an oversupply of bandwidth to users that are close to the BS.

A number of scheduling algorithms which assign resources to a set of selected users can be integrated into an OFDMA system. Queue and Channel aware algorithms are able to meet user QoS requirements, as one may need to sometimes schedule users whose delays/queues are becoming large even though their current channel state is not the most favorable. It was shown in [14] that Queue and Channel aware scheduling algorithms are throughput optimal, and that they lead to significant performance improvements for the LTE system [15]. In our work, equal power allocation across all sub-channels is assumed. It is noted in [16] that the throughput degradation arising from such an assumption is negligible when AMC is applied as with the case of LTE.

In order to maximize the throughput of the system whilst meeting the target BER of each user, a simple Queue and Channel aware algorithm will allocate sub-channel n to the user k^* for which the following holds

$$k^* = \arg\max_k P_{knm^*} R_{m^*} W_{k^*}(t) \tag{6}$$

where $W_k(t)$ is the head-of-line packet delay or queue length for user k during TTI t; and $P_{knm^*}R_{m^*}$ is the channel capacity that meets the target BER requirement assuming that the optimum MCS level m^* is selected according to (4). The throughput user k^* can achieve on subchannel n is

$$G_{k^*n} = P_{knm^*} R_{m^*} B \tag{7}$$

where B is the bandwidth of a subchannel.

For a subchannel n to be assigned in accordance with (6) the scheduler needs to search KM values of $P_{knm}R_m$ as the queue length can be considered a constant. Therefore, the computational complexity associated with allocating N subchannels to K users is $O(KMN)$.

B. Scheduling to provide a tradeoff between overhead and throughput/fairness

As the user velocity increases, the CSI has to be updated more frequently. Thus, large amounts of spectrum resources need to be reserved for overhead purposes if AMC is to be performed using CSI values that are correlated with the current value of the CSI. This leads to increased overhead requirements. The overhead load increases when a large number of active users are simultaneously present in the cell [4]. In particular, we require NKM bits per timeslot where M is the number of bits required to quantize a real number with negligible quantization error. This is clearly impractical for future mobile OFDMA systems such as LTE, as the capacity allocated for signaling purposes is limited [17]. Therefore it is useful to limit the amount of feedback bits. In this work, we confine the feedback to a set of users by making use of the following considerations.

In networks that support heterogeneous applications with diverse throughput requirements the call-admission control (CAC) unit becomes crucial. Firstly, it limits the number of incoming flows so that the required QoS can be provided to each flow. Secondly, it provides QoS guarantees by distributing the network throughput between the supported services. This is particularly important in networks that support a variety of services as one group of users may be more demanding than the rest, which results in an allocation of the network resources to the former and leaves the latter unsupported. Limiting the aggregate rate that the group of demanding subscribers receives imposes fairness and guarantees QoS for each service.

When the CAC unit functionality is accurate all users admitted into the network need to be satisfied in terms of QoS. A user situated at the edge of the cell requesting access to a specific service will need to be allocated more subchannels than a user with a high average SNR accessing the same service. By limiting periodic CSI feedback to the set of users with the lowest geometry (i.e., users SNR induced by the path-loss/shadowing model) more of the channels assigned by the scheduler will be loaded with CCSI. This scheme is also expected to increase the fairness of the system.

IV. NETWORK SIMULATION

In order to evaluate the importance of periodic CSI feedback as well as the strategy used to reduce the amount of feedback bits we perform system level simulations. Simulation parameters are based on [18] and these are typical values used for LTE simulation studies [14]. We consider a system with $10MHz$ of bandwidth divided into 666 subcarriers, 624 of which are used for data. The remaining 32 sub-carriers are used as guard sub-carriers which also need to be accounted for. The width of each carrier equals 15KHz. Resource allocation cannot be performed on a per sub-carrier basis due to the resulting overhead but is based on subchannels. In LTE [14] each subchannel consists of 12 subcarriers. Thus, N= 52 subchannels can be assigned to the users. The wireless environment is typical Urban Non Line of Sight (NLOS) and the carrier frequency equals 2GHz. The cell diameter is 1km; and the distance, d_k, between the kth user and the BS is a 2-D uniformly distributed random variable. The most suitable path loss model in this case is the COST 231 Walfisch-Ikegami (WI) [19] as it allows estimation of the pathloss from 20m [19]. The system level simulation parameters are summarized in Table I.

A schematic diagram of the simulation flow is given in Fig.2. When the simulation begins, each of the (K=25) users moves in a given random direction. The simulator updates the user location every 100 TTIs. During each TTI packets arrive for each user k's queue at a rate equal to the packet arrival rate. The packet size is selected such that the system capacity is roughly equal to 1 packet/user/TTI. In order to assign subchannels to these users so that packet transmission can occur the optimum MCS level m^* is required $\forall k, n$. When SCSI is used the pathloss model leads to the the average user SNR $\bar{\gamma}$ through which m^* can be obtained using (4). However, when CCSI is used, the values of $\hat{h}_{kn}$ are also needed. These depend on the power delay profile and the distribution of h_{kn} $(h_{kn}|\hat{h_{kn}} \sim NC(\rho\hat{h}_{kn}, \sqrt{1-\rho^2})$. Moreover, the values of ρ are also required. These are a function of τ (delay time between the channel estimation and the actual transmission) and the user velocity. The value of τ differs in each simulation run and is added to the CSI processing delay in order to obtain the total delay time. Using these values and (4) allows the optimum MCS level m^* to be found $\forall k, n$ for the case of CCSI. Finally, the queue and channel aware scheduler allocates subchannels to the users in accordance with (6). For each point in the figures presented in the Results section, we run the simulator for $1,000$ TTI's which for the LTE system is equivalent to a 1 second real-time period.

In order to reduce the computational load, link level simulation results are prepared in advance in the form of look-up tables for the throughput calculation, and these give the required SNR values needed to meet a specific target bit error rate. The defined MCS levels use coding rates between $1/8$ to $2/3$ combined with QPSK, 16QAM, and 64QAM modulation schemes. The MCS levels used in our simulations are shown in Table II.

TABLE I
KEY SIMULATION PARAMETERS

Parameter	Value	Comments
Carrier Frequency	2GHz	
Cell Configuration	single cell	
Cell Radius	1 km	
Channel Bandwidth	10MHz	In LTE the supported bandwidths are 1.4 MHz, 3 MHz, 5 MHz, 10 MHz, 15, MHz, 20 MHz[1]
subcarrier spacing	15KHz	This subcarrier spacing in LTE is 15KHz[1].
Total Number of data subcarriers	624	This results in 52 data subchannels.
BS Tx Power	46dBm	
BS Antenna Height	50m	
MS Antenna Height	2m	
Mean Buliding Heights	12m	
Mean Width of Streets	50m	
Mean Building Separation	100m	
Incident angle relative to street	90^o	
Path-Loss Model	COST 231 Walfisch-Ikegami	The Walfisch-Ikegami model is more appropriate for the cell size considered
Propagation Model	ITU Vehicular A	
Shadowing Log-Normal Deviation	8dB	
Thermal Noise Density	-174dBm/Hz	
Number of active Users	25	
Packet Size	500 bits	Packet size selected such that the system capacity is roughly equal to 1 packet/user/TTI
Packet Arrival Rate (P.A.R)	1,3 packets/user/TTI	
CSI Measurement Error	Ideal	Noisy channel estimation will not be a significant problem when a reasonably good estimator is used [3]
CSI Processing Delay	1 TTI	A 1 TTI processing delay is considered
CSI Reporting Period	2TTI	The BS requests feedback information every 2TTIs. When added to the CSI processing delay the feedback delay is equivalent to the baseline standard value in LTE [18]
TTI length	1msec	Length of a TTI in the LTE standard [1]

TABLE II
SELECTION OF MCS BASED ON RECEIVED SNR AND THE CORRESPONDING THROUGHPUT (TP)

SNR(dB)	Modulation	Coding Rate	Throughput (bps/Hz)
$\sim$ -5	No use		
-5 $\sim$ -1.9	QPSK	1/8	0.25
-1.9 $\sim$ 1.8	QPSK	1/4	0.5
1.8 $\sim$ 3.8	QPSK	1/2	1
3.8 $\sim$ 7.1	QPSK	2/3	1.33
7.1 $\sim$ 9.3	16QAM	1/2	2
9.3 $\sim$ 11.3	16QAM	2/3	2.67
11.3 $\sim$ 14.5	64QAM	1/2	3
14.5 $\sim$ 17.2	64QAM	2/3	4
17.2 $\sim$ 19.5	64QAM	0.81	4.86
19.5 $\sim$	64QAM	2/3	5.25

V. RESULTS

In this section, we present the impact of optimally selecting MCS levels on the system throughput when either CCSI or SCSI are used to perform AMC. By system throughput we refer to the maximum spectral efficiency that can be reliably transmitted. A comparison between the SCSI and CCSI resource allocation schemes in a fast fading environment is also presented. Then, we show that the limited resources reserved for feedback can be optimally used when the users with the lowest average SNR's send their CSI to the BS.

A. Impact of optimally selecting MCS levels

As AMC is always performed using imperfect CSI there will be a nonzero probability that the selected MCS level will not be optimized for the region where the current SNR lies. Fig.3 compares the throughput of a system when MCS levels are

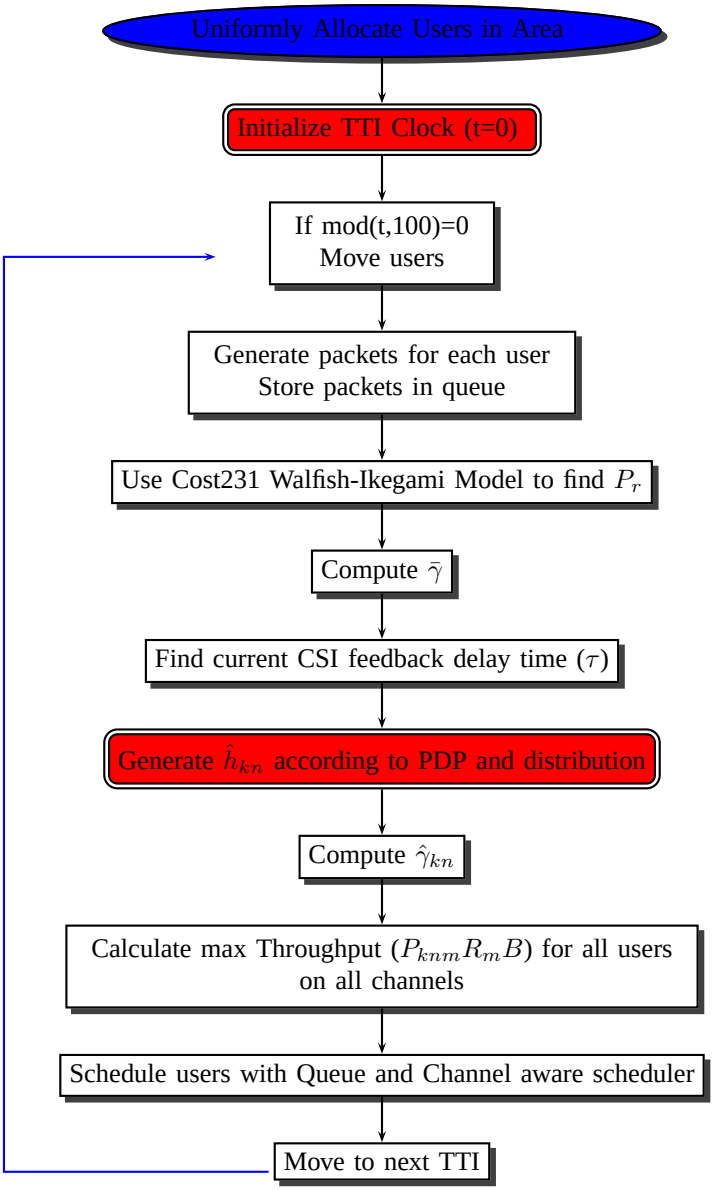

Figure 2. Block Diagram of Simulation Flow

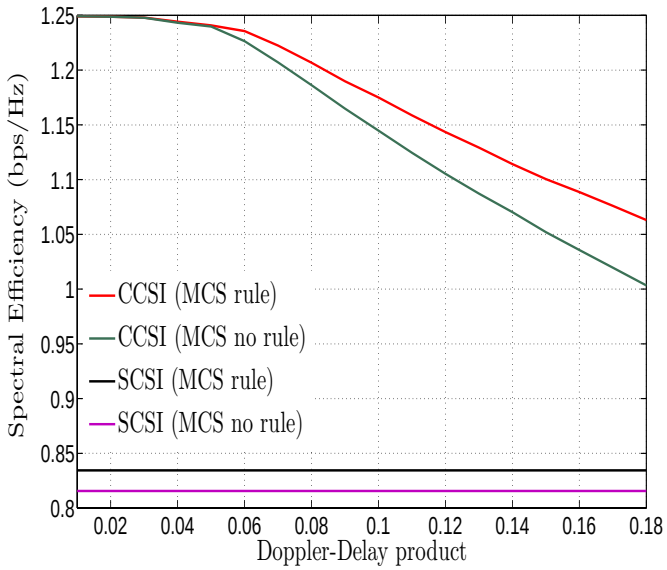

Figure 3. Spectral Efficiency vs $f_d\tau$ (packet arrival rate=1 packet/user/TTI)

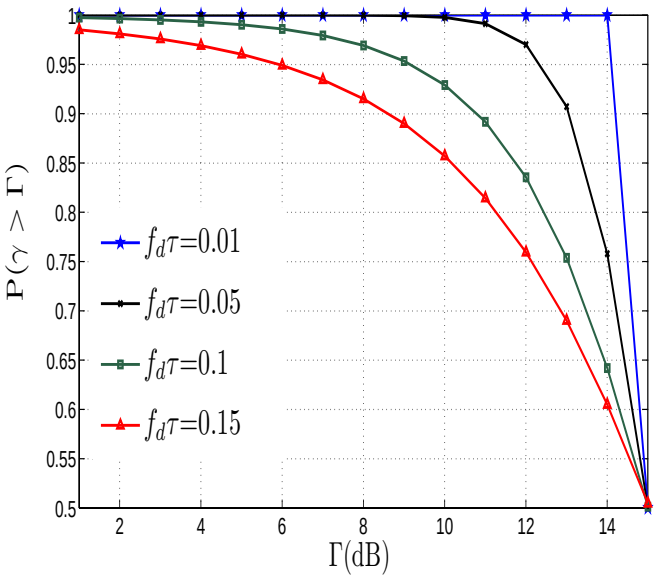

Figure 4. Probability of Exceeding an SNR threshold (Γ) vs Γ for different values of the Doppler-Delay product and $\hat{\gamma} = 15dB$

selected using the outdated/average SNR with the performance of the same system when (4) is used to perform AMC.

For the periodic CSI feedback scheme, these gains are lower when the value of the Doppler-Delay product $f_d\tau$ is small. As the value of $f_d\tau$ grows, the CSI becomes more outdated, and more MCS level selection errors occur. Therefore, the impact of the MCS level selection scheme is stronger. In Fig.4, we show that the probabilities of successful MCS level selection remain high as the value of $f_d\tau$ grows. This implies that high values of the throughput can be realized.

Using the rule of (4) to select MCS levels also leads to performance gains when SCSI is used to perform resource allocation. These results show that for the case where only a discrete number of modulation and coding levels are available maximizing the expected sum-rate leads to important throughput gains. These results are in agreement with those of [5] which focus on the continuous rate case (Shannon-capacity based formulation) and therefore have more theoretical rather than practical significance.

It is also important to present the impact of imperfect CSI on the bit error rate of the system as the value of $f_d\tau$ varies when a constraint on the target BER is not imposed on the system. As shown in [16], the instantaneous BER for M-QAM modulation schemes (as well as for BPSK) can be approximated for each user as

$$BER(\gamma) \approx 0.2 \exp^{-1.6\frac{\gamma}{2^{\lfloor r(\gamma) \rfloor}-1}}, \quad (8)$$

where $r(\gamma)$ denote the number of bits per symbol corresponding

to the applied modulation scheme and $\lfloor x \rfloor$ is the floor operation which provides the largest integer not greater than x. Fig.5 presents results showing the variation of the bit error rate with $f_d\tau$. Results show that in this case the use of CCSI leads to improved BER performance with the BER of the two cases approaching as the Doppler-Delay product grows.

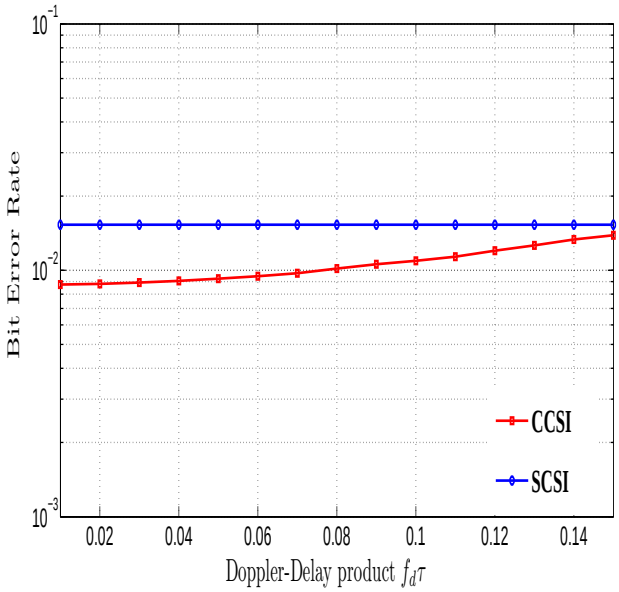

Figure 5. BER vs $f_d\tau$ for CCSI and SCSI based resource allocation schemes when a constraint is not imposed on the target BER

Fig.6 shows throughput vs velocity curves for a CSI measurement reporting period equal to 2 TTI's. The packet arrival rate for each user equals 1 packet/user/TTI. A processing delay time of one TTI is assumed with velocities ranging from 2km/h through 40km/h. Beyond these speeds, there is little correlation between the outdated and current CSI for the parameters considered. Results obtained for the case when the BS knows the instantaneous CSI (ICSI) are also plotted to provide a baseline comparison. When compared to SCSI, this figure shows that periodic CSI measurements lead to significant throughput gains for all of the velocities considered. In particular, a 43% throughput gain is observed when the user velocity equals $40km/h$.

B. Providing a tradeoff between overhead and throughput/fairness

It was established in the previous subsection that when the scheduler works with CSI that is correlated with its current state, significantly higher overall system throughput gains can be achieved. These gains are important even at high user velocities. However, they come at the cost of increased overhead requirements. This overhead load increases with user velocity and the number of active users present in the cell. Therefore, in a fast fading environment it is impractical to assume that all users feedback their CSI to the BS. In this section, we apply the strategy presented in Section 3 to the network under consideration. We divide the $K = 25$ active users present in the cell into two groups according to the value of their average SNR. The first group consists of the 13 users with the highest average SNR which are named Group A users. The remaining 12 users are called Group B. It is assumed that appropriate Connection Admission Control is performed so that the minimum user data rates are feasible for each user. For the duration of this simulation, users of Group B cannot move closer to the BS than any of the Group A users so that accurate results can be obtained.

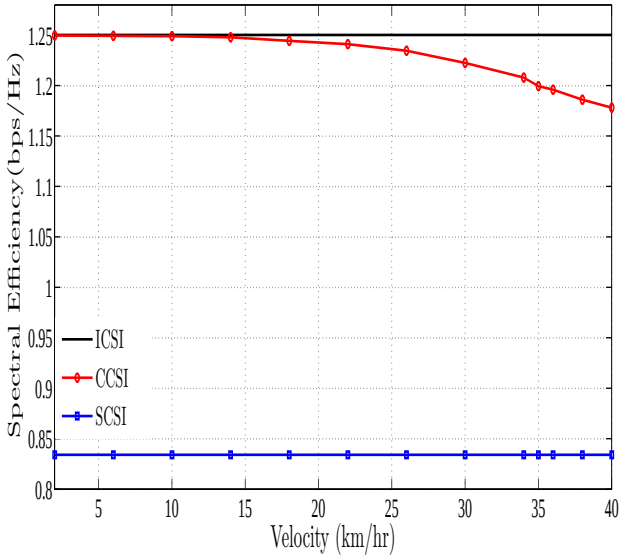

Figure 6. Spectral Efficiency vs Velocity when ICSI, SCSI and CCSI is used to perform resource allocation (packet arrival rate=1 packet/user/TTI)

The following cases are considered for evaluation
Case 1: Periodic CSI is received by the BS for all of the active users in the cell.
Case 2: Periodic CSI is received by the BS for only Group B users.
Case 3: 12 users (half from Group A and the other half from Group B) periodically send their CSI to the BS.
Case 4: Only Group A users send their CSI to the BS.
Case 5: No users send their CSI to the BS (only the average SNR of each active user is known by the BS).

In order to quantify the degree of fairness, we use Jain's fairness index which is defined as [20]

$$J = \frac{(\sum_{k=1}^{K} T_k)^2}{N \sum_{k=1}^{K} T_k^2} \tag{9}$$

where T_k is user $k's$ average throughput.

This factor measures the spread in the users' average throughputs T_k, and its value will always be within the range $1/N$ to 1 [20]. It can easily be verified that J = 1 indicates absolute fairness, whereas $J = 1/N$ indicates no fairness (all resources are allocated to a single user).

Figs 7 and 8 present the variation of the system's throughput and Jain's fairness factor with velocity for each of the cases considered. These figures show that when the users of Group B periodically send their CSI to the BS, higher throughput and fairness compared to the other cases (Case 3,4,5) is achieved. To see why Case 2 performs better we note that the employed CAC scheme has admitted 25 users into the network and that the packet arrival rate equals 1 packet/user/TTI. When Group A users do not periodically feedback their CSI their average queue lengths are not significantly affected as can be seen from the difference between Case 2 (Group A users do not feedback their CSI) and Case 4 (Group A users feedback their CSI) in Fig.9. This implies that allowing Group A users to feedback their

CSI does not lead to efficient usage of the resources allocated for overhead purposes. However, as users move further from the BS, they require more channels to meet their QoS demands. By enabling the users furthest from the BS to feedback their CSI a higher overall system throughput can be realized. This is because a higher number of allocated channels will have been bit-loaded with CCSI. Therefore, unlike [4], where only the users whose subchannel SNR exceeds a certain threshold feedback their channel quality, these results show that when a CAC unit is employed in conjunction with a scheduler, the queue states need to also be accounted for when deciding which users should feedback their CSI to the BS.

When there is no CAC functionality Case 4 (users with high average SNR feedback their CSI) yields the highest throughput. This is shown in Fig.10 where the 25 users each request a more bandwidth intensive service. The absence of CAC is depicted in Fig 12 which shows the very high queue lengths associated with Group B users when the packet arrival rate for each of the 25 users equals 3 packets/TTI. The absence of CAC functionality also leads to poor fairness as can be seen from Fig.11. In terms of fairness, the Jain factor remains higher for Case 2 regardless of the CAC scheme. This can be observed in Figs 8,11.

All these results show that as at high velocities, a high amount of overhead is needed for the BS to work with CSI that is correlated with the current CSI and the system-wide spectral resources available for feedback are limited; allowing only the users with the lowest average SNR to periodically send their CSI to the BS leads to a better tradeoff between the bandwidth occupied for feedback and throughput/fairness when an accurate CAC scheme is employed.

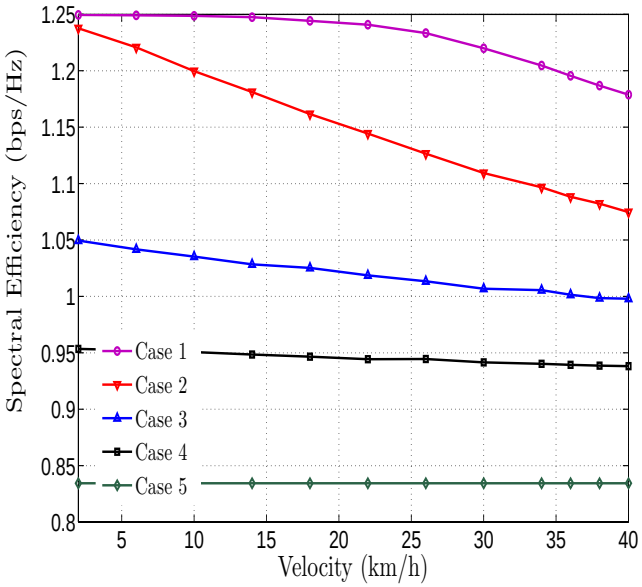

Figure 7. Spectral Efficiency vs user velocity for the 5 different cases considered (packet arrival rate =1 packet/user/TTI)

VI. Conclusion

This work shows that optimally selecting MCS levels leads to a performance enhancement when either SCSI or CCSI is used to perform resource allocation. A comparison between the SCSI and CCSI schemes shows that the use of CCSI leads to important throughput gains even under significant user mobility. Since in a fast fading environment, excessive overhead is required for the scheduler to continuously work with CCSI, we presented a strategy to optimally use the limited resources reserved for feedback purposes. Simulation results showed that this strategy leads to a higher overall fairness and system throughput when CAC functionality is considered.

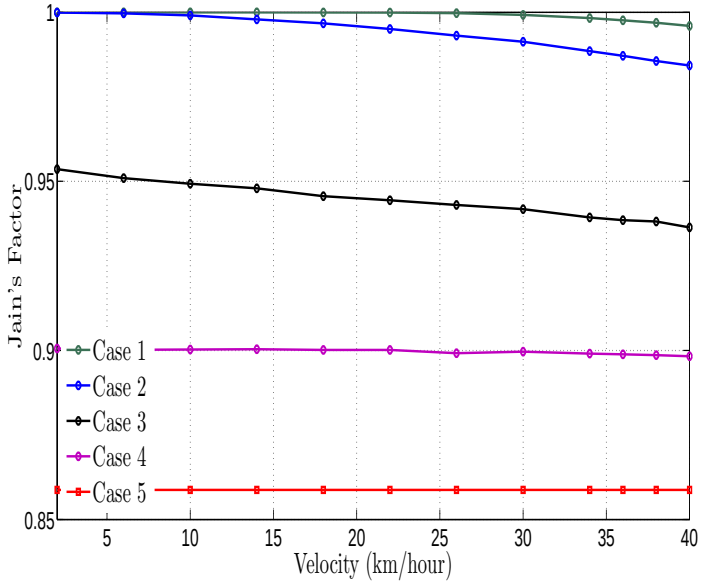

Figure 8. Jain Factor vs user velocity for the 5 different cases considered (packet arrival rate =1 packet/user/TTI)

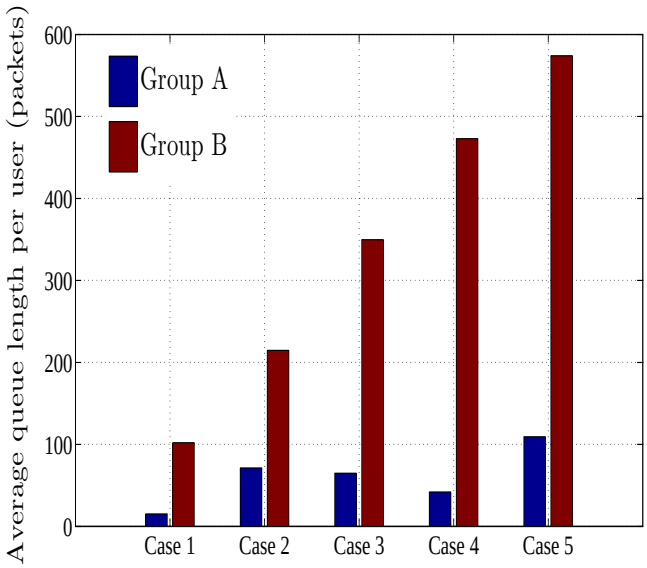

Figure 9. Average Queue length for the 5 different cases considered (packet arrival rate =1 packet/user/TTI, user velocity=40km/hour)

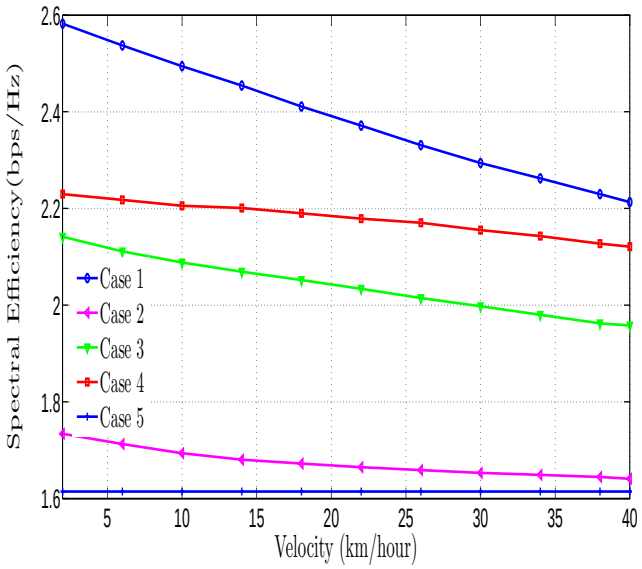

Figure 10. Spectral Efficiency vs user velocity when CAC unit not employed (packet arrival rate =3 packets/user/TTI)

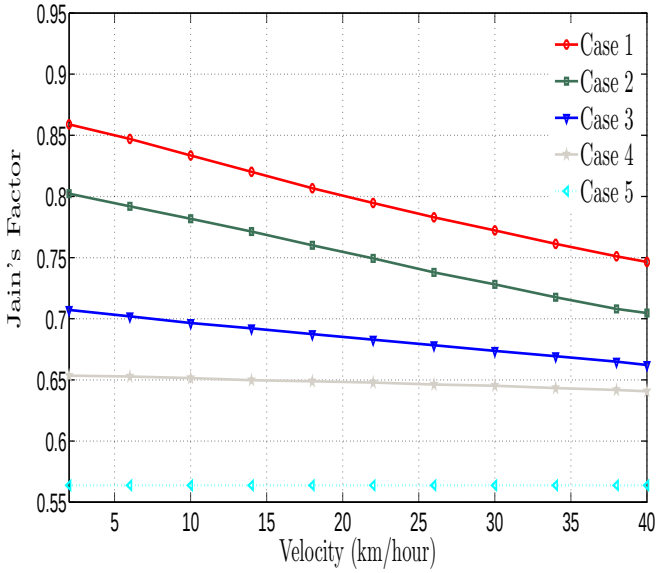

Figure 11. Jain Factor vs velocity when CAC unit not employed (packet arrival rate =3 packets/user/TTI)

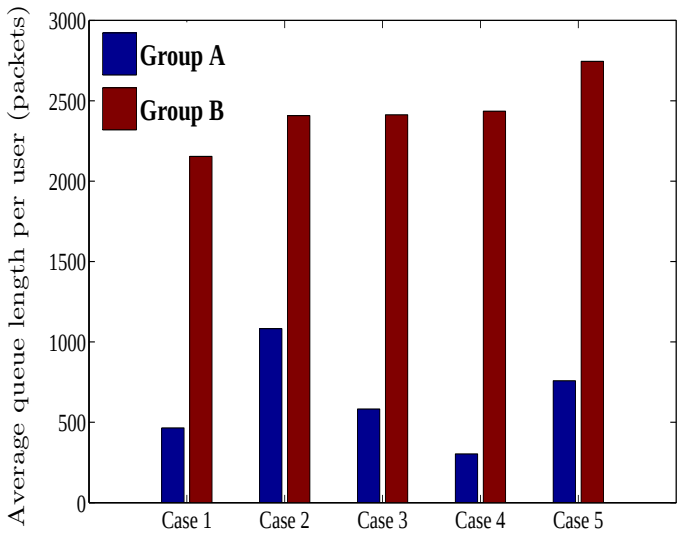

Figure 12. Average queue length when CAC unit not employed (packet arrival rate =3 packet/user/TTI, user velocity= 40km/hour)

REFERENCES

[1] S.Sesia, I.Toufik and M.Baker, LTE- The UMTS Long Term Evolution-From Theory to Practice, John Willey and Sons, 2009.

[2] B.Evans and B.I.Wong, Resource Allocation in Multiuser Multicarrier Systems, Springer Science and Media, 2008.

[3] Y.Sigen, R.Blum and L.Cimini, "Adaptive OFDM with Imperfect CSI," *IEEE Trans. Wireless Commun.*, vol. 5, no. 11, pp. 3255-3265, Nov. 2006.

[4] D.Gesbert and M.S. Alouini, "How much feedback is multi-user diversity really worth,?" *IEEE Int. Conf. on Commun.*, vol.1, pp. 234-238, Jun. 2004.

[5] F.Brah, J.Louveaux and L.Vandendorpe, "CDIT-Based Constrained Resource Allocation for Mobile WiMAX Systems," *EURASIP Journal on Wireless Communications and Networking*, vol. 2009, Article ID 425367, 8 pages, 2009.

[6] Y.Yao and G.B.Giannakis, Rate-Maximizing power allocation in OFDM based on partial CSI knowledge, *IEEE. Trans. Wireless Comm*, vol.4, pp. 1073-1083, May 2005.

[7] Y. Zhang and K. Letaief, Multiuser subcarrier and bit allocation along with adaptive cell selection for OFDM transmission, *Proc. IEEE Int. Conf. on Commun.*, vol. 2, pp. 861-865, Apr. 2002.

[8] D. Kivanc, G. Li, and H. Liu, Computationally efficient bandwidth allocation and power control for OFDMA, *IEEE Trans. Wireless Commun.*, vol. 2, no. 6, pp. 1150-1158, Nov. 2003.

[9] S.Stefanatos and N.Demetriou, "Downlink OFDMA Resource Allocation under partial Channel State Information," *IEEE Int. Conf. on Commun.*, pp. 1-5, June 2009.

[10] Sivridis. L, Choi, J and Li, Yue "A cost based resource allocation policy for multiservice mobile WiMAX networks," *IEEE ISWPC 2010*, pp. 489-494, May 2010.

[11] J.M.Holtzmann and A.Sampath," Adaptive averaging methodology for handoffs in cellular systems," *IEEE Trans.Veh.Technol.*, vol.44, pp. 59-66, Feb. 1995.

[12] J.Marcum, A statistical theory of target detection by pulsed radar: Mathematical appendix, RAND Corporation, California, Research Memo RM-753, July 1948.

[13] J.Proakis, Digital Communications, 4th ed. New York: McGraw-Hill, 2001.

[14] M.Andrews, A.Kumaran, A.Ramanan, A.Stolyar and P.Whiting, "Providing quality of service over a shared wireless link," *IEEE Comm. Mag.*, pp. 150-154, Feb. 2001.

[15] B.Sadiq, R.Madan and A.Sampath, "Downlink Scheduling for Multiclass traffic in LTE,"*EURASIP Journal on Wireless Communications and Networking*, vol. 2009, Article ID 510617, 18 pages, 2009.

[16] S. T. Chung , A. Goldsmith,"Degrees of Freedom in Adaptive Modulation: A Unified View," *IEEE. Trans. Commun.*, vol.49, pp. 1561-1571, Sep. 2001.

[17] H.Holma and A.Toskala, LTE for UMTS OFDMA and SC-FDMA based Radio Access, John Wiley and Sons, 2009.

[18] 3GPP TSG-RAN, TR25.814: Physical Layer Aspects for Evolved UTRA, Version 7.0.0, June 2006.

[19] IEEE 802.16 Broadband Wireless Access Working Group,Multihop Relay System Evaluation Methodology (Channel Model and Performance Metric), 2007.

[20] R.Jain, The art of computer systems performance analysis, John-Wiley and Sons, 1991.

Leonidas Sivridis is currently a Ph.D student at Swansea University, Swansea, U.K. He received his MSc degree in Communications and Radio Engineering from the Department of Electronic Engineering, Kings College London, London, U.K. His research interests include resource management in wireless networks and multiuser communications.

Dr. Xinheng (Henry) Wang is a senior lecturer in wireless communications at IAT. He graduated from Xian Jiaotong University with a BEng and an MSc degree in 1991 and 1994, respectively and obtained his PhD degree from Brunel University in 2001. He then worked as a post-doctoral research fellow at Brunel from June 2001. He joined Kingston University in 2003 as a senior research fellow and was promoted to a senior lecturer in June 2004. In September 2007 he joined the IAT to take up the senior lecturership. He is also a visiting professor at University of Electronic Science and Technology of China. His current research interests are wireless mesh and sensor networks, personal area networks, and their applications in healthcare.

Prof. Jinho Choi received his B.E. (magna cum laude) degree in electronics engineering in 1989 from Sogang University, Seoul, and his M.S.E. and Ph.D. degrees in electrical engineering from Korea Advanced Institute of Science and Technology (KAIST), Daejeon, in 1991 and 1994, respectively. He is currently working with the Wireless Research Group within IAT. His research interests include wireless communications and array/statistical signal processing. He authored a book entitled Adaptive and Iterative Signal Processing in Communications (Cambridge University Press, 2006).

A Reliable Routing Scheme for Post-Disaster Ad Hoc Communication Networks

Muhammad Ibrahim Channa, Kazi M. Ahmed
School of Engineering and Technology, Asian Institute of Technology, Thailand
Email: {muhammad.ibrahim.channa, kahmed}@ait.ac.th

***Abstract*— The natural or man-made disaster demands an efficient communication and coordination among first responders for successful emergency management operations. During emergency situations such as an earthquake or a flood, the traditional telecommunication infrastructure may be damaged and may not provide adequate communication services to emergency management teams. Mobile ad hoc networks are used in such type of situations for exchanging emergency related information. During emergency situation, the deployed ad hoc communication network may itself be prone to failures and vulnerable to malicious threats. The first responders use real-time applications for exchanging emergency related information, which may create network congestion. The significant loss of emergency related information may cause mismanagement of emergency response efforts. We propose a reliable routing scheme for post-disaster ad hoc communication networks, which finds the shortest possible routes with all reliable nodes. The proposed scheme also detects packet forwarding misbehavior caused by network fault or congestion in an active route and reroutes packets through other reliable route. The performance of the proposed scheme is evaluated in terms of packet delivery ratio, end-to-end delay and routing overhead through extensive simulations.**

***Index Terms*— Post-disaster communications, Mobile ad hoc network, Reliable routing, Broken nodes, Network congestion**

I. INTRODUCTION

It is a great challenge for public emergency services to cope with the crisis situations arising due to natural or man-made disasters. The most common disasters include earthquakes, floods and nuclear explosions. It is necessary to provide relevant information to concerned rescue workers in a timely manner for coping with such disasters in an effective and coordinated manner [1]–[4]. As coordination requires current information within and among various rescue organizations in real time, the deployment of an integrated information and communication system is essential for efficient, reliable and secure exchange of information [5]. A large scale emergency response operation involves multi-organizational teams including public authorities, volunteer organizations and the media. These entities work together as a virtual team to save lives and other community resources [6].

The availability of telecommunication services is of great importance during emergency situations, as it is the only means of communication among first responders, affected people and emergency management centers. During Hurricane Katrina [7], [8], the existing telecommunication infrastructure was badly damaged and the remaining parts of the network were not able to provide adequate communication services to the first responders [9]. In such type of situations, mobile ad hoc networks [10] are commonly used for exchanging emergency related information. These networks don't rely on existing infrastructure such as access points or base stations and configure automatically [11] when the network size varies dynamically. Figure 1 shows the deployment of an ad hoc communication network in a disaster affected area. The emergency site ad hoc communication network is connected with emergency management centers, hospitals, NGOs and media centers through gateway nodes and wide area network.

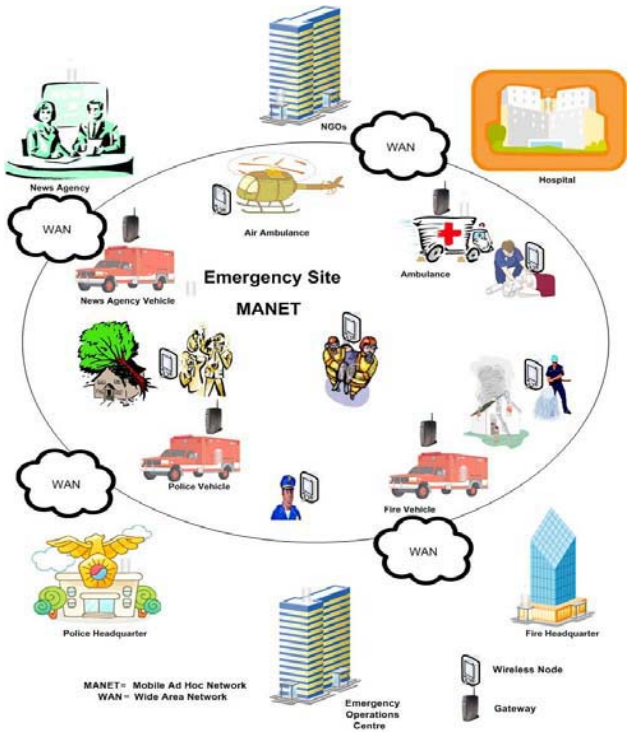

Figure 1. The deployment of an ad hoc communication network at emergency site

An emergency response network comprises of mobile devices such as smart phones and PDAs used by different rescue workers belonging to different rescue

Manuscript received February 05, 2011; revised April 30, 2011; accepted June 05, 2011

doi:10.4304/jcm.6.7.549-557

organizations. Reliable and robust communication is vital for successful emergency response operations [9]. The reliability of a network is its ability to perform a designated set of functions under dynamically changing conditions. During emergency situation, the deployed ad hoc communication network may itself be prone to failures and vulnerable to malicious threats [6]. An ad hoc communication network failure has life-or-death significance during emergency situations. A node may be broken by experiencing some software or hardware fault which prevents it from forwarding the packets successfully. A malicious node may launch a Denial of Service (DoS) attack [12] to create communication interruptions among first responders and is beyond the scope of this article. The first responders use real-time applications for exchanging emergency related information. The increasing number of simultaneous communications among first responders may create congestion in some parts of the network. A congested node may lack the CPU cycles, buffer space or available bandwidth to forward packets successfully. The significant loss of emergency related information may cause mismanagement of emergency response efforts.

Several reliable routing schemes have been proposed for mobile ad hoc networks. In weight-based reliable routing scheme [13], a route having more energy, less error rate and shorter length is selected for data transmissions. In cross-layer energy aware reliable routing scheme [14], the node's residual energy is used as a route selection metric. The mobility sensitive routing approach [15] is a multi-protocol scheme which activates an appropriate routing scheme based on the mobility pattern of the network nodes. In distributed long lifetime routing scheme [16], the source node forwards data through the shorter route while keeping longer route as backup. In reliable source routing scheme [17], the source node finds a route meeting the reliability requirements of the application. The stable and energy efficient routing scheme [18] uses node stability and energy efficiency as route selection metrics. The cross-layer reliable routing scheme [19] uses received signal strength to find reliable links in an stable route. The reliable multi-rate ad hoc routing protocol [20] uses route assessment index (RAI) to find the shortest possible route with high capacity links. The reliable dynamic source routing for video streaming [21] uses service feedback information to compute reliability of paths. The reliability map based routing (RMR) scheme [22] constructs reliability maps of deployment region and performs routing by avoiding compromised cells. The secure neighbor discovery scheme [23] prevents a legitimate or a malicious node from being incorrectly added to the neighbor list of another legitimate node. The network coding with imperfect overhearing scheme [24] improves overall system performance in cooperative relay networks. The secure packet transfer scheme [25] uses repeated games to identify malicious nodes in wireless sensor networks.

The proposed schemes use node energy [13], [14], [18], node mobility [15], route lifetime [16], successful data transmissions [17], signal strength [19], link capacity [20] and service feedback [21] as reliability metrics. None of the schemes addresses dynamic detection of packet forwarding misbehavior caused by network fault or congestion. We propose a reliable routing scheme for post-disaster ad hoc communication networks, which finds the shortest possible routes with all reliable nodes. The reliability of a node is computed by aggregating its packet forwarding behavior information. The proposed scheme also reroutes packets through other reliable route if some faulty or congested node performs packet forwarding misbehavior in an active route. The proposed scheme uses node reliability and end-to-end delay as route selection metrics.

The rest of the paper is organized as follows. Section II presents network model. Section III describes the proposed reliable routing scheme. Section IV comprises of the simulation results and section V concludes the paper.

II. Network Model

An ad hoc network is modeled as a graph $G = (V, E)$, where V represents the set of nodes and E represents the set of links between nodes. A path P of length l consists of a set of nodes $i, j, k, ..., n \in V$ and $(i, j) \in E$. We assume that the links are bidirectional, so if $(i, j) \in E$ then $(j, i) \in E$. Node i establishes wireless links with all its neighbors N_i, which are within its transmission range T_i. If the distance between node i and node j is greater than T_i, link (i, j) is assumed to be broken. All nodes are uniformly distributed over the network and each node moves independently in a random direction with a random speed. We model the behavior of a faulty or congested node j through a random variable $X(j)$, which follows the Bernoulli distribution as follows:

$$X(j) = \begin{cases} 1 & j \text{ forwards packet to } k \\ 0 & \text{otherwise} \end{cases} \quad (1)$$

We further assume that a faulty node performs packet forwarding misbehavior continuously by dropping random number of received packets. A reliable node may perform packet forwarding misbehavior randomly while experiencing significant congestion.

III. Proposed reliable routing scheme

The proposed reliable routing scheme comprises of three major components namely Reliability Manager, Route Setup and Route Maintenance. The *Reliability Manager* is responsible for maintaining reliability information about neighbor nodes and stores this information in reliability database. The *Route Setup* establishes the shortest possible route comprising of only reliable nodes. If some broken or congested node performs packet forwarding misbehavior in an active route, the *Route Maintenance* is initiated by Reliability Manager to inform the source node to establish a new reliable route.

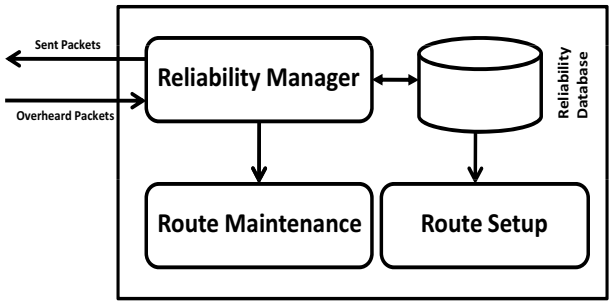

Figure 2. Reliable routing scheme model

The proposed reliable routing scheme is implemented by extending Ad Hoc On Demand Distance Vector (AODV) [26] routing protocol. The AODV routing protocol is preferred as it is on-demand, provides fresh enough routes and is more scalable. The on-demand approach enables AODV to find routes when desired and reduces control packet overhead. The sequence numbers act as time stamps and help AODV to find up-to-date route to a destination. In AODV, if a node is part of a route, it stores single entry for the destination in its routing table. This reduces storage overhead at each node and makes AODV more scalable. The proposed reliable routing scheme model is shown in figure 2.

A. Reliability Manager

The Reliability Manager maintains reliability information about neighbor nodes by overhearing their transmission in promiscuous mode [27] and identifies misbehaving nodes dynamically. In promiscuous mode, if node j is within transmission range of node i, node i can overhear transmission to and from node j even if those communications don't involve node i. When a data packet is sent by node i to node j, the Reliability Manager at node i stores the packet information such as packet ID, source address and destination address in its buffer and increments the value of $S_{i,j}$ by one. When node i overhears a packet from one of its neighbors, it compares the ID, source address and destination address of the overheard packet with all entries in its buffer. If there is a match, the Reliability Manager at node i assumes successful forwarding of the packet by node j to its next hop and increments the value of $F_{i,j}$ by one. The corresponding entry is then removed from the buffer at node i.

The Reliability Manager at node i evaluates the packet forwarding behavior of neighbor j for every n consecutively forwarded packets. This helps the Reliability Manager at node i to obtain the latest packet forwarding behavior of neighbor j. The value of n should be selected based on certain assumptions. First, the Reliability Manager at node i takes reasonable amount of time to evaluate packet forwarding behavior of neighbor j. Second, if node j is a broken node, the packet loss should be minimum. Third, if node j stay near the boundary of the transmission range of node i and starts moving away from node i, node i overhears n packets from node j to complete its behavior evaluation before node j moves out of its transmission range. The value of n is computed as the product of application's packet rate per second A_r and behavior evaluation time interval Δ_t as follows:

$$n = A_r \times \Delta_t \tag{2}$$

We assume that all applications generate the same number of packets per second. When the number of packets sent by node i to node j reaches n, the Reliability Manager at node i computes the packet forwarding ratio of node j as follows:

$$Pfr_{i,j} = \frac{F_{i,j}}{S_{i,j}} \tag{3}$$

where $S_{i,j} = n, F_{i,j} \leq n$ and $n > 0$

The Reliability Manager at node i categorizes the packet forwarding behavior of neighbor j in one of the two categories. If the packet forwarding ratio of node j is greater than or equal to packet forwarding threshold Th_{pfr}, it is known as positive behavior of node j observed at node i, otherwise; it is known as negative behavior of node j observed at node i. The positive and negative behaviors of node j observed at node i can be represented by $B_{p_{i,j}}$ and $B_{ni,j}$ respectively. If there is a positive behavior of node j observed at node i, $B_{p_{i,j}}$ is incremented by one as follows:

$$B_{p_{i,j}} = \begin{cases} B_{p_{i,j}} + 1 & Pfr_{i,j} \geq Th_{pfr} \\ B_{p_{i,j}} & Pfr_{i,j} < Th_{pfr} \end{cases} \tag{4}$$

Similarly, if there is a negative behavior of node j observed at node i, $B_{ni,j}$ is incremented by one as follows:

$$B_{ni,j} = \begin{cases} B_{ni,j} + 1 & Pfr_{i,j} < Th_{pfr} \\ B_{ni,j} & Pfr_{i,j} \geq Th_{pfr} \end{cases} \tag{5}$$

If there is a negative behavior of node j observed at node i, the Reliability Manager at node i initiates the *Route Maintenance* to inform the source node to establish a new reliable route. The value of Th_{pfr} should be selected in such a way that if node j drops significant number of received packets, the remaining packets may be rerouted through other reliable route. After each evaluation of node j made by node i, the value of $S_{i,j}$ and $F_{i,j}$ is reset to zero.

The Reliability Manager at node i uses Beta probability density function [28] to compute the expected probability of positive behavior of neighbor j. The Beta family of probability density functions is a continuous family of functions indexed by two parameters α and β. The Beta distribution $f(p|\alpha, \beta)$ can be expressed by using Γ function as follows:

$$f(p|\alpha, \beta) = \frac{\Gamma(\alpha + \beta)}{\Gamma(\alpha)\Gamma(\beta)} p^{(\alpha-1)}(1-p)^{(\beta-1)} \tag{6}$$

where $0 \leq p \leq 1, \alpha > 0$ and $\beta > 0$

If there is a binary process with two possible outcomes $\{x, \bar{x}\}, r$ represents the observed number of outcome x and s represents the observed number of outcome $\bar{x}$, then the probability density function of outcome x in future can be obtained by setting the values of α and β as follows:

$$\begin{aligned} \alpha &= r + 1 \\ \beta &= s + 1 \end{aligned} \tag{7}$$

where $r, s \geq 0$.

The probability expectation value of Beta distribution function is given by:

$$E(p) = \frac{\alpha}{\alpha + \beta} \tag{8}$$

Let r represents the number of positive behaviors of node j observed at node i i.e $B_{p_{i,j}}$, and s represents the number of negative behaviors of node j observed at node i i.e $B_{ni,j}$. The expected probability of the positive behavior of node j observed at node i can be computed by using Eq.(7) and Eq.(8) as follows:

$$E(p)_{i,j} = \frac{(B_{p_{i,j}} + 1)}{(B_{p_{i,j}} + 1) + (B_{ni,j} + 1)} \tag{9}$$

where $B_{p_{i,j}} \geq 0$, and $B_{ni,j} \geq 0$

The expected probability of positive behavior of a node also represents its reliability index. If a node's expected probability of positive behavior is higher, its reliability index is also higher and vice versa. During initial communications, a reliable node may experience congestion and may drop significant number of received packets exhibiting negative behavior. It is preferable to obtain at least m number of behavior evaluations of a node in order to predict its future behavior. The value of m should be selected in such a way that it gives a reasonable evidence about the packet forwarding behavior of a node. If a node performs packet forwarding misbehavior continuously due to some fault, the expected probability of its positive behavior decreases gradually. If a node performs packet forwarding misbehavior randomly due to congestion, the expected probability of its positive behavior varies accordingly.

Let $C_{i,j}$ represents the class of node j evaluated by node i. If node j is reliable, the value of $C_{i,j}$ will be 1 and 0 otherwise. Node i classifies node j based on the following criteria. If the number of behavior evaluations made by node i for node j is less than m, node i assumes node j as a reliable node. Node j is also said to be reliable if the total number of behavior evaluations made by node i for node j is greater than or equal to m, and the expected probability of the positive behavior of node j evaluated by node i i.e $E(p)_{i,j}$ is greater than or equal to positive behavior probability threshold Th_{prob}. If the value of

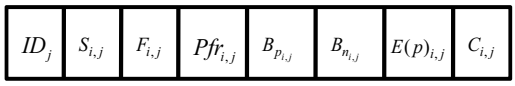

Figure 3. The structure of reliability database at node i

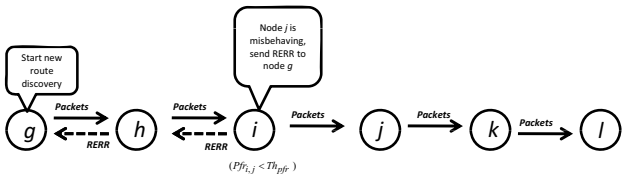

Figure 4. The route maintenance process

$E(p)_{i,j}$ is less than Th_{prob} after m behavior evaluations, node i assumes node j as unreliable as follows:

$$C_{i,j} = \begin{cases} 1 & B_{p_{i,j}} + B_{ni,j} < m \\ 1 & B_{p_{i,j}} + B_{ni,j} \geq m, E(p)_{i,j} \geq Th_{prob} \\ 0 & B_{p_{i,j}} + B_{ni,j} \geq m, E(p)_{i,j} < Th_{prob} \end{cases} \tag{10}$$

The value of Th_{prob} may be selected in such a way that the maximum number of reliable nodes may be used for routing packets. For example; a node having an equal probability of positive and negative behavior may be selected for routing packets. The Reliability Manager at node i stores the reliability information about neighbor j in reliability database as shown in figure 3.

B. Route Maintenance

In traditional AODV [26] routing protocol, the Route Maintenance is initiated when a link break occurs in an active route. In our proposed scheme, the Route Maintenance is also initiated when some node performs packet forwarding misbehavior in an active route. When an intermediate node along a given route identifies a link break or packet forwarding misbehavior, it generates a Route Error (RERR) message and sends it to the source node. All nodes including the source node and the reporting node invalidate the route to the destination and the source node initiates a new route setup process. The Route Maintenance process is described in figure 4. When the condition $Pfr_{i,j} < Th_{pfr}$ becomes true, the Reliability Manager at node i assumes node j as a misbehaving node and sends *RERR* message to source node g for finding a new reliable route. Node i, node h and node g delete the route to destination l from their routing tables and source node g starts a new route setup process as described in the following section.

C. Route Setup

The proposed scheme extends the route setup process of AODV [26] routing protocol to find the shortest possible route with all reliable nodes. The Route Setup uses node reliability and end-to-end delay as route selection metrics. The reliable nodes deliver the packets to destination with high probability. The shortest possible route

reduces power consumption in the network as fewer nodes participate in packet forwarding along a given route. We assume that the network topology does not change during the route setup process.

We assume a network where node e is the source and node k is the destination. When node e wants to send data to node k and it does not have route to the same, it starts route discovery by broadcasting Route Request (RREQ) message to its neighbors N_e. Node e specifies the packet rate per second A_r in the *RREQ* packet's *Reserved* field. The nodes in N_e compute the value of n as described earlier, make reverse route entry for node e and forward *RREQ* message to their neighbors. This process continues until the *RREQ* reaches at node k. Node k makes reverse route entry for node e and unicasts Route Reply (RREP) message to node e along the reverse route. If node k receives multiple *RREQ* messages from node e through different routes, it generates multiple *RREP* messages and unicasts them to node e along the reverse routes. This helps node e to select a route among available routes consisting of only reliable nodes, as a given route may have some broken nodes. Node j is said to be downstream neighbor of node i if node i sends *RREQ* message to node j. Similarly, node i is said to be upstream neighbor of node j if node i receives *RREP* message from node j.

The decision of route selection is made by the source and all intermediate nodes along a given route. When an intermediate node i receives *RREP* message from its downstream neighbor j and the downstream neighbor j is not the destination, node i checks for reliability information of node j from reliability database R_i. If node j is reliable, node i includes node j in route P_i, makes forward route entry for node k and forwards *RREP* message to its upstream node. If node j is unreliable, node i drops *RREP* message. This process continues until the *RREP* reaches at node e.

Let M represents the number of possible reliable routes between node e and node k with variable delay such that $P_1, P_2, P_3, ...P_M \in M$. Let $t_{i,j}$ represents the average transmission delay of link (i, j) on route P_i. If the length of route P_i is l hops, the average end-to-end delay of route P_i is computed as follows:

$$P_{id} = \sum_{i=1}^{l-1} t_{(i,j)_i} \tag{11}$$

The source node e selects the shortest possible route to destination node k from M available reliable routes as follows:

$$P_{e,k} = \min_{i=1}^{M} P_{id} \tag{12}$$

When the source node e selects the route, it makes forward route entry for destination node k and starts transmitting data over the established route.

Figure 5 shows the route setup process, where all network nodes are assumed to be reliable and one reliable route exists between source e and destination k. Figure 6

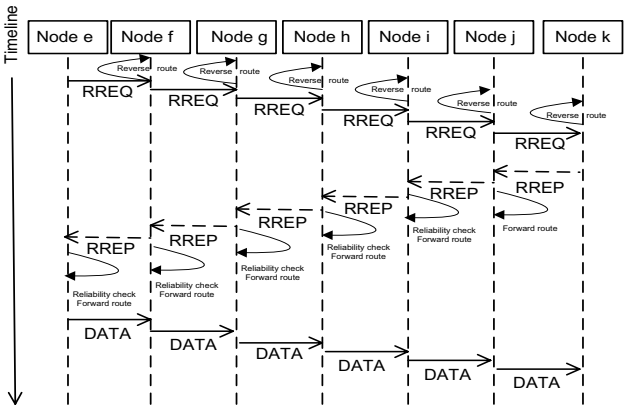

Figure 5. The route setup process in a network with all reliable nodes

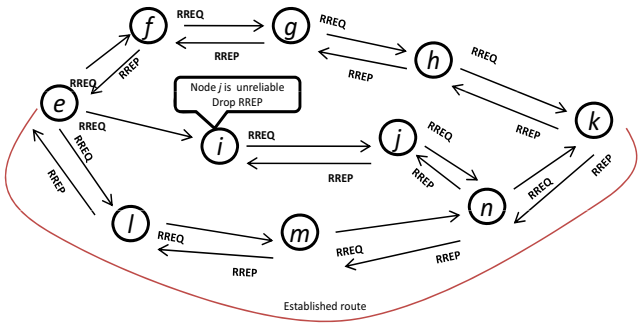

Figure 6. The route setup process in a network with some unreliable nodes

shows the route setup process in the presence of some unreliable nodes in the network and multiple reliable routes exist between source e and destination k. Node i drops *RREP* received from node j as node j is unreliable. Node e receives first *RREP* message from reliable neighbor l, makes forward route entry for node k and starts sending data over the route $e \rightarrow l \rightarrow m \rightarrow n \rightarrow k$. Node e ignores *RREP* message received afterwards from node f.

Consider a network with $k + 1$ nodes labeled as n_0, n_1, n_2,.. , n_k, with n_0 as the source and n_k as the destination. The current node is represented by n_i and R_i represents the reliability database at node n_i. The upstream neighbor of n_i is represented by n_{i-1} and the downstream neighbor of n_i is represented by n_{i+1}. Let N_i represents the neighborhood of node n_i such that $n_{i-1}, n_{i+1} \in N_i$. The $RREQ_b$ describes the broadcast of *RREQ* message and $RREP_u$ represents the unicast of *RREP* message. Moreover, $C_{i,i+1}$ and $C_{i,j}$ represent the same information. Algorithm 1 describes the route setup process.

IV. Simulation Scenario and Results

We simulate an emergency response scenario caused by an earthquake or a flood as shown in figure 1. The traditional telecommunication infrastructure is assumed to be totally collapsed and a mobile ad hoc network comprising of smart phones and PDAs has been established for exchanging emergency related information. The majority of first responders such as medical teams,

input : $C_{i,i+1}$
output: *Shortest route with all reliable nodes*
set $n_i = n_0$
if (n_i *has route to* n_k) **then**
  $n_i : Data \Rightarrow n_k$
end
else
  $n_i : RREQ_b \Rightarrow N_i$
  set $n_i = n_{i+1}$
end
repeat
  $n_i \Leftarrow RREQ : n_{i-1}$
  n_i computes $n = A_r \times \Delta_t$
  n_i makes reverse route entry for n_0
  $n_i : RREQ_b \Rightarrow N_i$
  set $n_i = n_{i+1}$
until ($n_i = n_k$ *AND* $n_i \Leftarrow RREQ : n_{i-1}$);
if ($n_i = n_k$ *AND* $n_i \Leftarrow RREQ : n_{i-1}$) **then**
  n_i makes reverse route entry for n_0
  $n_i : RREP_u \Rightarrow n_{i-1}$
  $n_{i-1} \Leftarrow RREP : n_i$
  n_{i-1} makes forward route entry for n_k
  $n_{i-1} : RREP_u \Rightarrow n_{i-2}$
  set $n_i = n_{i-2}$
end
repeat
  $n_i \Leftarrow RREP : n_{i+1}$
  $n_i \Leftarrow C_{i,i+1} : R_i$
  if ($C_{i,i+1} == 1$) **then**
    n_i makes forward route entry for n_k
    $n_i : RREP_u \Rightarrow n_{i-1}$
    set $n_i = n_{i-1}$
  end
  else if ($C_{i,i+1} == 0$) **then**
    $n_i : Drop \Leftarrow RREP : n_{i+1}$
  end
until ($n_i = n_0$ *AND* $n_i \Leftarrow RREP : n_{i+1}$);
if ($n_i = n_0$ *AND* $n_i \Leftarrow RREP : n_{i+1}$) **then**
  $n_i \Leftarrow C_{i,i+1} : R_i$
  if ($C_{i,i+1} == 1$) **then**
    n_i makes forward route entry for n_k
    $n_i : Data \Rightarrow n_k$
    n_i ignores pending $RREP$ messages
  end
  else if ($C_{i,i+1} == 0$) **then**
    $n_i : Drop \Leftarrow RREP : n_{i+1}$
  end
end

Algorithm 1: Route setup process

TABLE I.
SIMULATION PARAMETERS

Parameter	Value
Number of nodes	50
Coverage area	1000x1000 meters
Propagation model	Two ray ground
Mobility model	Random way point
MAC protocol	802.11
Routing protocol	AODV, $AODV_r$
Radio range	250 meters
Channel bandwidth	11Mbps
Traffic type	CBR
Packet size	512 bytes
Application's packet rate A_r	100 packets per second
Behavior evaluation time interval Δt	5 seconds
Node movement speed	0-10 meter per second
Interface queue size	100 packets
Positive behavior probability threshold Th_{prob}	0.5
Minimum number of behavior evaluations m	10
Packet forwarding threshold Th_{pfr}	0.2-0.8
Simulations time	1000 seconds

NGO teams and fire fighters are engaged in saving the life of trapped survivors at the disaster site. Some first responders use ambulance services to transfer the victims to remote hospitals. The mobile nodes choose random destinations and move towards those destinations with different movement speeds. The mobile nodes stay at a particular place for random period of time and then move to next destinations. We simulate the faulty node behavior as a node which drops alternate received packets. We assume that on average, there are three to five simultaneous communications in the network at a time and we name it as an average traffic load. The simulations are run by using NS2 [29] simulator. The performance of the proposed scheme is evaluated against the traditional AODV scheme in terms of packet delivery ratio, end-to-end delay and routing overhead. For convenience, we name our proposed scheme as reliable AODV and represent it by $AODV_r$. The simulation parameters are summarized in table I.

Figure 7, figure 8 and figure 9 show the packet delivery, end-to-end delay and routing overhead performance of the proposed scheme in a network having some broken nodes with an average network traffic and random node mobility speed. When all network nodes are reliable, the packet delivery ratio of AODV and $AODV_r$ is almost similar. The proposed scheme identifies and isolates faulty nodes dynamically, so its packet delivery ratio increases with the increasing number of faulty nodes against the traditional scheme. The end-to-end delay performance of the proposed scheme is also better as it switches to new routes while experiencing random congestion. The proposed scheme finds additional routes to avoid faulty or congested nodes, so its routing overhead increases against the AODV routing scheme. The overall performance of

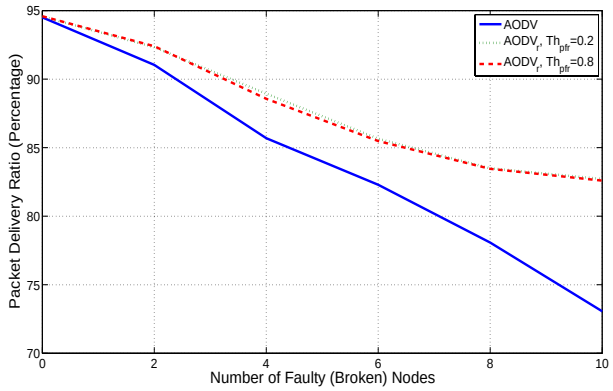

Figure 7. Packet delivery performance in a network having some broken nodes with an average network traffic and random node mobility speed

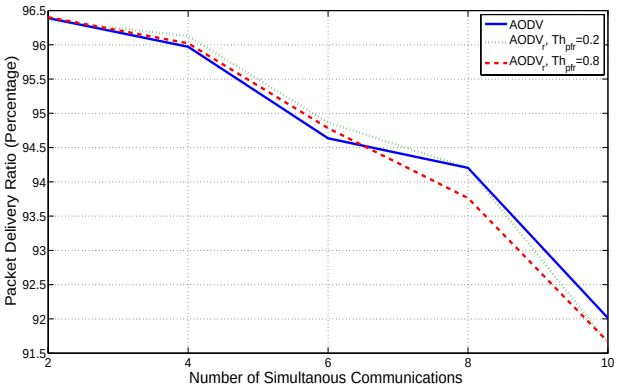

Figure 10. Packet delivery performance in a network having all reliable nodes with variable network traffic and random node mobility speed

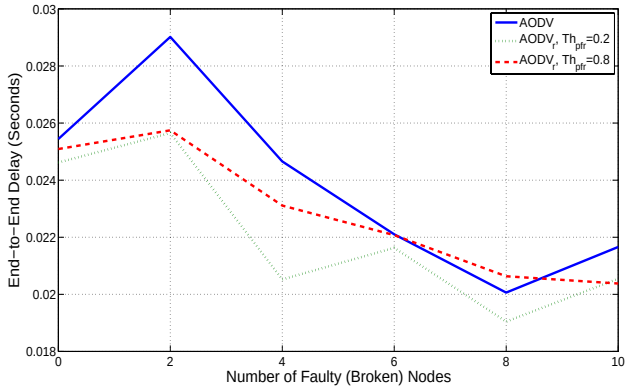

Figure 8. Delay performance in a network having some broken nodes with an average network traffic and random node mobility speed

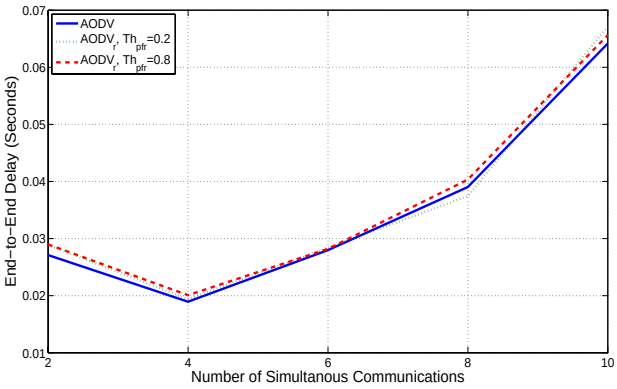

Figure 11. Delay performance in a network having all reliable nodes with variable network traffic and random node mobility speed

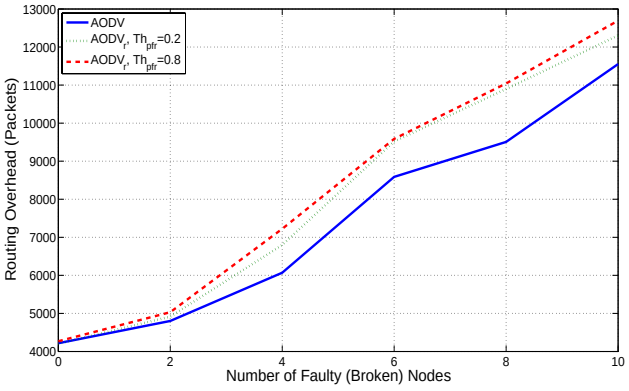

Figure 9. Routing overhead performance in a network having some broken nodes with an average network traffic and random node mobility speed

the proposed scheme improves at lower value of packet forwarding threshold, as the frequency of route maintenance calls decreases.

Figure 10, figure 11 and figure 12 show the packet delivery, end-to-end delay and routing overhead performance of the proposed scheme in a network having all reliable nodes with variable network traffic and random node mobility speed. At low traffic load, the packet delivery ratio of AODV and $AODV_r$ is almost similar as there is no significant congestion. As the network traffic increases and there is some random congestion, the packet delivery ratio of $AODV_r$ improves. When the network traffic increases significantly, the level of congestion also increases and the packet delivery ratio of $AODV_r$ degrades due to increasing number of route maintenance calls. The end-to-end delay of the proposed scheme remains almost similar to that of AODV for variable network traffic. The routing overhead of $AODV_r$ increases as the frequency of route maintenance calls increases to avoid significant network congestion.

Figure 13, figure 14 and figure 15 show the packet delivery, end-to-end delay and routing overhead performance of the proposed scheme in a network having all reliable nodes with an average network traffic and variable node mobility speed. The packet delivery ratio, end-to-end delay and routing overhead performance of AODV and $AODV_r$ is almost similar for lower packet forwarding threshold value. However, there is some overlapping in the packet delivery and end-to-end delay performance of AODV and $AODV_r$ if the value of packet forwarding threshold increases. The routing overhead of $AODV_r$ increases than AODV as the node mobility speed and the value of packet forwarding threshold increases.

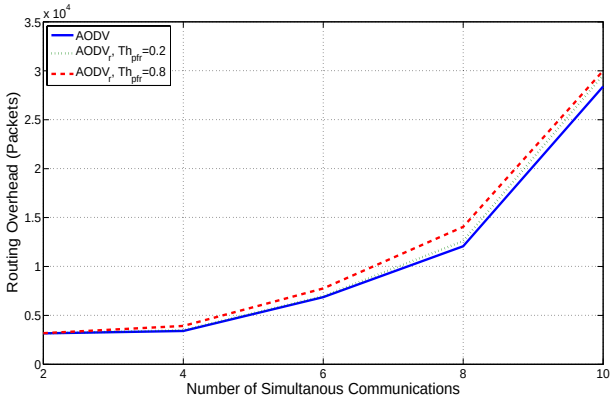

Figure 12. Routing overhead performance in a network having all reliable nodes with variable network traffic and random node mobility speed

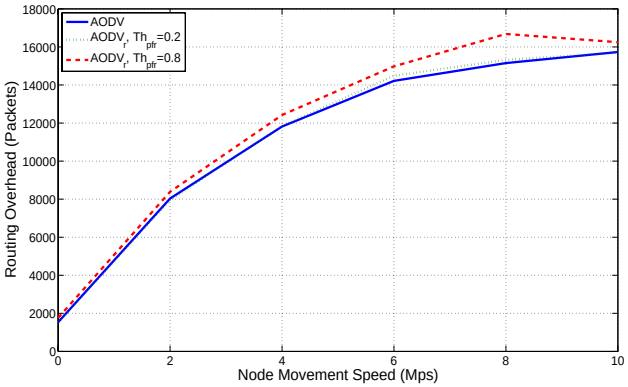

Figure 15. Routing overhead performance in a network having all reliable nodes with an average network traffic and variable node mobility speed

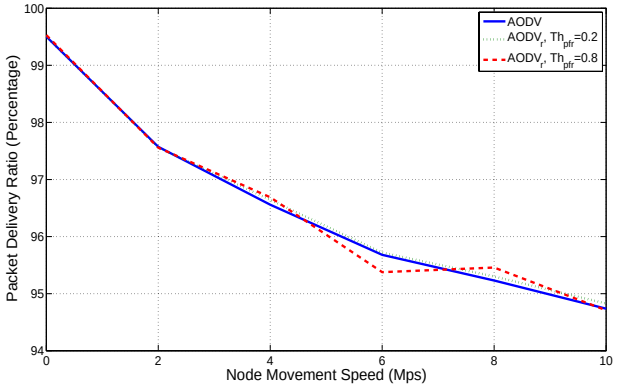

Figure 13. Packet delivery performance in a network having all reliable nodes with an average network traffic and variable node mobility speed

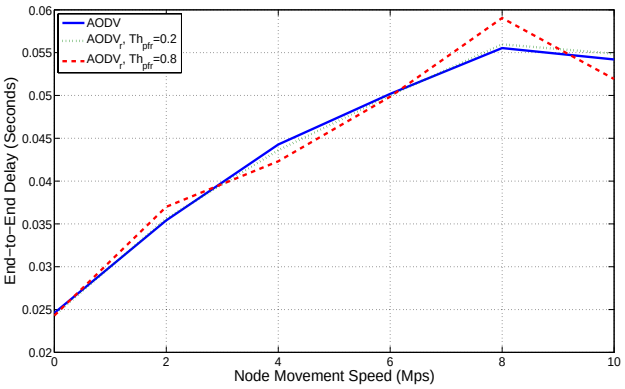

Figure 14. Delay performance in a network having all reliable nodes with an average network traffic and variable node mobility speed

V. Conclusion and Future Work

We propose a reliable routing scheme for post-disaster ad hoc communication networks, which finds the shortest possible routes with all reliable nodes. The proposed scheme also detects packet forwarding misbehavior dynamically and reroutes packets through other reliable routes. The performance of the proposed scheme is compared against the traditional scheme in terms of packet delivery ratio, end-to-end delay and routing overhead. The proposed scheme performs better in terms of packet delivery ratio and end-to-end delay with a reasonable increase in routing overhead, when the network contains some broken nodes, there is an average network traffic and the nodes move with random mobility speed. If the network contains all reliable nodes, there is variable network traffic and the nodes move with random mobility speed, the packet delivery ratio, end-to-end delay and routing overhead of the traditional and the proposed schemes almost match. The packet delivery ratio, end-to-end delay and routing overhead performance of the proposed scheme is almost similar to that of the traditional scheme, when the network contains all reliable nodes, there is an average network traffic, the nodes move with variable mobility speeds and the value of packet forwarding threshold decreases. However, the packet delivery and end-to-end delay performance of the traditional and the proposed schemes overlap with a little increase in routing overhead, if the value of packet forwarding threshold increases. We are in the process of extending the proposed scheme to address malicious node behavior in addition to network fault and congestion.

References

[1] E. Der Heide and R. Irwin, *Disaster response: principles of preparation and coordination*. Mosby, 1989.

[2] M. Kyng, E. Nielsen, and M. Kristensen, "Challenges in designing interactive systems for emergency response," in *Proceedings of the 6th conference on Designing Interactive systems*, 2006, pp. 301–310.

[3] H. Kirchner and T. Risse, "Challenges in information systems for disaster recovery and response," *3. GI/ITG KuVS Fachgespräch Ortsbezogene Anwendungen und Dienste*, pp. 16–19.

[4] B. Manoj and A. Baker, "Communication challenges in emergency response," *Communications of the ACM*, vol. 50, no. 3, pp. 51–53, 2007.

[5] A. Meissner, T. Luckenbach, T. Risse, T. Kirste, and H. Kirchner, "Design challenges for an integrated disaster management communication and information system," in *The First IEEE Workshop on Disaster Recovery Networks (DIREN 2002)*, 2002.

[6] S. Mehrotra, T. Znati, and C. Thompson, "Crisis management," *Internet Computing, IEEE*, vol. 12, no. 1, pp. 14–17, 2008.
[7] T. Lueck, "Grant to help city broaden radio network," *New York Times*, 2005.
[8] C. Thompson, "Talking in the dark," *New York Times Magazine*, 2005.
[9] M. Portmann and A. Pirzada, "Wireless mesh networks for public safety and crisis management applications," *IEEE Internet Computing*, pp. 18–25, 2008.
[10] J. Hubaux, T. Gross, J. Le Boudec, and M. Vetterli, "Toward self-organized mobile ad hoc networks: The terminodes project," *Communications Magazine, IEEE*, vol. 39, no. 1, pp. 118–124, 2001.
[11] M. Ad, C. Perkins, and S. Das, "Ip address autoconfiguration for ad hoc networks," Internet Draft draftietfmanetautoconf-01. txt, Internet Engineering Task Force, MANET WG, Tech. Rep., 2000.
[12] A. Wood and J. Stankovic, "Denial of service in sensor networks," *Computer*, vol. 35, no. 10, pp. 54–62, 2002.
[13] S. Rahebi and M. Asadi, "Wbrr: A weight based reliable routing method in mobile ad hoc network," *Australian Journal of Basic and Applied Sciences*, vol. 3, no. 3, pp. 1888–1897, 2009.
[14] F. Xie, L. Du, Y. Bai, and L. Chen, "Energy aware reliable routing protocol for mobile ad hoc networks," in *Wireless Communications and Networking Conference, 2007. WCNC 2007.*, 2007, pp. 4313–4317.
[15] A. Bamis, A. Boukerche, I. Chatzigiannakis, and S. Nikoletseas, "A mobility aware protocol synthesis for efficient routing in ad hoc mobile networks," *Computer Networks*, vol. 52, no. 1, pp. 130–154, 2008.
[16] Z. Cheng and W. Heinzelman, "Discovering long lifetime routes in mobile ad hoc networks," *Ad Hoc Networks*, vol. 6, no. 5, pp. 661–674, 2008.
[17] I. Jawhar, Z. Trabelsi, and J. Al-Jaroodi, "Towards more reliable source routing in wireless networks," in *International Conference on Networking, Architecture, and Storage, 2008. NAS'08*, 2008, pp. 167–168.
[18] V. Rishiwal, A. Kush, and S. Verma, "Stable and energy efficient routing for mobile adhoc networks," in *Fifth International Conference on Information Technology: New Generations*, 2008, pp. 1028–1033.
[19] B. Ramachandran and S. Shanmugavel, "Received signal strength-based cross-layer designs for mobile ad hoc networks," *IETE technical review*, vol. 25, no. 4, pp. 192–200, 2008.
[20] C. Hieu and C. Hong, "A reliable and high throughput multi-rate ad hoc routing protocol: Cross layer approach," in *International Conference on Information and Communication Technology Convergence (ICTC)*, 2010, pp. 362–367.
[21] J. Muñoz, O. Esparza, M. Aguilar, V. Carrascal, and J. Forné, "Rdsr-v. reliable dynamic source routing for video-streaming over mobile ad hoc networks," *Computer Networks*, vol. 54, no. 1, pp. 79–96, 2010.
[22] A. Gohari, R. Pakbaz, and V. Rodoplu, "Rmr: Reliability based multi-hop routing in wireless tactical networks," in *Proceedings of IEEE Military Communications Conference*, 2010, pp. 1106–1112.
[23] S. Hariharan, N. Shroff, and S. Bagchi, "Secure neighbor discovery through overhearing in static multihop wireless networks," in *Fifth IEEE Workshop on Wireless Mesh Networks (WIMESH 2010)*, 2010, pp. 1–6.
[24] H. Ning, C. Ling, and K. Leung, "Wireless network coding with imperfect overhearing," *Arxiv preprint arXiv:1003.4270*, 2010.
[25] Y. Reddy and R. Selmic, "Trust-based packet transfer in wireless sensor networks," in *Proceedings of the Tenth International Conference on Networks*, 2011, pp. 218–223.
[26] M. Ad, E. Royer, C. Perkins, and S. Das, "Ad hoc on-demand distance vector (aodv) routing," 1999.
[27] S. Marti, T. Giuli, K. Lai, and M. Baker, "Mitigating routing misbehavior in mobile ad hoc networks," in *Proceedings of the 6th annual international conference on Mobile computing and networking*, 2000, pp. 255–265.
[28] A. Jsang and R. Ismail, "The beta reputation system," in *Proceedings of the 15th Bled Electronic Commerce Conference*, 2002, pp. 41–55.
[29] T. Issariyakul and E. Hossain, *Introduction to Network Simulator NS2*. Springer Verlag, 2008.

Muhammad Ibrahim Channa was born in Pakistan. He completed M.Sc. in Computer Science from University of Sind, Pakistan, in 1995 and M.S. in Information Technology from National University of Science and Technology, Pakistan in 2005. He is enrolled as a PhD candidate at Asian Institute of Technology, Thailand since August 2007. His field of study is Information and Communications Technologies.

He is employed as Assistant Professor, Institute of Information Technology, Quaid-e-Awam University of Engineering, Science and Technology, Pakistan since March 2000. His research interest comprises of trust management, security, routing, and quality of service in mobile ad hoc networks.

Dr. Kazi M. Ahmed was born in Bangladesh. He did his Masters in Telecommunications Engineering from the then Leningrad Electrical Engineering Institute of Communications, former USSR, in 1978. He finished his Ph.D. in Electrical Engineering from the University of Newcastle, NSW, Australia in 1983.

At present, he is a Professor of Telecommunications and ICT at Asian Institute of Technology, Bangkok, Thailand. Dr. Ahmed has diverse interest in different fields of Telecommunications. His main research interest is in Wireless Communications and Communications Networks.

Dr. Ahmed is a Member, IEEE; Member, IEICE, Japan; Fellow of IE Bangladesh; and Member and Advisor of many international and national associations and steering committees.

Optimization of Control Parameters of Differential Evolution Technique for the Design of FIR Pulse-shaping Filter in QPSK Modulated System

Sudipta Chattopadhyay and Salil Kumar Sanyal
Department of Electronics & Telecommunication Engineering, Jadavpur University, Kolkata – 700 032, India
Email: sudiptachat@yahoo.com and s_sanyal@ieee.org

Abhijit Chandra
Department of Electronics & Telecommunication Engineering, Bengal Engineering & Science University, Shibpur, Howrah– 711 103, India
Email: abhijit922@yahoo.co.in

***Abstract*—Signal Processing in modern era, involves rigorous applications of various evolutionary algorithms such as Genetic Algorithm (GA), Particle Swarm Optimization (PSO) and Differential Evolution (DE) for the optimized design of aerodynamic shape, automated mirror, digital filter, computational intelligence etc. DE has been judged to be quite effective in designing different types of digital filter with good convergence behavior. The performance of the DE optimization technique could be improved to a further extent if the values of the two control parameters namely "Weighting Factor" and "Crossover Probability", be chosen properly. In this paper, the effect of these two control parameters on the design of low pass FIR digital filter has extensively been studied. The impact of these control parameters on the convergence behavior of the DE technique has also been presented. The performance of the DE optimized filter has been adjudicated in terms of its magnitude and impulse responses. In addition, the DE optimized filter has been utilized as a pulse-shaping filter in a Quadrature Phase Shift Keying (QPSK) modulated system and its performance has further been studied in terms of Bit Error Rate (BER). Finally, the optimized values of the ''Weighting Factor'' and "Crossover Probability" for this specific modulated system design problem has been recommended. Experimentally measured Eye diagrams have also confirmed the optimized values.**

***Index Terms*—Cost Function, Crossover Probability, DE, Eye diagram, Finite-Duration Impulse Response (FIR) filter, Pulse-Shaping Filter, Weighting Factor.**

I. Introduction

Digital Filters are frequency selective systems, which are used to pass a certain range of frequency and to stop another range of frequency. They are actually characterized by their impulse responses. Depending upon the duration of the impulse response, digital filters are classified as Finite-Duration Impulse Response (FIR) and Infinite-Duration Impulse Response (IIR) filters. Stable and linear phase FIR filter can be implemented quite easily under certain constraints [1]-[3]. These properties of FIR filter make it very much attractive for use in various digital communication systems. In mobile communication system, different types of FIR filters are being used as a transmitting pulse-shaping filter [4].

Different techniques have been used for the design of FIR filter, which includes window-based method, frequency sampling method and Parks-McClellan equiripple algorithm [1]. Of late, various evolutionary algorithms are also being used for this purpose.

An FIR filter design process using Genetic Algorithm (GA) has been presented in [5]. It requires a minimum number of GA parameter adjustments and the main part has been developed using the Gallops GA tool [6]. The frequency response of the designed FIR filter shows that for short transition band, it can be an alternative to the Parks-McClellan method [7]. It has also been mentioned in [5] that the design tool works well for symmetric, anti-symmetric, odd and even order FIR filters.

The design of low-pass and band-pass FIR digital filters using Particle Swarm Optimization (PSO) has been presented in [8]. In this paper, the utility of various error norms namely Least Mean Square (LMS) and Minimax along with their impact on the convergence behavior of the optimization technique has been focused. Finally, it has been established that PSO using Minimax strategy offers faster convergence speed than LMS strategy [8].

Shing-Tai Pan et.al. [9] have emphasized on the application of Differential Evolution (DE) algorithm for the design of robust and stable digital filter. It has been established that the performance of DE is much superior to that of GA in terms of the convergence behavior in the context of filter design problem with due consideration of robust stability.

Manuscript received January 31, 2011; revised April 25, 2011; accepted June 5, 2011.

doi:10.4304/jcm.6.7.558-570

The design of a linear-phase low-pass FIR filter using DE algorithm has also been described in [10]. The designed low-pass filter has further been extended as a pulse-shaping filter in a Quadrature Phase Shift Keying (QPSK) modulated system and the resulting system performance has been studied by means of various performance parameters such as Error Vector Magnitude (EVM), Signal to Noise Ratio (SNR) and Waveform Quality Factor. It has also been established that the proposed filter outperforms the standard Raised Cosine (RC) and Root Raised Cosine (RRC) filters in terms of the above mentioned parameters.

An efficient technique for adapting control parameter settings, associated with DE has been described in [11]. The algorithm presented in this paper shows good performance on numerical benchmark problems. It has been established that the self-adaptive control parameter setting algorithm performs better than or at least comparable to standard DE and other evolutionary algorithms found in the literature, as far as the quality of the solution is concerned.

The impact of the Weighting Factor on the convergence behavior of the DE algorithm for the design of low-pass filter has been critically studied in [12]. The performance of the designed filter has properly been analyzed and also been measured practically. From the experimental results, it has been established that the FIR filter designed with a Weighting Factor value of 0.7 gives the best performance in terms of convergence speed, magnitude response, impulse response and other performance parameters.

In this paper, we have critically studied the impact of two very important control parameters associated with DE, i.e., "Weighting Factor" and "Crossover Probability" on the convergence behavior of the algorithm for efficient design of low-pass FIR filter. The effect of these parameters on the performance of FIR pulse-shaping filter has also been evaluated in QPSK modulated system. The magnitude response, the impulse response and the Bit Error rate (BER) have mainly been measured with different combinations of "Weighting Factor" (F) and "Crossover Probability" (CR).

II. Theoretical Background

A. Differential Evolution

A new floating-point encoded DE algorithm for global optimization has been proposed by Storn and Price [13]. The effectiveness, efficiency and robustness of the DE algorithms are greatly dependent on the settings of the few control parameters [14]. The fundamental characteristics of evolutionary algorithm dictate that each population member should undergo initialization, mutation, recombination and selection processes, during each iteration [15].

The process of mutation expands the search space, where a mutant vector is generated in accordance with the following equation [15]:

$$v_{i,G+1} = x_{r_1,G} + F(x_{r_2,G} - x_{r_3,G}); i = 1,2,.....,P \quad (1)$$

where $x_{r_i,G}$ are the parameter vectors of the previous generation, $v_{i,G+1}$ is the mutant vector of the current generation and P is the total number of populations.

During the process of recombination, the elements of the donor vector enter the trial vector with a certain probability, named crossover probability. Thus the trial vector $u_{i,G+1}$ is of the form [15]:

$$u_{j,i,G+1} = \begin{cases} v_{j,i,G+1} & iff \ \ rand_{j,i} \le CR \vee j = I_{rand} \\ x_{j,i,G} & iff \ \ rand_{j,i} > CR \wedge j \ne I_{rand} \end{cases} \quad (2)$$

with $i = 1,2,...,P$, $j = 1,2,...,D$ and $rand_{j,i}$ is a random number within the set [0, 1] that has to be generated in each iteration of the algorithm for each population member and for each of the parameters that we want to optimize.

In the final step of DE, the trial vector is compared with the target vector of previous generation and the one with lower cost function is permitted to make an entry to the next generation. This has been summarized mathematically as follows [15]:

$$x_{i,G+1} = \begin{cases} u_{i,G+1} & iff \quad f(u_{i,G+1}) \le f(x_{i,G}) \\ x_{i,G} & iff \quad f(u_{i,G+1}) > f(x_{i,G}) \end{cases} \quad (3)$$

There are only two control parameters associated with the traditional DE algorithm. The choice of these two parameters, namely mutation control parameter and recombination control parameter, is very important in any design problem incorporating DE. It has been found in the literature that the value of mutation control parameter is more sensitive than the other.

Various methods of adapting two important control parameters of DE algorithm have been reported in [16]-[20]. A Self Adaptive Differential Evolution (SADE) has been proposed in [16] where an appropriate learning strategy and suitable control parameters have been self-adapted in accordance with some learning experience. Another new version of DE called Fuzzy Adaptive Differential Evolution (FADE) has been reported in [17] to control the DE parameters dynamically in a more efficient manner than traditional DE. Different versions of adaptive and self-adaptive DE algorithm have been compared in [18]. The comparison results show that the jDE algorithm performs better than FADE and DESAP algorithms and self-adaptive jDE-2 algorithm gives comparable result on benchmark functions as SADE algorithm. Different opinions regarding the choice of control parameters associated with DE technique have been discussed in [19]-[20] where it has been mentioned that DE algorithm is much more sensitive to the choice of weighting factor than the others. Determination of the suitable values for the control parameters of DE

algorithm, for a particular design problem is still a vast area of research.

The work carried out in [15] has not considered the variation of the control parameters to judge the performance of the application. Thus, from application point of view it is incomplete. In our work, we have further extended the ideas described in [15] to find out the optimized values of the two useful control parameters of DE algorithm applied to filter design problem, namely "Weighting Factor" and "Crossover Probability" in a particular fashion, which is widely different from those described in [16]-[20]. In order to accommodate the practical aspect of this design problem, it has been successfully used as a pulse-shaping filter in a QPSK modulated system and its performance has been studied. From this study, it has been established that the filter designed with the optimized values of the control parameters of DE algorithm also performs quite satisfactorily as a pulse-shaping filter in a QPSK modulated system.

B. Role of Pulse-shaping filter in communication system

In digital communication system, the symbols are transmitted in the form of different pulses over a band limited channel. However, due to practical channel impairment there is considerable spreading of these pulses in the time domain resulting in interference amongst the transmitted symbols. This phenomenon, well known as Inter Symbol Interference (ISI) is mainly responsible for making the overall system performance to deteriorate. Elimination of this interference as far as practicable, is of primary concern to the digital communication system designer [21]-[22]. The pulse-shaping technique has been used extensively in reducing system ISI to a great extent and thereby resulting in lower BER values.

Pulse shaping is usually done at the transmitter end prior to the digital modulation by means of a pulse-shaping filter [21]-[22]. In order to make a digital filter to act as a proper pulse-shaping filter, it has to satisfy the Nyquist minimum bandwidth criterion to ensure near zero ISI under the worst-case condition. Thus the transfer function of the Nyquist minimum bandwidth filter can be represented mathematically as follows [21]-[22]:

$$H_{Nyquist}(e^{j\omega}) = \begin{cases} 1, & 0 \le \omega \le \omega_{Nyquist} \\ 0, & \omega_{Nyquist} \le \omega \le \pi \end{cases} \quad (4)$$

where $\omega_{Nyquist} = 2\pi . f_{Nyquist}$ is the cut-off frequency in rad/pi and $f_{Nyquist} = f_s / 2$ is the cut-off frequency in Hz of the Nyquist filter and f_s is the symbol rate of the input data in Hz. The minimum bandwidth Nyquist filter is actually an ideal, brick-wall low pass filter that requires an infinite number of filter sections to synthesize the sharp attenuation slope in the stop band. This concept is very difficult to realize in practice. The practically realizable pulse shaping filters used in various digital communication systems include Raised Cosine (RC) and Root Raised Cosine (RRC) pulse shaping filters [21]-[22]. These filters can be realized with a finite number of filter sections and hence are widely accepted as a pulse-shaping filter in practice [23].

III. Problem Formulation

The main objective of this work has been to utilize DE technique to find out the optimum solution vector $\vec{h}_{opt}$ of dimension D over the search space S^D that can well represent the impulse response of a linear-phase low-pass FIR filter. The optimization procedure has been carried out in such a way that it takes care of the impact of various control parameters of DE. Mathematically, the choice of $\vec{h}_{opt}$ has been outlined as:

$$\Im(\overrightarrow{\mathrm{h}_{\mathrm{opt,F_{opt},CR_{opt}}}}) < \Im(\overrightarrow{\mathrm{h}_{\mathrm{F_{opt},CR_{opt}}}})$$

$$\forall\ \vec{h}, \overrightarrow{h_{opt}} \in \{S^D\} \quad (5)$$

where $\Im()$ signifies the associated cost function. Equation (5) has been implemented by considering the effect of two control parameters of DE, i.e. "Weighting Factor" (F) and "Crossover Probability" (CR). Since DE is more sensitive to the choice of Weighting Factor, it has been optimized first prior to the optimization of "Crossover Probability". The optimum value of "Weighting Factor" F_{opt}, from a vector of sample Weighting Factors $F_S = [F_1, F_2, ..., F_{m_1}]$ has been located according to:

$$\Im(\overrightarrow{\mathrm{h}_{\mathrm{opt,F,CR_{nom}}}})\Big\|_{\mathrm{F_{opt}}} < \Im(\overrightarrow{\mathrm{h}_{\mathrm{F,CR_{nom}}}})\Big\|_{\hat{\mathrm{F}}}$$

$$\exists\ F_{opt} \neq \hat{F}\ \&\ F_{opt}, \hat{F} \in F_S \quad (6)$$

In the above equation, the value of the Crossover Probability has been kept at its nominal value CR_{nom}. Thereafter, the value of F_{opt} has been employed in place of Weighting Factor in order to find out the most favorable value of Crossover Probability for this specific filter design problem. Selection of the most suitable Crossover Probability has been made from a vector of sample Crossover Probabilities $CR_S = [CR_1, CR_2, ..., CR_{m_2}]$. The necessary scheme has been illustrated as:

$$\Im(\overrightarrow{\mathrm{h}_{\mathrm{opt,F_{opt},CR}}})\Big\|_{\mathrm{CR_{opt}}} < \Im(\overrightarrow{\mathrm{h}_{\mathrm{F_{opt},CR}}})\Big\|_{\hat{\mathrm{CR}}}$$

$$\exists\ CR_{opt} \neq \hat{CR}\ \&\ CR_{opt}, \hat{CR} \in CR_S \quad (7)$$

The values of F_{opt} and CR_{opt}, as obtained from Equations (6) and (7) respectively, represent the optimum values of the two control parameters for this specific filter design problem.

The termination of any optimization process is largely determined by the choice of the cost function, associated with it. This paper attempts to observe the impact of control parameters on the effective design of low-pass FIR filter. Hence, the deviation of the magnitude response of the designed filter from that of the ideal one has been considered as a metric to realize the cost function of the design methodology.

The ideal frequency response of a low pass digital filter is given by the following equation [1], [21]:

$$H_{ideal}(e^{j\omega}) = \begin{cases} 1; & 0 \le \omega \le \omega_c \\ 0; & \omega_c \le \omega \le \pi \end{cases} \quad (8)$$

If the impulse response of the digital filter is of finite duration, then the transfer function of such a filter is related to its impulse response as shown [1], [21]:

$$H_{ideal}(e^{j\omega}) = \sum_{n=0}^{L} h_{ideal}[n] e^{-j\omega n} \quad (9)$$

where $h_{ideal}[n]$ is the impulse response of the ideal FIR filter of length L+1.

When the ideal frequency response is sampled in the frequency domain at an equal interval, the resultant sampled frequency response is of the following form :

$$H_{ideal}(k) = \left| H_{ideal}(e^{j\omega_k}) \right|, \omega_k = k\pi / N,$$
$$k = 1,2,.....,N \quad (10)$$

where N is the number of frequency samples.

DE technique can be used to find the impulse response of the low pass FIR digital filter. Let h (n) denotes the impulse response of the FIR filter obtained using the optimization technique. Then the resulting frequency response of the designed filter can be characterized mathematically as follows [1]:

$$H(e^{j\omega}) = \sum_{n=0}^{L} h[n] e^{-j\omega n} \quad (11)$$

The frequency-sampled version of the designed filter is defined by:

$$H(k) = \left| H(e^{j\omega_k}) \right|, \omega_k = k\pi / N \ \ k = 1,2,.....,N \quad (12)$$

The value of the sampled error function between the desired magnitude response and the DE obtained magnitude response at any frequency is given by:

$$E(k) = \left| H_{ideal}(k) - H(k) \right|, \ k = 1,2,.....,N \quad (13)$$

If the error value is lower, the actual magnitude response is closer to the ideal one. This can be achieved by using DE algorithm wisely. In our design problem, we have used the minimax error as the averaged cost function for the DE optimization technique. Here our goal is first to find out the maximum value of the sampled error function for all the members of the population and then to identify that particular member which yields the minimum of these maximum error values. So, the minimax error can now be written mathematically

$$Error = \max\{E(k)\},\ k = 1,2,.....,N \quad (14)$$

$$Mini\max Error = \min\{Error(i)\},\ i = 1,2,.....,P \quad (15)$$

Using (11), (13) and (14), equation (15) can be rewritten as:

$$Error = \max\{\sum_{j=1}^{N} \left| H_{ideal}(e^{jw_j}) - H(e^{jw_j}) \right|\} \quad (16)$$

where P is the number of populations and N is the total number of frequency samples. The primary objective behind this work is to reduce the error under the worst-case condition.

Based on the above mathematical model, the developed algorithm has been presented below:

Step 1: Choose the length of the FIR filter and the value of the cut-off frequency.

Step 2: Initialize the size of population, maximum iteration number, mutation strategy, crossover scheme, value of the weighting factor & crossover probability, threshold value of the cost function and initial value of each element of the population vector.

Step 3: Allow the process of mutation, crossover and selection to occur subsequently between the members of the population.

Step 4: Go to step 3 until and unless the value of the averaged cost function is less than the threshold specified during the initialization phase.

Step 5: Identify the member of the population yielding the minimum cost function and accept it as the impulse response of the designed FIR filter.

Various parameters of the above mentioned algorithm have been selected as follows:

Length of the FIR filter: 8

Value of the cut-off frequency: 0.5 rad /pi

Size of population: Three different population sizes, namely 40, 80 and 100.

Maximum iteration number: Nine different iteration numbers, namely 10, 20, 40, 60, 80, 100, 200, 400 and 500.

Mutation strategy: DE/rand/1

Crossover scheme: Binary

Sample value of the Weighting Factor: Four different

sample values, namely 0.3, 0.5, 0.7 and 1.0.
Sample value of the Crossover Probability: Four different sample values, namely 0.3, 0.5, 0.7 and 0.9.
Threshold value of the cost function: 0.0001
Initial value of each element of population vector: From the set [-1, 1].

IV. Simulation Results

Fig. 1 represents the convergence behavior of the DE optimization technique for four different values of Weighting Factors (F), namely 0.3, 0.5, 0.7 and 1.0 for a specific Crossover Probability of 0.5, using minimax error as the averaged cost function.

The comparison of the figures below shows that for F=0.3, the curves for the averaged cost function need a large number of iterations to converge for all the specified population sizes. When the value of the F is increased to 0.5, the algorithm needs only one fifth of its iterations to converge. This is a great achievement in respect of convergence speed of the DE algorithm. Further improvement in the convergence speed is observed when the value of the Weighting Factor (F) is increased from 0.5 to 0.7. However, if the value of F is increased further to 1.0, there is hardly any improvement in the convergence speed of the algorithm. Accordingly for the FIR pulse-shaping filter design problem, the optimized value of Weighting Factor (F) can now be recommended as 0.7 irrespective of Population sizes.

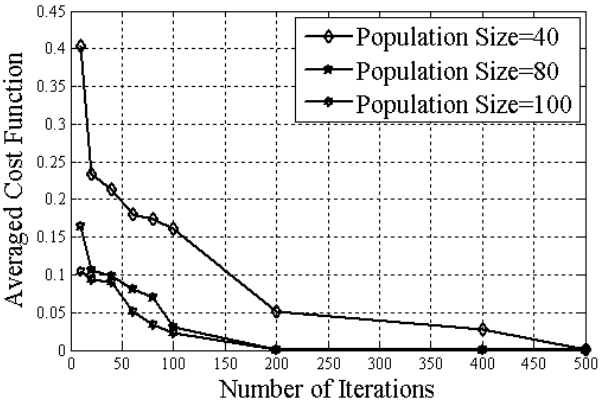

(a)

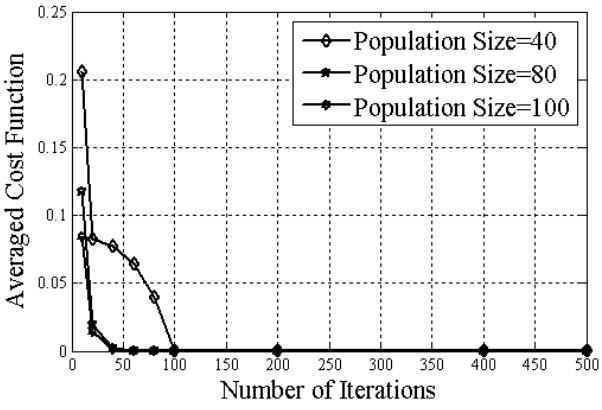

(b)

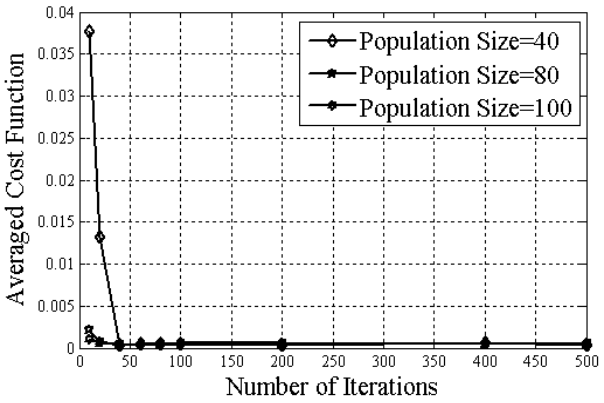

(c)

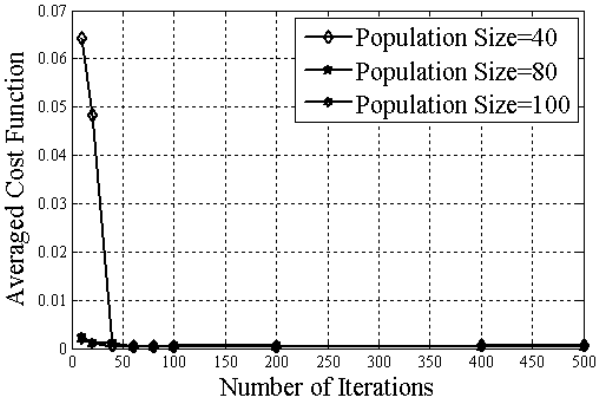

(d)

Figure 1. Convergence behavior of DE in design of low-pass FIR filter with CR=0.5 (a) F = 0.3 (b) F=0.5, (c) F=0.7 and (d) F=1.0

The above results can conveniently be summarized in a much compact form by plotting the variation of averaged cost function with Weighting Factor F as shown in Fig. 2. Fig. 2 confirms the fact that the lowest value of the averaged cost function i.e. error value is obtained for F=0.7, after which there is hardly any variation in the averaged cost function value.

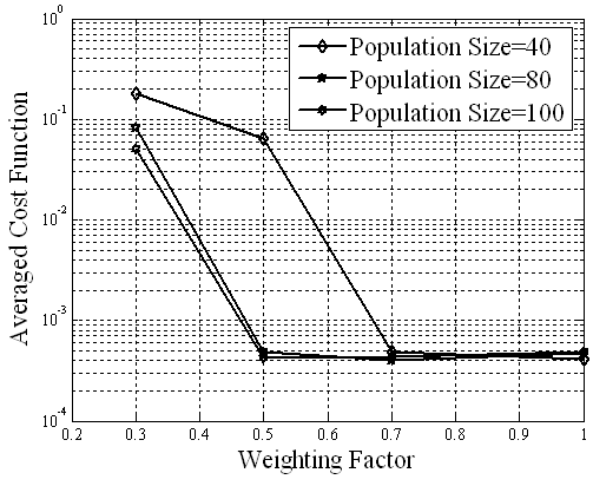

Figure 2. Variation of averaged cost function with Weighting Factor (F)

The performance of the FIR filter with the variation of F has been analyzed by plotting the magnitude response of the filter as shown in Fig. 3 with number of iterations being 100.

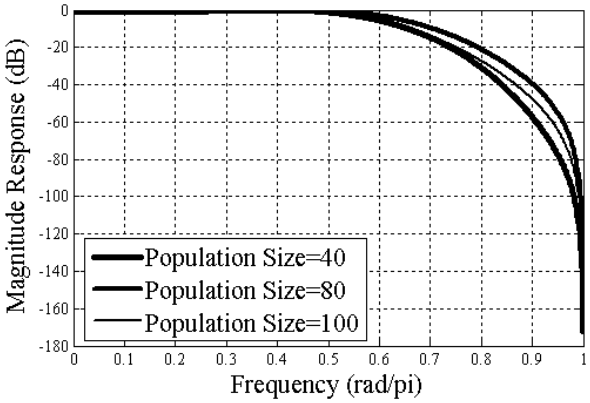

(a)

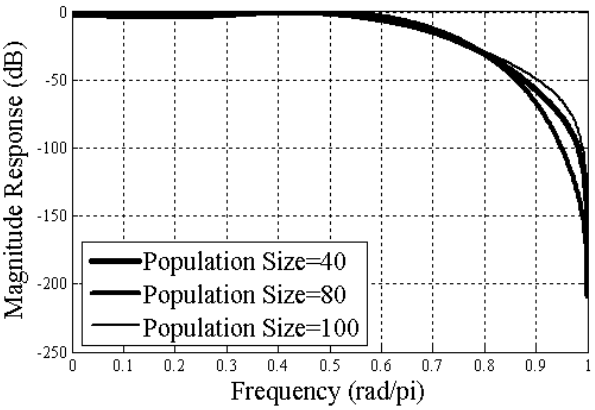

(b)

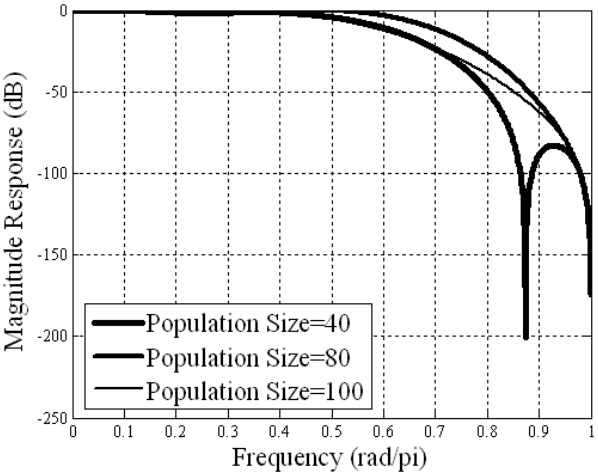

(c)

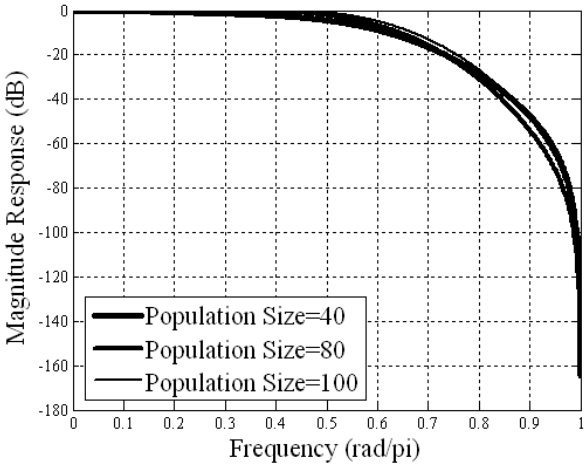

(d)

Figure 3. Magnitude response of designed low-pass FIR filter with CR=0.5 (a) F=0.3 (b) F=0.5 (c) F=0.7 (d) F=1.0

From the above figures, it can be clearly seen that the designed low-pass FIR filter shows better performance in terms of attenuation in the stop band, when the value of F is set to 0.7. More explicitly, when F is equal to 0.5 or 1.0, the maximum attenuation at a frequency of 0.8 rad/pi is almost equal to 30 dB. Whereas, for F = 0.7, the maximum attenuation at the same frequency is approximately found to be 50 dB. However, in terms of the performance in the pass band, FIR filter designed with the maximum population size exhibits a response, which is very close to the ideal one irrespective of the values of the Weighting Factor. Thus from these magnitude response plots we can infer that when the Weighting Factor (F) is set to a value of 0.7, the low-pass FIR filter shows the best result. Hence from the performance point of view, the optimized value of F is to be considered as 0.7 for the efficient design of low-pass FIR filter.

The performance of the FIR filter has also been evaluated in terms of its impulse response. The nature of the impulse response of the designed low-pass FIR filter for three different values of the Weighting Factor (F) has been depicted in Fig. 4 each for population size (P) = 100 and number of iterations (I) of 100.

From the figures below it is quite evident that the impulse response of the FIR filter with F = 0.7 gives the best result as it shows less amount of side lobe variation compared to others. Less number of side lobes with smaller amplitude will result in a lower value of ISI if the DE optimized FIR filter with F=0.7 is used as a pulse-shaping filter in a QPSK modulated system.

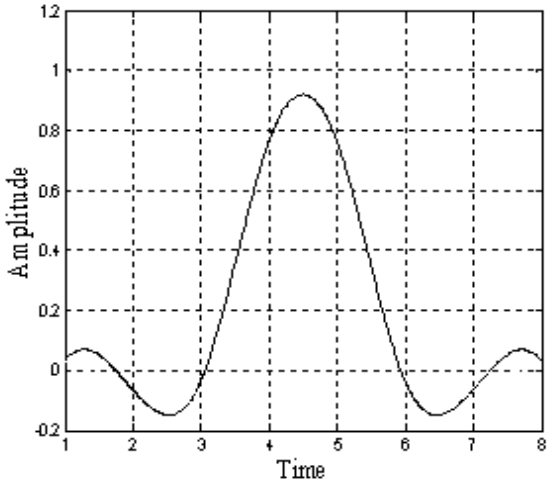

(a)

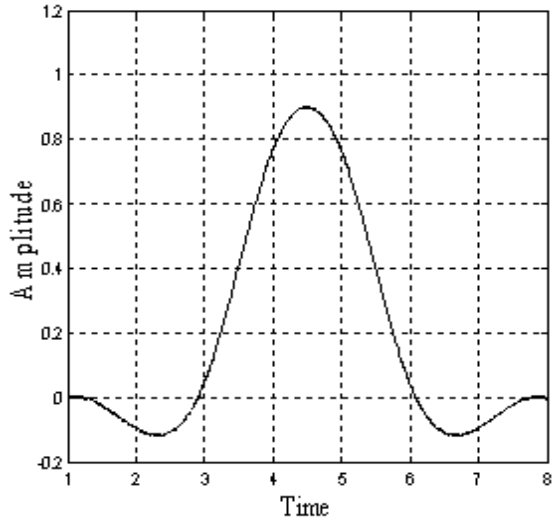

(b)

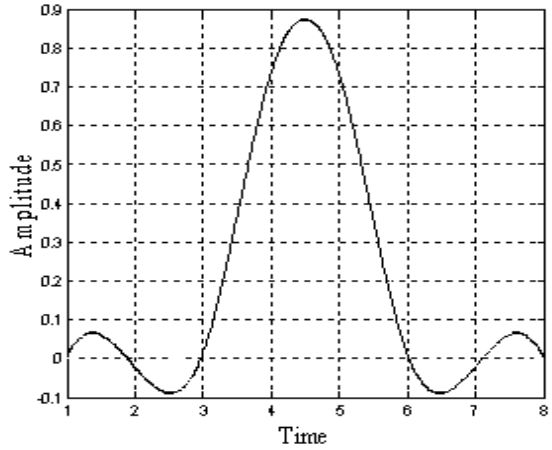

(c)

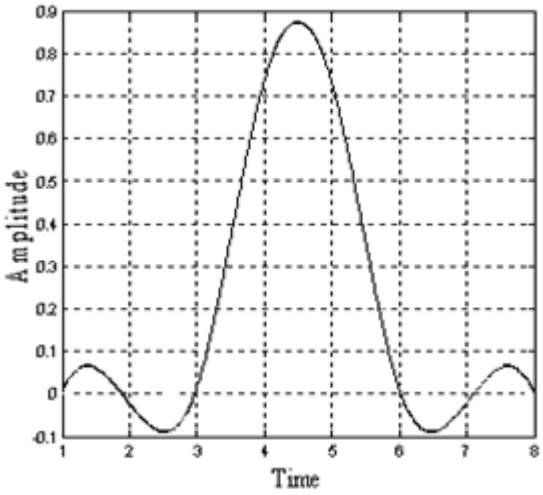

(d)

Figure 4. Impulse response of the designed low-pass filter with CR=0.5 (a) F = 0.3 (b) F=0.5, (c) F=0.7 and (d) F=1.0

Keeping the control parameter F at its optimized value of 0.7, the impact of another control parameter, namely Crossover Probability (CR) on the convergence behavior of the DE algorithm has next been studied, as presented in Fig. 5.

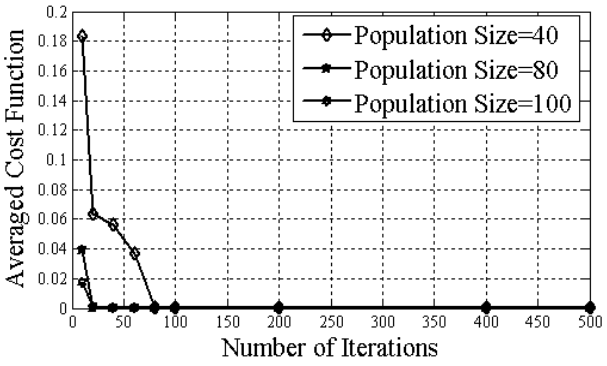

(a)

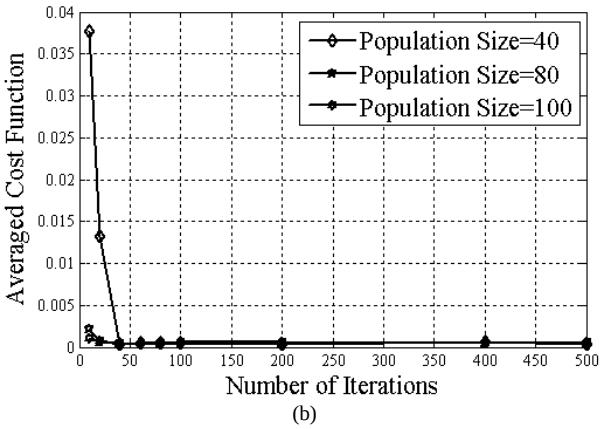

(b)

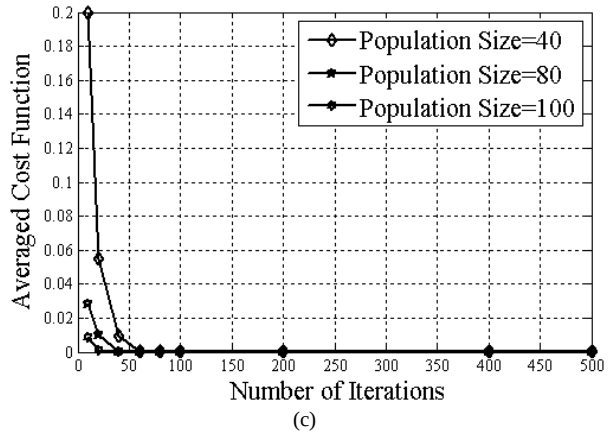

(c)

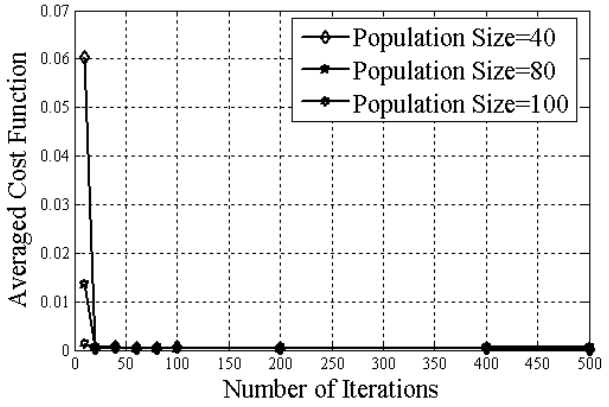

(d)

Figure 5. Convergence behavior of DE in design of low-pass FIR filter with F=0.7 (a) CR = 0.3 (b) CR=0.5, (c) CR=0.7 and (d) CR=0.9

It can be observed from Fig. 5 that the convergence behavior of DE is less sensitive to the control parameter "Crossover Probability" for population sizes of 80 and 100. But corresponding to population size of 40, it shows a considerable improvement in the convergence speed when the value of "Crossover Probability" is varied from 0.3 to 0.5. However, further higher values of "Crossover Probability" hardly show any considerable improvement in the convergence speed. Hence considering the above facts, the optimum value of "Crossover Probability" can be considered as 0.5 when F = 0.7.

The above facts have also been presented in a concise manner in Fig. 6, which clearly indicates that the optimum value of "Crossover Probability" could be considered as 0.5.

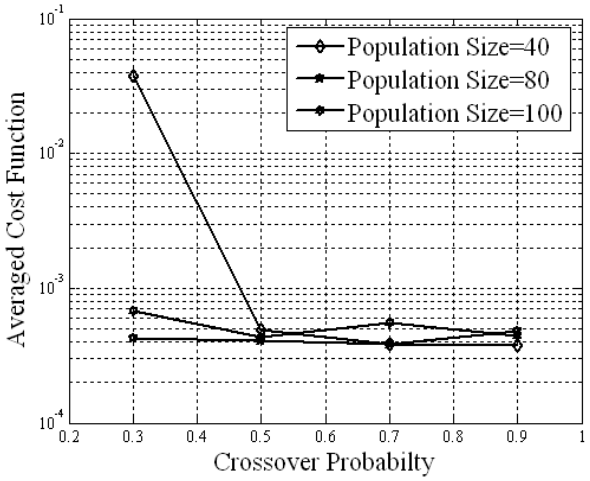

Figure 6. Variation of averaged cost function with Crossover Probability (CR)

The magnitude response of the FIR filter for different values of "Crossover Probability" has been presented in Fig. 7, with the optimized value of the "Weighting Factor" as 0.7. The curves corresponding to Fig. 7 have been plotted with the values of population size and number of iterations, both to be 100.

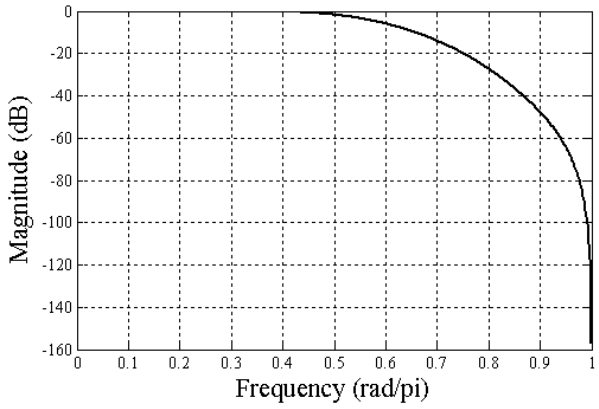

(a)

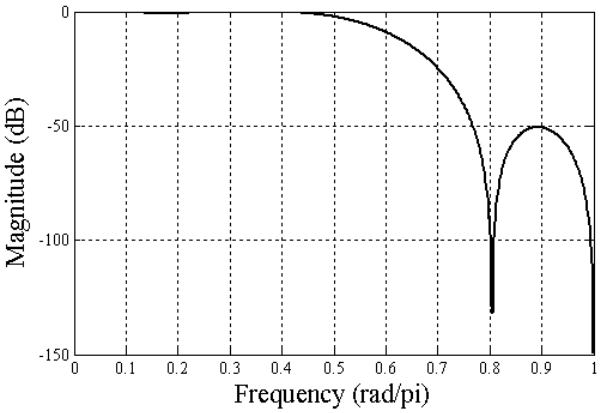

(b)

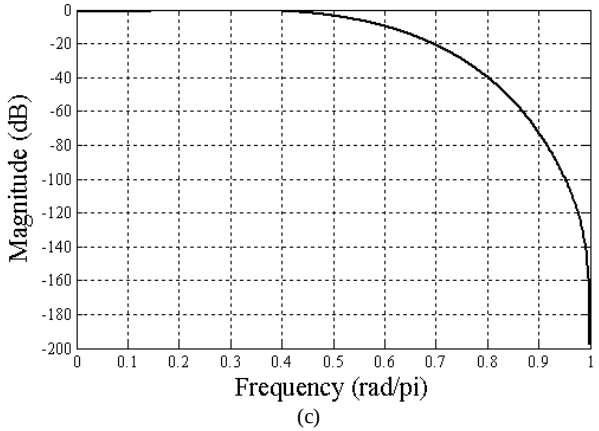

(c)

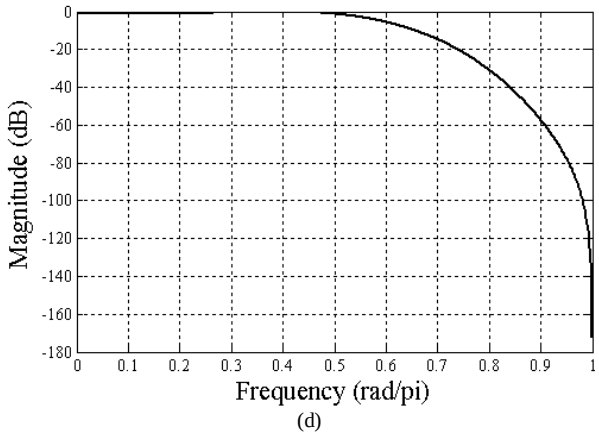

(d)

Figure 7. Magnitude response of designed low-pass FIR filter with F=0.7 (a) CR=0.3 (b) CR=0.5 (c) CR=0.7 (d) CR=0.9

A close inspection of the above curves shows that the pass band behavior of the designed filter for different values of "Crossover Probability" is almost similar. Where as the stop band behavior shows supremacy for CR = 0.5. This can be clearly explained by considering a particular frequency of 0.8 rad/pi. At this frequency, the stop band attenuation is around 120 dB for CR = 0.5, where as, for other values of CR, the stop band attenuation varies between 20 to 40 dB.

The nature of the impulse responses of the FIR filter, designed with the optimized value of F and four different sample values of CR, has been depicted in Fig. 8. Each of the impulse responses has been obtained with a population size (P) of 100 and number of iterations (I) also of 100.

Fig. 8 illustrates that impulse response obtained with a CR value of 0.5 yields the best response amongst the four as it includes less number of side lobes with quite insignificant amplitudes of them. Consequently, it will result in less interference amongst the succeeding and preceding pulses in a band limited digital communication system.

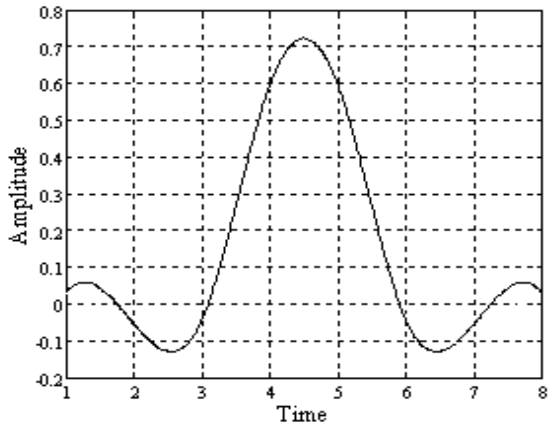

(a)

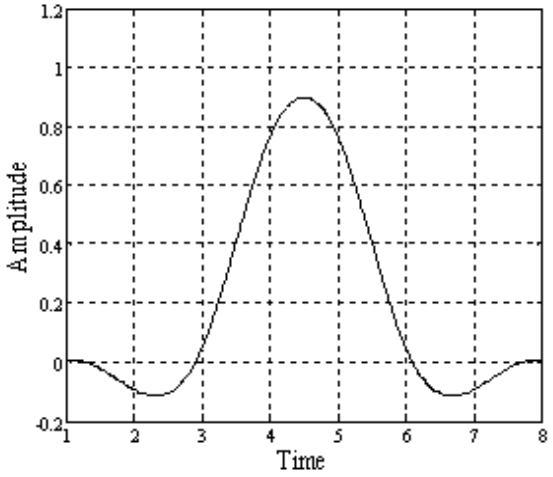

(b)

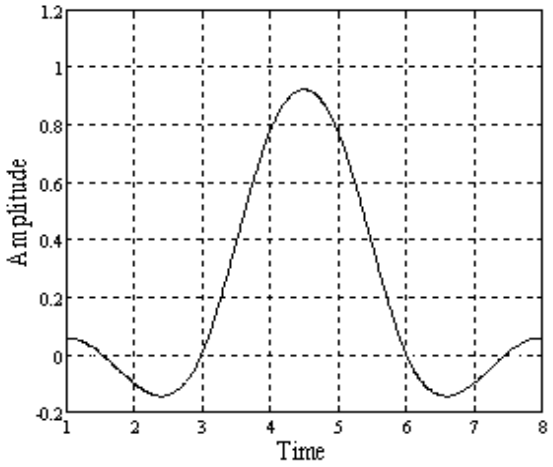

(c)

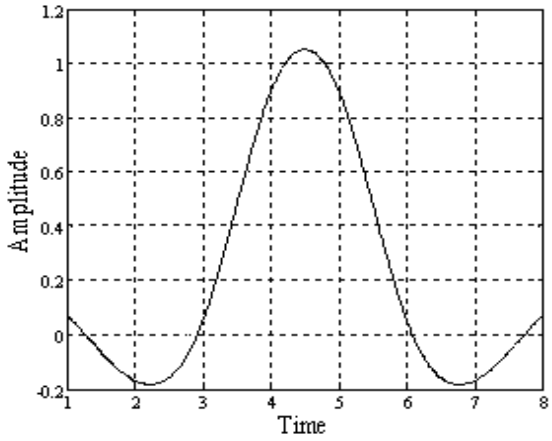

(d)

Figure 8. Impulse response of the designed low-pass filter with F=0.7 (a) CR = 0.3 (b) CR=0.5, (c) CR=0.7 and (d) CR=0.9

The above fact has also been substantiated by recording the In-phase Eye diagrams of the QPSK modulated system based on the DE designed FIR filter using Agilent E4438C 250 KHz–3 GHz ESG vector signal Generator (VSG), E4405B 9 KHz– 13.2 GHz ESA-E Series Spectrum Analyzer together with 89600 Vector Signal Analyzer (VSA) version 5.30 software, for F = 0.5, 0.7 and 1.0 as shown in Fig. 9, each for Population Size (P) = 100 and number of Iterations of 100.

During measurement, the VSG has been characterized in the following ways:

Baseband data	: pn-sequence of length 63
Symbol rate	: 25 Ksps
Pulse-shaping filter	: User defined FIR
Modulation type	: QPSK
Carrier amplitude	: 0dBm
Carrier frequency	: 10 MHz

Following options have been set in VSA software:

Reference filter	: user defined
Measurement filter	: off
Symbol rate	: 25 KHz
Modulation format	: QPSK
Result length	: 256 symbols
Points/symbol	: 5

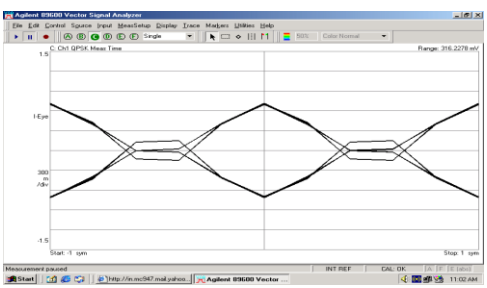

(a)

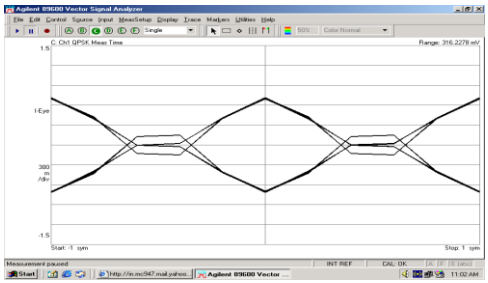

(b)

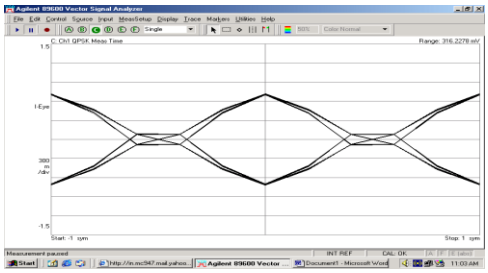

(c)

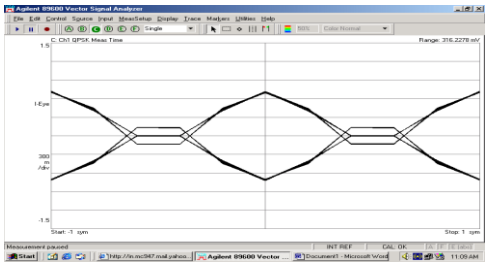

(d)

Figure 9. Eye diagram of the designed low-pass filter with CR=0.5 (a) F = 0.3 (b) F=0.5, (c) F=0.7 and (d) F=1.0

Comparison of the above figures shows that the Eye width and hence the Eye opening for the FIR filter with F=0.7 is slightly more than those with F=0.5 and F=1.0. Since the open part of the Eye represents the time over which the signal can be sampled with fidelity, larger the Eye opening, less the effect of ISI. It is also prominent that the effective crossover region of the Eye diagram and hence the amount of jitter present in the signal is less for F=0.7 as compared to others. Hence from the system ISI point of view, the FIR filters with F=0.7 provides the optimized performance.

The effect of "Crossover Probability" (CR) on the In-phase Eye diagrams of the QPSK modulated system has also been demonstrated in Fig. 10. Fig. 10 reflects the fact that the best Eye diagram is obtained with CR = 0.5, which again supports the other measured results.

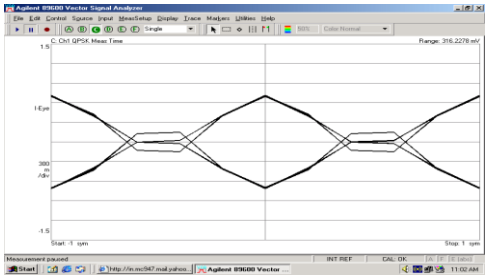

(a)

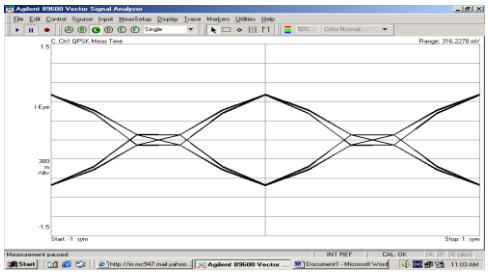

(b)

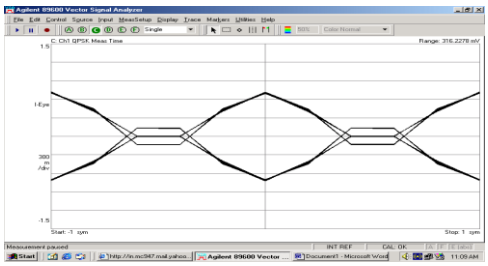

(c)

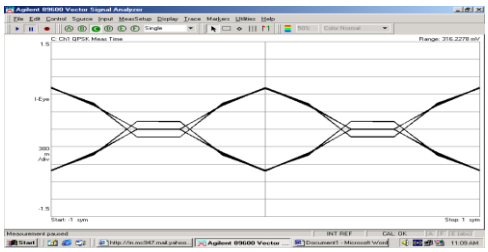

(d)

Figure 10. Eye diagram of the designed low-pass filter with F=0.7 (a) CR = 0.3 (b) CR=0.5, (c) CR=0.7 and (d) CR=0.9

To study the effect of the "Weighting Factor" (F) on the BER performance of the QPSK modulated system, the DE optimized filter has been used as a pulse-shaping filter. Table I depicts the variation of the BER with Weighting Factor (F) when the parameter "Crossover Probability" (CR) has been maintained at a value of 0.5.

TABLE I
VARIATION OF BER WITH WEIGHTING FACTOR (F)
(CR=0.5)

Population Size	F=0.3	F=0.5	F=0.7	F=1.0
40	0.4762	0.4921	0.5079	0.4603
80	0.4762	0.4921	0.4286	0.4556
100	0.4687	0.4603	0.3651	0.3810

Table I clearly indicates that the resulting BER value largely depends on the choice of the Weighting Factor. It is quite apparent that for the larger population size, the BER of QPSK modulated system attains its minimum value when the Weighting Factor is chosen to be 0.7.

The effect of another control parameter "Crossover Probability" (CR) on the BER performance of QPSK modulated system has been presented in Table II when the value of "F" has been maintained at its optimized value i.e. 0.7.

TABLE II
VARIATION OF BER WITH CROSSOVER PROBABILITY (CR)
(F=0.7)

Population Size	CR=0.3	CR=0.5	CR=0.7	CR=0.9
40	0.4762	0.4921	0.4762	0.4921
80	0.4762	0.4286	0.4603	0.4603
100	0.4762	0.3651	0.4762	0.4603

From the numerical data presented in Table II, it is clear that once the control parameter "F" is maintained at its optimized value of 0.7, the corresponding optimized value of "CR" is found to be 0.5.

From the detailed discussion of the above measurement results, the final outcome of this work i.e. the optimized values of the control parameters "F" and "CR" have been presented in Table III.

TABLE III
OPTIMIZED VALUES OF "F" & "CR"

Different values of "F" used	Optimized value of "F"	Different values of "CR" used	Optimized value of "CR"
0.3	0.7	0.3	0.5
0.5		0.5	
0.7		0.7	
1.0		0.9	

Finally it is now recommended that the FIR filter designed with a "Weighting Factor" of 0.7 and "Crossover Probability" of 0.5 provides the best performance in terms of convergence speed, magnitude response, impulse response and BER performance, supported with practically measured Eye diagrams when used as a pulse-shaping filter in a QPSK modulated digital communication system.

V. CONCLUSION

DE is a very useful optimization technique that exhibits a very good convergence property using less number of control parameters. The values assigned to those parameters have a great impact on the convergence speed of the algorithm since the averaged cost function depends significantly on those parameter values. Accordingly, the right choice of these parameters is of paramount importance in any particular application utilizing this evolutionary algorithm. In this paper, we have investigated the effect of two control parameters of DE, namely "Weighting Factor" (F) and "Crossover

Probability" (CR) on the convergence behavior of the algorithm, applied in FIR filter design problem. Analyzing our simulation results, we have recommended the optimized value for the Weighting Factor (F) and the Crossover Probability (CR) for this specific design problem when used as a pulse-shaping filter in a QPSK modulated system. The optimized value of the control parameters have also been equally supported by experimentally measured Eye diagrams.

REFERENCES

[1] S.K. Mitra, *Digital Signal Processing: A Computer-based Approach*, McGraw-Hill, 2001.

[2] A. Antoniou, *Digital Filters: Analysis, Design and Applications*, McGraw-Hill, 2001.

[3] B. Somanathan Nair, *Digital Signal Processing: Theory, Analysis and Digital-filter Design*, Prentice-Hall, 2004.

[4] S. Haykin, *Communication Systems*, John Wiley & Sons, 2007.

[5] A. M. Barros, A. L. Stelle and H.S. Lopes, "A FIR filter design tool using genetic algorithms", *COBENGE 2006*, pp. 1.799-1.811, 2006.

[6] G. Venkataraman, S. M. Reddy and I. Pomeranz, "GALLOP: Genetic algorithm based low power FSM synthesis by simultaneous partitioning and state assignment", in *Proc. of International Conference on VLSI Design*, pp. 533–538, 2003.

[7] L. R. Rabiner, J. H. McClellan and T. W. Parks, "FIR digital filter design techniques using weighted Chebyshev approximation", in *Proc. of the IEEE. New York*, vol. 63, no. 4, pp. 595-610, 1975.

[8] M. Najjarzadeh and A. Ayatollahi, "FIR digital filters design: particle swarm optimization utilizing LMS and minimax strategies", in *Proc. of IEEE International Symposium on Signal Processing and Information Technology*, pp. 129-132, December, 2008.

[9] Shing-Tai Pan, Bo-Yu Tsai and Chao-Shun Yang, "Differential evolution algorithm on robust IIR filter design and implementation", in *Proc. of Eighth International Conference on Intelligent Systems Design and Application*, pp. 537-542, December, 2008.

[10] S. Chattopadhyay, S. K. Sanyal and A. Chandra, "Design of FIR filter based on differential evolution optimization technique & to study its effect as a pulse-shaping filter in a QPSK modulated system", *International Journal of Computer Science and Network Security*, vol.10, no. 1, pp. 313-321 January, 2010.

[11] J. Brest, S. Greiner, B. Boskovic , M. Mernik, and V. Zumer, "Self-adapting control parameters in differential evolution: a comparative study on numerical benchmark problems", *IEEE Transactions on Evolutionary Computation*, vol. 10, no. 6,pp. 646-657, December, 2006.

[12] S. Chattopadhyay, S. K. Sanyal and A. Chandra, "Optimization of control parameter of differential evolution algorithm for efficient design of FIR filter", in *Proc. of International Conference on Computer and Information Technology (ICCIT-2010)*, Dhaka, Bangladesh, December, 2010.

[13] R. Storn and K. V. Price, "Differential evolution- a simple and efficient adaptive scheme for global optimization over continuous spaces", *ICSI*, Berkeley, TR-95-012, 1995.

[14] J. Liu and J. Lampinen, "On setting the control parameter of the differential evolution method", in *Proc. 8th Int. Conf. Soft Computing (MENDEL 2002)*, pp. 11–18, 2002.

[15] S. Das, A. Abraham and A. Konar, "Particle swarm optimization and differential evolution algorithms: technical analysis, applications and hybridization perspectives", *Studies in Computational Intelligence (SCI)* , 116, 1-38, 2008.

[16] A. K. Qin and P. N. Suganthan, "Self-adaptive differential evolution algorithm for numerical optimization", *IEEE Congress on Evolutionary Computation CEC2005*, vol. 2, pp. 1785-1791.

[17] J. Liu and J. Lampinen, "A fuzzy adaptive differential evolution algorithm", *Soft Computing—A Fusion of Foundations, Methodologies and Applications*, vol. 9, no. 6, pp. 448–462, 2005.

[18] J. Brest, B. Boskovic, S. Greiner, V. Zumer, and M. Sepesy Maucec, "Performance comparison of self-adaptive and adaptive differential evolution algorithms", *Technical Report #2006-1-LABRAJ*, University of Maribor, Faculty of Electrical Engineering and Computer Science, Slovenia, 2006.

[19] K. Price and R. Storn, "Differential evolution: a simple evolution strategy for fast optimization", *Dr. Dobb's J. Software Tools*, vol. 22, no. 4, pp. 18–24, April 1997.

[20] R. Gämperle, S. D. Müller and P. Koumoutsakos, "A parameter study for differential evolution", *WSEAS NNA-FSFS-EC 2002*, Interlaken, Switzerland, WSEAS, Feb.11-15, 2002.

[21] John G. Proakis, *Digital Communications*, 3rd Edition, Chapter 9, McGraw-Hill Book Co., 1995.

[22] T. S. Rappaport, *Wireless Communications: Principles and Practice*, 2nd Edition, Chapter 6, Prentice Hall of India Pvt. Ltd., 2007.

[23] K. Feher, *Wireless Digital Communications, Modulation & Spread Spectrum Analysis*, Chapter 4, Prentice Hall of India Pvt. Ltd., 2005.

Sudipta Chattopadhyay received her B. Tech in Instrumentation Engineering in 1994 from Calcutta University, Kolkata- 700 009, India and M.E.Tel.E in 2001 from Jadavpur University, Kolkata – 700 032, India.

She was a Lecturer in the Department of Electronics and Communication Engineering at Institute of Technical Education and Research, Bhubaneswar, India, from 1996-2001 and also worked as Lecturer, Sr. Lecturer and Asst. Professor in the Department of Electronics and Communication Engineering at Netaji Subash Engineering College, Kolkata – 700 152, India, from 2001-2006. She is now working as an Assistant Professor in the Department of Electronics and Telecommunication Engineering, Jadavpur University, Kolkata – 700 032, India since 2006. She has published a number of papers in International/National Conferences. Her current research interests include Digital/Mobile Communication, Coding Theory and Digital Signal Processing.

Mrs. Chattopadhyay is a member of IEEE since last 10 years. She is also an Executive Committee member of the Affinity Group "Women in Engineering" under IEEE Calcutta Section.

Salil Kumar Sanyal received his B.E.Tel.E, M.E.Tel.E and Ph. D (Engg.) in 1977, 1979 and 1990 respectively all from Jaduvpur University, Kolkata –700 032, India.

He joined the Department of Electronics and Telecommunication Engineering, Jadavpur University as Lecturer in 1982 and currently he is a Professor of the same department. His current research interests include Analog/Digital/Radar/Genomic Signal Processing, Mobile and Digital Communication and Tunable Micostrip Antenna. He has published more than 125 papers in International/National Conferences and in International Journals of repute.

Dr. Sanyal is a Senior Member of IEEE. He also served as the Chairman of IEEE Calcutta section during 2006-2008 and at present he is the Chair of Circuits and Systems Society Chapter of IEEE Calcutta Section.

Abhijit Chandra received his B.E. in Electronics & Telecommunication Engineering in 2008 from Bengal Engineering & Science University, Shibpur, Howrah-711 103, India and M.E.Tel.E. with specialization in Communication Engineering in 2010 from Jadavpur University, Kolkata-700 032, India.

Currently, he is working as an Assistant Professor in the Department of Electronics & Telecommunication Engineering at Bengal Engineering & Science University, Shibpur. He has published few papers in International/National Conferences. His research area includes Digital Signal Processing, Evolutionary Optimization Techniques, Digital/Mobile Communication Systems, Information and Coding Theory.

Mr. Chandra has received President's Gold Medal from Bengal Engineering & Science University, Shibpur in 2010 for being First in the faculty of Engineering and Technology at B.E. examination 2008. He has also received University Medal from Jadavpur University in 2010 for standing First in order of merit at M.E. Tel. E. examination 2010.

Adaptive Receiver Power Routing Protocol for Mobile Ad Hoc Wireless Network

Lawal Bello, Panos Bakalis, Predrag Rapajic, Kwashie A. Anang and Titus I. Eneh
Mobile and Wireless Communications Research Centre, University of Greenwich, Chatham, UK
Email: {L.Bello, P.Bakalis, P.Rapajic, K.Anang, T.Eneh}@greenwich.ac.uk

***Abstract*— In this paper, an Adaptive Receiver Power Routing (ARPR) protocol technique for Mobile Ad Hoc wireless network is proposed. The adaptive receiver power routing (ARPR) protocol evaluates the effect of environment, and signal path loss on a mobile ad hoc wireless network quality of service (QoS) and throughput performance. The proposed technique is incorporated into Dynamic Source Routing (DSR) protocol. Mathematical analysis supported by computer simulations is used to validate the scalability of the proposed technique. The simulation results showed that when ARPR is incorporated into DSR the throughput performance increased by 62.5 %, compared to the conventional DSR protocol model, without ARPR. The simulation result also showed that the average received power for individual nodes was 1.0×10^{-10} watt for the proposed ARPR model and 5.0×10^{-2} watt for conventional model.**

***Index Terms*— adaptive receiver, DSR routing protocol, mobile ad hoc networks, power-routing**

I. Introduction

Power is consumed in mobile ad hoc wireless network due to excessive utilization during network routing operations. Thus, a node may cease to function as a result of power depletion. This problem consequently leads to mobile nodes behaving selfishly and thus affecting the entire performance of the network [1]. In [2], [3], selfish nodes were described as nodes that lack network resources such as transmit power and bandwidth to carry out their network operation. Selfish nodes are nodes participating in routing operations but may not be willing to use their computing and energy resources to forward packets that are not directly beneficial to them. They may be dropping packets instead of forwarding packets to their respective destinations.

MANET are used in areas where infrastructured network are not possible without having any centralized administration, such as disaster areas, battlefield, emergency and rescue places. These areas are severely affected by different environmental conditions such as hill shade, which consequently affect the received signal power strength, network routing operation and the entire performance of the network [4]. Different routing protocols have been proposed, these protocols can be classified either as reactive or proactive protocols [5]. The reactive routing protocols sends out route request for routes-to-destination if the source node have data packets to send. The proactive routing protocols uses routing tables which are maintained via periodic updates from all other nodes in the network, irrespective of the fact that the network may not be active in terms of data traffic. Yuvaraju et. al in [1], reported that proactive routing protocols consumes more power as compare to reactive routing protocols, which is due to continuous periodic update of the proactive routing protocols. Routing protocols ensures the proper routing of packets from source to destination via intermediate nodes. The total power consumption and the received signal power strength depends on the distance between mobile nodes, signal path loss, network environmental conditions and the type of application running. Currently, most research work carried out in the area of routing protocols uses free space path loss model to represent the network environment [4], [3], [2], [6]. However, free space path loss model does not include the effects of other environmental conditions; such as hill shade, when evaluating the received signal power.

Manuscript received January 31, 2011; revised; June 10, 2011; accepted June 14, 2011.

II. Related Work

Anderegg and Eidenbenz in [7], proposed an energy-efficient routing protocol (Ad Hoc-VCG protocol) for detecting selfish nodes, to ensure that a packet from a source node-to-destination gets routed along the most energy-efficient path via intermediate nodes. The Ad Hoc-VCG protocol works efficiently for networks where communications session between mobile nodes does not change frequently during a session. However, considering the nature of MANETs, where mobile nodes are free to move randomly and network topology changes rapidly and unpredictably. Thus, this routing protocol is not suitable for practical applications in MANET. There are two general techniques in detecting selfish nodes within a network; these are Watchdog and Pathrater [8]. These techniques are combined with the standard reactive routing protocol in MANET and the selfish nodes are recognized by listening to the next nodes to observe if the packets are forwarded, and if not the node is marked as selfish node after some time. However, watchdog and pathrater techniques are detective rather than preventive techniques; they might not detect selfish nodes in the presence of limited transmission power, network congestions and partial dropping of packets due to link or routing failure. Nie and Zhou in [9] proposed a model

doi:10.4304/jcm.6.7.571-580

which detects selfish nodes and forced them to cooperate. However, forcing a node with limited network resources to cooperate can affect other cooperative mobile nodes in the network. Researches carried out by Yuvaraju et. al in [1] and Ramachandran et. al in [6], showed that as network capacity increases, the total power consumption increases concurrently, thus requiring more routes to reach the destination, consequently increasing the end-to-end delay. Routing are distributed overall the participating nodes and this can be critical under resource consumptions especially when the network size increases [10]. Our research focused on designing an adaptive receiver power routing protocol, which will improve the quality of service and the throughput performance of MANET routing protocols.

The rest of the paper is organized as follows. Section II present a summary of related works. Section III gives an overview of Dynamic Source Routing protocol. Section IV describes the proposed ARPR power model for Dynamic Source Routing protocol. Section V presents the simulation; model and environment. Section VI presents results and disussion. Finally VII presents conclusions.

III. OVERVIEW OF DYNAMIC SOURCE ROUTING PROTOCOL (DSR)

Dynamic Source Routing is a simple, efficient and an On-demand routing protocol designed specifically for use in multi-hop wireless ad hoc networks of mobile nodes that uses source routing rather than hop-by-hop routing approach [12]. Each packet to be routed carries in its header, a complete ordered list of nodes through which the packet passes. The advantage of this protocol is that, intermediate nodes do not need to maintain up-to-date routing information in order to route the packets they forward. Due to the on-demand characteristics of DSR, periodic route updates and neighbor detection are eliminated to minimize bandwidth consumption [5], [13]. DSR has two basic mechanisms of operations, Route Discovery process by flooding the network with a route request (RREQ) packets to all its neighboring nodes containing the IP address of both sender and receiver in the packet header as shown in Fig. 1(a), whilst Route reply returns the route reply messages (RREP). The route reply contains the list of the best routes from the source initiator to the target destination as shown in Fig. 1(b).

Performance evaluation conducted on both proactive and reactive protocols in [12], [14], [15], [16], [17], showed that DSR performs better than Ad Hoc On demand Distance Vector (AODV) and other proactive protocols in terms of throughput, end-to-end delay, and packets drop. The DSR performance is attributed to its characteristics of having multiple routes to other destination. In case of link failure, it does not require a new route discovery processes. Because of this, end-to-end delay is reduced, less packet dropping and less energy consumption. Reference [18], [19], [20] showed that, the DSR has less energy consumption in the entire network as compared to its counterpart AODV, which losses energy due to broadcasting hello messages to update its routes. Hence, the DSR protocol was chosen as genial candidate for carrying out this research.

A. Conventional DSR Packet Format

To improve the communication performances and reliability; traffic data sent between mobile nodes are subdivided into packets headers. The DSR protocol uses specific headers to carry information. The header must be a multiple of 4 bytes in case other headers follow the DSR Options header. The DSR header format is shown in Table I.

TABLE I.
CONVENTIONAL DSR HEADERS

Next Header	Reserved	Payload	Options	Data
8 bits	8 bits	16 bits	0 bits	0 bits

The packets formats are defined as follows:

- **Next Header:** The size of the Next Header field is 8 bits. The Next Header field shows either the type of the first extension (if any extension header is available) or the protocol in the upper layer such as TCP, UDP.
- **Payload Length:** Specifies the length of the payload, in bytes, that the packet is encapsulating. The value of the Payload Length field defines the total length of all options carried in the DSR Options header such as route request option, route reply option.

B. Convention DSR Protocol

Routing protocol is responsible of routing packets from the IP datagram between mobile nodes, and also verifies if the packet is coming from the upper layer or lower layer of the network protocol stack and makes a decision of where to forward the packet protocol (appendix A) [21]. Figure 2, shows the network protocol stack and the process model for the conventional DSR routing protocol. DSR protocol is implemented at the network layer; IP dispatch is the root process for network layer, and has as a child process; manet manager. Manet manager acts as manager process for DSR and provides an interface to DSR routing protocols.

C. Modification Cost of DSR Protocol

Sheetalkumar et. al in [3], gave the modification cost for existing dynamic source routing protocol as shown in Table II. The authors in [3], considered the minimum route maintenance energy, which involved the modification of routing software and 802.11; without considering the proper modification of DSR routing algorithm and transmits power control. Also to the best of our knowledge this modification have not being applied to existing version of the DSR protocol to achieve an optimized quality of service. The routing algorithm modification cost involves the cost of changes made to existing routing algorithm. In our work we considered modification of the routing software and power control.

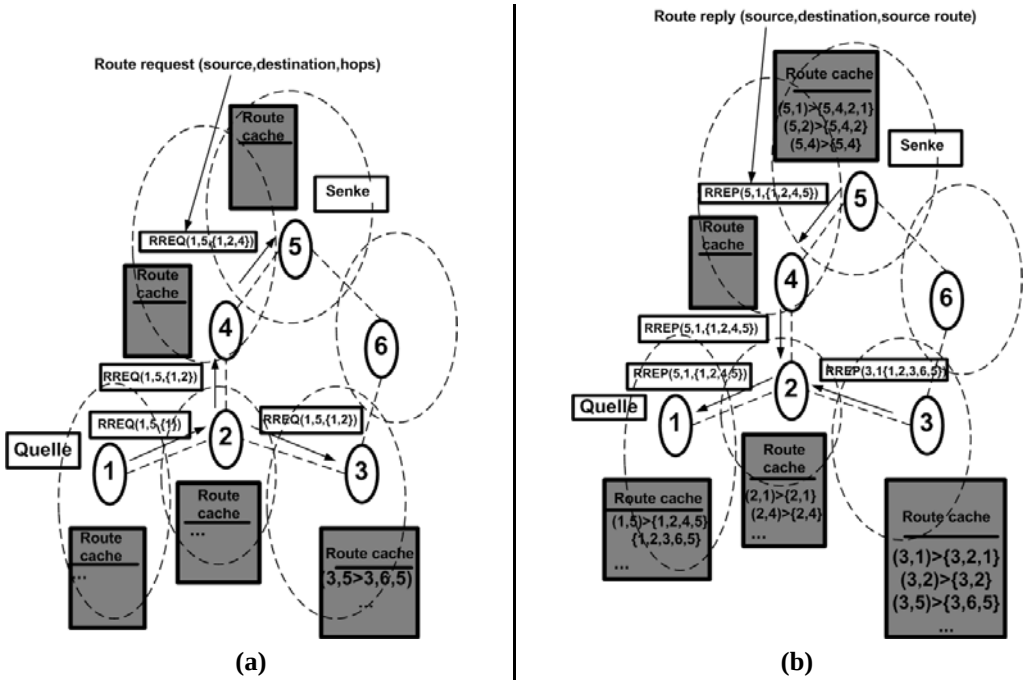

Figure 1. Overview of DSR protocol: (a) Route request process. (b) Route reply process [11].

TABLE II.
MODIFICATION COST

Routing features of power routing protocol	Routing software modification	IEEE 802.11 modification	Radio hardware modification
Link energy cost	Yes	No	No
Tx power control	Yes	Yes	Yes
Route discovery min. energy route	Yes	No	No
Route maintenance min. energy	Yes	No	No
Link cache	Yes	No	No

IV. PROPOSED ADAPTIVE RECEIVER POWER CONTROL PROTOCOL

Considering current MANET applications, it is important for existing routing algorithm for MANET to be modified to specifically accommodate power model for better routing in the network. However the free space path loss model only takes into account distance between mobile nodes and the frequency of transmission. The free space model is limited in its ability to accurately predict signal path loss in most network environments. Our technique takes into account the modification of existing routing algorithm for dynamic source routing protocol (DSR), modification of power control and the inclusion of mathematical model to represent other environmental conditions.

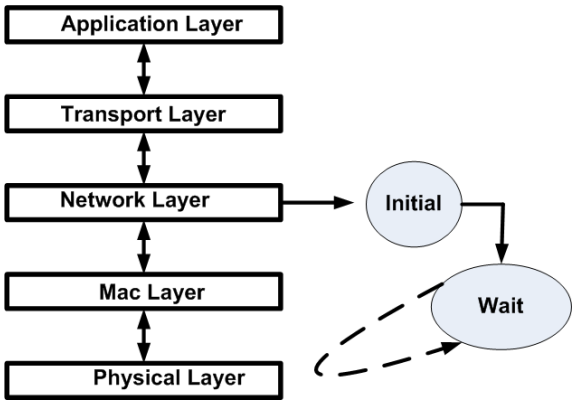

Figure 2. Conventional DSR Protocol

A. DSR Packet Format with Power Values

In this section, we describe changes made to the conventional DSR packet format. We added four power values to the conventional DSR packet format; which included, transmit power level, received power level, minimum transmit power level and minimum receive power level as shown in Table III.

For successful transmission and reception of data packets the minimum transmit and minimum received power levels are required. These power values are made available to the DSR protocol of the protocol stack.

B. DSR Protocol with Power Model

DSR protocol is implemented at the network layer, with addition of power model process (appendix B). The Physical layer, wireless mac layer, sends the measured values of transmit power, minimum transmit power, received signal

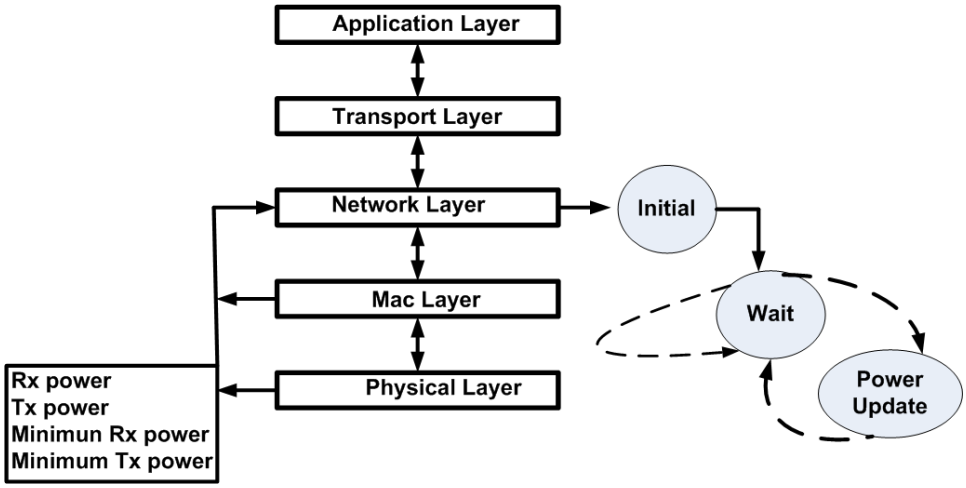

Figure 3. Modified DSR Protocol with Power Model

TABLE III.
MODIFIED DSR PACKET FORMAT

Header	Reserved	Payload	Options	Data
(8 bits)	(8 bits)	(16 bits)	(0 bits)	(0 bits)
Rx Power (W) 0 bit	Tx Power (W) 0 bit	Min Tx Power (W) 0 bit	Min Rx Power (W) 0 bit	

power and the minimum received signal power to network routing layer (refer to figure 3) along the DSR packets, where it is stored and used for routing decision making process. Manet manager is responsible for spawning the DSR child process when a node is configured for DSR with power model

C. Power Management in DSR Protocol

The setbacks to power management in ad hoc mobile communications is choosing transmit power. The transmit power level determines the quality of the received signal. Most of the transmit power is consumed during the network routing processes. The idea behind power routing is to avoid unnecessary waste of packets as well as network resources that can make nodes to behave selfishly. At the network layer, the routing algorithms must select the best route that satisfies the probabilistic power condition as describe below.

If $((P_{Tx} >= Min_{tx})\&\&(P_{Rx} >= MinRx))$
{
Route Request send = True
}
Else
{
New routing search
}

D. Adaptive Receiver Power Model

We present the adaptive power model used for our analysis. This model assist us to analyze the effect of signal path loss, and other environmental conditions on the received signal power and the general performance of the network. The environmental conditions can be in different forms depending on the network operating environment. In urban areas, the environmental conditions may include cars engine noise, horns, trains, construction machines, and aircrafts noise etc. While in rural areas, it may include sounds from farm animals, and wildlife.

For a given environmental condition, the environmental constant Env_{const}, is the sum of the ambient noise level and boltzmann constant, which is given as:

$$Env_{const} = A_{noiselevel} + k_B \quad (1)$$

where $\text{A}_{noiselevel}$ is the ambient noise level, which is the sound pressure level at a given location and k_B is the Boltzmann constant, which is the physical constant value relating energy to individual particle level with temperature. Env_{const} includes noises from transport, industries, and recreation activities.

Assuming no obstructions between a transmitting mobile node and a receiving mobile node; signals will be transmitted through free space to a receiver located at a distance D [m]. The free space path loss model used in our analysis is given by [22], as:

$$P_L = \frac{\lambda^2}{(4\pi D)^2} \quad (2)$$

where P_L is the free space path loss, D is the distance between any two mobile nodes and λ is the carrier wave length.

The general loss (G_L) over the transmission channel is the sum of the free space path loss propagation model and the environmental constant value and can be written as

$$G_L = P_L + Env_{const} \quad (3)$$

From [23], the received signal power P_{Rx}, can be written as

$$P_{Rx} = P_{tx} + Env_{const} - 10P_L \times 10log10(D) + T \quad (4)$$

where P_{tx}, is the transmitted signal power and T is the terrain. However, due to frequent topology changes

associated with movements of mobile nodes in the network, the transmit power level for each mobile node is not the same. The minimum transmit and receive power, Min_{tx}, Min_{Rx} for successful transmission and reception of data/control packets requires to meet the probabilistic power condition given in (5) and (6)

$$Min_{tx} \geq \beta_0 \times \eta_0 \times g(u,v) \quad (5)$$

$$Min_{Rx} \geq \beta_0 \times \eta_0 \quad (6)$$

where β_0 is the signal to noise ratio, η_0 is ambient noise level strength and *g(u,v)* is the transmitter and receiver antenna gain.

V. SIMULATION MODEL

OPNET Modeller (version 16.0), developed by OPNET Technologies is used for all our simulations [21]. Details about the simulation model and environment are presented in the rest of this section.

OPNET Technologies, Inc. is a leading provider of solutions for IT service assurance. OPNET's best-in-class solutions address: application performance management, network performance management, and Network Research and Development. OPNET Solution delivers broad visibility and monitoring across infrastructure, infrastructureless domains as well as deep data collection and analysis to enable powerful root cause diagnosis. OPNET's solutions have been operationally proven in thousands of customer environments worldwide, including corporate and government enterprise, defense agencies, network service providers, and network equipment manufacturers [21].

A. Simulation Parameters

The adaptive receiver power model was computed and incorporated into DSR protocol. We simulated a network with 80 mobile nodes, using file transfer protocol (ftp) applications with medium load, which are randomly selected (sources and destinations) within a topology area of 700 $\times$ 500 meters. Constant Bit Rate (CBR) agents, with packets sizes of 4096 bits were used for traffic generation in the network. The simulation time was 3600 seconds real time, each simulation scenario was repeated 10 times, which enabled the simulation to converge for accurate result. The basic parameters used for the simulations are summarized in Table IV.

TABLE IV.
SIMULATION PARAMETERS

Parameters	Values
Simulation time	3600 seconds
Topology area	700 $\times$ 500 m
Number of nodes	80 nodes
Simulator	OPNET 16.0 wireless suite version
Node Mobility Model	Random Way point
Data rate (bits)	5.5 Mbps
Physical Characteristics	802.11g
Data rate (bits)	5.5 Mbps
Transmit power	0.100 W
Packet size (bits)	4096 bits
Packet inter-arrival time	0.5 seconds
Routing protocol	DSR
Boltzmann constant	1.379e-23 J/K
number of trials	10
Ambient Noise Level	1.0e-26

B. Performance Metrics

We use the following metrics to compare the performance of DSR protocol with proposed adaptive receiver power control protocol to conventional DSR protocol without adaptive receiver power control protocol.

- **Throughput:** represents the total number of successful packets in (bits/sec) received from all WLAN nodes of the network.
- **Bit Error Rate:** is the number of bit errors divided by the total number of transferred bits during a simulated time.
- **Bandwidth Utilization:** this metric measures the total bandwidth consumption, a value of 100.0 % indicates full usage of bandwidth.
- **Delay:** represents the end-to-end delay of all the packets received by the wireless LAN of the mobile nodes in the network.
- **Received Power (W):** this measures the power that is received by the individual nodes in the network.

VI. SIMULATION RESULTS AND DISCUSSION

Simulation results are presented in this section. Figure 4, shows the performance throughput with and without ARPR power model. The initial rise in throughput is due to route discovery processes initiated by the routing protocol. This shows that more control information in the form of route request (RREQ) and route reply (RREP) were forwarded by all nodes in the network, which lead to a higher throughput. As the network stabilized and more network routes are discovered, the DSR throughput performance with ARPR protocol was approximately 800000 bit/sec as compared to 480000 bits/sec for DSR without ARPR power model, and both remained constant throughout the simulation period.

The BER is an important performance metric, which determines the success of packets transfer over a wireless channel. Bit errors causes packets to be corrupted, resulting in data segments or acknowledgments lost. When acknowledgements do not arrive at the sender (source mobile node) within a given time, the sender retransmits the data segment, and exponentially backs off its retransmit timer for the next retransmission. Repeated errors result in a small congestion window at the sender and causes low throughput as experienced by conventional DSR protocol without ARPR power model as shown in Figure 4. Figure 5, shows the BER curves for DSR protocol with- and without ARPR power model. For the DSR protocol with ARPR power model, the BER is approximately 0.009 as compared to 0.019 for the conventional DSR protocol without ARPR. This shows the noise level in the wireless channel affects the throughput performance of the entire network. Transmission of packets over the

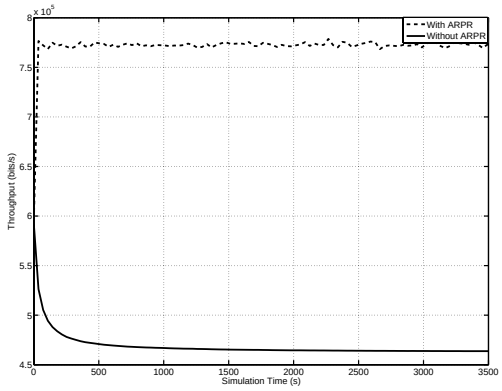

Figure 4. The throughput (b/s); a comparison of DSR protocol with and without ARPR

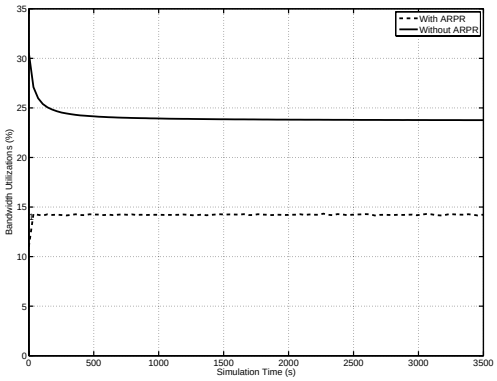

Figure 6. The bandwidth utilization; a comparison of DSR protocol with and without ARPR

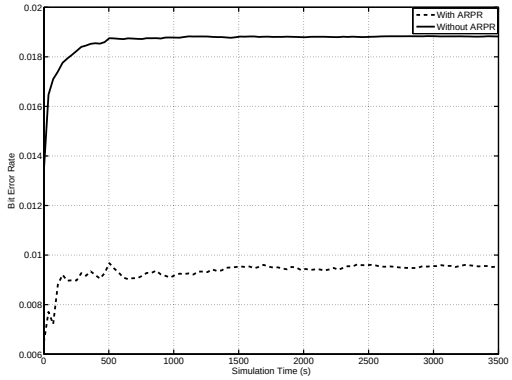

Figure 5. The bit error rate; a comparison of DSR protocol with and without ARPR

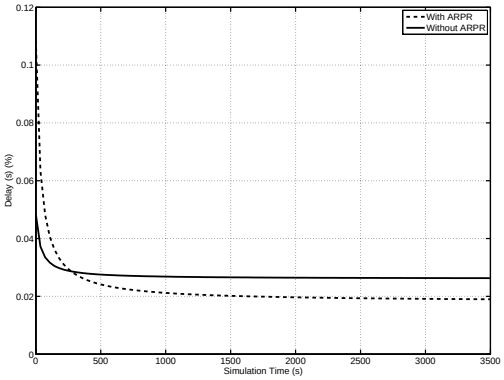

Figure 7. The delay; a comparison of DSR protocol with and without ARPR

wireless channel has been scheduled in accordance to probabilistic power condition and mobility models (refer to table I), and these helps to reduces interference noise in the wireless link channel.

The ARPR power model assist in controlling the data traffic delivery and avoids traffic redundancy, which can lead to channel bandwidth consumption. Figure 6 shows that DSR protocol with ARPR power model has 14 $\%$ bandwidth utilization rate as compared to 24 $\%$ for the conventional DSR protocol without power model. A value of 100 $\%$ indicates full usage of the channel. The higher rate of bandwidth consumption by DSR protocol without ARPR model is due to packet drop by the mobile nodes, which do not have enough power to participate in network routing operation. Hence DSR have to retransmit data/control packets.

Figure 7 shows the delay curves for DSR protocol with-and without ARPR power model. The curves, shows that the packet delay increases initially, which is due to the DSR protocol trying to find the valid routes to destinations. When the network stabilized, the DSR protocol with ARPR model delay reduced and remained constant at 0.02 seconds compared to 0.03 seconds for the conventional DSR protocol without ARPR power model.

Figure 8 shows the power consumed at each node after 3600 seconds real time of simulation. Each node has an initial transmit power of 0.1 watts and the figure shows that with ARPR power model, the received power consumption for the individual nodes was 1.0×10^{-10} watt as compared to 5.0×10^{-2} watt for DSR protocol without ARPR power model.

From the simulation results we conclude that using probabilistic ARPR power model to find the routes save mobile nodes to die away as a result of power depletion during the network routing operation which consequently leads to mobile nodes behaving selfishly and thus affecting the quality of service and performance throughput of the entire network. Our protocol performs better in terms of power saving, bandwidth consumption, delay reduction, low bit error rate as compared to work in [2], [6], [24], despite the fact that they have used different mobility parameters as well as routing protocols. However, [24] agreed that their approach was extremely expensive in terms of power consumption and this warrant investigation into more approach that can save more power of the mobile nodes.

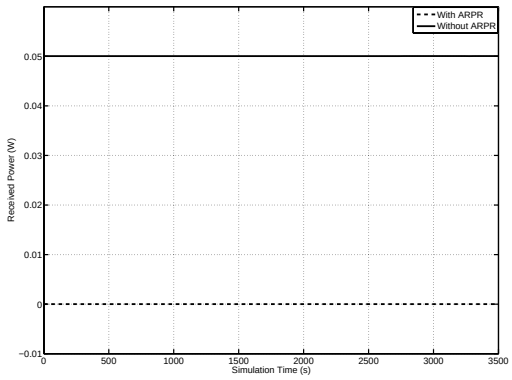

Figure 8. The received signal power; a comparison of DSR protocol with and without ARPR

VII. Conclusion

In this paper, we have proposed an adaptive receiver power routing (ARPR) protocol technique, which is incorporated into Dynamic Source Routing Protocol (DSR) for better throughput performance. OPNET wireless suite simulator was used to evaluate the effect of environmental conditions, signal path loss on quality of service and throughput performance of Mobile Ad hoc Wireless Network. With the proposed ARPR power model, there is a significant power saving. For example, for a practical power model, our simulations show that the network life time with the proposed ARPR model is twice better than the conventional model.

Simulation results shows that the longevity of the network was achieved in terms of throughput of 800000 bits/sec with proposed ARPR power model as compared to 480000 bits/sec of conventional DSR protocol without ARPR power model. However, the power received by individual nodes for the proposed ARPR power model was 1.0×10^{-10} watt as compared to 5.0×10^{-2} watt without ARPR power model.

Appendix A

```
/* Create the DSR packet*/

dsr_pkptr =
dsr _pkt_support_pkt_create(IpC_Protocol_Unspec);
/*Set the route request option in DSR packet header*/
dsr_pkptr =
dsr_pkt_support_option_add(dsr_pkptr,dsr_tlv_ptr);0.1in
/*Set the DSR packet in a newly created IP datagram */
/*The source address of the IP datagram is the */
/*node's own IP address and the destination address*/
/*of the IP datagram is the limited broadcast address */
/*(255.255.255.255) for IPv4 or the all node link */
/*layer multicast address for IPv6*/
 if(inet_address_family_get(&dest_address)

==InetC_Addr_Family_v4)
{
ip_pkptr =
dsr_rte_ip_datagram_create (dsr_pkptr,
InetI_Broadcast_v4_Addr,
InetI_Broadcast_v4_Addr, OPC_NIL);
}
else
{
ip_pkptr =
dsr_rte_ip_datagram_create (dsr_pkptr,
InetI_Ipv6_All_Nodes_LL_Mcast_Addr,
InetI_Ipv6_All_Nodes_LL_Mcast_Addr, OPC_NIL);
op_ici_install (ip_iciptr);
}
if (LTRACE_ACTIVE)
{
inet_address_print (dest_hop_addr_str, dest_address);
inet_address_to_hname (dest_address, dest_node_name);
sprintf (temp_str, "destined to node %s (%s) with ID
(%d)",
dest_hop_addr_str, dest_node_name,
route_request_identifier);
op_prg_odb_print_major
("Broadcasting a route request option in packet",
temp_str, OPC_NIL);
}
/*Increment the route request identifier/*
route_request_identifier++;
/* Access the IP datagram fields/*
op_pk_nfd_access(ip_pkptr, "fields", &ip_dgram_fd_ptr);


  /* If the non-propagating route request feature/*
/* has been enabled, set the TTL field in the /*
/* route request packet to one/*
if (non_prop_route_request)
{
/* Set the TTL to one /*
ip_dgram_fd_ptr− >ttl = 1;
}
else
{
/* Set the TTL to the default /*
ip_dgram_fd_ptr− >ttl = IPC_DEFAULT_TTL;
}


  /*Insert the originating route request information in
/*
/*  the originating route request table/*
dsr_route_request_originating_table_entry_insert
(route_request_table_ptr, dest_address,,
ip_dgram_fd_ptr− > ttl);


  /*Update the statistic for the total traffic sent /*
dsr_support_total_traffic_sent_stats_update
(stat_handle_ptr, global_stathandle_ptr, ip_pkptr);


  /* Update the statistics for the routing traffic sent /*
dsr_support_routing_traffic_sent_stats_update
(stat_handle_ptr, global_stathandleptr, ip_pkptr);
/* Update the statistic for the total number of route
```

```
requests sent/*
dsr_support_route_request_sent_stats_update
(stat_handle_ptr, global_stathandle_ptr,non_
prop_route_request);

   /* Send the packet to the CPU which will broadcast
it/*
/* after processing the packet/*
manet_rte_to_cpu_pkt_send_schedule_with_jitter
(module_data_ptr, parent_prohandle, parent_pro_id,
ip_pkptr);
```

APPENDIX B

```
   /* Create the DSR packet/*
dsr_pkptr =
dsr_pkt_support_pkt_create(IpC_Protocol_Unspec);
//Get the power levels from DSR packet
rec_pow = op_pk_nfd_get_dbl (dsr_pkptr, "rx_power",
&rx_power);
tx_pow = op_pk_nfd_get_dbl (dsr_pkptr, "tx_power",
&tx_power);
mini_tx = op_pk_nfd_get_dbl (dsr_pkptr, "min_tx",
&min_tx);
mini_rx = op_pk_nfd_get_dbl (dsr_pkptr, "min_rx",
&min_rx);

   /* Set the route request option in the DSR packet
header /*
dsr_pkt_support_option_add (dsr_pkptr, dsr_tlv_ptr);

   /* Set the DSR packet in a newly created IP datagram
/*
/*The source address of the IP datagram is the node's
/*
/* own IP address and the destination address of the /*
/*IP datagram is the limited broadcast address/*
/* (255.255.255.255) for IPv4 or the all node link/*
/* layer multicast address for IPv6/*
if (inet_address_family_get (&dest_address)==
InetC_Addr_Family_v4)
{
ip_pkptr = dsr_rte_ip_datagram_create (dsr_pkptr,
InetI_Broadcast_v4_Addr,
InetI_Broadcast_v4_Addr, OPC_NIL);
}
else
{
ip_pkptr = dsr_rte_ip_datagram_create (dsr_pkptr,
InetI_Ipv6_All_Nodes_LL_Mcast_Addr,
InetI_Ipv6_All_Nodes_LL_Mcast_Addr, OPC_NIL);

   /* Install the ICI for IPv6 case /*
ip_iciptr = op_ici_create ("ip_rte_req_v4");
op_ici_attr_set (ip_iciptr, "multicast_major_port",
mcast_major_port);
op_ici_install (ip_iciptr);
}

   if (LTRACE_ACTIVE)
{
inet_address_print (dest_hop_addr_str, dest_address);
inet_address_to_hname (dest_address, dest_node_name);
sprintf (temp_str, "destined to node %s (%s) with ID
(%d)", dest_hop_addr_str, dest_node_name,
route_request_identifier);
op_prg_odb_print_major ("Broadcasting a route request
option in packet", temp_str, OPC_NIL);
}

   /* Increment the route request identifier /*
route_request_identifier++;

   /* Access the IP datagram fields /*
op_pk_nfd_access (ip_pkptr, "fields", &ip_dgram_fd_ptr);

   /* If the non-propagating route request feature /*
/* has been enabled, set the TTL field in the /*
/* route request packet to one/*
if (non_prop_route_request)
{
/* Set the TTL to one /*
ip_dgram_fd_ptr_ ttl = 1;
}
else
{
/* Set the TTL to the default /*
ip_dgram_fd_ptr ttl = IPC_DEFAULT_TTL;
}

   /* Insert the originating route request information
in/*
/* the originating route request table/*
dsr_route_request_originating_table_entry_insert
(route_request_table_ptr, dest_address, rec_pow,tx_pow,
mini_tx, ip_dgram_fd_ptr ttl);

   /* Update the statistic for the total traffic sent/*
dsr_support_total_traffic_sent_stats_update (stat_handle_ptr,
global_stathandle_ptr, ip_pkptr);

   /* Update the statistics for the routing traffic sent /*
dsr_support_routing_traffic_sent_stats_update
(stat_handle_ptr, global_stathandle_ptr, ip_pkptr);

   /* Update the statistic for the total number of route
requests sent /*
dsr_support_route_request_sent_stats_update
(stat_handle_ptr, global_stathandle_ptr,
non_prop_route_request);

   /* Send the packet to the CPU which will broadcast
it/*
/* after processing the packet/*

   if ((tx_pow = mini_tx) && (rec_pow = mini_rx))
```

manet_rte_to_cpu_pkt_send_schedule_with_jitter (module_data_ptr, parent_prohandle, parent_pro_id, ip_pkptr);

ACKNOWLEDGMENT

The authors would like to thank the OPNET Technology Group for providing the software used for the simulations (OPNET Modeler Simulator).

REFERENCES

[1] B. N. Yuvaraju, T. Mohit, and N. C. Niranjan, "Enhancing the Performance of MANETs by Monitoring the Energy Consumption and Use of Mobile Relays," in *Proceedings of the IEEE International Association of Computer Science and Information Technology - Spring Conference*, Singapore, Apr. 2009, pp. 85 – 89.

[2] S. Singh, M. Woo, and C. S. Raghavendra, "Power-Aware Routing in Mobile ad Hoc Networks," in *Proceedings of the 4th annual ACM/IEEE international conference on Mobile computing and networking Dallas*, 1998, pp. 181 – 190.

[3] S. Doshi, S. Bhandare, and X. Timothy, "An On-demand Minimum Energy Routing Protocol for a wireless ad Hoc Network," in *ACM SIGMOBILE Mobile Computing and Communications Review.*, vol. 6, no. 3, jun 2002, pp. 50 – 66.

[4] X. Y. Li, Y. Wang, H. Chen, X. Chu, Y. Wu, and Y. Qi, "Reliable and energy-efficient routing for static wireless ad hoc networks with unreliable links," *IEEE Transactions on Parallel and Distributed Systems*, vol. 10, no. 20, pp. 1408 – 1421, Aug. 2009.

[5] D. B. Johnson, D. A. Maltz, and J. Broch, "The Dynamic Source Routing Protocol for Multi-HopWireless Ad hoc Networks," in *Networks.Computer Science Department Carnegie Mellon*, University, Pittsburgh, PA 15213-3891.

[6] B. Ramachandran and S. Shanmugavel, "Received Signal Strength-based Cross-layer Designs for Mobile Ad Hoc Networks," *IETE Technical Review*, vol. 25, no. 4, 2008.

[7] L. Anderegg and S. Eidenbenz, "Ad hoc-vcg: A truthful and cost-efficient routing protocol for mobile ad hoc networks with selfish agents," in *Proceedings of the 9th annual international conference on Mobile computing and networking (MobiCom '03)*, San Diego, California, USA, Sept. 2003, pp. 245 – 259.

[8] S. Marti, T. J. Giuli, and M. Baker, "Mitigating routing misbehaviour in mobile ad hoc networks," in *Proceedings of the 6th annual international conference on Mobile computing and networking (MobiCom '00)*, Boston, MA, USA, Aug. 2000, pp. 255 – 265.

[9] J. Nie and Z. Zhou, "An energy based power-aware routing protocol in ad hoc networks," in *Proceedings of the International Symposium on Communications and Information Technologies (ISCIT '04)*, vol. 1, Sapporo, Japan, Oct. 2004, pp. 280 – 285.

[10] M. Conti, E. Gregori, and G. Maselli, "Cooperation issues in mobile ad hoc networks," in *Proceedings of the 24 International Conference on Distributed Computing Systems Workshops (ICDCSW '09)*, vol. 7, 2009, pp. 803 – 808.

[11] "Interoperability laboratory for security in ad-hoc networks," http://www.uni.lu/secan-lab/.

[12] SreeRangaRaju and J. Mungara, "Performance Evaluation of ZRP over AODV and DSR in Mobile Adhoc Networks using Qualnet," *European Journal of Scientific Research*, vol. 45, pp. 658–674, 2010.

[13] S. Basagni, M. conti, S. Giordano, and I. Stojmenovic, *Mobile Ad Hoc Networking*. IEEE Press, 2004.

[14] N. Qasim, fatin Said, and H. Aghvami, "Mobile Ad hoc Networking Protocols Evaluation through Simulation for Quality of service," *IAENG International Journal of Computer Science*, vol. 36, no. 1, 2009.

[15] B. R. A. Kumar, L. C. Reddy, and P. S. Hiremath, "Performance Comparison of Wireless Mobile Ad Hoc Network Routing Protocols," *IJCSNS International Journal of Computer Science and Network Security*, vol. 8, no. 1, 2008.

[16] J. Broch, D. A. Maltz, D. B.Johnson, Y.-C. Hu, and J. Jetcheva, "A Performance Comparison of Multi-Hop Wireless Ad Hoc Network Routing Protocols," in *Networks.Computer Science Department Carnegie Mellon*, University, Pittsburgh, PA 15213-3891, 1998.

[17] M. A. Rahman, M. S. Islam, and A. Talevski, "Performance Measurement of Various Routing Protocols in Ad Hoc Network," in *Proceedings of the International MultiConference of Engineers and Computer Scientist*, vol. I IMECS, Hong Kong, 2009.

[18] S. Z. Yang, B. Qi, and J. He, "Simulation comparison of four wireless Ad hoc routing protocols," *Information Technology Journal*, vol. 3, no. 3, pp. 219 – 226, 2004.

[19] A. Boukerche, *Algorithm and Protocls for Wireless and Mobile Ad Hoc Networks*. Wiley Seris on Parallel and Distributed Computing.

[20] L. Quakil, S. Senouci, and G. Pujolle, "Performance Comparison of Ad Hoc Routing Protocols Based on Energy Consumption," in *Ambience Workshop*, Torino, Italy, 2002.

[21] "Opnet simulator," http://www.opnet.com/.

[22] A. Goldsmith, *Wireless communication*. New York, NY: Cambridge University, 2005, pp. 31–35.

[23] G. Zanca, F. Zorzi, A. Zanella, and M. Zorzi, "Experimental comparison of rssi-based localization algorithms for indoor wireless sensor networks," in *Workshop on Real-World Wireless Sensor Networks (RealWSN'08)*, Glasgow, UK, Apr. 2008.

[24] B. Chen, K. Jamieson, and H. Balakrishnan, "Span: An energy-efficient coordination algorithm for topology maintenance in ad hoc wireless networks," in *Proceedings of the 7th ACM MOBICOM*, Rome, Italy, Jul. 2001.

Lawal Bello received his BSc degree in Computer Science in 2004 from Usmanu Danfodiyo University Sokoto, Nigeria and MSc degree in Computer Networking engineering from University of Greenwich, UK. He is currently a PhD student with the mobile and wireless research centre at the school of Engineering, University of Greenwich, United Kingdom. His research interest includes design and performance evaluation of routing protocols in mobile ad hoc wireless networks.

Dr Panos S Bakalis received his BSc in Electrical Engineering, Athens, 1975, and his PG Diploma in Electronics and Control in 1980, at CLP London. He received his MSc in Systems Engineering 1982, and his PhD in Control Engineering both at City University London. From 1986 - 92 he was Senior Lecturer at Thames Polytechnic, London and from 1992 - 96 became Senior Lecturer in the School of Computing at the University of Greenwich. Since then, he moved to the Department of Computer and Communications at the Medway School of Engineering, University of Greenwich where he has worked as a Senior Lecturer in Computer Networking. His research interests are in computer process control and optimization of large-scale systems. He has published papers in international Control Conferences and Journals. From 2008 he has widened his research interests to include the field of Ad Hoc Wireless Computer Networks Protocols (MANET) using OPNET Modeler. He has published several papers in International Communications Conferences and Journals. As MSc Programme Leader in Computer Networking he is supervising students for MSc projects and PhD thesis, in the capacity of MANET field.

Prof. Predrag Rapajic received his BE in 1982, University of Banjaluka, Bosnia and Herzegovina, ME in 1988, University of Belgrade and his PhD in 1994 from the University of Sydney, Australia. Before and after his PhD, he held several full time industrial positions, the latest one in 1996 with Motorola, Sydney. He held academic positions at the University of Sydney 1990-1995, the Australian National University, Canberra, Australia 1996-2000 and the University of New South Wales, Sydney, Australia 2000-2005. He is currently holding chair as Professor of Communication Systems and he is director of research program in Computer and Communications Engineering, University of Greenwich, UK. Prof. Rapajic's research interests include adaptive multi-user detection, equalization, error control coding, mobile communication systems, multi-user information theory, information capacity and modelling of time variable communication channels. Prof Rapajic has published more than 180 highly influential research papers in IEEE Transactions, books, peer-refereed international journals and conferences in the area of mobile communications

Kwashie A Anang received his Diploma in Electrical and Electronic Engineering from the Kwame Nkrumah University of Science and Technology, Kumasi, Ghana in 1997 and his BEng degree in Electrical and Electronic Engineering and MSc degree in Wireless Communication from University of Greenwich in 2005 and 2007. He is currently doing his PhD with the University of Greenwich. His research interest includes next generation cellular wireless systems, mobile ad hoc wireless networks routing protocols and antenna design.

Titus Ikechukwu ENEH received his Bsc in Electrical and Electronic Engineering in 1999 from Enugu State University of Science and Technology (ESUT) Enugu, Nigeria. Msc in Electrical and Electronic Engineering from University of Greenwich Uk in 2005. Currently doing his PhD with the University of Greenwich. His research interest includes adaptive Multi-user detection, Information capacity and MIMO OFDM.

A Hybrid Satellite-Terrestrial Cooperative Network over Non Identically Distributed Fading Channels

Arif Iqbal and Kazi M. Ahmed
School of Engineering and Technology, Asian Institute of Technology, Thailand
Email: {Arif.Iqbal,kahmed}@ait.ac.th

Abstract— **This paper investigates a hybrid satellite-terrestrial cooperative relaying communications network (HSTCN) under independent and non-identical shadowed Rician and Nakagami-m fading channels. It evaluates the performance of such a network using amplify-and-forward (AF) cooperative relaying protocol. The maximal ratio combining (MRC) technique is used at the destination to combine the signals received from the source and cooperating relay nodes. An analytical approach is derived to evaluate the performance of the system in terms of outage probability and symbol error rate (SER). The closed form expressions for the probability density function (PDF), cumulative distribution function (CDF) and moment generating function (MGF) of the end-to-end signal to noise ratio (SNR) are also derived. The derived analytical expressions are applied to the general operating conditions with the help of satellite channel data available from the literature. The analytical results are compared with Monte Carlo simulations. The results show the improvement in the performance of the HSTCN under challenging fading conditions with the help of fixed multiple terrestrial relay nodes.**

Index Terms— **Hybrid satellite-terrestrial, cooperative relay, amplify and forward, fading channels, combined probability density function, moment generating function, outage probability, symbol error rate.**

I. Introduction

The demand for high bit rate transmission supporting a variety of multimedia services is increasing day by day. Satellite technology can address this concern as it can be used to develop a global communication system. In this scenario, the differences between terrestrial and satellite communication systems as well as between fixed and mobile networks will cease to exist in the global coverage by wireless communication system.

Cooperative relaying networks are useful in the satellite-terrestrial networks as it can extend the satellite coverage especially in the areas where terrestrial networks are not able to provide services due to lack of coverage, emergency conditions, and network overloads. Many efficient physical layer techniques like adaptive coding and modulation (ACM), satellite channel modeling, synchronization and estimation are proposed, but these techniques are not able to provide satellite coverage inside buildings and shopping malls due to lack of signal from the satellites [1]. In such situations, a cooperative relaying satellite-terrestrial network can play an important role as it offers services inside covered areas as well as supports low cost user terminals with satellite transmission and reception capabilities. The relay node operates in two strategies, i.e. Amplify and Forward (AF), and Decode and Forward (DF) [2]. Hence, diversity gain can be achieved through multiple signal paths. As a result, a high data rate is achieved and transmission becomes more reliable in terms of symbol error rate (SER) and outage probability [2]. Many standardization groups have incorporated relaying techniques into their emerging standards such as IEEE 802.16 and IEEE 802.11 [3].

The concept of a hybrid satellite-terrestrial cooperative system is presented in [4]–[7]. In [4], transmit diversity technique using space time coding (STC) is proposed and diversity gain is achieved with the use of multiple terrestrial relay nodes with encoding capabilities, while additional coding gain can be achieved at the destination node by combining different parity symbols as shown in [5]. Moreover, a comparison of AF and DF techniques in a cooperative satellite communication network is discussed in [6]. In [8], the architecture of a satellite based mobile multimedia broadcasting is presented, while cooperative relaying for DVB-SH is discussed in [9] - [10]. The outage performance of multiple relay cooperative system using Nakagami-m fading channel is discussed in [11] - [12].

In a cooperative relaying satellite-terrestrial system, a hybrid channel consisting of satellite and terrestrial components is perceived by the destination node. Furthermore, the conventional channel models used in terrestrial radio propagation cannot be used to characterize the satellite channel because of the remarkable differences observed in the line-of-sight (LOS) and shadowing links. In order to model such a satellite channel, a combination of different probability distributions is necessary [13]. In [5]–[7] and [14], a hybrid satellite-terrestrial channel is considered in which fadings in the source(satellite)-relay (S-R) and source(satellite)-destination (S-D) links are assumed to be Rician distributed, while Rayleigh fading is assumed between the relay-destination (R-D) link. In [4], [10] and [15], lognormal distribution is considered in S-R and S-D links. While evaluating the BER performance of single

Manuscript received December 1, 2010; revised May 20, 2011; accepted Jun 12, 2011.

doi:10.4304/jcm.6.7.581-589

and multichannel reception, lognormal based models can be complex especially for the mathematical computations. Thus, the shadowed Rician channel model [16] which is simple and accurate in terms of mathematical computations and much closer to the measured satellite data can be used.

In this paper, we investigate the performance of multi-hop AF HSTCN under non-identically distributed fading links between $S \rightarrow D$, $S \rightarrow R_i$ and $R_i \rightarrow D$. To the best of our knowledge, the performance analysis of a HSTCN over independent and non-identically shadowed Rician and Nakagami-m fading channels with closed form analytical expressions has not yet been investigated. Hence, we derive the closed form expressions to evaluate the performance in terms of outage probability and SER for some important modulation schemes under various fading scenarios. We also compare the theoretical results with Monte Carlo simulations of these different scenarios.

Section II of this paper introduces the network and fading models. In Section III, we derive the closed form expressions for the combined PDF, CDF and MGF of the bounded end-to-end SNR of the relay path. The Land Mobile satellite Channel (LMSC) parameters for various fading conditions are used to analyze the performance of the system in Section IV. Finally, concluding remarks are given in Section V.

Mathematical Notations and Functions: $X \rightarrow Y$ describes the link between node X and Y, $E[\cdot]$ denotes the expectation. $K_v(\cdot)$, ${}_1F_1(\cdot,\cdot,\cdot)$, $\Gamma(\cdot)$, γ_{xy}, $\bar{\gamma}_{xy}$, $\mathcal{M}_\gamma(s)$ and ${}_2F_1(\cdot,\cdot,\cdot;\cdot)$ denote the vth order modified Bessel function of the second kind, the hypergeometric function, gamma function, instantaneous SNR of the $X \rightarrow Y$ link, average SNR of the $X \rightarrow Y$ link, the MGF of the equivalent SNR (γ) and the Gauss hypergeometric function, respectively.

II. System Model

A. Network Model

A HSTCN with multiple cooperative terrestrial fixed relays (R_i) where $i = 1..., N$ and single destination (D) is assumed as shown in Fig. 1. Independent and non-identical fading paths exist between the source (S), N relay nodes and the destination. It is assumed that each node is equipped with single antenna. The source transmits information signal to the relay nodes and the destination. The independent faded copies of the information signal are received at the destination node, one directly from the satellite and the other through the N relay nodes. This technique of transmitting information from different locations makes communication possible even in bad channel conditions and provides spatial diversity at the destination. To explain the system in a less complex manner, the AF cooperative protocol is used at all relay nodes to forward information received from a source to the destination node, where the distance between the relay nodes and a stationary destination node is same. Specifically, the whole transmission is accomplished in two phases as illustrated in Fig. 1. In the first phase

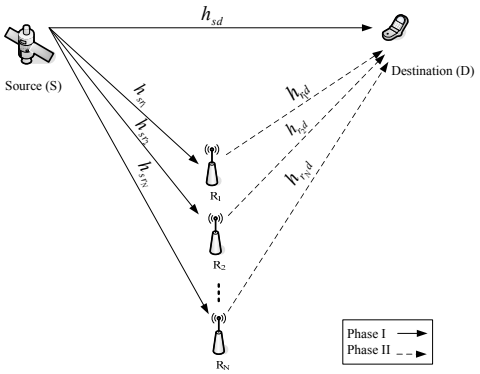

Figure 1. System model of a hybrid satellite-terrestrial cooperative network

of cooperative communication, the source broadcast the signal (information), destination and N terrestrial relay nodes receive. In the second phase, the relay nodes amplified the receive signal and forward the scaled version of the signal to the destination while the source keeps silent. The destination node combines all received signals from the source and N relays using MRC. Further, for the sake of mathematical tractability it is assumed that the signals transmitted by the source and relay nodes are perfectly synchronized at the destination node.

B. Fading Model

In the proposed system independent and non-identical fading channels are assumed. The shadowed Rician distribution is assumed between $S \rightarrow D$, and $S \rightarrow R_i$, which is a more accurate distribution for analyzing the performance of wireless land mobile satellite communication (LMSC) systems [16]. The fading coefficient for $S \rightarrow D$ and R_i nodes are represented as h_{sd} and h_{sr_i} respectively as shown in Fig. 1. The channel coefficient between $R_i \rightarrow D$ follows the Nakagami-m distribution because there are multiple paths due to small buildings, trees and other objects and fading coefficient is denoted by h_{r_id}. The instantaneous SNR of the combined signal at the output of MRC at the destination node can be written as:

$$\gamma_{\text{MRC}} = \gamma_{\text{sd}} + \sum_{i=1}^{N} \gamma_{r_i} \tag{1}$$

where $\gamma_{sd} = |h_{sd}|^2 E_s/N_0$ is the instantaneous SNR of the $S \rightarrow D$ and γ_{r_i} is the instantaneous SNR between the source and *i*th relay, and between the *i*th relay and destination. For the tractable analytical evaluation of outage probability and SER, γ_{r_i}, can be determined by

$$\gamma_{r_i} = \frac{\gamma_{\text{sr}_i}\gamma_{r_id}}{\gamma_{\text{sr}_i} + \gamma_{r_id}} \tag{2}$$

where $\gamma_{sr_i} = |h_{sr_i}|^2 E_s/N_0$ is the instantaneous SNR of $S \rightarrow R_i$ channel while $\gamma_{r_id} = |h_{r_id}|^2 E_{r_i}/N_0$ is the instantaneous SNR of $R_i \rightarrow D$ channel. While E_s and E_{r_i} are the transmit power of the S and the R_i node. The received noise at the *i*th relay and at the destination node

is modeled as additive white Gaussian (AWGN) noise with variance N_0. Fading coefficients between the $S \to D$ and $S \to R_i$ are assumed as shadowed Rician distribution and PDF of SNR per symbol is given by [16] as

$$f_{\gamma_{\text{xy}}}(\gamma) = \frac{1}{2b_o\bar{\gamma}_{\text{xy}}}\left(\frac{2b_om_o}{2b_om_o+\Omega}\right)^{m_o}\exp\left(\frac{-\gamma}{2b_o\bar{\gamma}_{\text{xy}}}\right) \times {}_1F_1\left(m_o, 1, \frac{\Omega\gamma}{2b_o\bar{\gamma}_{\text{xy}}\left(2b_om_o+\Omega\right)}\right) \quad (3)$$

Here, Ω is the average power of the LOS component, $2b_o$ is the average power of the multipath component. Here, m_o is allowed to vary over the wider range of $m_o \geq 0$. We can model different types of LOS conditions for the land mobile satellite channels, i.e. very small values of m_o corresponds to the urban areas, while the value of $0 < m_o < \infty$ is associated with suburban and rural areas with partial obstruction of the LOS.

The PDF of the instantaneous SNR per symbol between the $R_i \to D$ is distributed according to the Nakagami-m distribution which covers a broad variety of fading scenarios for the different values of m-fading parameter [17],

$$f_{\gamma_{r_id}}(\gamma) = \frac{1}{\Gamma(m)}\left(\frac{m}{\bar{\gamma}_{r_id}}\right)^m\gamma^{m-1}\exp\left(-\frac{m}{\bar{\gamma}_{r_id}}\gamma\right) \quad (4)$$

where m is the traditional Nakagami multipath fading parameter which ranges from ≥ 0.5 to ∞.

III. Performance Analysis

This section presents a comprehensive performance analysis of the proposed HSTCN. The PDF, CDF and MGF of the end-to-end relaying SNR, γ_{r_i}, are derived, and based on such statistics, we obtained exact closed form expressions of the outage probability and symbol error rate (SER).

A. Statistical characterization of end-to-end relaying SNR

The combined PDF of two independent and non-identical distributions (3) and (4), can be calculated by using [18], (as explained in Appendix A) and expressed as the following equation,

$$f_{\gamma_{r_i}}(\gamma) = \frac{1}{2b_o\bar{\gamma}_{\text{sr}_i}}\left(\frac{2b_om_o}{2b_om_o+\Omega}\right)^{m_o}\frac{1}{\Gamma(m)}\left(\frac{m}{\bar{\gamma}_{r_id}}\right)^m \times \exp\left[-\left(\frac{1}{2b_o\bar{\gamma}_{\text{sr}_i}}+\frac{m}{\bar{\gamma}_{r_id}}\right)\gamma\right]\sum_{x=0}^{\infty}\frac{1}{(x!)} \times \frac{\Gamma(m_o+x)}{\Gamma(m_o)\Gamma(1+x)}\lambda^x\sum_{y=0}^{m+x+1}\binom{m+x+1}{y} \times 2\gamma^{m+x}\left(\sqrt{\frac{\bar{\gamma}_{r_id}}{2b_om\bar{\gamma}_{\text{sr}_i}}}\right)^{m-y} \times K_{(m-y)}\left(2\gamma\sqrt{\frac{m}{2b_o\bar{\gamma}_{\text{sr}_i}\bar{\gamma}_{r_id}}}\right) \quad (5)$$

where $\lambda = \left(\frac{\Omega}{2b_o\bar{\gamma}_{\text{sr}_i}(2b_om_o+\Omega)}\right)$. The average SNR between $S \to R_i$ is represented by $\bar{\gamma}_{sr_i} = E_s/N_0$ while $\bar{\gamma}_{r_id} = E_{r_i}/N_0$ is the average SNR between $R_i \to D$. The following are some special cases where the above derived PDF can be applicable.

Case 1: Applying $m_o = 0$ and $m = 1$ in (5), the link from $S \to R_i$ and $R_i \to D$ is converted into a Rayleigh distribution. The combined PDF of the independent and non-identical Rayleigh channels can be calculated using (6), the result of which is the same as that obtained in [12]

$$f_{\gamma_{r_i}}(\gamma) = \frac{2\gamma}{\bar{\gamma}_{sr_i}\bar{\gamma}_{r_id}}\exp\left[-\left(\frac{1}{\bar{\gamma}_{sr_i}}+\frac{1}{\bar{\gamma}_{r_id}}\right)\gamma\right]\Big[2K_0 \times\left(\frac{2\gamma}{\sqrt{\bar{\gamma}_{sr_i}\bar{\gamma}_{r_id}}}\right)+\left(\sqrt{\frac{\bar{\gamma}_{sr_i}}{\bar{\gamma}_{r_id}}}+\sqrt{\frac{\bar{\gamma}_{r_id}}{\bar{\gamma}_{sr_i}}}\right) \times K_1\left(\frac{2\gamma}{\sqrt{\bar{\gamma}_{sr_i}\bar{\gamma}_{rd_i}}}\right)\Big] \quad (6)$$

Case 2: In this case substituting $m_o = \infty$ in (5), the link between $S \to R_i$ act as Rician distribution. While if $m = 1$ in (5), the channel between $R_i \to D$ works as a Rayleigh distribution and the expression (7) is obtained,

$$f_{\gamma_{r_i}}(\gamma) = \frac{(1+K_{sr_i})}{\bar{\gamma}_{sr_i}\bar{\gamma}_{r_id}}\exp\left(-K_{sr_i}-\mu\right)\sum_{x=0}^{\infty}\frac{1}{(x!)^2} \times\left(\frac{K_{sr_i}(1+K_{sr_i})}{\bar{\gamma}_{sr_i}}\right)^x\sum_{k=0}^{x+2}\binom{x+2}{k} \times 2\gamma^{x+1}\left(\sqrt{\frac{(1+K_{sr_i})\bar{\gamma}_{rd_i}}{\bar{\gamma}_{sr_i}}}\right)^{(1-k)} \times K_{(1-k)}\left(2\gamma\sqrt{\frac{(1+K_{sr_i})}{\bar{\gamma}_{sr_i}\bar{\gamma}_{r_id}}}\right) \quad (7)$$

where $\mu = \frac{(1+K_{sr_i})\gamma}{\bar{\gamma}_{sr_i}} - \frac{\gamma}{\bar{\gamma}_{r_id}}$. This is the combined PDF of two independent and non-identical Rician and Rayleigh fading channels as shown in [19].

An exact closed form expression for the CDF of the end-to-end relaying SNR γ_{r_i}, in (2) can be derived as

$$F_{\gamma_{r_i}}(\gamma) = 1 - \frac{1}{2b_o\bar{\gamma}_{\text{sr}_i}}\left(\frac{2b_om_o}{2b_om_o+\Omega}\right)^{m_o}\sum_{n=0}^{m-1}\frac{1}{n!} \times\left(\frac{m}{\bar{\gamma}_{r_id}}\right)^n\text{Exp}\left[-\gamma\left(\frac{1}{2b_o\bar{\gamma}_{\text{sr}_i}}+\frac{m}{\bar{\gamma}_{r_id}}\right)\right] \times\sum_{k=0}^{\infty}\frac{1}{k!}\frac{\Gamma(m_o+k)}{\Gamma(m_o)\Gamma(1+k)}\lambda^k\sum_{j=0}^{n+k}\binom{n+k}{j} \times 2\gamma^{n+k+1}\left(\sqrt{\frac{2b_om\bar{\gamma}_{\text{sr}_i}}{\bar{\gamma}_{r_id}}}\right)^{k-j+1} \times K_{k-j+1}\left(2\gamma\sqrt{\frac{m}{2b_o\bar{\gamma}_{\text{sr}_i}\bar{\gamma}_{r_id}}}\right) \quad (8)$$

*P*roof: The proof is provided in Appendix B

The MGF-based approach is a simple and efficient method to evaluate the average SER and outage probability in fading conditions and the MGF can be obtained from the expression given by

$$\mathcal{M}_{\gamma_{r_i}}(s) = E\left[e^{-s\gamma}\right] \quad (9)$$

$$\begin{aligned}\mathcal{M}_{\gamma_{r_i}}(s) =& \frac{1}{2b_o\bar{\gamma}_{sr_i}}\left(\frac{2b_om_o}{2b_om_o+\Omega}\right)^{m_o}\frac{1}{\Gamma(m)}\left(\frac{m}{\bar{\gamma}_{r_id}}\right)^{m}\sum_{x=0}^{\infty}\frac{1}{x!}\frac{\Gamma(m_o+x)}{\Gamma(m_o)\Gamma(1+x)}\lambda^x\sum_{y=0}^{m+x+1}\binom{m+x+1}{y}\\ &\times 2\left(\sqrt{\frac{\bar{\gamma}_{r_id}}{2b_om\bar{\gamma}_{sr_i}}}\right)^{m-y}\frac{\sqrt{\pi}(2\beta)^{m-y}}{(\alpha+\beta)^{2m+x-y+1}}\frac{\Gamma(2m+x-y+1)\Gamma(x+y+1)}{\Gamma(m+x+3/2)}\\ &\times {}_2F_1\left(2m+x-y+1, m-y+\tfrac{1}{2}, m+x+\tfrac{3}{2}, \tfrac{\alpha-\beta}{\alpha+\beta}\right)\end{aligned} \tag{10}$$

In order to provide a powerful tool for calculating the average SER and outage probability, a closed form expression for the MGF can be obtained using the combined PDF given in (5). After some mathematical manipulations and from [18], the MGF of γ_{r_i} is expressed as in (10). where

$$\alpha = \left[\frac{1}{2b_o\bar{\gamma}_{sr_i}} + \frac{m}{\bar{\gamma}_{r_id}} + s\right] \tag{11}$$

and

$$\beta = 2\sqrt{\frac{m}{2b_o\bar{\gamma}_{sr_i}\bar{\gamma}_{r_id}}} \tag{12}$$

After substituting (3) in (9) and using [18], the MGF of γ_{sd} can be shown as

$$\mathcal{M}_{\gamma_{\text{sd}}}(s) = \frac{(2b_om_o)^{m_o}\left(2b_os\bar{\gamma}_{\text{sd}}+1\right)^{m_o-1}}{\left[\left(2b_om_o+\Omega\right)\left(2b_os\bar{\gamma}_{\text{sd}}+1\right)-\Omega\right]^{m_o}} \tag{13}$$

where $\bar{\gamma}_{\text{sd}} = E_s/N_0$ is the average SNR of $S \to D$. Using the assumed non-identical fading channels, a closed form expression of the moment generating function of γ_{ub} can be obtained by multiplying the MGF of the γ_{sd} and γ_{r_i}

$$\mathcal{M}_{\gamma_{\text{ub}}}(s) = \mathcal{M}_{\gamma_{\text{sd}}}(s)\prod_{i=1}^{N}\mathcal{M}_{\gamma_{r_i}}(s) \tag{14}$$

B. Outage Probability

1) Without direct link: In this scenario, it is assumed that the link between $S \to D$ is not available due to heavy shadowing and the source is communicating with destination node with the help of multiple fixed relay nodes. In noise limited systems, outage probability is an important performance measure and is defined as the probability that the received SNR, γ_{r_i}, falls below a certain threshold value γ_{th}. This threshold is a protection value for the SNR, below of which the quality of service is deemed to be unsatisfactory. The outage probability of dual hop system without direct link can be obtained by using (8) as follows

$$P_{\text{outage}}^{w/o} = F_{\gamma_{r_i}}(\gamma_{th}) \tag{15}$$

2) With MRC (direct and relaying path): Consider the case when the destination node is receiving the signal from multiple fixed relays and as well as from the source node. In this case the outage probability at the destination node is given by

$$P_{\text{outage}} = \Pr\left[\gamma_{\text{MRC}} < \gamma_{\text{th}}\right] \tag{16}$$

where $\gamma_{\text{th}} = 2^{2R} - 1$. The SNR can be approximated by its upper bound

$$\gamma_{\text{MRC}} = \gamma_{\text{ub}} = \gamma_{\text{sd}} + \gamma_{r_i} \tag{17}$$

Therefore, the outage probability can be written as

$$P_{\text{outage}} = \Pr\left[\gamma_{\text{ub}} < \gamma_{\text{th}}\right] \tag{18}$$

Moreover, the closed form expression of $\mathcal{M}_{\gamma_{\text{ub}}}(s)$ can be used to calculate the outage probability as

$$P_{\text{outage}} = \mathcal{L}^{-1}\left(\frac{\mathcal{M}_{\gamma_{\text{ub}}}(s)}{s}\right)\Bigg|_{\gamma_{\text{th}}} \tag{19}$$

where $\mathcal{L}^{-1}$ is the inverse Laplace transform. Using MGF-based approach, the end-to-end outage probability can be calculated by using any of the numerical techniques [20]-[21].

C. Symbol Error Rate

1) Without direct link: The average SER (ASER) rate is one of the important measures of the performance of wireless communication systems. The ASER of the various commonly used modulation schemes at certain SNR is shown in [17] and can be obtained as follows

$$P_{\text{ASER}}^{w/o} = aQ\left(\sqrt{b\gamma}\right) \tag{20}$$

where $Q(\cdot)$ is the Gaussian Q function which is defined as $Q(\alpha) = \frac{1}{\sqrt{2\pi}}\int_{\alpha}^{\infty}\exp\left(-\frac{t^2}{2}\right)dt$, and a and b are constants depending upon the specific modulation type. For example, $(a = 1, b = 2)$ and $(a = 1, b = 1)$ are used to calculate the exact bit error rate (BER) of binary phase shift keying (BPSK) and binary frequency shift keying (BFSK), respectively. Similarly, for the SER of M-PAM $(a = 2(M-1)/M)$ and $(b = 6\log_2 M\,/M^2 - 1)$ are used. Further, the SER of other modulation schemes have approximate forms such as *M*-PSK $(a = 2, b = 2\sin^2\pi/M$ and *M*-ary quadrature amplitude modulation (M-QAM) $(a = 4, b = 3/(M-1))$. The results in this study show that there is a close approximation for these modulation schemes.

An accurate closed form expression for the average SER approximation can be obtained by integrating $P_{\text{ASER}}^{w/o}$ over the CDF of the relaying SNR γ_{r_i} as follows:

$$P_{\text{ASER}}^{w/o} = \frac{a}{\sqrt{2\pi}}\int_0^{\infty}F_{\gamma_{r_i}}\left(\frac{x^2}{b}\right)\exp\left(\frac{x^2}{2}\right)dx \tag{21}$$

By using (8) and after some variable transformations, and applying [18, eq.(6.619.3)], the exact closed form expression of the relaying path can be calculated as shown in (22), with the value of α and β given in (23) and (24)

$$\alpha = \frac{1}{2b_o\bar{\gamma}_{sr_i}b} + \frac{m}{b\bar{\gamma}_{r_id}} + \frac{1}{2} \tag{23}$$

$$P_{\text{ASER}}^{w/o} = \frac{a}{2} - \frac{1}{2b_o\bar{\gamma}_{sr_i}}\left(\frac{2b_om_o}{2b_om_o+\Omega}\right)^{m_o}\sum_{n=0}^{m-1}\frac{1}{n!}\left(\frac{m}{\bar{\gamma}_{r_id}}\right)^{n}\sum_{x=0}^{\infty}\frac{1}{x!}\frac{\Gamma(m_o+x)}{\Gamma(m_o)\Gamma(1+x)}\left(\frac{\Omega}{2b_o\bar{\gamma}_{sr_i}(2b_om_o+\Omega)}\right)^{x}\sum_{y=0}^{n+x}$$
$$\times\binom{n+x}{y}\left(\sqrt{\frac{2b_om\bar{\gamma}_{sr_i}}{\bar{\gamma}_{r_id}}}\right)^{x-y+1}\frac{a}{\sqrt{2}b^{n+2x-y+2}}\left(4\sqrt{\frac{m}{2b_o\bar{\gamma}_{sr_i}\bar{\gamma}_{r_id}}}\right)^{x-y+1}\frac{\Gamma(n+2x-y+5/2)\Gamma(n+y+1/2)}{(\alpha+\beta)^{n+2x-y+5/2}\Gamma(n+x+2)} \quad (22)$$
$$\times\ {}_2F_1\left(n+2x-y+5/2, x-y+3/2, n+x+2, \frac{\alpha-\beta}{\alpha+\beta}\right)$$

and

$$\beta = \frac{2}{b}\sqrt{\frac{m}{2b_o\bar{\gamma}_{sr_i}\bar{\gamma}_{r_id}}} \quad (24)$$

Equation (22) provides a simple and efficient way of evaluating the error rate performance of all modulation schemes that have SER of form indicated in (20).

2) With MRC (direct and relaying path): A unified MGF based approach which is an easy and efficient method to evaluate the SER performance of wireless systems, is given as:

$$P_{\text{ASER}} = a\int_0^{\text{b}\pi}\mathcal{M}_{\gamma_{\text{sd}}}(g;\bar{\gamma}_{\text{sd}})\prod_{i=1}^{N}\mathcal{M}_{\gamma_{r_i}}(g;\bar{\gamma}_{\text{sr}_i},\bar{\gamma}_{r_id})\,d\theta \quad (25)$$

where the parameters a, b and g are determined by the the specific modulation type used. For *M*-ary phase shift keying (MPSK) and *M*-ary quadrature amplitude modulation (MQAM) these values are given as:

MPSK: $a = \frac{1}{\pi}$, $b_{PSK} = \frac{M-1}{M}$, $g = sin^2\left(\frac{\pi}{M}\right)$

MQAM:

$a_1 = \frac{4}{\pi}\left(1-\frac{1}{\sqrt{M}}\right)$, $b_1 = \frac{1}{2}$, $g_1 = \frac{3}{2(M-1)}$

$a_2 = \frac{4}{\pi}\left(1-\frac{1}{\sqrt{M}}\right)^2$, $b_2 = \frac{1}{4}$, $g_2 = \frac{3}{2(M-1)}$

IV. Numerical and Simulation Results

This section presents the numerical and simulation results of SER and the outage probability of a hybrid satellite-terrestrial cooperative system under non-identical fading channels. About 10^7 BPSK and QPSK symbols are randomly generated for simulation in the Matlab. The AWGN samples are complex Gaussian variables with zero mean and variance N_0, while the three channel variables, such as the shadowed Rician h_{sr_i}, h_{sd} and Nakagami h_{r_id} are independently generated. The analytical results are evaluated using the Mathematica program. The performance curves of the direct path under the shadowed Rician fading and the relaying path under shadowed Rician and Nakagami-m fading with cooperative MRC at destination are plotted in terms of outage probability and SER versus the average SNR of the transmitted signal. Since, the source transmits simultaneously to the destination and to the relay nodes, the signal energy through the links $S \to D$ and $S \to R$ is same. We have assumed that the channel between the source and the relay nodes has LOS communication $(m_o = 26)$ and the channel between the relay and destination node experience multipath fading. In this case we can allocate equal power at both the source and relay nodes [6]. The targeted threshold rate R is chosen as 1 bit/sec/Hz

TABLE I.
Land Mobile Satellite Channel Parameters [16]

Channel state	m_o	b_o	Ω
Frequent deep shadowing	2.56	0.0158	0.123
Moderate shadowing	7.64	0.0129	0.372
Infrequent light shadowing	26	0.005	0.515

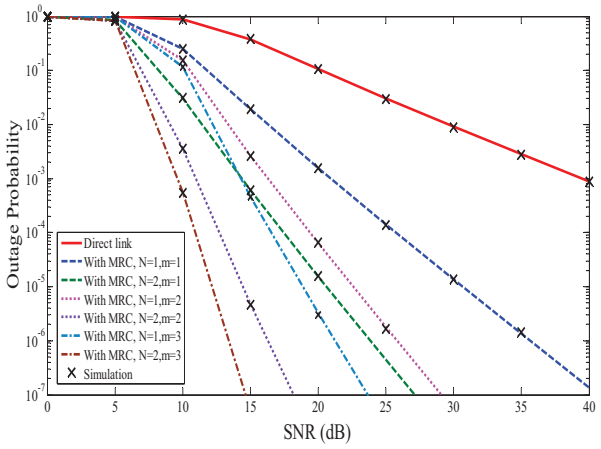

Figure 2. Outage probability versus the SNR performance of the proposed system when the direct channel experience the deep fading, $m_o = 2.56$, $S \to R_i$ channel have LOS, $m_o = 26$, and the $R_i \to D$ channel experience Nakagami-m fading associated with $m = 1, 2, 3$

to evaluate the outage probability of the system. The numerical values of the LMSC are taken from [16], as shown in Table. I. The LMSC parameter m_o in the direct channel and relay channel shows the intensity of fading. The m_o values in Table. I decreases as the amount of fading increases. We show the analytical results by the colored curves while the simulation results are shown by $(\times)$ mark on all the figures for comparison.

Firstly, the outage probability performance in relation to the average SNR using different number of relay nodes $(N = 1, 2)$ is determined. Fig. 2 compares the performance of the hybrid satellite-terrestrial cooperative system at multiple relay nodes in different and non-identical fading channels. The LMSC parameter $m_o = 2.56$ shows deep fading in the direct path while the path between $S \to R_i$ is under light fading $(m_o = 26)$. It is observed from the figure that the outage probability decreases as the number of relay nodes and m increase. The figure further show that the system with cooperation performs better than the system without any cooperation in terms of outage probability. For example, at the outage probability of 10^{-3}, the system with $(N = 1, m = 1)$ and $(N = 2, m = 1)$ offers a gain of 19 dB and 26

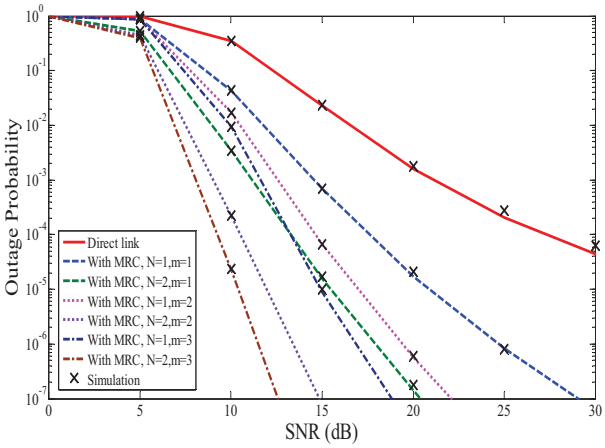

Figure 3. Outage probability versus the SNR performance of the proposed system when the direct channel experience the moderate fading, $m_o = 7.64$, $S \rightarrow R_i$ channel have LOS, $m_o = 26$, and the $R_i \rightarrow D$ channel experience Nakagami-m fading associated with $m = 1, 2, 3$

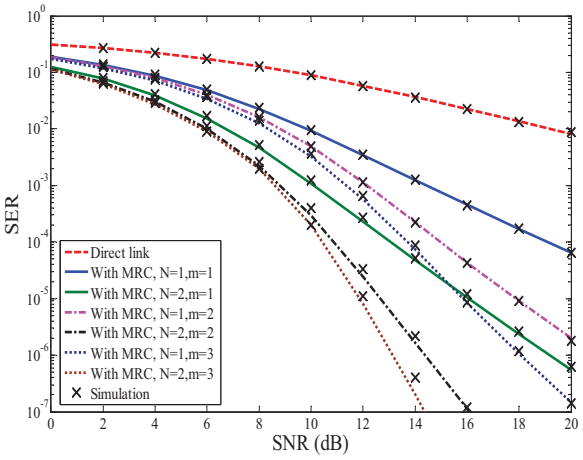

Figure 4. Symbol error rate (SER) versus the SNR performance of the proposed system using BPSK modulation scheme, when the direct channel experience the deep fading, $m_o = 2.56$, $S \rightarrow R_i$ channel have LOS, $m_o = 26$, and the $R_i \rightarrow D$ channel experience Nakagami-m fading associated with $m = 1, 2, 3$

dB over the system without cooperation. Similarly, the system with $(N = 2, m = 3)$ provides a gain of 3.5 dB over the system with $(N = 2, m = 2)$ at outage rate of 10^{-4}. At $m = 1$ the channel between $R_i \rightarrow D$ acts as Rayleigh fading. Fig. 3 illustrates the outage curves when the direct link of the destination with satellite suffers from moderate fading. It is also observed that the theoretical results agree quite well with the Monte Carlo simulations, confirming the accuracy of the analysis.

Fig. 4 shows the SER performance of the hybrid satellite-terrestrial system with and without cooperation using the BPSK baseband modulation scheme when the direct link is under deep fading at $m_o = 2.56$. The figure shows that the performance of the system gets better as the Nakagami factor m increases and the slope of the curve gets deeper. The system with $N = 2$ and $m = 1$, $N = 2$ and $m = 2$, and $N = 2$ and $m = 3$, produces cooperation gain of about 6 dB at the SER of 10^{-4}, 7 dB at the SER of 10^{-5}, and 5 dB at the SER of 10^{-6} respectively, over the system using single relay cooperative communication.

The case when the direct link is under moderate fading at $m_o = 7.64$ is presented in Fig. 5, where the system with $N = 2$ and $m = 1$, $N = 2$ and $m = 2$, and $N = 2$ and $m = 3$, produce cooperation gain of about 4.5 dB, 3.6 dB , and 3 dB at 10^{-6} respectively, over the system using single relay cooperative communication.

Furthermore, Fig. 6 shows the SER performance of the system that uses the QPSK baseband modulation scheme when the direct link is under deep fading at $m_o = 2.56$. The multiple relay satellite-terrestrial cooperative communication system with $N = 2$ and $m = 1$, $N = 2$ and $m = 2$, and $N = 2$ and $m = 3$, produces cooperation gain of about 5 dB at the SER of 10^{-3}, 4.5 dB at the SER of 10^{-4}, and 4.3 dB at the SER of 10^{-5} respectively, over the system using single relay cooperative communication. The case when the direct link is under moderate fading at $m_o = 7.64$ is presented in Fig. 7. The exact agreement

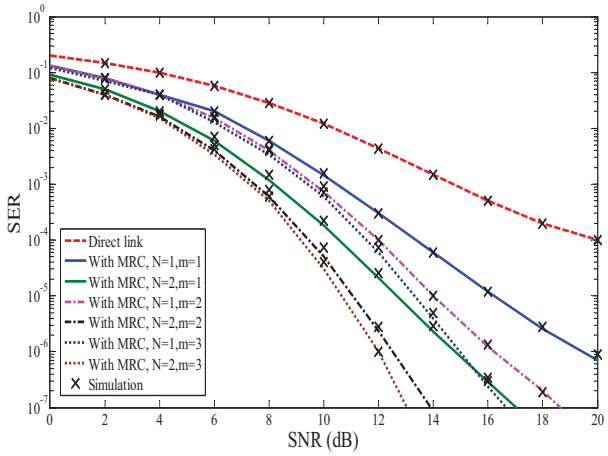

Figure 5. Symbol error rate (SER) versus the SNR performance of the proposed system using BPSK modulation scheme, when the direct channel experience the moderate fading, $m_o = 7.64$, $S \rightarrow R_i$ channel have LOS, $m_o = 26$, and the $R_i \rightarrow D$ channel experience Nakagami-m fading associated with $m = 1, 2, 3$

between the SER curves and the Monte Carlo simulation results validates the computational accuracy of our analysis.

V. Conclusion

In this paper, a rigorous analysis is carried out to derive the closed form expressions for the combined PDF, CDF and the MGF of non-identical relaying channel with bounded SNR. The results obtained are examined by evaluating the outage probability and the SER performances under various scenario of multiple relay hybrid satellite-terrestrial cooperative network using an AF protocol.

Using land mobile satellite channel statistical experimental data of different fading conditions obtained from literatures, the analyses of the study are verified using the results of the numerical computations and simulation.

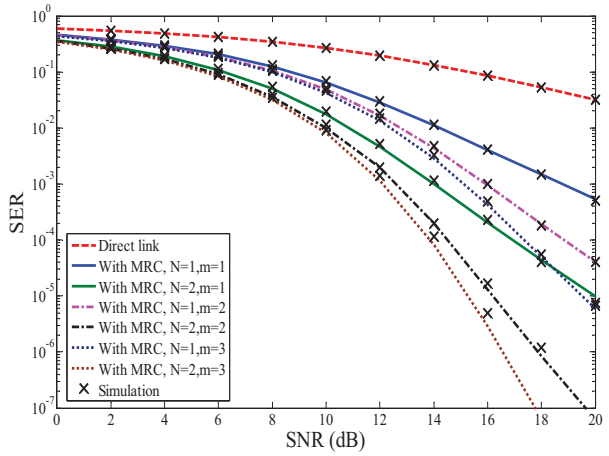

Figure 6. Symbol error rate (SER) versus the SNR performance of the proposed system using QPSK modulation scheme, when the direct channel experience the deep fading, $m_o = 2.56$, $S \rightarrow R_i$ channel have LOS, $m_o = 26$, and the $R_i \rightarrow D$ channel experience Nakagami-m fading associated with $m = 1, 2, 3$

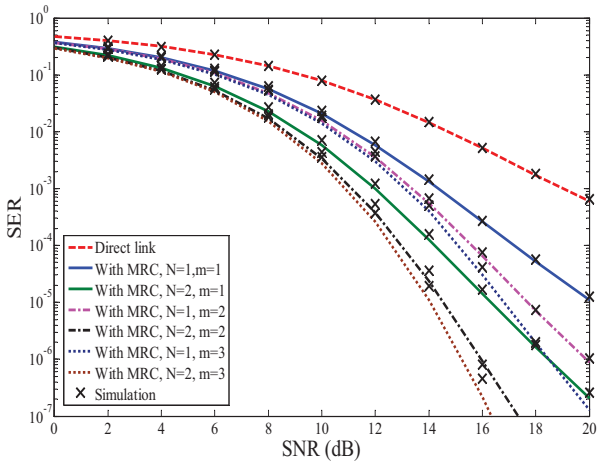

Figure 7. Symbol error rate (SER) versus the SNR performance of the proposed system using QPSK modulation scheme, when the direct channel experience the moderate fading, $m_o = 7.64$, $S \rightarrow R_i$ channel have LOS, $m_o = 26$, and the $R_i \rightarrow D$ channel experience Nakagami-m fading associated with $m = 1, 2, 3$

The results show that the multi-hop cooperative satellite-terrestrial communication has a diversity of advantages. The proposed system can provide a stable improved performance of future 4G services even in covered areas. The performance of the proposed system may also be extended to the DF cooperative communication scenario.

ACKNOWLEDGMENT

The first author would like to thank the Higher Education Commission (HEC) Pakistan for providing funds for his higher studies.

APPENDIX I
DERIVATION OF THE COMBINED PDF OF RELAY PATH $f_{\gamma_{r_i}}(\gamma)$

The combined PDF of two independent and non-identical distributions is given in [12] as

$$f_{\gamma_{r_i}}(\gamma) = \int_{\gamma}^{\infty} \frac{z^2}{(z-\gamma)^2} f_{\gamma_{\mathrm{sr}_i}}\left(\frac{\gamma z}{z-\gamma}\right) f_{\gamma_{r_i}}(z) dz \quad (26)$$

After applying $f_{\gamma_{\mathrm{sr}_i}}$ and $f_{\gamma_{r_i d}}$ from (3) and (4) in the above equation and carrying out some variable transformations, (26) can be written as

$$\begin{aligned} f_{\gamma_{r_i}}(\gamma) = {} & \frac{1}{2b_o\bar{\gamma}_{\mathrm{sr}_i}}\left(\frac{2b_o m_o}{2b_o m_o+\Omega}\right)^{m_o} \frac{1}{\Gamma(m)}\left(\frac{m}{\bar{\gamma}_{r_i d}}\right)^{m} \\ & \times \exp\left[-\left(\frac{1}{2b_o\bar{\gamma}_{\mathrm{sr}_i}}+\frac{m}{\bar{\gamma}_{r_i d}}\right)\gamma\right]\int_0^{\infty}\left(\frac{z+\gamma}{z}\right)^{m+1} \\ & \times z^{m-1}\ \exp\left[-\left(\frac{\gamma^2}{2b_o\bar{\gamma}_{\mathrm{sr}_i} z}+\frac{mz}{\bar{\gamma}_{r_i d}}\right)\right] \\ & \times\ {}_1F_1\left(m_o, 1, \frac{\Omega\gamma(z+\gamma)}{2b_o\bar{\gamma}_{\mathrm{sr}_i}(2b_o m_o+\Omega)z}\right) dz \end{aligned} \quad (27)$$

Now substituting ${}_1F_1(\cdot,\cdot,\cdot)$ with series expression by using [18, eq.(9.14.1)], (27) can be written as

$$\begin{aligned} f_{\gamma_{r_i}}(\gamma) = {} & \frac{1}{2b_o\bar{\gamma}_{\mathrm{sr}_i}}\left(\frac{2b_o m_o}{2b_o m_o+\Omega}\right)^{m_o} \frac{1}{\Gamma(m)}\left(\frac{m}{\bar{\gamma}_{r_i d}}\right)^{m} \\ & \times \sum_{x=0}^{\infty}\frac{1}{x!}\gamma^x \frac{\Gamma(m_o+x)}{\Gamma(m_o)\Gamma(1+x)}\lambda^x \\ & \times \int_0^{\infty}\left(\frac{z+\gamma}{z}\right)^{m+x+1} z^{m-1} \\ & \times \exp\left[-\left(\frac{\gamma^2}{2b_o\bar{\gamma}_{\mathrm{sr}_i} z}+\frac{mz}{\bar{\gamma}_{r_i d}}\right)\right] dz \end{aligned} \quad (28)$$

Upon expanding the term $\left(1+\frac{\gamma}{a}\right)^{m+x+1}$ according to [18, eq.(1.111)], we can reach

$$\begin{aligned} f_{\gamma_{r_i}}(\gamma) = {} & \frac{1}{2b_o\bar{\gamma}_{\mathrm{sr}_i}}\left(\frac{2b_o m_o}{2b_o m_o+\Omega}\right)^{m_o} \frac{1}{\Gamma(m)}\left(\frac{m}{\bar{\gamma}_{r_i d}}\right)^{m} \\ & \times \exp\left[-\left(\frac{1}{2b_o\bar{\gamma}_{\mathrm{sr}_i}}+\frac{m}{\bar{\gamma}_{r_i d}}\right)\gamma\right]\sum_{x=0}^{\infty}\frac{1}{x!} \\ & \times \frac{\Gamma(m_o+x)}{\Gamma(m_o)\Gamma(1+x)}\lambda^x \\ & \times \sum_{y=0}^{m+x+1}\binom{m+x+1}{y}\gamma^{x+y}\int_0^{\infty} z^{m-y-1} \\ & \times \exp\left[-\left(\frac{\gamma^2}{2b_o\bar{\gamma}_{\mathrm{sr}_i} z}+\frac{mz}{\bar{\gamma}_{r_i d}}\right)\right] dz \end{aligned} \quad (29)$$

Now with the help of [18, eq.(3.471.9)], the combined PDF of $f_{\gamma_{r_i}}(\gamma)$ can be shown as (5).

APPENDIX II
DERIVATION OF RELAY PATH CDF $F_{\gamma_{r_i}}(\gamma)$

The PDF of SNR per symbol of $S \rightarrow R_i$ link is given in (4) and the CDF of $R_i \rightarrow D$ link for the integer values

of m is given by

$$\Gamma\left(m, \frac{m\gamma}{\bar{\gamma}_{r_i d}}\right) = 1 - \exp\left(-\frac{m\gamma}{\bar{\gamma}_{r_i d}}\right) \sum_{n=0}^{m-1} \frac{1}{n!} \left(\frac{m\gamma}{\bar{\gamma}_{r_i d}}\right)^n \tag{30}$$

Then, the CDF of the relaying path can be calculated with the help of (2) as

$$\begin{aligned} F_{\gamma_{r_i}}(\gamma) &= \Pr\left(\gamma_{r_i} \leq \gamma\right) = \Pr\left(\frac{\gamma_{\mathrm{sr}_i}\gamma_{r_i d}}{\gamma_{\mathrm{sr}_i} + \gamma_{r_i d}} \leq \gamma\right) \\ &= \int_0^{\gamma} \Pr\left(\gamma_{r_i d} \geq \frac{\gamma\gamma_{\mathrm{sr}_i}}{\gamma_{\mathrm{sr}_i} - \gamma}\right) f_{\gamma_{\mathrm{sr}_i}}\left(\gamma_{\mathrm{sr}_i}\right) d\gamma_{\mathrm{sr}_i} \\ &+ \int_{\gamma}^{\infty} \Pr\left(\gamma_{r_i d} \leq \frac{\gamma\gamma_{\mathrm{sr}_i}}{\gamma_{\mathrm{sr}_i} - \gamma}\right) f_{\gamma_{\mathrm{sr}_i}}\left(\gamma_{\mathrm{sr}_i}\right) d\gamma_{\mathrm{sr}_i} \\ &= 1 - \int_{\gamma}^{\infty} \Pr\left(\gamma_{r_i d} \geq \frac{\gamma\gamma_{\mathrm{sr}_i}}{\gamma_{\mathrm{sr}_i} - \gamma}\right) f_{\gamma_{\mathrm{sr}_i}}\left(\gamma_{\mathrm{sr}_i}\right) d\gamma_{\mathrm{sr}_i} \\ &= 1 - \frac{1}{2b_o\bar{\gamma}_{\mathrm{sr}_i}} \left(\frac{2b_o m_o}{2b_o m_o + \Omega}\right)^{m_o} \sum_{n=0}^{m-1} \frac{1}{n!} \left(\frac{m}{\bar{\gamma}_{r_i d}}\right)^n \\ &\times \int_{\gamma}^{\infty} \exp\left[-\left(\frac{\gamma_{\mathrm{sr}_i}}{2b_o\bar{\gamma}_{\mathrm{sr}_i}} + \frac{m\gamma\gamma_{\mathrm{sr}_i}}{\bar{\gamma}_{r_i d}\left(\gamma_{\mathrm{sr}_i} - \gamma\right)}\right)\right] \\ &\times \left(\frac{\gamma\gamma_{\mathrm{sr}_i}}{\gamma_{\mathrm{sr}_i} - \gamma}\right)^n \\ &\times {}_1F_1\left(m_o, 1, \frac{\Omega\gamma_{\mathrm{sr}_i}}{2b_o\bar{\gamma}_{\mathrm{sr}_i}\left(2b_o m_o + \Omega\right)}\right) d\gamma_{\mathrm{sr}_i} \end{aligned} \tag{31}$$

After integral substitution $x = \gamma_{sr_i} - \gamma$ and applying [18, eq.(9.14.1)] and [18, eq.(1.111)] we can reach

$$\begin{aligned} F_{\gamma_{r_i}}(\gamma) &= 1 - \frac{1}{2b_o\bar{\gamma}_{\mathrm{sr}_i}} \left(\frac{2b_o m_o}{2b_o m_o + \Omega}\right)^{m_o} \sum_{n=0}^{m-1} \frac{1}{n!} \\ &\times \left(\frac{m}{\bar{\gamma}_{r_i d}}\right)^n \exp\left[-\left(\frac{\gamma}{2b_o\bar{\gamma}_{\mathrm{sr}_i}} + \frac{m\gamma}{\bar{\gamma}_{r_i d}}\right)\right] \\ &\times \sum_{k=0}^{\infty} \frac{1}{k!} \frac{\Gamma(m_o + k)}{\Gamma(m_o)\Gamma(1 + k)} \left(\frac{\Omega}{2b_o\bar{\gamma}_{\mathrm{sr}}\left(2b_o m_o + \Omega\right)}\right)^k \\ &\times \sum_{j=0}^{n+k} \binom{n+k}{j} \gamma^{n+j} \\ &\times \int_0^{\infty} \exp\left[-\left(\frac{x}{2b_o\bar{\gamma}_{\mathrm{sr}_i}} + \frac{m\gamma^2}{x\bar{\gamma}_{r_i d}}\right)\right] x^{k-j} dx \end{aligned} \tag{32}$$

Now with the aid of [18, eq.(3.471.9)] and solving the above integral, we can get the closed form CDF expression in (8).

REFERENCES

[1] A. Vanelli-Coralli, G. Corazza, G. Karagiannidis, P. Mathiopoulos, D. Michalopoulos, C. Mosquera, S. Papaharalabos, and S. Scalise, "Satellite communications: Research trends and open issues," in *proceeding of the International Workshop on Satellite and Space Communications, IWSSC'07.*, 2007, pp. 71–75.

[2] J. Laneman, D. Tse, and G. Wornell, "Cooperative diversity in wireless networks: Efficient protocols and outage behavior," *IEEE Transactions on Information Theory*, vol. 50, no. 12, pp. 3062–3080, 2004.

[3] V. Genc, S. Murphy, Y. Yu, and J. Murphy, "IEEE 802.16 j relay-based wireless access networks: an overview," *IEEE Wireless Communications*, vol. 15, no. 5, pp. 56–63, 2008.

[4] S. Kim, H. Kim, and K. Kang, "Performance enhancement in future mobile satellite broadcasting services," *IEEE Communications Magazine*, vol. 46, no. 7, pp. 118–124, 2008.

[5] D. Ahn, S. Kim, H. Kim, and D. Park, "A cooperative transmit diversity scheme for mobile satellite broadcasting systems," *International Journal of Satellite Communications and Networking*, vol. 28, no. 5-6, pp. 352–368, 2010.

[6] Y. Labrador, M. Karimi, D. Pan, and J. Miller, "An approach to cooperative satellite communications in 4G mobile systems," *Journal of Communications*, vol. 4, no. 10, pp. 815–826, 2009.

[7] C. Warty, "Cooperative communication for multiple satellite network," in *porceeding of the IEEE Aerospace Conference*, 2010, pp. 1–7.

[8] S. Lee, S. Lee, K. Kim, and J. Seo, "Personal and mobile satellite DMB services in Korea," *IEEE Transactions on Broadcasting*, vol. 53, no. 1, pp. 179–187, 2007.

[9] N. Chuberre, O. Courseille, P. Laine, L. Roullet, T. Quignon, and M. Tatard, "Hybrid satellite and terrestrial infrastructure for mobile broadcast services delivery: an outlook to the unlimited mobile TV system performance," *International Journal of Satellite Communications and Networking*, vol. 26, no. 5, pp. 405–426, 2008.

[10] S. Morosi, E. Del Re, S. Jayousi, and R. Suffritti, "Hybrid satellite/terrestrial cooperative relaying strategies for DVB-SH based communication systems," in *proceeding of the European Wireless Conference,. EW'09.*, 2009, pp. 240–244.

[11] S. Ikki and M. Ahmed, "Performance analysis of cooperative diversity wireless networks over Nakagami-m fading channel," *IEEE Communications Letters*, vol. 11, no. 4, pp. 334–336, 2007.

[12] L. Yang and H. Chen, "Error probability of digital communications using relay diversity over Nakagami-m fading channels," *IEEE Transactions on Wireless Communications*, vol. 7, no. 5, pp. 1806–1811, 2008.

[13] F. Fontán, M. Vazquez-Castro, C. Cabado, J. Garcia, and E. Kubista, "Statistical modeling of the LMS channel," *IEEE Transactions on Vehicular Technology*, vol. 50, no. 6, pp. 1549–1567, 2001.

[14] H. Kim, K. Kang, and D. Ami, "Distributed space-time coded transmission for mobile satellite communication using ancillary terrestrial component," in *proceeding of the IEEE International Conference on Communications,. ICC'07.*, 2007, pp. 4426–4431.

[15] A. Perez-Neira, C. Ibars, J. Serra, A. del Coso, J. Gomez, and M. Caus, "MIMO applicability to satellite networks," in *in proceeding of the IEEE 10th International Workshop on Signal Processing for Space Communications, 2008. SPSC.*, 2008, pp. 1–9.

[16] A. Abdi, W. Lau, M. Alouini, and M. Kaveh, "A new simple model for land mobile satellite channels: first-and second-order statistics," *IEEE Transactions on Wireless Communications*, vol. 2, no. 3, pp. 519–528, 2003.

[17] M. Simon and M. Alouini, *Digital communication over fading channels*. Wiley-IEEE Press, 2005, vol. 86.

[18] I. Ryzhik, A. Jeffrey, and D. Zwillinger, *Table of integrals, series and products*. Academic Press, 2007.

[19] A. Iqbal and K. Ahmed, "SER analysis of cooperative satellite-terrestrial network over non identical fading channels," in *proceeding of the IEEE 5th Advanced satellite multimedia systems conference (ASMA) and the 11th signal processing for space communications workshop (SPSC)*, 2010, pp. 329–334.

[20] J. Abate and W. Whitt, "Numerical inversion of Laplace

transforms of probability distributions," *ORSA Journal on Computing*, vol. 7, pp. 36–36, 1995.

[21] Y. Ko, M. Alouini, and M. Simon, "Outage probability of diversity systems over generalized fading channels," *IEEE Transactions on Communications*, vol. 48, no. 11, pp. 1783–1787, 2000.

Arif Iqbal received the B.E. degree in Electronic Engineering from Dawood College of Engineering and Technology, Karachi, Pakistan in 2002 and M.E. degrees in Telecommunication Engineering from the Asian Institute of Technology, Thailand, in 2009. He is currently working towards the PhD. degree at the Telecommunications, School of Engineering and Technology, Asian Institute of Technology, Thailand.

Mr. Iqbal's research interest includes performance analysis of hybrid satellite-terrestrial system; cooperative MIMO relaying system, land mobile satellite communications systems (LMSS) and cooperative diversity schemes.

Dr. Kazi M. Ahmed was born in Bangladesh. He did his Masters in Telecommunications Engineering from the then Leningrad Electrical Engineering Institute of Communications, former USSR, in 1978. He finished his Ph.D. in Electrical Engineering from the University of Newcastle, NSW, Australia in 1983.

At present, he is a Professor of Telecommunications and ICT at Asian Institute of Technology, Bangkok, Thailand.

Dr. Ahmed has diverse interest in different fields of Telecommunications. His main research interest is in Wireless Communications and Communications Networks.

Dr. Kazi Ahmed is a Member, IEEE; Member, IEICE, Japan; Fellow of IE Bangladesh; and Member and Advisor of many international and national associations and steering committees.

Call for Papers and Special Issues

Aims and Scope.

Journal of Communications (JCM) is a scholarly peer-reviewed international scientific journal published monthly, focusing on theories, systems, methods, algorithms and applications in communications. It provide a high profile, leading edge forum for academic researchers, industrial professionals, engineers, consultants, managers, educators and policy makers working in the field to contribute and disseminate innovative new work on communications.

JCM invites original, previously unpublished, research, survey and tutorial papers, plus case studies and short research notes, on both applied and theoretical aspects of communications. These areas include, but are not limited to, the following topics:

- Signal Processing for Communications
- Multimedia Processing and Communications
- Communication QoS and Performance Modeling
- Cross-layer Design and Optimization
- Communication and Information Theory
- Communication Software and Services
- Protocol and Algorithms for Communications
- Wireless Communications and Networking
- Wireless Ad-hoc and Sensor Networking
- Broadband Wireless Access
- Cooperative Communications and Networking
- Optical Communications and Networking
- Broadband Networking and Protocols
- Internet Services, Systems and Applications
- P2P Communications and Networking
- Pervasive Computing and Grid Networking
- Communication Network Security
- Cognitive Radio Communications and Networking
- Hardware Architecture for Communications and Networking
- Parallel and Distributed Computing
- Satellite and Space Communications
- Emerging Communication Technology and Standards

Special Issue Guidelines

Special issues feature specifically aimed and targeted topics of interest contributed by authors responding to a particular Call for Papers or by invitation, edited by guest editor(s). We encourage you to submit proposals for creating special issues in areas that are of interest to the Journal. Preference will be given to proposals that cover some unique aspect of the technology and ones that include subjects that are timely and useful to the readers of the Journal. A Special Issue is typically made of 8 to 12 papers, with each paper 8 to 12 pages of length, and the papers include:

- A Guest Editorial;
- 2-3 Invited Survey papers from world well-known scientists in the specific area;
- 6-10 Research papers reflecting the latest advances in the specific area.

The following information should be included as part of the proposal:

- Proposed title for the Special Issue
- An initial version of Call for Papers with specific topics covered in the Special Issue
- Name, contact, position, affiliation, and biography of the Guest Editor(s)
- Tentative time-table for the call for papers and reviews
- Potential authors and topics for the Invited Survey papers
- List of potential reviewers
- Plans for advertising the Call for Paper and attracting high-quality paper submissions

If a proposal is accepted, the guest editor will be responsible for:

- Submitting a final “Call for Papers” to be included on the Journal’s Web site.
- Distribution of the Call for Papers broadly to various mailing lists and sites.
- Leading a fair and strict review process for the paper submissions, collecting 2-3 reviews for each paper before the final decision making. Authors should be informed the Author Instructions.
- Providing JCM the completed and approved final versions of the papers formatted in the Journal’s style, together with all authors’ contact information.
- Writing a one- or two-page introductory editorial to be published in the Special Issue.

In the Guest Editor Team building process, it is highly recommended that a world well-known scientist (e.g., IEEE or ACM Fellow) in the area is involved in this effort to promote the visibility of the Special Issue in the society. On the other hand, it is suggested to consider the geographic coverage of the team. Due to conflict-of-interest, the Guest Editors are not encouraged to submit their own papers to the Special Issue.

Recommended Papers from an International Conference

JCM accept recommendations from well-known International conferences. The conference organizer can recommend the best papers (top 5% of the accepted papers) to be considered in either JCM regular issue or a JCM special issue. A fast-track review process would be conducted by a JCM Editor for these recommended papers and the final decisions are made based on the review feedback.

The following information should be included as part of the proposal:

- The name of the conference/workshop, and the URL of the event
- A brief description of the event, including: number of submitted and accepted papers, and number of attendees. If these numbers are not yet available, please refer to previous events. First time conference would NOT be considered.
- Tentative time-table for the paper submission.

If a proposal is accepted, the conference organizer needs to submit the following items at a later stage:

- The list of the best papers (top 5% of the accepted papers) for recommendation
- The submitted conference paper draft and review feedbacks

If a conference contributes more than 5 papers that are finally accepted by JCM, the organizer would be invited to serve as a Guest Co-Editor of a JCM annual Special Issue, “SI on the Latest Advances in Communications and Networking”, and these accepted papers would be included in the same Special Issue. Otherwise, the accepted papers would be published in JCM regular issues.

More information is available on the web site at http://www.academypublisher.com/jcm/.

(Contents Continued from Back Cover)

REGULAR PAPERS